From Molecules to Cooper Pairs: Experiments in the BEC-BCS Crossover

Dissertation

zur Erlangung des Doktorgrades an der
Fakultät für Mathematik, Informatik und Physik
der Leopold-Franzens-Universität Innsbruck

vorgelegt von

Markus Bartenstein

durchgeführt am Institut für Experimentalphysik
unter der Leitung von
Univ.-Prof. Dr. Rudolf Grimm

Februar 2005

per Anna

Abstract

We explore the crossover from a molecular Bose-Einstein condensate (BEC) to a Bardeen-Cooper-Schrieffer (BCS) superfluid of "Cooper paired" fermions with an ultracold gas of fermionic ^{6}Li atoms. The crucial parameter in the crossover is the coupling strength between the paired atoms. At sufficiently low temperatures a BEC of tightly bound molecules is formed in the strong coupling limit, while in the weak coupling limit a BCS state of delocalized pairs is created.

A magnetically tunable scattering resonance at a magnetic field of about 834 G serves as the experimental key to explore various coupling regimes. Through this Feshbach resonance we control the interactions in the gas and vary the coupling strength over a broad range. The starting point for our experiments is a molecular BEC of tightly bound pairs that we produce by evaporative cooling of an optically trapped ^{6}Li spin mixture. Exploiting the Feshbach tuning, we explore the BEC-BCS crossover by studying elementary macroscopic and microscopic properties of the gas.

The analysis of density profiles of the trapped cloud in the BEC-BCS crossover shows that it is smooth and reversible. Moreover, from the measured cloud size on resonance we are able to determine the value of an universal parameter, which characterizes the interaction energy of the unitary limited quantum gas.

To investigate the collective dynamics of the gas in the BEC-BCS crossover we excite energetically low-lying collective modes in the axial and radial directions of our cigar shaped trap. The collective oscillations of the modes in the axial direction show the expected behavior of a gas in the BEC-BCS crossover with a particularly small damping rate in the vicinity of the Feshbach resonance. The modes in the strongly confined radial direction, however, show an abrupt change in the collective oscillation frequency at a magnetic field value that corresponds to a Fermi gas in the strongly interacting regime. A plausible explanation for the observed breakdown of the hydrodynamic behavior is the coupling of the collective oscillation to the pairs in the strongly interacting Fermi gas, which leads to pair breaking.

Employing radio-frequency spectroscopy, we study the pairing energy in the BEC-BCS crossover. We demonstrate the dependence of the pairing energy on the coupling strength, temperature, and Fermi energy. The observation of an early onset of the pairing in the evaporative cooling process strongly suggests that for full evaporation the strongly interacting Fermi gas is in the superfluid phase.

Our experiments open up intriguing prospects for further experiments on the fascinating properties of strongly correlated many-body regimes that are of great relevance for several fields of physics; like quantum fluids, neutron stars, and most prominently high T_c superconductors.

Zusammenfassung

Mit einem ultrakalten Gas fermionischer ^{6}Li Atome erforschen wir den Übergang von einem molekularen Bose-Einstein Kondensat (BEC) zu einem superfluiden Bardeen-Cooper-Schrieffer (BCS) Zustand aus zu Cooper-Paaren gebundenen Fermionen. Die ausschlaggebende Größe bei diesem Übergang ist die Stärke der Kopplung zwischen den gepaarten Atomen. Bei ausreichend tiefen Temperaturen bildet sich im Bereich extrem starker Kopplung ein BEC fest gebundener Moleküle, während sich im Grenzfall äußerst schwacher Kopplung ein BCS Zustand delokalisierter Paare ausbildet.

Eine magnetisch abstimmbare Streuresonanz bei einem Feld von etwa 834 G dient uns als experimenteller Schlüssel zur Erforschung verschiedenster Kopplungsbereiche. Durch diese Feshbach-Resonanz kontrollieren wir die Wechselwirkungen im Gas und variieren die Kopplungsstärke über einen großen Bereich. Ausgangspunkt unserer Experimente ist ein molekulares BEC aus fest gebundenen Paaren, das wir durch Verdampfungskühlung eines optisch gefangenen ^{6}Li Spingemisches erzeugen. Mit Hilfe der Feshbach-Resonanz stellen wir die Kopplungsstärke ein und erfroschen den BEC-BCS Übergang indem wir elementare makroskopische und mikroskopische Eigenschaften des Gases untersuchen.

Die Auswertung von Dichteprofilen im BEC-BCS Übergang zeigt, daß er stetig und reversibel ist. Darüberhinaus können wir durch die auf der Resonanz gemessene Größe der Wolke den Wert eines universellen Parameters bestimmen, welcher die Wechselwirkungsenergie des unitär limitierten Quantengases charakterisiert.

Zur Untersuchung der kollektiven Dynamik des Gases im BEC-BCS Übergang regen wir energetisch tiefliegende kollektive Schwingungen in der axialen und radialen Richtung unserer zigarrenförmigen Falle an. Die kollektiven Schwingungen in axialer Richtung weisen das für ein Gas im BEC-BCS Übergangsbereich erwartete Verhalten auf, wobei wir eine besonders geringe Dämpfung in unmittelbarer Nähe der Feshbach-Resonanz beobachten. Das Verhalten der Moden in der stark eingeschlossenen, radialen Richtung zeigt hingegen eine abrupte Änderung der Oszillationsfrequenz bei einem Magnetfeld, bei dem eine stark wechselwirkendes Fermi-Gas vorliegt. Eine plausible Erklärung für den beobachteten Einbruch des hydrodynamischen Verhaltens ist dass die Paare im stark wechselwirkenden Fermi-Gas durch eine Kopplung an die kollektiven Schwingungen aufgebrochen werden.

Durch Verwendung von Radiofrequenz-Spektroskopie untersuchen wir die Paarungsenergie im BEC-BCS Übergang. Wir zeigen die Abhängigkeit der Paarungsenergie von der Kopplungsstärke, der Temperatur und der Fermi-Energie. Der beobachtete frühzeitige Beginn der Paarung während der Kühlung legt nahe, dass sich das stark wechselwirkende Fermi-Gas am Ende des Kühlprozesses im superfluiden Zustand befindet.

Unsere Experimente eröffnen einzigartige Möglichkeiten für weiterführende Untersuchungen der faszinierenden Eigenschaften stark korrelierter Vielteilchensysteme. Diese Systeme sind von größter Bedeutung für eine Vielzahl physikalischer Arbeitsgebiete wie der Untersuchung von Quantenflüssigkeiten, Neutronensternen und, vor allem, der Untersuchung von Hochtemperatursupraleitern.

Contents

Chapter 1

Introduction

All particles can be classified into two types, bosons[1] and fermions[2]. In atomic gases the distinct quantum statistical description of these two classes of matter becomes apparent when the gas is cooled to such low temperatures that the quantum mechanical wave packets of the particles begin to overlap. For bosons this marks the onset of Bose-Einstein condensation (BEC). This phase transition into the superfluid condensate is characterized by a macroscopic occupation of the ground state. Identical fermions are far less social and have to occupy different quantum states. This rule is expressed by the Pauli exclusion principle, which forces fermions at low temperature to stack up in the lowest quantum states. In contrast to a Bose-Einstein condensate such a "Fermi sea" arrangement is obtained without passing through a phase transition. At even lower temperatures a Fermi gas with attractive interactions is predicted to undergo a phase transition into a superfluid Bardeen-Cooper-Schrieffer (BCS) state where two fermions are paired up in a "Cooper pair".

The experimental realization of a Bose-Einstein condensate in dilute atomic gases was a milestone in physics [And95, Dav95]. Since then the field of atomic condensates has been progressing rapidly and is driven by the combination of new experimental techniques and theoretical advances [Ang02].

The quest for a superfluid Fermi gas poses the challenge of reaching the even lower temperatures that yield the phase transition into pairing and superfluidity [Pit02]. The cooling of fermions is hindered by the Pauli exclusion principle, which suppresses collisions between identical fermions at low temperature. To partially overcome this limitation most experiments use a spin mixture of different hyperfine states of the same fermionic isotope. The two most prominent fermionic atoms that are used in the field of cold atoms are ^{40}K and, as in our experiment, ^{6}Li.

Since the first experimental realization of a degenerate Fermi gas of ^{40}K atoms in 1999 [DeM99b], and of ^{6}Li in 2001 [Tru01, Sch01] tremendous progress has been achieved in the field of ultracold Fermi gases. In particular the ability to control the two-body coupling strength by a magnetically tunable scattering resonance turned

[1] Named after the Indian physicist Satyendrah Nath Bose.

[2] Named after the Italian physicist Enrico Fermi-

out to be a powerful tool [Ino98]. Based on such a Feshbach resonance a strongly interacting Fermi gas was realized in 2002 [O'H02a]. In the following year several groups succeeded in the formation of ultracold composite bosons by pairing of fermions in the vicinity of the resonance [Reg03b, Cub03, Str03, Joc03b]. The pairing of fermions to composite bosons profoundly changes the properties of the gas. The finding that these molecules are rather long lived, triggered a "hot race" [Cho03] that found its first highlight in the creation of a molecular Bose-Einstein condensate [Joc03a, Gre03, Zwi03, Bou04, Hul04].

This molecular condensate of tightly bound fermions corresponds to a BEC type superfluid in the strong coupling limit. Exploiting Feshbach tuning, recent experiments explore the crossover to a Cooper paired superfluid in the weak coupling BCS limit [Bar04b, Reg04b, Zwi04, Bou04, Kin04a, Bar04a, Chi04a, Gre04, Kin04b, Kin05].

These experiments studied the elementary properties of the system under variable interaction conditions. The internal interaction energy was measured by detecting the cloud size of a trapped gas [Bar04b] and by observing the expansion of the gas after release [Bou04]. The condensed nature of fermionic atom pairs was demonstrated by rapid conversion of the "Fermi condensate" into a molecular BEC [Reg04b, Zwi04]. The study of collective excitation modes [Kin04a, Bar04a, Kin04b] provided first insight into changes of the equation of state and hydrodynamics of the system in the crossover. Spectroscopic measurements of the pairing energy [Chi04a] showed the crossover from a two-body molecular pairing regime to the many body dominated BCS regime. The results of these experiments provide strong evidence of superfluidity in strongly interacting Fermi gases [Ho04a].

The BEC-BCS crossover has been the subject of great theoretical interest for more than three decades [Eag69, Leg80, Noz85, Che04]. The theoretically compelling crossover is closely linked to a predicted "resonance superfluidity" [Hol01, Tim01, Oha02, Sta04] and the universal behavior of a Fermi gas with resonant interactions [Hei01, Ho04c]. The crossover is of great relevance for several fields of physics like quantum fluids, neutron stars, and most prominently high T_c superconductors [Cho03, Wei04]. Ultracold Fermi gases now offer unique possibilities to experimentally explore the crossover under well defined conditions with variable coupling strength between the particles. Therefore these systems allow to test the various theoretical approaches.

This thesis reports on our experiments with a degenerate fermi gas of ^{6}Li atoms in the BEC-BCS crossover. It is structured as follows: Chapter two and three provide a summary of the theoretical concepts that are relevant for our experiments. Chapter two introduces the description of degenerate Bose and Fermi gases and gives a very brief introduction into the description of the BEC-BCS crossover. Chapter three is devoted to interactions and collective dynamics in ultracold gases. The first part of this chapter introduces the general description of ultracold collisions and the concept of magnetically tunable Feshbach resonances. Both sections focus on the specific properties of fermionic ^{6}Li atoms. The second part of this chapter presents the description of collective oscillations of gases in different harmonic traps and under different conditions.

Chapter four and five briefly summarize our experimental setup and the creation of a molecular Bose-Einstein condensate, respectively. A detailed description of these two topics is found in the Ph.D. thesis of Selim Jochim [Joc04].

Our measurements with a degenerate Fermi gas in the BEC-BCS crossover are presented in chapter six. They are the main result of this thesis. This chapter starts with the presentation of the measured cloud size when the molecular BEC is converted into a strongly interacting Fermi gas. The observation of a smooth and reversible crossover is the most important finding of this first series of experiments. In the following section we show our measurements of collective excitations in the BEC-BCS crossover. Our measurements of the axial and radial breathing mode both show a very pronounced dependence of the frequency and damping rate on the coupling strength. Of particular interest is the observed sharp transition in the radial collective mode frequency which indicates a transition from a hydrodynamic to a collisionless gas. In a further series of experiments we employed radio-frequency spectroscopy measurements in the BEC-BCS crossover. Applying this high resolution spectroscopic technique we were able to observe the pairing gap in the strongly interacting Fermi gas. The experimental results show the gradual change of the pairing gap from the two-body molecular regime to the many-body BCS regime. The high precision radio-frequency spectroscopy on weakly bound molecules also allowed us to precisely determine the ultracold collision parameters of ^{6}Li. These data enable a quantitative comparison of the experimental results with the predictions of the crossover theory and are used throughout this thesis.

The experiments in the BEC-BCS crossover support the expected superfluidity of the strongly interacting Fermi gas. The next great challenge is a direct proof of the superfluidity. In chapter seven we present our ideas to achieve this next major goal.

Chapter 2

Degenerate Quantum Gases

For a gas at sufficiently high temperature and low density, the thermodynamic description is independent of the quantum statistical properties of the particles. In this classical limit the gas can be treated as point-like particles with an occupation of the single particle states that is given by the Maxwell-Boltzmann distribution function (see also figure 2.1). Because the mean occupation per quantum state is usually much smaller than one, it does not make a difference whether or not the constituents of the gas are treated as indistinguishable particles.

The quantum mechanical properties of the gas become important as soon as the gas is cooled to such a low temperature T that the mean occupation per state is no longer negligibly small. The quantum statistical description in combination with the indistinguishability of the particles gives rise to the Bose and Fermi statistics. The different statistics are a direct consequence of the symmetric and antisymmetric wave functions that describe bosons and fermions, respectively. The distinct Bose and Fermi statistics result in a drastically different thermodynamic behavior of ultracold Bose and Fermi gases [Hua87].

In a simplified picture, the particles can be regarded as quantum mechanical wave packets with an extent given by the thermal de Broglie wavelength

$$\lambda_{\mathrm{dB}} = \sqrt{\frac{2\pi\hbar^2}{m k_{\mathrm{B}} T}}, \tag{2.1}$$

where m is the mass of the particle and k_{B} is the Boltzmann constant. At sufficiently low temperature the wave packets begin to overlap and the gas is said to become degenerate. In a gas of density n the interparticle spacing is given by $n^{-1/3}$ and the condition for degeneracy can be expressed by

$$D = n\lambda_{\mathrm{dB}}^3 \approx 1, \tag{2.2}$$

where D defines the phase-space density, which in a classical gas is a measure of the typical occupancy number of a single particle state.

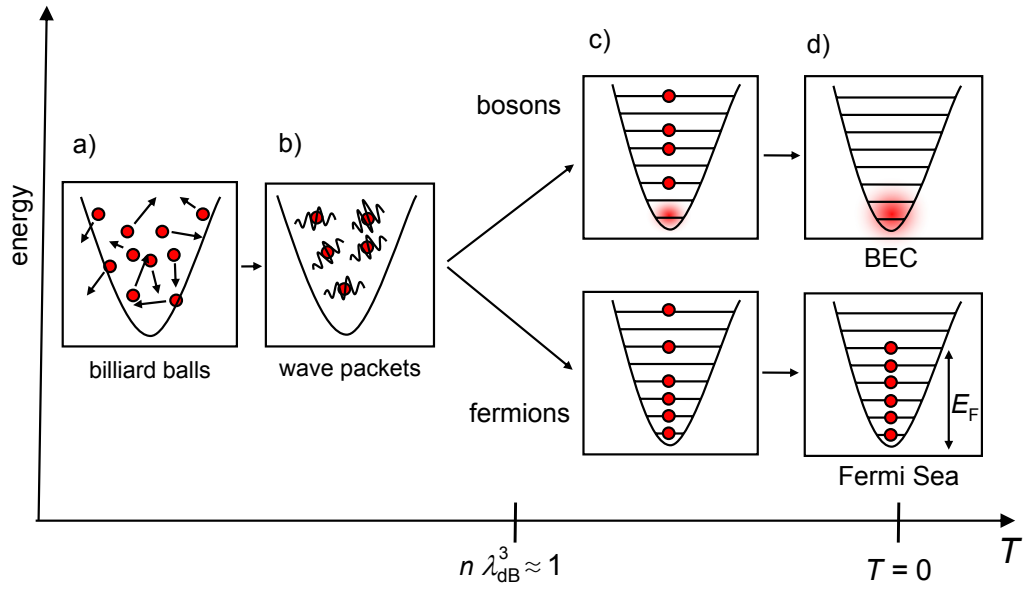

Figure 2.1: Illustration of the transition from a classical gas of identical particles into a quantum mechanically governed degenerate gas. At high temperature the mean interparticle distance is much larger than the size of the particles and they can be treated as point-like (a). If the temperature is lowered, the quantum statistical properties of the particles become important (b). For temperatures where the de Broglie wavelength is on the order of the interparticle spacing ($n\lambda_{\mathrm{dB}}^3 \approx 1$), bosons begin to form a BEC and occupy the ground state of the trap (c, upper row); While fermions fill up the lowest lying states, occupying each state by only one particle (c, lower row). In the limit of $T = 0$ a pure BEC and a Fermi sea are formed, respectively (d).

For a phase space density approaching unity bosons and fermions show a strikingly different thermodynamic behavior (see also figure 2.1). For bosons a phase space density of about one marks the onset of the so-called Bose-Einstein condensation. This phase transition is a purely statistical phenomenon characterized by an macroscopic occupation of the ground state. Such degenerate Bose gases are described in more detail in section 2.1. Fermions however, obey the Pauli exclusion principle that forbids two identical fermions to occupy the same quantum state. Thus a phase space density of one implies that up to a certain energy E_{F} each state is filled with exactly one atom. The energy E_{F} of the highest occupied state is referred to as the Fermi energy. In analogy to the case of bosons such a Fermi gas is called a degenerate Fermi gas, although physically speaking the opposite is true. The properties of degenerate Fermi gases are summarized in section 2.2.

In contrast to the case of bosons the formation of a degenerate Fermi gas is not accompanied by a phase transition. For a Fermi gas with weak attractive interactions, however, a phase transition into a so-called BCS state exists at much lower temperatures than the Fermi temperature T_{F} which marks the onset of quantum degeneracy ($k_{\mathrm{B}}T_{\mathrm{F}} = E_{\mathrm{F}}$). As will be explained in section 2.2 the fermions in this BCS state form Cooper pairs of bosonic nature.

For a composite particle like an atom, the number of elementary particles decides, whether it belongs to the group of bosons or fermions. In degenerate quantum gases the composite nature of these bosons or fermions has usually not to be taken into account and the particles can be treated as point-like particles obeying Bose or Fermi statistics, respectively. The reason for this lies in the fact that in a degenerate gas, the internal degree of freedom is frozen out because the available energies are all much smaller than the energy required for an internal excitation.

This condition, however, is no longer fulfilled if the Fermi energy is on the order of the binding energy E_b of the composite particles. Depending on the exact value of the Fermi energy with respect to the binding energy, the particles are bound ($E_\mathrm{F} \ll E_\mathrm{b}$) or not ($E_\mathrm{F} \gg E_\mathrm{b}$). In particular, a pair of composite fermions is said to be in the strong coupling BEC limit if the binding energy is large with respect to the Fermi energy, while for binding energies that are small with respect to the Fermi energy, the system is in the weak coupling BCS limit. In ultracold gases, magnetically tunable scattering resonances allow the control of the two-body coupling strength. The ability to tune continuously the coupling strength from the strong to the weak coupling limit, opens the door to experimentally investigate the BEC-BCS crossover. Section 2.3 gives a brief description of this theoretically compelling BEC-BCS crossover.

2.1 Bose-Einstein condensates

The theory of Bose-Einstein condensation in dilute gases is covered in several excellent textbooks [Pet02, Pit03] and review articles [Ket99, Dal99a]. Therefore only an overview of the main aspects relevant for this thesis will be given.

The section starts with a short description of the occurrence of the phase transition in an ideal gas of free, and harmonically trapped bosons. In the second part interactions between the particles are taken into account. This leads to the Gross-Pitaevskii equation and the widely used Thomas-Fermi approximation.

2.1.1 Phase transition in an ideal gas

For noninteracting bosons in thermodynamic equilibrium, the mean occupation number of a single particle state ν with energy ϵ_ν is given by the Bose-Einstein distribution function

$$n(\epsilon_\nu) = \frac{1}{\exp\left[(\epsilon_\nu - \mu)/k_\mathrm{B}T\right] - 1}. \tag{2.3}$$

The chemical potential μ is fixed by the normalization condition $N = \sum_\nu n(\epsilon_\nu)$ and can be calculated as a function of T and N.

At high temperatures the mean occupancy number of any state is much less than one. In other words $\exp\left[(\epsilon_\nu - \mu]/k_\mathrm{B}T\right) \gg 1$ for all states and thus the chemical potential has to be much smaller than the energy ϵ_0 of the lowest single particle state. In

this limit the distribution function given in equation 2.3 is well approximated by the classical Maxwell-Boltzmann distribution.

When the temperature is lowered with constant atom number N, the chemical potential rises to conserve $N = \sum_\nu n(\epsilon_\nu)$. An upper limit for the chemical potential is given by ϵ_0. If the chemical potential would reach or exceed this value the occupation number of the lowest energy state would lead to an unphysical negative value. When μ approaches ϵ_0 the occupation number of the ground state

$$N_0 = n(\epsilon_0) = \frac{1}{\exp\left[(\epsilon_0 - \mu)/k_B T\right] - 1} \tag{2.4}$$

becomes increasingly large. This mechanism is the origin of Bose-Einstein condensation.

To obtain the criteria for Bose-Einstein condensation one considers the number of atoms in the excited states $N_\mathrm{T} = N - N_0$. For a given temperature T the number of thermal atoms N_T reaches a maximum for $\mu \to \epsilon_0$. This maximum number is given by

$$N_\mathrm{T}^\mathrm{max} = \sum_{\nu>0} \frac{1}{\exp\left[(\epsilon_\nu - \epsilon_0)/k_B T\right] - 1}. \tag{2.5}$$

If the temperature drops below a certain value T_c, the maximum number of atoms in the excited states $N_\mathrm{T}^\mathrm{max}$ becomes smaller than N. To satisfy the normalization condition $N = N_0 + N_\mathrm{T}$ the number of atoms in the ground state N_0 has to be on the order of N. The temperature T_c where $N_\mathrm{T}^\mathrm{max} = N$ is called the critical temperature and marks the onset of the Bose-Einstein condensation, i.e. the macroscopic occupation of a single particle state.

BEC in a harmonic trapping potential

In most experiments with atomic gases, the particles are confined by a harmonic potential. In the following a brief discussion of the properties of a BEC in a three-dimensional harmonic oscillator potential $V(\mathbf{r})$ with trap frequencies ω_i $(i = x, y, z)$ is given.

Assuming that the temperature of the gas is much larger than the level spacing between the single particle states ($k_\mathrm{B} T \gg \hbar\omega_i$), the so-called semiclassical approximation can be applied. For a BEC, this condition is satisfied if $N \gg 1$. Because the condition implies that $k_\mathrm{B} T_\mathrm{c}$ is much larger than the zero point energy of the harmonic oscillator potential, this energy is neglected in the following.

In the semiclassical approximation the sum over the single particle states (see for example equation 2.5) can be replaced by integrals. The approximation of the discretized single particle levels by a continuum also justifies the concept of the density of states. For a three-dimensional harmonic oscillator the density of states is given by $g(\epsilon) = \epsilon^2/2(\hbar\omega_\mathrm{ho})^3$, where $\omega_\mathrm{ho} = (\omega_x \omega_y \omega_z)^{1/3}$ is the geometric average of the oscillator

frequencies. The number of thermal atoms then becomes

$$N_{\mathrm{T}} = \int_0^\infty g(\epsilon) n(\epsilon)\, d\epsilon, \tag{2.6}$$

and the evaluation of the integral with $\mu = 0$ and $N_{\mathrm{T}} = N$ defines the critical temperature given by [Pet02]

$$k_{\mathrm{B}} T_{\mathrm{c}} = \hbar\omega_{\mathrm{ho}} \left(\frac{N}{\zeta(3)} \right)^{1/3} = 0.94 \hbar\omega_{\mathrm{ho}} N^{1/3}, \tag{2.7}$$

where $\zeta(\alpha)$ is the Riemann zeta function[1].

The temperature dependence of the condensate fraction N_0/N is found using the normalization condition $N = N_0 + N_{\mathrm{T}}$ and equation 2.6 [Dal99a]

$$\frac{N_0}{N} = 1 - \left(\frac{T}{T_{\mathrm{c}}} \right)^3 . \tag{2.8}$$

In a pure BEC all atoms are condensed in the lowest single particle state and the density distribution $n(r)$ reflects the shape of the ground state wave function, which is given for a harmonic oscillator by

$$\varphi_0(\mathbf{r}) = \left(\frac{m\omega_{\mathrm{ho}}}{\pi\hbar} \right)^{3/4} \exp\left[-\frac{m}{2\hbar} (\omega_x x^2 + \omega_y y^2 + \omega_z z^2) \right]. \tag{2.9}$$

The density distribution is given by $n(\mathbf{r}) = N|\varphi_0(\mathbf{r})|^2$ and grows with N. The size of the condensate however, is independent of N and is fixed by the harmonic oscillator length

$$a_{\mathrm{ho}} = \left(\frac{\hbar}{m\omega_{\mathrm{ho}}} \right)^{1/2}, \tag{2.10}$$

which corresponds to the geometric average of the width of the Gaussian function given in equation 2.9. For ^{6}Li in our weakest trap with $\omega_{\mathrm{ho}}/2\pi \approx 110\,\mathrm{Hz}$ the harmonic oscillator length would be about $2.8\,\mu$m.

The density distribution of a gas obeying classical statistics, however, depends on the temperature and is proportional to $\exp[-V(\mathbf{r})/k_{\mathrm{B}}T]$. The $1/e$-width B_i of the distribution is given by [Pet02]

$$B_i^2 = \frac{2k_{\mathrm{B}}T}{m\omega_i^2}, \tag{2.11}$$

and is, under typical experimental conditions, much broader than the corresponding width of the condensate $a_i^2 = \hbar/m\omega_i$. Consequently, when the gas is cooled below the transition temperature T_{c} the formation of the condensate shows up as a narrow peak in the spatial distribution with a weight that increases with decreasing temperature (see also chapter 5).

[1] The Riemann zeta function is defined as $\zeta(\alpha) = \sum_{l=1}^{\infty} l^{-\alpha}$.

2.1.2 Interacting condensates

So far interactions between particles have not been taken into account and in principle the ground state of a system including two-body interactions can be directly calculated from the corresponding Hamiltonian [Kra96]. To solve the many-body Schrödinger equation exactly, heavy numerical efforts are necessary, which might even fail at large N. Therefore mean field approaches are commonly used to describe interacting systems. In these approaches the interactions are not taken explicitly into account on length scales smaller than the interparticle spacing[2].

Assuming that the s-wave scattering amplitude a (see section 3.1) is the relevant interaction parameter, E. Gross [Gro61] and L. Pitaevskii [Pit61] showed independently that at $T = 0$ and in the limit of $N \gg 1$ the condensate wave function $\Phi(\mathbf{r}, t)$ (also referred to as the order parameter) obeys the following equation

$$i\hbar\frac{\partial}{\partial t}\Phi(\mathbf{r}, t) = \left(-\frac{\hbar^2\nabla^2}{2m} + V_{\text{ext}}(\mathbf{r}) + g|\Phi(\mathbf{r}, t)|^2\right)\Phi(\mathbf{r}, t), \tag{2.12}$$

where $g = 4\pi\hbar^2 a/m$ is the coupling constant. The density and the condensate wave function are related by $n(\mathbf{r}, t) = |\Phi(\mathbf{r}, t)|^2$.

In the case of stationary solutions the wave function evolves in time according to [Pit03]

$$\Phi(\mathbf{r}, t) = \Phi(\mathbf{r}) \exp\left(\frac{-i\mu t}{\hbar}\right), \tag{2.13}$$

where the time dependence is fixed by the chemical potential, which is given by the normalization condition $\int d\mathbf{r}\, |\Phi(\mathbf{r})|^2 = N$. The Gross-Pitaevskii equation 2.12 then becomes

$$\left(-\frac{\hbar^2\nabla^2}{2m} + V_{\text{ext}}(\mathbf{r}) + g|\Phi(\mathbf{r})|^2\right)\Phi(\mathbf{r}) = \mu\Phi(\mathbf{r}). \tag{2.14}$$

This equation has the form of a Schrödinger equation in which the potential acting on the particles is the sum of the external potential V_{ext} and a nonlinear term $g|\Phi(\mathbf{r})|^2$ that takes into account the mean field produced by the other bosons. Note that in contrast to the Schrödinger equation the eigenvalue is the chemical potential and not the energy per particle.

In the following the external potential $V_{\text{ext}}(\mathbf{r})$ is again assumed to be a three dimensional harmonic oscillator. By directly integrating equation 2.14 one finds the useful expression [Pit03]

$$\mu = \frac{1}{N}\left(E_{\text{kin}} + E_{\text{ho}} + 2E_{\text{int}}\right) \tag{2.15}$$

for the chemical potential in terms of the different contributions to the energy. The quantum kinetic energy (also referred to as the quantum pressure term) E_{kin}, the harmonic oscillator energy E_{ho} and the two-body interaction energy E_{int} are related to each other by the virial relation [Pit03]

$$2E_{\text{kin}} - 2E_{\text{ho}} + 3E_{\text{int}} = 0. \tag{2.16}$$

[2] Interactions at low energy are discussed in more detail in section 3.1.3.

The validity of the Gross-Pitaevskii equation is based on the condition that the scattering length a is much smaller than the average distance $d = n^{-1/3}$ between the particles fixed by the average density n of the gas. The condition $|a| \ll n^{-1/3}$ is equivalent to the requirement that the value of the gas parameter is very small, i.e. $n|a|^3 \ll 1$. In this case the gas is said to be dilute or weakly interacting. The terminology however, can be misleading since the condition of $n|a|^3 \ll 1$ does not necessarily imply that the interactions can be neglected. The effects of interactions have to be compared with the kinetic energy. Taking the kinetic energy of the ground state of a harmonic oscillator, one finds [Dal99a]

$$\frac{E_{\text{int}}}{E_{\text{kin}}} \propto \frac{N|a|}{a_{\text{ho}}}. \tag{2.17}$$

Even for a dilute gas this parameter can easily be larger than one, leading to a non-ideal behavior of the gas.

Thomas-Fermi limit

For noninteracting bosons ($g = 0$) the solution of the Gross-Pitaevskii equation is found to be $\Phi(\mathbf{r}) = \sqrt{N}\varphi_0(\mathbf{r})$, where $\varphi_0(\mathbf{r})$ is the ground state wave function given in equation 2.9.

In the presence of interactions, however, the shape of the cloud will change significantly. In case of attractive (repulsive) interactions the central density is raised (lowered) and the radius of the cloud consequently will decrease (increase). If the effect of interactions is very significant, i.e $Na/a_{\text{ho}} \gg 1$, the width of the gas will become so large and the density profile so smooth that the kinetic energy term in the Gross-Pitaevskii equation can be ignored. This limit is called the Thomas-Fermi approximation and is well satisfied in most experiments. In this limit the density profile is given by

$$n(\mathbf{r}) = \frac{1}{g}[\mu - V_{\text{ext}}(\mathbf{r})], \tag{2.18}$$

for $\mu > V_{\text{ext}}$ and $n(\mathbf{r}) = 0$ elsewhere [Bay96]. The chemical potential is fixed by the normalization condition $\int d\mathbf{r}\, n(\mathbf{r}) = N$ and takes the value

$$\mu = \frac{\hbar\omega_{\text{ho}}}{2}\left(\frac{15Na}{a_{\text{ho}}}\right)^{2/5}. \tag{2.19}$$

The density profile in the Thomas-Fermi limit thus takes the form of an inverted parabola. The density vanishes at the classical turning point and the characteristic radius (also called the Thomas-Fermi radius) R_i ($i = x, y, z$) of the cloud is given by the relation

$$\mu = \frac{1}{2}m\omega_i^2 R_i^2. \tag{2.20}$$

Combining this with equation 2.19, the Thomas-Fermi radius can be written as

$$R_i = a_{\text{ho}}\left(\frac{15Na}{a_{\text{ho}}}\right)^{1/5}\frac{\omega_{\text{ho}}}{\omega_i}, \tag{2.21}$$

and the density profile of the condensate in a three dimensional harmonic trap is given by

$$n(\mathbf{r}) = \frac{15N}{8\pi \prod_i R_i} \max\left(1 - \sum_i \frac{r_i^2}{R_i^2}, 0\right). \tag{2.22}$$

From the thermodynamic relation $\mu = \partial E/\partial N$ the total energy per particle in the Thomas-Fermi limit is found to be

$$\frac{E}{N} = \frac{5}{7}\mu. \tag{2.23}$$

From equation 2.16, with the quantum pressure term E_{kin} set to zero, the interaction energy per particle is found to be $E_{\mathrm{int}}/N = (2/7)\,\mu$ while the potential energy is $E_{\mathrm{ho}}/N = (3/7)\,\mu$ [Pit03].

It should be noted again that all the results presented so far are only valid if the gas is sufficiently dilute, i.e. $n|a|^3 \ll 1$. For typical parameters in trapped atomic gases this condition is well fulfilled. However, in the vicinity of a Feshbach resonance the scattering length can become very large, making it necessary to include corrections to the above mean field description. These beyond mean field corrections and their influence to the dynamic behavior of the gas are briefly described in section 3.3.5.

Critical temperature and condensate fraction

In order to discuss the effects of repulsive interactions on the thermodynamic behavior of the gas, it is convenient to estimate the relevant energies of the system. The interaction energy of zero-temperature BEC in the Thomas-Fermi limit is given by $E_{\mathrm{int}}/N = (2/7)\,\mu$. By comparing the interaction energy or equivalently the chemical potential $\mu(T = 0)$ with the thermal energy $k_{\mathrm{B}}T$, one expects the interactions to be important if $k_{\mathrm{B}}T$ is smaller than $\mu(T = 0)$. If instead the thermal energy is larger than the chemical potential, interactions will provide only perturbative corrections. Note that for temperature above the critical temperature the interaction effects become much smaller as the condensate is absent and consequently the density in the central region of the trap is significantly lower [Pit03].

A useful parameter to estimate the interaction effects is the ratio $\eta = \mu(T = 0)/k_{\mathrm{B}}T_{\mathrm{c}}^0$ of the chemical potential μ calculated at $T = 0$ in the Thomas-Fermi approximation and the critical temperature T_{c}^0 for noninteracting particles in the same trap[3]. The ratio can be expressed by

$$\eta = \frac{\mu(T = 0)}{k_{\mathrm{B}}T_{\mathrm{c}}^0} \approx 1.57\left(N^{1/6}\frac{a}{a_{\mathrm{ho}}}\right)^{2/5} \approx 2.24(na^3)^{1/6}, \tag{2.24}$$

where n is the density at the center of the trap evaluated at $T = 0$. The power of $1/6$ entering the last relation leads to large values for η on the order of 1 even if the

[3]The Thomas-Fermi parameter Na/a_{ho} on the other hand expresses the value of the chemical potential in units of the harmonic oscillator energy.

gas parameter is very small. In our molecular BEC $\eta \approx 0.5 - 0.6$ [Joc04] and thus one expects that interaction effects are still visible for values of T on the order of T_c^0 [Pit03].

In a BEC with repulsive interactions the central density is lowered with respect to the noninteracting case and therefore one expects that the transition temperature is decreased with respect to the noninteracting case. However at the onset of Bose-Einstein condensation, the system is very dilute and consequently the corrections due to interactions are expected to be small.

By treating the interactions in a mean field approximation the shift of the critical temperature can be estimated. Using a theory where the motion of thermal atoms is described by a single particle Hamiltonian S. Giorgini *et al.* found for the temperature shift $\delta T_c = T_c - T_c^0$ [Gio96]

$$\frac{\delta T_c}{T_c^0} = -1.32 N^{1/6} \frac{a}{a_{ho}} = -0.43 \eta^{5/2}. \tag{2.25}$$

The shift is proportional to a and is, as expected, small for typical experimental parameters. Taking for example $\eta = 0.55$ the critical temperature is reduced by about 10%.

At temperatures below the transition temperature the effects of the interactions are expected to be larger. The calculation of the effects on the condensate fraction yield to lowest order in η [Nar98]

$$\frac{N_0}{N} = 1 - t^3 - \alpha \eta t^2 (1 - t^3)^{2/5}, \tag{2.26}$$

where $t = T/T_c^0$ and $\alpha = \zeta(2)/\zeta(3) \approx 1.37$ is a numerical factor. Assuming again $\eta = 0.55$ and $t = 0.5$, the number of atoms in the condensate is reduced by about 20% with respect to the ideal gas prediction (see equation 2.8).

2.2 Degenerate Fermi gases

For identical bosons a phase space density of about one marks the onset of the phase transition into a Bose-Einstein condensate as explained in the previous section. This macroscopic occupation of the lowest ground state is a direct consequence of Bose statistics for particles with a symmetric wave function. Unlike bosons, the wave function of fermions has an odd symmetry, which prevents the occupation of one single particle state by more than one Fermion – a fact that is expressed by the well known Pauli-exclusion principle. Consequently at $T = 0$ fermions fill up all single particle states up to the maximum available energy – the so called Fermi energy E_F (see also figure 2.1 on page 18). The corresponding Fermi temperature $T_F = E_F/k_B$ is on the same order of magnitude as the critical temperature for a BEC and for temperatures $T < T_F$ the Fermi gas is said to be quantum degenerate. However in contrast to bosons,

the quantum degenerate state evolves smoothly from the non-degenerate Fermi gas and the system does not undergo any phase transition.

This section summarizes the properties of ultracold fermionic gases relevant for our experiments. A detailed description of noninteracting fermions in a harmonic trapping potential is found in D. Butts *et al.* [But97]. Their analysis is extended in the article of G. Bruun *et al.* to include the effects of interactions in the mean field approximation [Bru98]. The topic of fermionic quantum gases is also covered in the two textbooks [Pet02, Pit03].

2.2.1 Trapped atomic Fermi gases

In a gas of identical fermions, all in the same internal state, the Pauli exclusion principle requires that any single particle state is occupied by no more than one atom. The resulting kinetic energy is sometimes called the Fermi motion and gives a major contribution to the total energy of the system. Moreover at low temperature the dominant s-wave interactions are absent (see section 3.1.2) and the properties of the fermi gas can be obtained by treating it as noninteracting [But97]. This highlights the difference to the case of Bose-Einstein condensates, where in most cases the interaction term dominates the kinetic energy (see section 2.1.2).

Assuming a gas of N identical fermions the occupation probability $f(\epsilon)$ for a single particle state with energy ϵ is given by the Fermi-Dirac distribution

$$f(\epsilon) = \frac{1}{\exp\left[(\epsilon - \mu)/k_{\mathrm{B}}T\right] + 1}, \tag{2.27}$$

where the chemical potential μ is fixed by the normalization condition

$$N = \int g(\epsilon) f(\epsilon) d\epsilon. \tag{2.28}$$

As already mentioned, the density of states for a three-dimensional harmonic potential is given by $g(\epsilon) = \epsilon^2/2(\hbar\omega_{\mathrm{ho}})^3$.

An important quantity is the chemical potential at $T = 0$, which defines the energy of the highest occupied state. This value of the chemical potential is the Fermi energy $E_{\mathrm{F}} = \mu(T = 0)$ and the corresponding temperature is referred to as the Fermi temperature $T_{\mathrm{F}} = E_{\mathrm{F}}/k_{\mathrm{B}}$. The Fermi energy is obtained by integrating equation 2.28 at $T = 0$, resulting in

$$E_{\mathrm{F}} = \hbar\omega_{\mathrm{ho}}(6N)^{1/3}. \tag{2.29}$$

Thomas-Fermi approximation

To obtain the density distribution the semiclassical local density approximation, that consists of labelling each state by a position $\mathbf{r}$ and a wave vector $\mathbf{k}$ is used. According to this approximation the properties of the gas at a point $\mathbf{r}$ are assumed to be those of

a uniform gas having a density equal to the local density $n(\mathbf{r})$. In general, the validity of the local density approximation requires that the thermal energy is much larger than the level spacing of the harmonic trapping potential. For fermions at low temperature this condition is fulfilled due to the Pauli principle. On the other hand, degenerate bosons with repulsive interactions satisfy this conditions due to strong correlation in the condensate. In both cases the zero-temperature semiclassical approximation for dilute gases is usually referred to as the Thomas-Fermi approximation.

Due to the Pauli exclusion principle, a volume $d\mathbf{r}d\mathbf{k}$ in phase space can accommodate only $d\mathbf{r}d\mathbf{k}/(2\pi)^3$ fermions. Hence at $T = 0$ and a given local density $n(\mathbf{r})$, the particles will have wave numbers within the interval $0 \leq k \leq k_{\mathrm{F}}(\mathbf{r})$, where

$$\frac{4}{3}\pi k_{\mathrm{F}}^3(\mathbf{r}) = (2\pi)^3 n(\mathbf{r}). \tag{2.30}$$

At a given position $\mathbf{r}$ the most energetic particles have an energy equal to the local Fermi energy $\hbar^2 k_{\mathrm{F}}^2(\mathbf{r})/2m$ plus the energy of the position dependent potential $V(\mathbf{r})$. Assuming equilibrium implies that the energy required to add a particle at any point inside the cloud is the same, i.e.

$$\frac{\hbar^2 k_F^2(\mathbf{r})}{2m} + V(\mathbf{r}) = E_{\mathrm{F}}. \tag{2.31}$$

In combination with equation 2.30, the spatial density profile of a noninteracting Fermi gas in the Thomas-Fermi limit can be written as [Møl98]

$$n(\mathbf{r}) = \frac{1}{6\pi^2}\left[\frac{2m}{\hbar^2}\left(E_{\mathrm{F}} - V(\mathbf{r})\right)\right]^{3/2} \tag{2.32}$$

for $V(\mathbf{r}) < E_{\mathrm{F}}$ and zero otherwise.

The boundary of the cloud at $T = 0$ is defined by $V(\mathbf{r}) = E_{\mathrm{F}}$. Therefore the characteristic size of the trapped Fermi gas is given by the turning point of a classical particle with total energy E_{F} in the trapping potential. In case of a harmonic potential with trap frequencies ω_i along the three directions $i = x, y, z$ one finds

$$E_{\mathrm{F}} = \frac{1}{2}m\omega_x^2 R_x^2 = \frac{1}{2}m\omega_y^2 R_y^2 = \frac{1}{2}m\omega_z^2 R_z^2. \tag{2.33}$$

Inserting the relation for the Fermi energy given in equation 2.29 the characteristic size of the Fermi gas is

$$R_i = a_{\mathrm{ho}}(48N)^{1/6}\frac{\omega_{\mathrm{ho}}}{\omega_i}. \tag{2.34}$$

Thus for an axially symmetric trap with trapping frequencies $\omega_\perp$ and $\omega_\parallel$ along the radial R and axial Z directions the density distribution is found to be

$$n(\mathbf{r}) = \frac{8}{\pi^2}\frac{N}{R^2 Z}\left(1 - \frac{r^2}{R^2} - \frac{z^2}{Z^2}\right)^{3/2}. \tag{2.35}$$

The corresponding momentum distribution can be derived in the same way as equations 2.32 and 2.35 were derived. The width of the momentum distribution is fixed by the maximum occupied Fermi wave number $k_\mathrm{F} = \sqrt{2mE_\mathrm{F}/\hbar^2}$ or

$$k_\mathrm{F} = (48N)^{1/6}/a_\mathrm{ho}, \tag{2.36}$$

and the momentum distribution is given by

$$n(\mathbf{k}) = \frac{8}{\pi^2}\frac{N}{k_F^3}\left(1 - \frac{k^2}{k_F^2}\right)^{3/2}. \tag{2.37}$$

Equation 2.30 shows that the maximum wave number k_F is on the order of the inverse interparticle separation.

Comparison with a BEC in the Thomas-Fermi limit

It is worth comparing the above results for the density and momentum distribution of an ideal Fermi gas at $T = 0$ with the corresponding distributions for an interacting, zero-temperature BEC in the Thomas-Fermi limit.

The shape of the density profiles in coordinate space are very similar. However, the characteristic radius of a Fermi gas scales more slowly on the atom number ($\propto N^{1/6}$) compared to the Thomas-Fermi radius of the BEC ($\propto N^{1/5}$). In a similar way the Fermi energy scales as $N^{1/3}$ while the zero-temperature chemical potential of a BEC varies more rapidly ($\mu \propto N^{2/5}$). Nevertheless the physical origin of the chemical potential is in both cases very different. For bosons it is fixed by the interactions of the atoms while for fermions it is given by the Pauli exclusion principle. For typical experimental parameters ($Na_\mathrm{ho}/a \gg 1$) the radius of a cloud of fermions is generally a few times larger than the Thomas-Fermi radius of a BEC with the same number of particles. This effect of the Fermi pressure has been observed in two elegant experiments [Tru01, Sch01].

In momentum space the distributions differ significantly. For a gas of noninteracting fermions the velocity distribution is isotropic independent of the trapping potential (see equation 2.37). For an interacting BEC the momentum distribution is the square of the fourier transform of $\sqrt{n(\mathbf{r})}$, which is anisotropic in an asymmetric trap [Bay96]. Furthermore the momentum width of a trapped BEC scales as $\hbar/R$ and consequently decreases with increasing N, while in a trapped Fermi gas the momentum width is given by $m\omega_\mathrm{ho}R$ and increases with increasing N.

Role of interactions

For an ultracold spin-polarized Fermi gas of identical particles, the ideal gas model presented in the previous section provides a very good approximation. In such a cold gas the particles interact only via s-wave collisions (see also section 3.1) and for identical fermions these collisions are forbidden due to the Pauli exclusion principle. In

the presence of a spin mixture this is no longer the case. Here two-body interactions may become important and lead to a modification of the above model [Bru98].

Consider a gas of N fermionic atoms in two different spin states, hereafter called 1 and 2. Assuming an equal number of atoms per spin state ($N_1 = N_2 = N/2$) and equal densities ($n_1 = n_2 = n/2$), the relevance of interactions can be estimated by comparing the mean field interaction energy $E_{\mathrm{int}} = (g/4)\int n^2(\mathbf{r})d\mathbf{r}$ with the oscillator energy $E_{\mathrm{ho}} = \int V(\mathbf{r})n(\mathbf{r})d\mathbf{r}$. Approximating the density distribution $n(\mathbf{r})$ with the Thomas-Fermi distribution of a noninteracting Fermi gas (see equation 2.35) one finds [Vic99]

$$\frac{E_{\mathrm{int}}}{E_{\mathrm{ho}}} \approx 0.5N^{1/6}\frac{a}{a_{\mathrm{ho}}} \approx 0.3k_{\mathrm{F}}a, \tag{2.38}$$

where $k_F = (24N)^{1/6}/a_{\mathrm{ho}}$ is the peak Fermi wave number of the harmonically trapped spin mixture.

As noted already the value of k_{F}^{-1} is on the order of the mean interparticle spacing. In a dilute gas the interatomic distance is much larger than the scattering length, leading to a small value of the interaction parameter $k_{\mathrm{F}}a$. Therefore it is expected that particle interactions have only little effect on the thermodynamics of a trapped Fermi gas unless the scattering length is very large. However interactions are crucial for a Fermi gas to undergo a phase transition into a superfluid phase as described in the next section.

2.2.2 BCS phase transition

When a Fermi gas is cooled to temperatures below the Fermi temperature T_{F}, the system gradually evolves into a degenerate quantum gas. In contrast to a bosonic gas, the quantum degenerate state is reached without passing through any phase transition.

At temperatures much below the degeneracy temperature T_{F}, a Fermi gas with attractive interactions, however, can undergo a phase transition into a superfluid state. This phase transition is similar to the phase transition in a solid when it becomes superconducting due to the pairing of the electrons. This effect was first explained by the ground-breaking BCS theory of Bardeen, Cooper and Schrieffer [Bar57]. A good introduction to the theoretical concept of the BCS theory is found in the textbook of Tinkham [Tin66].

The BCS theory shows that in a degenerate Fermi gas, two fermions with opposite spin and momentum can be coupled by an effective attractive interaction to form a bound state of delocalized, composite particles. Being composed of two fermions, these Cooper pairs [Coo56] obey Bose-Einstein statistics and can undergo Bose-Einstein condensation. It should be noted, that in the traditional BCS theory, the formation of the Cooper pairs and the condensation process are not two independent phenomena but rather occur simultaneously. In the following a brief summary of the most relevant results of the BCS formalism for a uniform dilute Fermi gas is given.

As a consequence of the pairing mechanism a gap occurs in the excitation spectrum of the superfluid state. For a uniform Fermi gas at zero-temperature, that interacts with

attractive s-wave interactions, the pairing gap is found to be [Gor61]

$$\Delta = \left(\frac{2}{e}\right)^{7/3} E_\mathrm{F} \exp\left(-\frac{\pi}{2k_\mathrm{F}|a|}\right) \approx 0.49 E_\mathrm{F} \exp\left(-\frac{\pi}{2k_\mathrm{F}|a|}\right). \tag{2.39}$$

The critical temperature T_c for the transition from the normal to the superfluid phase is directly related to the value of the zero-temperature value of the gap and is given by [Gor61]

$$k_\mathrm{B} T_\mathrm{c} = \frac{e^C}{\pi}\left(\frac{2}{e}\right)^{7/3} E_\mathrm{F} \exp\left(-\frac{\pi}{2k_\mathrm{F}|a|}\right) = 0.28 E_\mathrm{F} \exp\left(-\frac{\pi}{2k_\mathrm{F}|a|}\right), \tag{2.40}$$

where C is Euler' s constant ($C \approx 0.577$). The result shows that due to an exponential factor the critical temperature in a dilute gas ($k_\mathrm{F}|a| \ll 1$) is much smaller than the Fermi energy.

Note that due to the inclusion of induced interactions by L. Gorkov *et al.* [Gor61] the result for the gap (see equation 2.39) is reduced by a factor of ~2.2 with respect to the standard BCS result $\Delta = 8e^{-2} E_\mathrm{F} \exp(-\pi/2k_\mathrm{F}|a|)$. Nevertheless both calculations predict the same proportionality constant between the gap and the critical temperature for the phase transition $k_\mathrm{B} T_\mathrm{c} = e^C \Delta/\pi \approx 0.567\Delta$.

The size χ_pair of the Cooper pairs can be shown to be essentially temperature independent and is approximately given by [Tin66, Hou97]

$$\chi_\mathrm{pair} \approx \frac{\hbar v_\mathrm{F}}{\Delta}, \tag{2.41}$$

where $v_\mathrm{F} = \hbar k_\mathrm{F}/m$ is the Fermi velocity corresponding to the Fermi energy. In a dilute Fermi gas the size of the Cooper pairs is much larger than the average particle spacing ($\chi_\mathrm{pair} \gg 1/k_\mathrm{F}$), which leads to the strong correlations in the superfluid phase.

To evaluate the critical temperature in the case of a harmonic trapping potential it is convenient to apply the local density approximation [Hou97]. This requires that the correlation length is much smaller than the length scale over which the density changes, i.e. $\chi_\mathrm{pair} \ll R$. From equation 2.41 and equation 2.33 one finds that this condition is equivalent to the requirement that the gap has to be larger than the oscillator energy ($\Delta \gg \hbar\omega_\mathrm{ho}$).

An estimate of the transition temperature for typical parameters used in our experiment can be obtained from the useful relation $k_\mathrm{F} a = 1.70 N^{1/6} a/a_\mathrm{ho}$, which is valid for a two component spin mixture of N atoms ($N_1 = N_2 = N/2$). Assuming a total number of $N = 4 \times 10^5$ atoms, a scattering length of $a = -2140\, a_0$ and a trap with a harmonic oscillator length of $a_\mathrm{ho} = 2.5\,\mu$m results in $k_\mathrm{F} a \approx -0.66$ and a transition temperature of $T_\mathrm{c}/T_\mathrm{F} \approx 0.026$. It should be noted, that this result is only a rough estimate because the expression for the critical temperature is only correct in the limit of $k_\mathrm{F}|a| \ll 1$ as BCS theory was used in the derivation. In the BCS limit however, the predicted critical temperature is much smaller than the Fermi energy. Assuming for example $k_\mathrm{F} a = -0.1$ results in a transition temperature of $T_\mathrm{c}/T_\mathrm{F} \approx 4 \times 10^{-8}$, which is far below the temperatures obtained in current experiments with ultracold Fermi gases.

Nevertheless it can be shown that the result for the transition temperature is accurate to 30% for $k_F|a| = 1/2$ and $\Delta \approx 2\hbar\omega_{ho}$ [Car04].

2.2.3 Universal Fermi gas and resonance superfluidity

In the vicinity of a Feshbach resonance the scattering length can become arbitrarily large, exceeding the characteristic range of the scattering potential ($|a| \gg r_c$). In this case three density regimes have to be distinguished, namely the low density (or dilute) regime ($k_F^{-1} \gg |a|$), the high density ($k_F^{-1} \leq r_c$), and the intermediate regime ($r_c \leq k_F^{-1} \leq |a|$). The later regime is realized in our experiments and is considered in the following discussion.

On resonance the scattering length a diverges and the scattering cross section reaches the unitarity limit with a maximum cross section given by $4\pi/k^2$, where k is the relative wave number of the two scattering atoms (see also section 3.1.3). In this limit the scattering length a is no longer a relevant length scale and the thermodynamic properties of the gas are expected to depend only on the temperature and the density [Hei01, Ho04c, Car03, Ho04b]. Because the properties of the gas become independent of the specific details of the interaction, the gas is said to be universal. A recent discussion of the condition for universality at Feshbach resonance is found in [Die04] and references therein.

In a universal quantum gas the only relevant length scale is the interparticle spacing given by $n^{-1/3}$ and the relevant energy scale is the Fermi energy [Ho04b]. Therefore the effective mean field potential, the collision rate, the superfluid transition temperature (see next paragraph) and the associated pairing gap of the gas are expected to become proportional to the Fermi energy with different proportionality constants [Hei01].

In the following a simple heuristic description of a universal gas is given [O'H02a, Geh03b]. Two-body interactions give rise to a mean field potential U_{MF} which in a two-component Fermi gas of equal density $n/2$ is given by

$$U_{MF} = \frac{4\pi\hbar^2 a_{eff}}{m}\frac{n}{2}, \tag{2.42}$$

where $a_{eff} = a/(1 + k^2a^2)$ is the effective scattering length (see section 3.1.3). In the weakly interacting case ($k_F a \ll 1$) the effective scattering length is energy independent and equal to the scattering length a. At intermediate densities ($r_c \ll k_F^{-1} \ll |a|$) obtained in the vicinity of a Feshbach resonance, the effective scattering length is unitarity limited to $|a_{eff}| \approx 1/k_F$ [Geh03b]. Further employing the relation $n \propto k_F^3$ the mean field potential can then be written as

$$U_{MF} = \beta E_F, \tag{2.43}$$

where β is a universal scaling parameter.

The equation of state for a uniform interacting Fermi gas is given by [Geh03b, Men02]

$$\mu = E_F + U_{MF} \tag{2.44}$$

This reveals that on resonance, where $U_{\mathrm{MF}} = \beta E_{\mathrm{F}}$, the equation of state no longer depends on the value of the scattering length nor on its sign. Here the equation of state becomes proportional to one of an ideal Fermi gas

$$\mu = (1+\beta)\frac{\hbar^2}{2m}(3\pi^2 n)^{2/3}, \tag{2.45}$$

with the characteristic density dependence of $n^{2/3}$. For a trapped Fermi gas at zero temperature it can be shown that the mean field in the unitarity limited region scales the Fermi energy of the trapped cloud without changing the shape from a Thomas-Fermi distribution [O'H02a, Geh03b]. This fact allows us to determine the universal parameter β from in situ images of our molecular BEC in the unitarity limit as described in section 6.1.2.

Detailed calculations by H. Heiselberg [Hei01] using a self-consistent many-body approach, show that the universal parameter β is independent of the sign and magnitude of $k_{\mathrm{F}}a$. Employing a Wigner-Seitz cell approximation H. Heiselberg predicts $\beta = -0.33$ while he obtains $\beta = -0.67$ from the Galitskii integral equations [Hei01]. G. Baker obtains $\beta = -0.43$ and $\beta = -0.67$ from two different Padé approximations of the ladder series for the energy [Bak99]. Using effective field theory Steel yields $\beta = -0.56$ [Ste00]. A similar result of $\beta = -0.545$ is obtained from the BEC-BCS crossover theory [Per04b]. From a Monte Carlo calculation with ~40 particles J. Carlson *et al.* find $\beta = -0.56(1)$ [Car03], in agreement with results from similar Monte Carlo calculations by G. Astrakharchik *et al.* covering the hole BEC-BCS crossover, which yield $\beta = -0.58(1)$ [Ast04].

These theoretically predicted values for β, as well as measured values [Bar04b, Bou04, Kin05], yield consistently values larger than -1. This means that the attractive mean field never exceeds the repulsive Fermi pressure and the two component interacting Fermi gas is mechanically stable even at the Feshbach resonance [Geh03b]. This is an important requirement toward the production of a fermionic superfluid in the vicinity of a Feshbach resonance (see below).

It should be noted that the universality hypothesis[4] does not depend on the statistics of the particles. Thus also a Bose gas in the unitarity limit, if stable, is predicted to have a fermionic energy density [Cow02, Ho04b].

Large and negative scattering lengths are of particular interest for the investigation of the phase transition into a superfluid Fermi gas. Because the transition temperature depends exponentially on the scattering length (see equation 2.40) an arbitrarily large a should in principle result in a critical temperature on the order of the Fermi temperature.

However the situation poses a number of fundamental theoretical problems that must be addressed in order to provide an adequate description of the critical temperature. First of all the theory of a dilute gas is based on a perturbative approach that relies on the expansion of the small gas parameter $n|a|^3$. Formally, when the scattering

[4]The universal behavior has so far only been proven in the Boltzmann regime [Ho04c].

length is increased, the gas parameter $n|a|^3$ might become on the order of one, indicating the break down of the conventional perturbation theory. The theoretical description of such a strongly interacting Fermi gas would have to explicitly treat higher-order correlations.

Nevertheless it is possible to derive an effective mean field theory even in the direct vicinity of a Feshbach resonance, where the resonance occurs due to the coupling to a molecular state [Tim01, Hol01]. These resonance superfluidity theories explicitly treat the coupling between the atomic and molecular gases. The theories again replace the diluteness criterion ($k_F a \ll 1$) by the weaker condition that the characteristic range of the interparticle potential r_c is smaller than the interparticle spacing, i.e. $k_F r_c \ll 1$. A detailed description of the resonance superfluid theories is found in the article by S. Kokkelmans *et al.* [Kok02]. The current estimates for the transition temperature into the superfluid state range from about 0.5 to 0.2 T_F [Hol01, Mil02, Chi02, Oha02].

2.3 BEC - BCS crossover

As described in the previous sections, the behavior of a dilute gas of bosons and fermions is quite different when the phase space density becomes on the order of unity. While bosons undergo a phase transition into a superfluid state, fermions stack up in a Fermi sea.

However at even lower temperatures fermions interacting with attractive interactions can also undergo a phase transition into a superfluid state. The phase transition is predicted to occur even for very weak attractive interactions. In this weak coupling or BCS limit, fermions pair up into so-called Cooper pairs with a bosonic character and a size much larger than the interparticle spacing. In the other limit of strong coupling, paired fermions form localized bosons. Due to the strong coupling the size of the pairs can be neglected and the particles are described as point-like bosons, that can undergo Bose-Einstein condensation. The BEC and BCS limits are connected by a smooth BEC-BCS crossover that has been a subject of great theoretical interest for more than thirty years [Eag69, Leg80, Noz85]. For an introduction into the field the reader is referred to the review article by M. Randeria [Ran95] and the recent review article by Q. Chen *et al.* [Che04].

2.3.1 Early studies of the crossover

The first discussion of the possibility of a crossover from a BCS state to a BEC state was given by D. Eagles in the context of a theory of superconductivity in low carrier concentration systems [Eag69]. Later, A. Leggett [Leg80] studied a dilute gas at $T = 0$ and showed the existence of a smooth crossover from a BCS ground state, with Cooper pairs overlapping in real space, to a condensate of tightly bound diatomic molecules. In the following the model employed by A. Leggett is briefly described.

The model considers N fermions of mass m interacting via an attractive central potential $V(r)$ with finite range l_0. The parameters of $V(r)$ are chosen such that they are near the critical value for binding of a single two-particle state. As explained further in section 3.2 the scattering length a resonantly changes when the parameters of the potential are varied from just below the critical value for binding a two-particle-state to just above it. The model assumes that the parameters of the potential are varied around the critical value such that $|a| \gg l_0$. If one further assumes that the system is at intermediate densities ($k_\mathrm{F} l_0 \ll 1$), the properties of the system at $T = 0$ should be functions of the single dimensionless variable $k_\mathrm{F} a$ [Leg80]. This variable characterizes the coupling strength in the system. For $1/k_\mathrm{F} a \to -\infty$ the system is in the weak coupling BCS limit while for $1/k_\mathrm{F} a \to +\infty$ the strong coupling BEC limit is obtained.

Employing a $T = 0$ variational approach with the BCS wave function the self consistency conditions are given by the two equations which are referred to as the "gap" and "number" equation, respectively [Leg80, Che04]

$$\frac{m}{4\pi\hbar^2 a} = \sum_k \left[\frac{1}{2\epsilon_k} - \frac{1}{2E_k} \right] \tag{2.46}$$

$$n = 2 \sum_k \left[1 - \frac{\epsilon_k - \mu}{E_k} \right], \tag{2.47}$$

where $E_k = \sqrt{(\epsilon_k - \mu)^2 + \Delta^2}$ and $\epsilon_k = \hbar^2 k^2 / 2m$ is the fermion energy dispersion. From these two equations the gap Δ and the chemical potential μ can be calculated as a function of the interaction strength.

In the limit of strong coupling ($1/k_\mathrm{F} a \to +\infty$) these equations describe the Bose-Einstein condensation of tightly bound diatomic molecules formed by two paired fermions. In this BEC limit of tightly bound molecules the chemical potential is negative and approaches $\mu = -E_\mathrm{b}/2$, where $E_\mathrm{b} = \hbar / m a^2$ is the binding energy. In this strong coupling limit the gap Δ approaches zero [Leg80].

The weak coupling limit ($1/k_\mathrm{F} a \to -\infty$) corresponds to the standard BCS result. In this regime the chemical potential is positive and given by the noninteracting Fermi energy, i.e. $\mu = E_\mathrm{F}$. For the gap one obtains the standard BCS result $\Delta = 8 e^{-2} E_\mathrm{F} \exp(-\pi / 2 k_\mathrm{F} |a|)$ [Leg80].

In the weak and the strong coupling limits the values of the chemical potential μ correspond to the energy required to extract one fermion from the Fermi sea and to extract one atom from a bound molecule, respectively.

It can be shown that the energy of a single particle excitation is given by the minimum of E_k [Leg80]. This minimum energy E_min or "energy gap" is a consequence of the pairing mechanism in the superfluid ground state and is given by

$$E_\mathrm{min} = \begin{cases} \Delta & \text{for } \mu > 0 \\ \sqrt{\mu^2 + \Delta^2} & \text{for } \mu < 0. \end{cases} \tag{2.48}$$

Thus in the BEC limit with $\Delta = 0$ one obtains $E_\mathrm{min} = |\mu| = E_\mathrm{b}/2$.

Smooth crossover

The Leggett model allows at least for a qualitative analysis of the system when the coupling strength is varied from the weak coupling BCS limit to the strong coupling BEC limit. One important question is, whether there is a phase transition while crossing from the weak coupling to the strong coupling limit. As already pointed out by A. Leggett [Leg80], the occurrence or non occurrence of the two-particle bound state has no significance on the many-body problem. Moreover, even at the point where $\mu = 0$ no singularity occurs [Ran95]. Nevertheless for $\mu > 0$ the system has a Fermi surface and is said to be "fermionic" while for $\mu < 0$ the Fermi surface is gone and the system is called "bosonic".

As noted in section 2.2.2, the size of the pairs in the BCS limit is much larger than the interparticle spacing, i.e $\chi_{\text{pair}} \approx \hbar v_F/\Delta \gg k_{\text{F}}^{-1}$. With increasing coupling strength the pair size decreases monotonically. In the BEC limit the size of tightly bound molecules is given by $\chi_{\text{pair}} \approx a$, which is much smaller than the mean interparticle separation k_{F}^{-1} [Ran95].

The smoothness of the crossover was further confirmed by P. Nozières and S. Schmitt-Rink [Noz85] who extended the previous models to finite temperature. Their studies showed that the transition temperature T_{c} for the phase transition into the superfluid phases evolves smoothly as a function of the attractive coupling from the BCS to the BEC limit (see also below).

2.3.2 Recent calculations

Quite generally, the theoretical approaches to study the BCS-BEC crossover rest on solving the two coupled equations for the order parameter Δ and the chemical potential μ. While the first theoretical studies of the BEC-BCS crossover at zero temperature are based on the mean field BCS equations more sophisticated approaches take into account the effects of fluctuations [Pie00, Pie04b] or include explicitly the bosonic molecular field [Hol01, Oha03].

The BEC-BCS crossover is theoretically compelling, because a small parameter is absent and approximations that are valid on one side of the crossover are not necessarily valid on the other side. In these strongly correlated systems quantum Monte Carlo techniques provide valuable information [Car03, Cha04, Ast04]. In particular the recent quantum Monte Carlo study of G. Astrakharchik *et al.* [Ast04] allowed the calculation of the equation of state in the BEC-BCS crossover and in the following a briefly report on the main findings is given.

In the strong coupling BEC region ($1/k_{\text{F}}a \gg 1$), the authors find a gas of molecules with mass $m_{\text{mol}} = 2m$, whose repulsive interactions are well described by the dimer-dimer scattering length $a_{\text{mol}} = 0.6a$. This relation between the molecular and atomic scattering length was previously calculated by D. Petrov *et al.* [Pet04]. The energy per particle in the molecular BEC region agrees with the equation of state of a homoge-

neous gas of bosonic molecules of density $n/2$

$$\frac{E}{N} - \frac{E_\mathrm{b}}{2} = E_\mathrm{F}\frac{1}{6\pi}k_\mathrm{F}a_\mathrm{mol}\left(1 + \frac{128}{15\sqrt{6\pi^3}}(k_\mathrm{F}a_\mathrm{mol})^{3/2} + \ldots\right), \tag{2.49}$$

which in the limit $1/k_\mathrm{F}a \to \infty$ approaches the binding energy per particle $E_\mathrm{b}/2$. The first term in the above equation corresponds to the mean field energy of the molecular gas and the second term corresponds to the first beyond mean-field correction [Lee57].

In the unitarity limit obtained at $1/k_\mathrm{F}a = 0$ the calculation yields

$$\frac{E}{N} = \xi\frac{3}{5}E_\mathrm{F}, \tag{2.50}$$

where $\xi = 0.42(1)$ which corresponds to $\beta = 1 - \xi = 0.58(1)$.

In the BCS region obtained for $1/k_\mathrm{F}a < -1$ the energy per particle agrees well with the perturbation expansion of a weakly attractive gas of fermions [Hua57]

$$\frac{E}{N} = E_\mathrm{F}\left(\frac{3}{5} + \frac{2}{3\pi}k_\mathrm{F}a + \frac{4(11 - 2\log 2)}{35\pi^2}(k_\mathrm{F}a)^2 + \ldots\right). \tag{2.51}$$

Superfluid transition temperature

In the weak coupling BCS limit, the pair formation and their condensation occurs at the same temperature T_c. With increasing attraction the pair formation temperature T^* and the condensation temperature T_c become more and more separated (see figure 2.2). In the intermediate coupling regime at temperatures below T^*, preformed pairs exist before superfluidity is reached. Reference [Sta04, Che04] further explains the role of these preformed pairs which lead to a so-called “pseudo gap” regime. In the strong coupling BEC limit one finds tightly bound pairs with binding energy E_b. Here the pair formation sets in at a temperature T^* on the order of E_b/k_B which is much larger than the critical temperature T_c for the phase transition into the superfluid condensate.

Comparing the dependence of the transition temperature T_c on the coupling strength shows further differences in the two limiting cases. In the weak coupling BCS limit $k_\mathrm{B}T_\mathrm{c} = e^C\Delta/\pi$ and thus T_c strongly depends on the coupling strength. However, in the BEC limit the transition temperature is independent of the coupling strength and approaches $T_\mathrm{c} = 0.518T_\mathrm{F}$ in a trapped gas [Oha03].

It should be stressed again that even though the weak and strong coupling limits appear to be very different at first sight, there is no phase transition as a function of coupling strength predicted [Ran95].

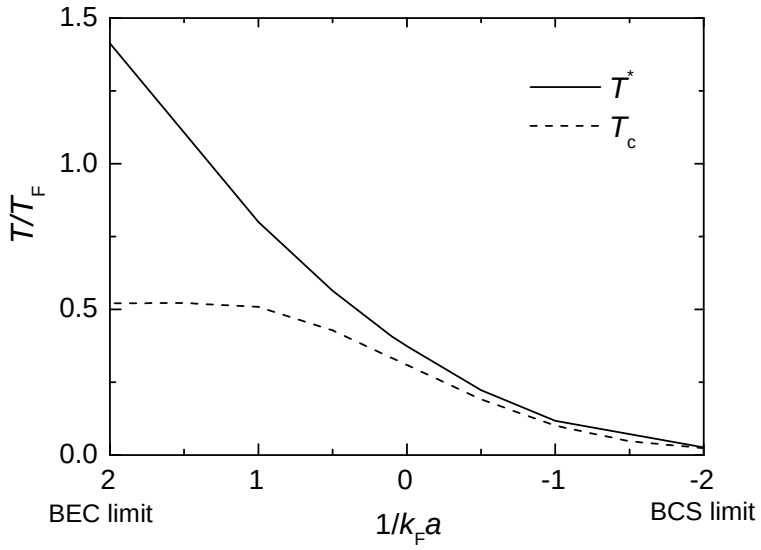

Figure 2.2: Phase diagram for a trapped gas in the BEC-BCS crossover. Shown is the pair breaking temperature T^* and the critical temperature T_c for the transition into the superfluid phase as a function of the coupling strength. Each temperature is normalized to the Fermi temperature T_F. The weak coupling BCS limit is realized for $1/k_F a \to -\infty$. Here the pair formation and the condensation occur at the same temperature. In the BEC limit ($1/k_F a \to +\infty$) the pair formation and their condensation are two independent processes with widely separated energy scales (data courtesy from [Per04a]).

Chapter 3

Collisions and collective dynamics in ultracold gases

Collisions govern the properties of ultracold gases and play a key role in our experiment. By exploiting a magnetically tunable scattering resonance in ^{6}Li , we are able to continuously tune the molecular energy level structure relative to the scattering continuum, thereby varying the interatomic interactions in a large range from effectively repulsive to attractive.

The tunability of the interatomic interactions offers great prospects. A large collision rate ensures fast thermalization of the sample and therefore a very efficient evaporative cooling process. In the past years the focus in the investigation of ultracold fermionic gases has been directed to the observation of the superfluid phase. In the BCS regime the temperature of the phase transition depends exponentially on the interaction strength and the tunability of the scattering length offers great prospects in the investigation of these highly correlated systems. This was first highlighted in the observation of a strongly interacting Fermi gas in the group of J. Thomas [O'H02a].

Besides the tunability of the scattering properties in the quantum gas, Feshbach resonances have far more to offer. The presence of the weakly bound molecular state enables the creation of weakly bound molecules, which was first demonstrated in the group of C. Wieman in a ^{85}Rb BEC [Don02]. In the group of D. Jin the next big step was made by coupling two fermionic ^{40}K atoms to a bosonic molecule, thereby altering the quantum statistics of the system [Reg03b]. Thereafter the successful formation of ultracold molecules was reported from bosonic atoms [Her03, Dür04, Xu03] and fermionic ^{6}Li atoms [Cub03, Str03, Joc03b]. The collisional stability of both kinds of molecules, however, is strikingly different. While molecules formed from bosonic atoms show a very fast decay, the observed lifetime in dimers formed from fermionic atoms can be extraordinarily long. This large collisional stability is due to the Fermi statistics of the underlying atoms [Pet04] and in combination with the large elastic collision rate, paved the way to the successful evaporative cooling into a molecular Bose-Einstein condensate [Joc03a, Gre03, Zwi03, Bou04, Hul04].

By varying the coupling strength of these molecules it is possible to experimen-

tally investigate the crossover from a molecular BEC of tightly bound molecules to a Bardeen-Cooper-Schrieffer (BCS) state of overlapping, correlated pairs [Bar04b, Reg04b, Zwi04, Bou04, Kin04a, Bar04a, Chi04a, Gre04, Kin04b].

The experimental access to the BEC-BCS crossover in dilute gases offers great possibilities to test fundamental theoretical predictions. In particular there is a crossover from the equation of state of a dilute BEC to the one of a superfluid Fermi gas. As a general consequence of superfluidity the macroscopic dynamics of these highly correlated many-body systems is hydrodynamic. The first observation of hydrodynamic behavior in a strongly interacting Fermi gas was obtained by K. O'Hara *et al.* [O'H02a]. However, the observation of a hydrodynamic behavior is not a direct proof of superfluidity as hydrodynamic behavior is also expected for a gas in which the collision rates are sufficiently large. Nevertheless, the careful investigation of the hydrodynamic behavior can provide unique information on the underlying equation of state. For this purpose, a perfectly suited method is the investigation of the collective modes in the BEC-BCS crossover [Str04a, Hei04a, Hu04, Com04b, Com04a, Kim04b, Kim04a, Man04, Bul04]. The ability to experimentally measure the frequencies of the modes with high precision allows for the comparison with predictions from many-body theories beyond the mean field picture. Collective modes in the BEC-BCS crossover were investigated in [Kin04a, Kin04b] and in our group [Bar04a]. Our experimental results are presented in section 6.2.

This chapter is organized as follows: in the first part the basic concepts of interactions in ultracold gases are briefly summarized. The discussion starts with the description of the interatomic scattering potentials and their dependency on the individual spin state of the colliding atoms. This is followed by a summary of the basic ideas of the scattering theory. Of special interest for our experiments are the scattering properties at ultra low temperatures. Section 3.2 discusses Feshbach resonances in atomic gases and starts with the description of various scattering resonances to point out the key role played by a bound molecular level close to the scattering continuum. Afterwards the general concept of the magnetically tunable scattering resonances is presented, which is followed by a more detailed discussion of the broad Feshbach resonances that occur in ^{6}Li. Different schemes to create weakly bound molecules in the vicinity of the Feshbach resonance are presented in section 3.2.4. In addition the expected properties of these ultracold, diatomic molecules are briefly summarized.

The second part of this chapter is dedicated to the collective modes in ultracold trapped gases. The description starts with an introduction to the hydrodynamic equations that are expected to describe a gas in the BEC-BCS crossover. These dynamic equations allow the calculation of the collective mode frequencies for different trap geometries and are presented in section 3.3.2. The calculation of the modes in an elongated trap shows the sensitivity of their frequencies to the underlying equation of state, which makes them perfectly suited to investigate the BEC-BCS crossover. Section 3.3.3 describes the expected frequency and damping of these modes for a gas in the normal, non superfluid, state when the system changes from the hydrodynamic to a collisionless regime. In section 3.3.4 the influence of mean field corrections in Fermi

gases is discussed. As expected, these effects are small due to the Pauli exclusion principle, which reduces the density with respect to a BEC. On the other hand, strong interactions in a BEC can lead to corrections beyond the mean field description. The influence of these beyond mean field corrections to the collective modes is described in section 3.3.5. Finally, predictions for the collective mode frequency in the BEC-BCS crossover are briefly discussed in section 3.3.6.

3.1 Basic scattering theory

After introducing the characteristics of the interatomic scattering potentials, a brief reminder on the quantum mechanical scattering theory is given. As this topic is covered in many standard textbooks on quantum mechanics (see for example [Sak94]) this section only summarizes the main results that are relevant for our research.

The same restriction holds for the discussion of the scattering properties in ultracold gases. A very good introduction to the field of ultracold collisions is, for example, found in a review article by J. Weiner *et al.* [Wei99] and the lectures of J. Dalibard [Dal99b]. A more recent introduction covering the topics of Feshbach resonances and molecule formation can be found in a review article by K. Burnett *et al.* [Bur02].

3.1.1 Interatomic potentials

In the following, we consider the interatomic potential of two alkali atoms in their ground state. The individual atoms have an electronic spin of $S = 1/2$ and the electronic spin state of the pair of atoms can either be in a singlet or a triplet state. The relative orientation of the two spins significantly effects the interatomic potential as will be described below (see also figure 3.1).

At large interatomic distance r, the interaction potential is independent of the spin state and can be expressed in terms of inverse powers of r, i.e. $V(r) = -C_6 r^{-6} - C_8 r^{-8} + \cdots$. The leading term is the van der Waals interaction and arises from the interaction between the induced electric dipole moments. The next higher coefficient is due to the dipole-quadrupole interaction and can, as well as higher orders, be neglected at large interatomic distances. The van der Waals potential leads to a characteristic length scale [Wil99][1]

$$r_c = \frac{1}{2}\left(\frac{mC_6}{\hbar^2}\right)^{1/4}. \tag{3.1}$$

For ^{6}Li the C_6 coefficient has been calculated to be $C_6 = 1393.39(16)\,\text{au}$ [Yan96] ($1\,\text{au} = 9.57344 \times 10^{-26}\,\text{J nm}^6$), which leads to a characteristic range of $r_c = 31.25\,a_0$, where a_0 is the Bohr radius ($a_0 \approx 0.0529\,\text{nm}$).

[1] A discussion of several length scales relevant for an attractive C_6/r^6 potential is found in the appendix of this reference.

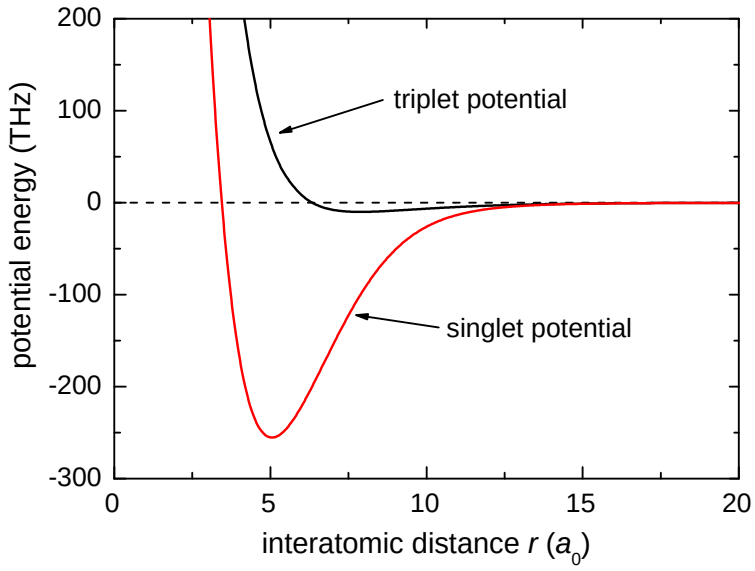

Figure 3.1: Potential energy of two colliding ^{6}Li atoms in a pure singlet and triplet state, respectively. The calculation of the potentials was performed in the group of Paul Julienne [Sim04].

When the atoms get close to each other, such that the electronic wave functions begin to overlap, the exchange term becomes dominant. The exchange term occurs due to the required antisymmetry of the electronic wave function and vanishes exponentially at large separation [Côt94]. In the case where the two colliding alkali atoms have their valence electrons in an antisymmetric spin state (singlet state), the electrons can occupy the same orbit and thus their probability to be between the two nuclei is non zero. This lowers the total energy, as the electrons shield the repulsive force of the two nuclei. The same effect is responsible for covalent bonding. However, if the two electrons are in a symmetric spin state (triplet state), their spin wave function is symmetric and thus the spatial wave function has to be antisymmetric. Here the probability for the two electrons to be between the two nucleons is zero and therefore the reduction of the energy due to the shielding is absent. Hence the singlet potential is generally much deeper than the triplet potential, although both potentials are deep enough to support many bound states. For example, in case of collisions in ^{6}Li the triplet and singlet potentials have 9 and 38 vibrational levels, respectively [Abr97]. Finally for very small distances the interactions are in both cases are dominated by a strong repulsive force due to the overlapping electron clouds (see also figure 3.1).

The interatomic potentials shown in figure 3.1 correspond to the purely singlet and triplet scattering potentials of two ^{6}Li atoms [Sim04]. The calculations have been fine adjusted by our radio-frequency spectroscopy measurements of weakly bound $^6Li_2$ dimers and are further described in section 6.3.2.

In most scattering processes, however, the valence electrons from each atom are coupled through the hyperfine interaction into a superposition of singlet and triplet

states and the scattering potential is neither described by the pure triplet nor by the singlet potential. In such a complex system quantitative results can only be obtained numerically. Nevertheless the outcome of such multi-channel calculations is often expressed in terms of these model potentials and their associated scattering lengths.

In case of fermionic ^{6}Li the scattering lengths of the singlet and triplet potentials are found to be $a_s = 45.167(8)\,a_0$ and $a_t = -2140(18)\,a_0$, respectively [Bar04c]. The large negative triplet scattering length results from a zero energy resonance (see section 3.2.1) and made ^{6}Li an early prime candidate to access the superfluid state in atomic Fermi gases [Sto96].

3.1.2 A brief reminder on scattering theory

The collisional dynamics of two colliding atoms are commonly described by considering the scattering of a particle with reduced mass $m_r = m/2$ in the potential $V(\mathbf{r})$. For neutral atoms in the ground state the interaction potential is spherical symmetric $V(\mathbf{r}) = V(r)$. This results in the stationary Schrödinger equation

$$\left(\frac{p^2}{2m_r} + V(r)\right)\psi_k(r) = E_k\psi_k(r) \tag{3.2}$$

for the effective particle with reduced mass and energy $E_k = \hbar^2k^2/2m_r$. The asymptotic solution is expected to be a superposition of the incident plane wave and a scattered wave function

$$\psi_k(r) \sim e^{ikz} + f(k,\theta)\frac{e^{ikz}}{r}. \tag{3.3}$$

The scattering amplitude $f(k,\theta)$ depends only on the energy of the colliding particles and the scattering angle θ, defined as the angle between the relative momentum before and after the scattering process. From the value of the scattering amplitude the differential scattering cross section can be determined by

$$\frac{d\sigma}{d\Omega} = |f(k,\theta)|^2. \tag{3.4}$$

To take advantage of the symmetry of the problem the incident and scattered wave function can be expanded in terms of Legendre polynominals. This partial wave expansion leads to a one dimensional Schrödinger equation for the unknown radial wave functions with an effective potential

$$V_{\text{eff}}(r) = \frac{\hbar^2 l(l+1)}{2m_r r^2} + V(r). \tag{3.5}$$

For partial waves with $l = 0$ the potential V_{eff} is simply the interatomic potential $V(r)$ (see previous section) while for all other partial waves a centrifugal barrier is added. This situation is illustrated in figure 3.2.

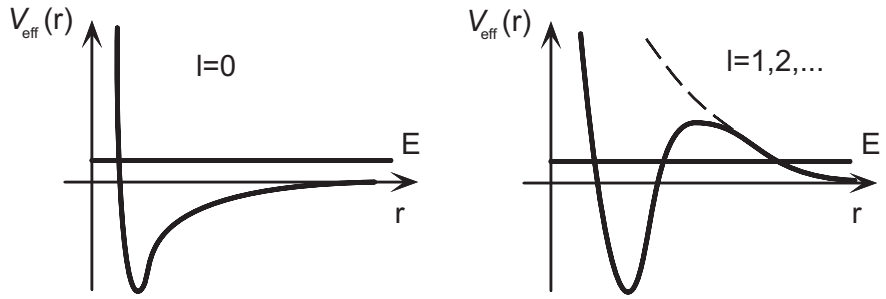

Figure 3.2: Schematic of the effective potential entering the radial Schrödinger equation for s-wave scattering (left) and scattering with partial waves $l > 0$ (right) where an additional centrifugal barrier (dashed line) proportional to $l(l+1)$ is added. For sufficient low collision energy E the barrier leads to a suppression of collisions with $l > 0$. (figure adapted from [Dal99b]).

The cross section for each partial wave l is found to be

$$\sigma_l(k) = \frac{4\pi}{k^2}(2l+1)\sin(\delta_l(k)), \tag{3.6}$$

where $\delta_l(k)$ is the phase shift that, in the limit of $k \to 0$ is found to be

$$\delta_l(k) \propto k^{2l+1} \text{ modulo } \pi. \tag{3.7}$$

Thus in the limit of low energy, the cross section of partial waves with $l \neq 0$ is given by $\sigma_l(k) \propto k^{4l}$ and goes to zero for $k \to 0$. Consequently at low energy only the partial wave with $l = 0$ contributes to the total cross section. This regime is called the s-wave limit and is characterized by an isotropic scattering amplitude. The corresponding scattering cross section is given by

$$\lim_{k\to 0} \sigma_{l=0}(k) = 4\pi a^2, \tag{3.8}$$

where the scattering length a is defined by

$$a = -\lim_{k\to 0} \frac{\tan\delta_0(k)}{k}. \tag{3.9}$$

That higher partial waves ($l > 0$) freeze out at sufficient low temperatures can also be qualitatively understood. For partial waves $l \neq 0$ the interacting atoms see in addition to the pure atomic potential $V(r)$ a centrifugal barrier with an hight proportional to l. In case of lithium the barrier for the $l = 1$ partial wave amounts to $\sim k_B \times 7\,\text{mK}$ [Jul92]. For sufficient small interaction energies the atoms are "reflected" at the barrier and do not get close enough to interact through the potential $V(r)$ (see figure 3.2, right).

In general the total cross section is given by the sum over all partial waves l, i.e. $\sigma(k) = \sum_{l=0}^{\infty} \sigma_l(k)$. Taking into account the symmetry constrains for bosons (fermions) the contributions of the even (odd) partial waves doubles while the odd (even) contributions cancels [Dal99b]. Consequently identical fermions do not interact at sufficient low temperatures as they scatter only through partial waves with $l = 1, 3, \ldots$ whose cross section tends to zero at low temperature. This suppression of elastic collisions hinders the evaporative cooling of a polarized fermionic gas to ultra low temperatures [DeM98]. To circumvent this limitation experimenters use Fermi gases consisting of a spin mixtures of different hyperfine states or employ sympathetic cooling by using a mixture of different atomic species. In contrast, the s-wave interaction for identical bosons is not suppressed at low temperatures and the total scattering cross section is given by $\sigma = 8\pi a^2$.

In our experiment a spin mixture of the two lowest hyperfine states of fermionic ^{6}Li is used and cooled by evaporation in an optical dipole trap (see chapter 5). The reached temperatures are well below 1 mK and therefore only s-wave interactions have to be taken into account. The scattering properties of such an ultracold dilute gas are described in the next section.

3.1.3 Interactions in ultracold dilute gases

In a dilute gas with a typical density of about $n = 10^{12}\,\mathrm{cm}^{-3}$ the mean interparticle separation is $n^{-1/3} \approx 1\,\mu\mathrm{m}$. In contrast the range of the interatomic potential r_c is typically on the order of some nm. This justifies the usage of the asymptotic expression for the wave function of the scattering state (see above) and shows that the dominant scattering processes are two-body interactions.

For a dilute gas in the s-wave limit, it is possible to show, that the macroscopic properties of the gas depend only on the s-wave scattering length and do not depend on the detailed form of the two-body interaction potential [Pit03]. This allows one to obtain a many-body formalism, where the microscopic potential is replaced by an effective short range potential that reproduces the correct scattering length.

The simplest interaction between two particles is the contact interaction. In this case, the relation between the s-wave scattering amplitude and the scattering length a is found to be [Dal99b]

$$f(k) = -\frac{a}{1 + ika}, \tag{3.10}$$

where k is the relative wave number of the colliding particles. The real part of $-f(k)$ is sometimes referred to as the effective scattering length, i.e. $a_\mathrm{eff} = a/(1 + k^2a^2)$ [Geh03b]. Using equation 3.4 the total cross section for elastic collisions of nonidentical particles is determined to be

$$\sigma(k) = \frac{4\pi a^2}{1 + k^2a^2}. \tag{3.11}$$

In the limit of weak interactions ($ka \ll 1$) the result reduces to the energy independent cross section $\sigma = 4\pi a^2$. In the strongly interacting case ($k|a| \gg 1$) the scattering cross

section is energy dependent and approaches the unitarity limited value of $\sigma(k) = 4\pi/k^2$. This maximum cross section is proportional to λ_{dB}^2.

A particle in medium of density n experiences an effective potential resulting from the scattering with all other particles. Assuming again contact interactions between the particles, the mean field potential is readily calculated to be [Joc04]

$$U_{\mathrm{MF}} = \frac{4\pi\hbar^2 an}{m} = gn, \tag{3.12}$$

where $g = 4\pi\hbar^2 a/m$ is the coupling constant[2]. For negative (positive) scattering length the atoms feel an effectively attractive (repulsive) potential where the strength of the interaction is determined by the magnitude of $|a|$.

3.2 Feshbach resonances and weakly bound molecules

A powerful tool to vary the interaction in an atomic gas are magnetically tunable scattering resonances. Originally formulated in the context of nuclear physics [Fes58], the possibility for using Feshbach resonances to manipulate interactions in atomic gases was pointed out by E. Tiesinga *et al.* [Tie93]. Feshbach resonances were first observed in a BEC by a dispersive variation of the scattering length by a factor of more than ten and enhanced inelastic processes [Ino98]. Thereafter they became a powerful tool to dramatically alter the properties in bosonic gases [Cor00, Don01, Don02, Kha02, Str02, Web03] and to tune the interaction strength in fermionic gases [O'H00, Die02, Joc02, O'H02b, O'H02a, Reg03a, Bou03].

Besides the ability to resonantly control the scattering properties of the gas, Feshbach resonances turned out to be perfectly suited to produce ultracold weakly bound molecules. The first direct observation of molecules formed from fermionic ^{40}K by adiabatically sweeping the magnetic field across the resonance was reported by the group of D. Jin [Reg03b]. Shortly after researchers around the world succeeded in the formation of ultracold molecules formed from bosonic Cesium [Her03], Rubidium [Dür04], Sodium [Xu03] and fermionic ^{6}Li atoms [Cub03, Str03, Joc03b]. The observed short lifetime of the molecules formed from bosonic samples inhibited so far their condensation. However the long lifetime observed for molecules made from fermionic atoms allowed for a successful Bose-Einstein condensation [Joc03a, Gre03, Zwi03, Bou04, Hul04]. Moreover the Feshbach resonance enables a continuous variation of the coupling strength in these molecular condensates from the strong coupling BEC limit towards the weak coupling BCS limit. In combination with the low temperature obtained in the molecular BEC, these systems therefore provide a perfect starting point to explore the BEC-BCS crossover in an atomic Fermi gas [Bar04b, Bou04, Reg04b, Zwi04, Kin04a, Bar04a, Chi04a, Gre04, Kin04b, Kin05].

[2]Note that for a Fermi gas with two spin components the density n refers to the density of each species.

3.2.1 Scattering resonances

The position of the last bound state in the scattering potential has generally a crucial effect on the scattering properties [Dal99b].

The strong modification of the scattering length due to small changes in the scattering potential are already visible if one considers the scattering at a simple square potential barrier (see for example [Dal99b]). Looking for solutions as a function of the potential depth, one finds a diverging scattering length exactly at a potential depth where a new bound state appears. The calculation shows that a weakly bound state just below the continuum gives rise to a large positive scattering length while a (virtual) bound state just above the continuum results in a large negative scattering length.

In the following a brief report on different scattering resonances related to the existence of a weakly bound (virtual) state is given. Here the discussion is restricted to the case that the bound state belongs to the scattering potential of the two colliding atoms. The more general case that the bound state and the scattering state belong to different interaction potentials is described in the next section and gives rise to Feshbach resonances.

Zero energy resonance

This type of resonances is found when a bound state of the interatomic scattering potential is close to the continuum. As mentioned above for the square well potential, a bound state just below threshold gives rise to a large positive scattering length while a virtual bound state just above threshold leads to a large negative scattering length.

Consider for example ^{6}Li. The asymptotic behavior of the scattering potential is given by the the van der Waals potential (see section 3.1.1) and allows to determine the average or "mean" scattering length [Gri93]

$$\bar{a} = \frac{\Gamma(3/4)}{\sqrt{2}\Gamma(1/4)} r_c \approx 0.956 r_c. \tag{3.13}$$

In case of ^{6}Li we find $\bar{a} = 29.9 a_0$. Because the van der Waals coefficient C_6 is independent of the hyperfine state, the mean scattering length for the singlet and triplet scattering potential is the same.

In contrast to this prediction from the asymptotic shape of the van der Waals potential, the triplet scattering length is found to be $a_t = -2140(18)\, a_0$ [Bar04c]. The reason for this extraordinary magnitude of the scattering length is found in the exact shape of the triplet scattering potential that gives rise to a virtual bound state just above continuum. If the potential would be less then 0.03% deeper the virtual state would become bound and the scattering length would change sign [Abr97].

The scattering length for the singlet potential instead amounts to $a_s = 45.167(8)\, a_0$ [Bar04c]. Here the estimation of $\bar{a}$ from the asymptotic behavior is in reasonable agreement with the exact value.

Shape resonances

To understand the basic concept of a shape resonance we consider a scattering processes that is in the low energy s-wave limit. In this case the effective potential for partial waves with $l \neq 0$ is a combination of the attractive van der Waals potential and a centrifugal barrier as shown in figure 3.2 (right). This effective potential can confine quasi-bound states that can decay via tunnelling through the barrier. A shape resonance occurs when the incident energy E of the scattering state matches the energy of such a quasi-bound state. For fermionic atoms a p-wave shape resonance was observed in ultracold ^{40}K [DeM99a].

3.2.2 Magnetically tunable Feshbach resonances

In the scattering resonance considered in subsection 3.2.1 the bound state and the scattering state belonged to the same internal state of the colliding atoms. In a Feshbach resonance however, the continuum state and the bound state belong to different internal states, corresponding to different spin configurations of the two colliding atoms.

A scattering channel is characterized by the internal spin configuration of the two atoms at infinite distances. In ^{6}Li with a nucleus spin of $I = 1$ and an electronic spin of $S = 1/2$, the hyperfine interaction gives rise to six internal spin states. In an external magnetic field these states split and can be denoted in order of increasing energy by $|1\rangle - |6\rangle$ (see also appendix A). In the following the scattering state of one atom in state $|a\rangle$ and one in state $|b\rangle$ is denoted by (a, b). A scattering channel is said to be open (closed), if its energy at large interatomic distances is smaller (larger) than the total energy of the two colliding atoms.

In a multichannel scattering process the incoming (open) channel may be coupled during the collision to other open or closed channels. Since the two coupled channels correspond to two different internal atomic states, they can respond in a different way to external electro-magnetic fields. Provide the open and closed channel have different magnetic moments, the relative energy ΔE of the two states can be tuned by changing an external magnetic field ($\Delta E = \Delta\mu \times B$).

A Feshbach resonance occurs when the energy of a bound state in the closed channel coincides with the energy of the incoming channel [Fes58]. The coupling between the open and the closed channels gives rise to the resonant interaction. In experiments with cold atoms the coupling of the different channels is due to the hyperfine interaction. The physical picture of a Feshbach resonance is the following (see also figure 3.3). Due to coupling between the closed and the open channel, the effective scattering potential of the two colliding atoms is slightly modified. Just below resonance it provides a new bound state giving rise to a large positive scattering length. By changing the magnetic field B this weakly bound state can be tuned across threshold. At threshold ($B = B_0$) the scattering length approaches infinity. For fields above the resonance ($B > B_0$) the presence of the virtual bound state leads to a large negative scattering length. With increasing field this state is tuned further away from the continuum and

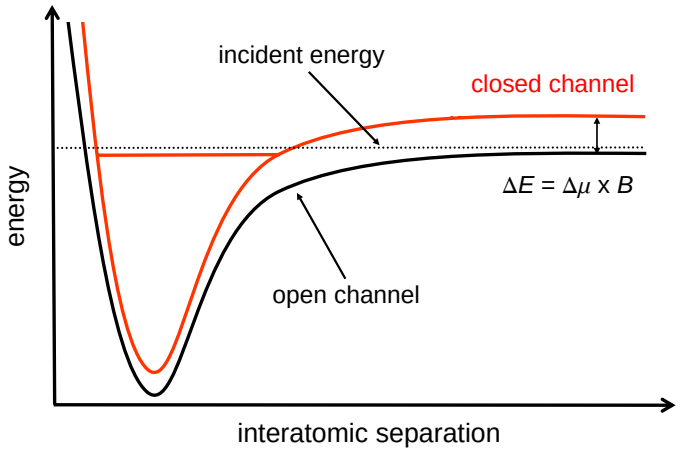

Figure 3.3: Schematic of a Feshbach resonance: the scattering length is resonantly altered if the energy of a bound state of a closed channel matches the energy of the initial scattering channel. Provide the two channel have a different magnetic moment the relative energy and hence the scattering properties can be tuned by simply changing an external magnetic field.

the scattering length approaches its original value a_{bg}, which characterizes the scattering potential in the absence of the coupling to the closed channel. The resulting scattering length can be written in terms of the background scattering length a_{bg} and the magnetic field of the resonance position B_0 as [Moe95]

$$a = a_{\mathrm{bg}}\left(1 + \frac{\Delta B}{B - B_0}\right). \tag{3.14}$$

The width of the resonance ΔB depends on the magnetic moments of the states and the coupling between the channels and characterizes the range of magnetic fields over which the resonance significantly affects the scattering length.

The possibility to vary the energy of a weakly bound molecular state and thereby resonantly tune the scattering properties makes Feshbach resonances a very powerful tool in exploring the properties of ultracold atomic gases and the creation of weakly bound molecules. In the next section the description of Feshbach resonances is focused on different ^{6}Li spin mixtures.

3.2.3 Feshbach resonance in ^{6}Li

Feshbach resonances in fermionic spin mixtures are of great interest as a large scattering length allows the investigation of strongly interacting Fermi gases. Of particular interest is the ability to obtain large negative scattering length, which is favorable for the experimental realization of a fermionic superfluid [Sto96, Hou97, Bar98, Com99, Tim01, Hol01, Hof02, Mil02, Kok02, Chi02, Oha02].

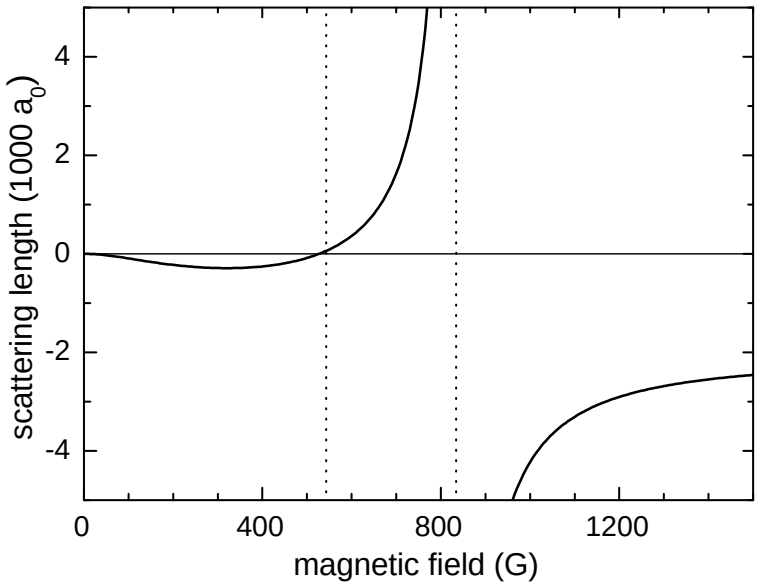

Figure 3.4: Magnetic field dependent scattering length for ^{6}Li atoms colliding in the (1,2) scattering channel [Bar04c]. The vertical dotted lines mark the position of the narrow and the broad Feshbach resonance at magnetic fields of about 543 G and 834 G, respectively.

Feshbach resonances in the (1,2) channel

In figure 3.4 we show the magnetic field dependence of the scattering length for a spin mixture of ^{6}Li atoms in the two lowest hyperfine states $|1\rangle$ and $|2\rangle$. The calculation of the scattering length is based on the best knowledge of the cold collision parameters of ^{6}Li [Bar04c] (see also section 6.3.2). The figure shows in addition to a broad Feshbach resonance at a magnetic field of 834.1(1.5) G a small Feshbach resonance at about 543 G.

The broad Feshbach resonance was first predicted by M. Houbiers *et al.* from full coupled channel calculations [Hou98]. At large magnetic fields the (1,2) scattering channel is an almost pure triplet state with a small singlet admixture and the resonance is due to the coupling with the most weakly bound vibrational level ($\nu = 38$) of the singlet potential [Hou98]. The narrow resonance arises due to the coupling of the scattering state with a different hyperfine component of the same weakly bound singlet state [O'H02b] and was first observed in [Die02].

The description of the molecular state at large magnetic field is most conveniently done in the basis of the quantum numbers for the total electronic spin $\mathbf{S} = \mathbf{S}_1 + \mathbf{S}_2$, the total nuclear spin $\mathbf{I} = \mathbf{I}_1 + \mathbf{I}_2$ and the orbital angular momentum $\mathbf{L}$. As already mentioned, at zero magnetic field the molecules belong to the singlet potential with a spin quantum number $S = 0$. In our s-wave Feshbach resonance[3] the quantum number of the angular momentum is $L = 0$. The nuclear spin of the two ^{6}Li atoms

[3]Feshbach resonances involving higher partial waves have been observed in ultracold fermionic gases [Reg03c, Zha04, Sch04].

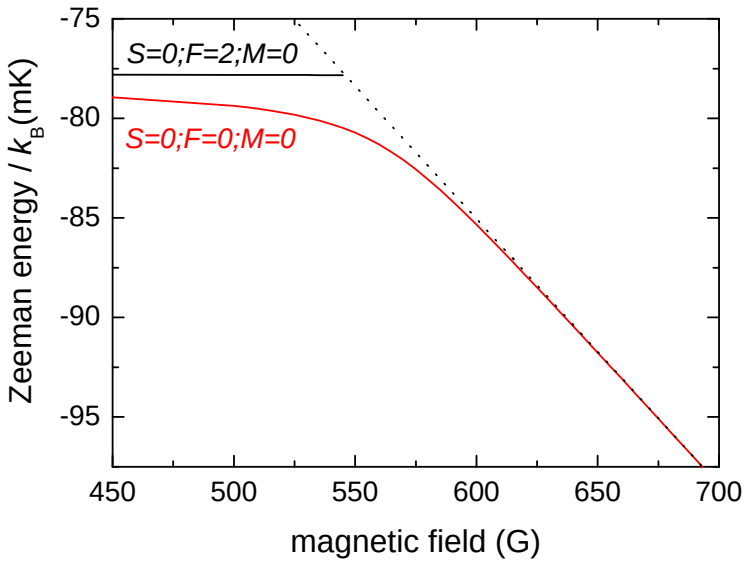

Figure 3.5: Energy structure of atoms in the scattering channel (1,2) (dotted line) and molecular states (solid lines). The molecular state of the singlet potential splits due to the hyperfine interaction into two states $F = 2, M_F = 0$ and $F = 0, M_F = 0$ giving rise to the two Feshbach resonances at magnetic fields of 543 and 834 G, respectively.

can in principle add up to the nuclear quantum numbers $I = 0, 1, 2$. Due to symmetry considerations the total wave function has to be antisymmetric with respect to the exchange of the two atoms and therefore the molecular states has to be $I = 0$ or $I = 2$. Hence the two Feshbach resonances at 543 G and 834 G are due to the coupling of the (1,2) scattering channel with the two molecular hyperfine states characterized by a total angular momentum $F = 2, M_F = 0$ and $F = 0, M_F = 0$, respectively.

The magnetic field dependent energy structure of the two molecular states with $F = 2, M_F = 0$ and $F = 0, M_F = 0$ is shown in figure 3.5 together with the Zeeman energy of the free atoms in the scattering channel (1,2). The unperturbed molecular state $F = 2, M_F = 0$ corresponds to a nearly pure singlet potential that is characterized by a vanishing magnetic moment. Consequently the molecular state shows no magnetic field dependent energy. However, when the magnetic field is close to the resonance field the molecular state couples to the (approximately) triplet atomic scattering state and the states become mixed. When the molecular state is tuned into the continuum, the mixing results in an adiabatic connection of the molecular state with the scattering continuum. This effect is analogous to an avoided crossing in a two level system. The corresponding bending of the states shows up in a very pronounced way for the $F = 2, M_F = 0$ molecular state (see figure 3.5). This leads to a very slow crossing of the bound state through threshold and hence to the very broad Feshbach resonance. Note that the resonance field of about 834 G is outside the magnetic field range shown in figure 3.5. The reason for this behavior is an interplay between the open channel zero energy resonance (see the discussion above) and the Feshbach res-

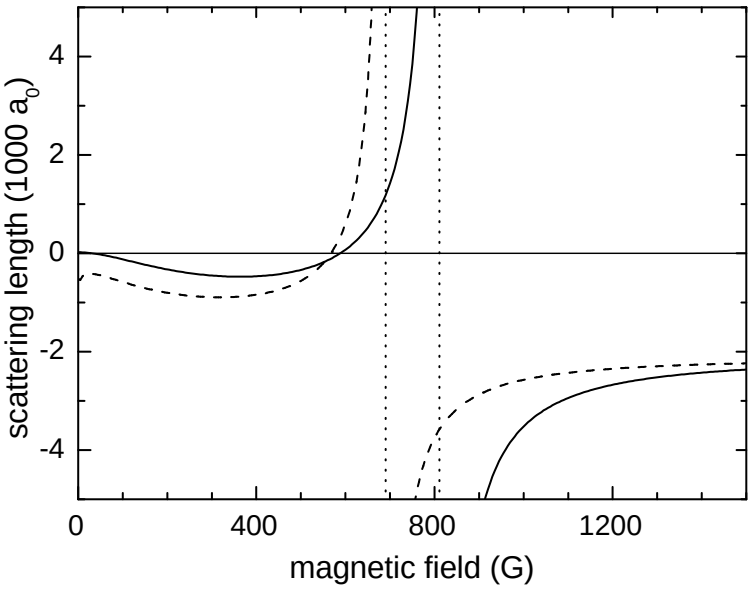

Figure 3.6: Calculated s-wave scattering length for ^{6}Li atoms in the scattering channel (1,3) (solid line) and in the channel (2,3) (dashed line). The vertical dotted lines indicate the resonance position of 811.2(1.0) G and 690.4(5) G, respectively [Bar04c].

onance [Mar04, Kem04]. In the absence of the zero energy resonance the Feshbach resonance would occur around 550 G [Sch04].

Feshbach Resonances in the (1,3) and (2,3) channel

In this paragraph we present the calculated magnetic field dependent s-wave scattering length for atoms interacting in the scattering channel (1,3) and (2,3). In both channels the existence of Feshbach resonances offer the possibility to resonantly alter the interactions. Moreover in the presence of an external magnetic field the scattering channel (1,3) was observed to be stable against inelastic decay [O'H00].

In all cases the resonances are due the coupling of the scattering channel with the the most weakly bound vibrational state of the singlet molecular potential with a total angular momentum $F = 2$. For two atoms colliding in the (1,3) channel, the total projection number of the total angular momentum is given by $M_F = -1$ and the resonance with the bound molecular state $F = 2, M_F = -1$ occurs at a field of 690.4(5) G and is characterized by a width of about 120 G [Bar04c]. Two colliding atoms in the scattering channel (2,3) have a total angular momentum $M_F = -2$. For this scattering state the Feshbach resonance arises at a magnetic field of 811.2(1.0) G [Bar04c] and is due to the coupling with the $F = 2, M_F = -2$ molecular state. The width of this resonance is about 220 G. Figure 3.6 shows the magnetic field dependent scattering length for both states.

Table 3.1: Parameters for formula given in equation 3.15. The function reproduces the calculated scattering length to better than 99% over a magnetic field range or 600 to 1200 G.

Channel	a_b (a_0)	B_0 (G)	ΔB (G)	α (kG)$^{-1}$
(1,2)	-1405	834.149	300	0.4
(1,3)	-1490	811.22	222.3	0.395
(2,3)	-1727	690.43	123.3	0.2

Fitting the numerical results

It is very convenient to have an analytic function that reproduces the results from the numerical calculation of the scattering length over the range of interest to BEC-BCS crossover experiments.

We find that over the magnetic field range of 600 to 1200 G the calculated scattering length can be fitted to better than 99% by the formula

$$a = a_{\mathrm{bg}}\left(1 + \frac{\Delta B}{B - B_0}\right)(1 + \alpha(B - B_0)). \tag{3.15}$$

The expression includes the standard resonance term given in equation 3.14 and a leading order correction parameterized by α. The respective values for the scattering channels (1,2), (1,3) and (2,3) are summarized in table 3.1.

3.2.4 Weakly bound molecules

As discussed in the previous section the tunability of the weakly bound molecular state enables the resonant control of the atomic scattering properties. Moreover the tunability of the weakly bound molecular level relative to the scattering continuum enables an efficient creation of ultracold diatomic molecules.

The following paragraphs briefly describe different techniques to create these exotic weakly bound molecules, their binding energies and their collisional stability. A detailed theoretical investigation of their properties is for example found in the articles by D. Petrov *et al.* [Pet03, Pet04, Pet05].

Our experimental study of dimers created at the broad Feshbach resonance at 834 G is found in our publication [Joc03b] and in the Ph.D. thesis of Selim Jochim [Joc04].

Creation of ultracold weakly bound molecules

The first observation of ultracold molecules was demonstrated in the beautiful experiments in the group of D. Jin [Reg03b]. In these experiments an adiabatic sweep of the magnetic field across the Feshbach resonance was performed to transfer an ultracold degenerate gas of fermionic atoms into weakly bound molecules.

This technique is now used in many laboratories to create ultracold molecules [Her03, Cub03, Xu03, Str03, Dür04].

Inspired by the previous work with Potassium at JILA [Reg03b], Cesium in our group [Her03] and Lithium at the ENS in Paris [Cub03] that had produced the molecules either from a BEC or a degenerate Fermi gas, we investigated the possibility to create molecules from a thermal gas of atoms [Joc04].

Our experiments showed a very efficient formation of molecules at magnetic fields close to the Feshbach resonance [Joc03b]. Here the molecular binding energy is small and a strong coupling between the atomic and the molecular gas exists. The exchange between the atomic and molecular gas is due to three-body collisions [Sun03, Pet03]. Our measurements showed that the exchange between the atomic and the molecular fraction is nearly lossless and the experimental data are found to be in good agreement with a theoretical model that assumes a thermal atom-molecule equilibrium [Chi04b, Joc04]. The main result of the model is the following relation between the molecular phase space density ϕ_{mol} and the atomic phase space density ϕ_{at} [Chi04b][4]

$$\phi_{\mathrm{mol}} = \phi_{\mathrm{at}}^2 \, \mathrm{e}^{E_{\mathrm{b}}/k_{\mathrm{B}}T}, \tag{3.16}$$

where E_{b} is the molecular binding energy.

The result shows that if the molecular state is far below the atomic continuum, all particles should accumulate the lower molecular state and the number of unbound atoms is exponentially suppressed. However applying the result to cold atoms has to be done with some care as the atom-molecule formation heats up the sample and reduces the atomic phase space density and limits the molecule fraction [Chi04b].

Molecular binding energy

The small binding energy E_{b} of the molecules is controlled by the value of the magnetic field and is related to the scattering length by [Gri93]

$$E_{\mathrm{b}} = \frac{\hbar}{m(a-\bar{a})^2}, \tag{3.17}$$

where $\bar{a}$ is the mean scattering length, which is on the order of the characteristic range of the van der Waals potential (see equation 3.13). In many cases the scattering length a is much larger than r_{c} and the above formula reduces to the well know result $E_{\mathrm{b}} = \hbar/ma^2$ [Lan77].

Figure 3.7 shows the calculated binding energy of $^6Li_2$ molecules formed in the scattering channel (1,2). The molecular level connects at 834.1(1.5) G steadily to the scattering continuum. Note that for magnetic fields below approximately 600 G equation 3.17 starts to deviate because the scattering length approaches the zero crossing at about 527 G.

[4] A similar model taking into account a quantum degenerate molecular gas is found in [Kok04, Wil04].

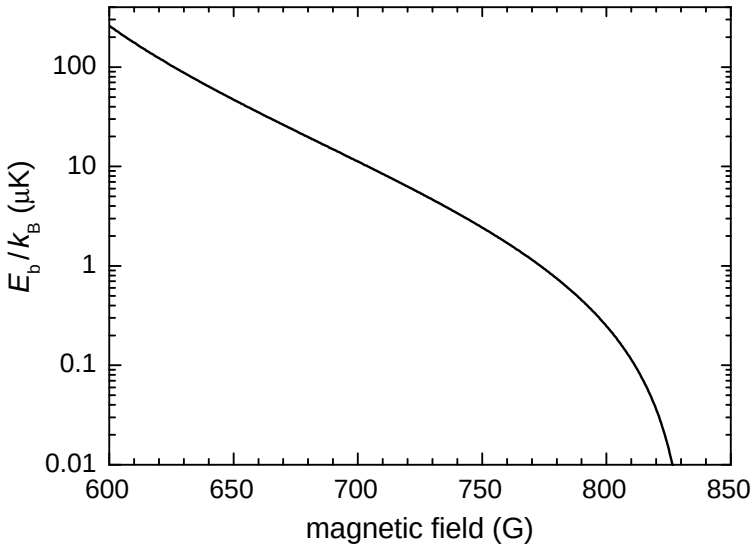

Figure 3.7: Calculated molecular binding energy for molecules formed in the (1,2) scattering channel. The calculation is based on equation 3.17 and the most up to date values for the scattering length [Bar04c].

Collisional stability and elastic dimer-dimer scattering

The small binding energy of the molecule corresponds to a large size, which is on the order of the atomic scattering length a [Pet04]. This large size[5] in combination with the Pauli exclusion principle is responsible for the remarkable collisional stability of the dimers created from fermionic atoms. The size of the deeply bound molecules is on the order of the characteristic range of interactions r_c ($r_c \approx 30\,a_0 \ll a$) and the collisional relaxation requires the presence of at least three fermions at distances on the order of r_c from each other. Because two of them are necessarily identical, the process is suppressed due to Fermi statistics for the atoms [Pet04]. Furthermore due to the large size of the weakly bound dimers the spatial Franck-Condon overlap of the weakly bound molecules with the tightly bound states is rather low.

While the later argument holds for all weakly bound molecules, the first one applies only to molecules created from fermionic atoms. This explains the observed extraordinarily large molecular lifetimes of molecules formed from fermionic atoms [Cub03, Joc03b, Reg04a] that allowed the successful creation of a molecular Bose-Einstein condensate [Joc03a, Gre03, Zwi03, Bou04, Hul04]. Experiments with molecules created from bosonic gases, however show a rapid collisional decay [Her03, Dür04, Xu03] that inhibited so far the creation of a molecular BEC.

As the size of the molecules depends on the scattering length, one expects a weakening of the above effects for smaller a. Assuming $r_c \ll a$, the detailed calculation of

[5] Note that in the vicinity of the Feshbach resonance a is on the order of some $1000\,a_o$.

atom dimer collisions leads to a rate constant of

$$\alpha_{\mathrm{ad}} \propto \frac{\hbar r_{\mathrm{c}}}{m}\left(\frac{r_{\mathrm{c}}}{a}\right)^{3.33} \tag{3.18}$$

for the relaxation of the weakly bound dimers into deeply bound states [Pet04]. Note that the proportionality factor depends on the individual system. Similar the relaxation rate constant α_{dd} in dimer-dimer collisions is found to be [Pet04]

$$\alpha_{\mathrm{dd}} \propto \frac{\hbar r_{\mathrm{c}}}{m}\left(\frac{r_{\mathrm{c}}}{a}\right)^{2.55}. \tag{3.19}$$

Both processes decrease with increasing scattering length. In the limit of large scattering length ($r_{\mathrm{c}}/a \to 0$) the dominant relaxation process are dimer-dimer collisions. The predicted strong decrease of the relaxation rate with increasing a is consistent with experimental findings in ultracold molecular $^{40}K_2$ and $^{6}Li_2$ gases [Reg04a, Bou04].

Calculations of the dimer-dimer scattering length yield to [Pet04]

$$a_{\mathrm{mol}} = 0.6a. \tag{3.20}$$

This relation is in agreement with experimental findings [Joc03a, Cub03] and a recent Monte Carlo calculation of the equation of state in the BEC-BCS crossover [Ast04] (see section 2.3). The atom-dimer scattering length is calculated to be $a_{\mathrm{ad}} = 1.2a$ [Pet05].

Thus the inelastic rate constant is much smaller than the rate constant of elastic collisions [Pet04]. This excellent ratio of "good" to "bad" collisions allows for a very efficient evaporative cooling of the dimers [Pet04, Chi04b, Joc04] (see also chapter 5).

3.3 Collective Oscillations

The previous discussion of the static properties of trapped degenerate Bose and Fermi gases showed the strikingly different influence of the interaction effects in both systems (see chapter 2). In this section the studies are extended to collective excitations in these quantum systems, which again point out the important role played by the interactions and quantum correlations. The study of collective modes is of particular interest as the collective frequencies of a trapped cloud can be measured with high precision and therefore allow for a detailed comparison with the theory.

Over the past years collective modes have been extensively studied in trapped BECs and revealed their sensitivity to interaction and correlation effects [Dal99a]. An excellent introduction to the theoretical description is found in the textbooks of C. Pethick and H. Smith [Pet02], and L. Pitaevskii and S. Stringari [Pit03]. A good overview of the dynamic behavior of superfluid Bose liquids is also found in the textbook of Nozieres and Pines [Noz90].

The equations characterizing the macroscopic behavior of a superfluid at zero temperature are presented in section 3.3.1. These equations have the form of irrotational

hydrodynamic equations and hold for Bose as well as Fermi superfluids. Moreover, the linearized collective modes of a gas in the normal, non superfluid state, are described by the same equations of motion, if the collisions are frequent enough to ensure the gas to be in local thermodynamic equilibrium.

The corresponding collective modes of a gas that are described by the hydrodynamic equations are presented in section 3.3.2 for different harmonic traps. Of particular interest for our measurements of the collective modes in the BEC-BCS crossover (see section 6.2) are the low-lying collective modes in an elongated trap.

The dynamics of a non-degenerate quantum gas are described by the classical Boltzmann equation. This equation has two asymptotic regimes: the collisional or hydrodynamic regime, and the collisionless regime. The behavior of the mode frequency and damping rate between these two limits is presented in section 3.3.3 for the axial and radial collective oscillation in an elongated harmonic potential.

While mean field effects play a key role in dilute BECs, their effects are much less pronounced in interacting Fermi gases, where the density is reduced due to the Pauli exclusion principle. Nevertheless, the ability to measure the collective modes with high precision should allow the observation of the (small) mean field corrections to the collective mode frequencies in a Fermi gas. These corrections are presented in section 3.3.4 for a Fermi gas in the collisionless and hydrodynamic regimes.

Corrections of the collective modes for a BEC beyond the mean field level are presented in section 3.3.5. In general these effects are expected to be small but might become visible when the BEC enters the strongly interacting regime.

This section ends with a brief discussion of the theoretical calculations of the collective modes in the BEC-BCS crossover.

3.3.1 Hydrodynamic equations of motion

The time dependent Gross-Pitaevskii equation was introduced in section 2.1.2 and describes the general time dependence of the order parameter (condensate wave function). The Gross-Pitaevskii equation conserves the particle number N and therefore obeys the continuity equation [Pet02]

$$\frac{\partial n}{\partial t} + \nabla(\mathbf{v}n) = 0, \tag{3.21}$$

where the the density n and the (superfluid) velocity field $\mathbf{v}$ are related to the order parameter $\Phi(\mathbf{r}, t) = |\Phi(\mathbf{r}, t)|e^{iS(\mathbf{r},t)}$ through the relationships

$$n(\mathbf{r}, t) = |\Phi(\mathbf{r}, t)|^2 \tag{3.22}$$

and

$$\mathbf{v}(\mathbf{r}, t) = \frac{\hbar}{m}\nabla S(\mathbf{r}, t). \tag{3.23}$$

From the definition of the velocity of the condensate flow it is obvious that the motion of the condensate is irrotational, i.e $\nabla \times \mathbf{v}(\mathbf{r}, t) = 0$. It should be noted however, that

this result fails if the condensate phase $S(\mathbf{r}, t)$ is singular, as is, for example, the case in a vortex core [Pet02].

Inserting the expression for the order parameter $\Phi(\mathbf{r}, t) = |\Phi(\mathbf{r}, t)|e^{iS(\mathbf{r},t)}$ into the Gross-Pitaevskii equation results in the equation for the phase S

$$\hbar\frac{\partial}{\partial t}S + \left(\frac{1}{2}m\mathbf{v}^2 + V_{\text{ext}}(\mathbf{r}) + gn - \frac{\hbar^2}{2m\sqrt{n}}\nabla^2\sqrt{n}\right) = 0. \tag{3.24}$$

This equation together with the continuity equation 3.21 provides two coupled differential equations that are exactly equivalent to the original Gross-Pitaevskii equation.

Equation 3.24 can be further simplified if the quantum pressure term proportional to $\hbar^2$ can be neglected. For this assumption to be valid the density of the gas has to change slowly in space. Denoting the typical distance characterizing the density variation by R, the quantum pressure term scales as $\nabla^2\sqrt{n}/\sqrt{n} = R^{-2}$. According to equation 3.24 the quantum pressure term can be neglected if the length scale of the density variation R is much larger than the characteristic length [Pit03]

$$\xi = \frac{\hbar}{\sqrt{2mgn}}. \tag{3.25}$$

This characteristic length is called the healing length. For a uniform BEC the healing length marks the transition from a single particle spectrum to a phonon like spectrum. For excitations with a wavelength larger than ξ the particles move collectively, while for shorter wavelengths they behave as free particles [Pet02, Pit03].

Assuming collective oscillations with a length scale of the oscillation that is larger than the healing length, equation 3.24 can be written as [Pit03]

$$\frac{\partial\mathbf{v}}{\partial t} = -\nabla\left(\frac{\mathbf{v}^2}{2} + \frac{V_{\text{ext}}(\mathbf{r})}{m} + \frac{\mu(n)}{m}\right), \tag{3.26}$$

where $\mu(n)$ is the chemical potential of a homogeneous system evaluated at the density n. The functional form of the chemical potential in a homogeneous system represents the equation of state. In the case of a weakly interacting BEC, the equation of state is linear in the density ($\mu(n) = gn$).

The equations 3.21 and 3.26 have the typical structure of the dynamic equations for superfluids at zero temperature [Noz90], and are referred to as the equations of irrotational hydrodynamics. They have been systematically used to predict the effects of superfluidity on the dynamic behavior of Bose-Einstein condensates [Dal99a, Pet02, Pit03].

The same equations of hydrodynamics also hold for a superfluid Fermi gas [Coz03]. However, in this case the equation of state can be very different due to the Pauli exclusion principle. For example, in a weakly interacting, very dilute Fermi gas of two spin states with equal density $n/2$, the equation of state is given by [Men02]

$$\mu(n) = \frac{\hbar^2}{2m}(3\pi^2 n)^{2/3}. \tag{3.27}$$

Conversely, the equation of state of a BEC is fixed by the interactions ($\mu(n) = gn$).

It should be noted that the applicability of the hydrodynamic equations for superfluids is only valid if [Zam01]:

- the non superfluid component is negligible which implies that the temperature is much smaller than the transition temperature to the normal phase (see also below).
- the size of the sample is large enough to ensure the validity of the local density approximation for the chemical potential. Or alternatively the healing length has to be much smaller than the size of the sample.
- the length scale of the oscillation is larger than the healing length.

Description of the non superfluid phase

Provided that the rate of collisions in the normal, non superfluid, state is sufficiently large to ensure a local thermodynamic equilibrium, a hydrodynamic description is possible. In this case the fluid can be described by the local density, local velocity, and local temperature. At zero temperature the system is fully described by the local density and the local velocity. Moreover, the expansion and the linearized collective oscillations of a classical gas in the collisional (hydrodynamic) regime and a superfluid gas are described by the same irrotational hydrodynamic equations [Coz03][6].

For a classical gas in the hydrodynamic regime, as well as for a superfluid condensate, it is the ability to describe the system in terms of a local density and velocity that enables the usage of the hydrodynamic equations. In the classical gas the thermodynamic equilibrium is ensured by the high collision rate. On the other hand the condensate at zero temperature is in the collisionless regime (see below). However, the presence of the macroscopic order parameter validates a hydrodynamic description [Pet02].

Scaling solution

It was noted by C. Menotti *et al.* [Men02] that the equations of irrotational hydrodynamics admit simple scaling solutions in harmonic traps if the equation of state is given by

$$\mu(n) \propto n^{\gamma}. \tag{3.28}$$

Such an equation of state is referred to as a polytropic equation of state and applies to many systems. For example an interacting BEC has $\mu = gn$ and hence $\gamma = 1$. On the other hand an ideal Bose gas in the normal state as well as an ideal Fermi gas both have $\gamma = 2/3$ [Coz03, Hei04a]. In the next section the corresponding collective modes of the linearized hydrodynamic equations are discussed.

[6] Strictly speaking this is only valid, if the initial state does not contain any velocity flow.

Superfluids at finite temperature

At zero temperature all bosonic particles are in the condensate and the relaxation time τ of the collective modes is much larger than the collective frequency ($\omega\tau \gg 1$). In this collisionless regime the restoring force is only due to the mean field interaction and the collective oscillation in a uniform system is referred to as Bogoliubov sound or zero sound. A detailed discussion of the collective excitations of a Bose gas in the collisionless regime is found in the article by S. Giorgini [Gio00].

At finite temperature, collisions become more important and one eventually reaches the collisional or hydrodynamic regime ($\omega\tau \ll 1$). For temperature $T < T_c$ the dynamic equations have to be generalized to the equation of two-fluid hydrodynamics [Noz90, Pet02, Pit03]. This regime is characterized by the occurrence of two distinct oscillations, which in a uniform system are called first and second sound. While first sound mainly involves the oscillation of the thermal cloud and reduces to hydrodynamic sound above T_c, second sound is the oscillation of the condensate and disappears above T_c. A discussion of these hydrodynamic sound modes in uniform Bose gases is found in [Gri97b], while a detailed discussion of trapped Bose gases in this regime is found in the article of E. Zaremba *et al.* [Zar99]. A discussion of the low energy collective modes of trapped Fermi superfluids at various temperatures is found in [Bru01a].

At temperatures above T_c the system reaches the classical regime that is well described by the Boltzmann equation and is further discussed in section 3.3.3.

The damping of the collective modes in a zero-temperature BEC [Fed98] as well as in a superfluid trapped Fermi gas, is expected to be very small [Bar00]. For the superfluid Fermi gas this can be understood by considering that at zero temperature a low energy collective mode cannot decay because the presence of an energy gap in the excitation spectrum prevents the formation of excitations. On the other hand for temperatures just below the critical temperature the collective modes in a superfluid Fermi gas are expected to be strongly damped [Bar00]. The general description of the damping in inhomogeneous systems at finite temperature is very complex and we refer to the literature [Fed98, Gio00, Bar00] and references therein.

3.3.2 Collective Modes in the hydrodynamic regime

From the linearized hydrodynamic equation of motion the collective modes can be calculated [Pet02]. In the following, a polytropic equation of state with $\mu(n) = n^\gamma$ is assumed.

To reveal the role of interactions in the collective modes of a gas in the hydrodynamic regime, the modes have to be compared with the predictions of the ideal gas model for a harmonically confined gas. Here the discrete mode frequencies are sums of integer multiples of the trap frequency ω_0.

To reveal the role of interactions they have to be compared with the predictions of the ideal gas model confined in a harmonic potential. Here the discrete mode frequen-

cies are sums of integer multiples of the trap frequency ω_0.

Isotropic trapping potential

For isotropic harmonic traps with trapping frequency ω_0, the collective modes are characterized by their orbital angular momentum l and the number of radial nodes n_r (see for example [Str96, Amo99, Pet02]). The corresponding eigenfrequencies of the modes are found to be [Hei04a]

$$\omega^2/\omega_0^2 = l + 2n_r\,(\gamma(n_r + l + 1/2) + 1)\,. \tag{3.29}$$

For a dilute, interacting BEC with $\gamma = 1$ this reduces to the mode frequencies found by S. Stringari *et al.* [Str96]. For a superfluid and a collisional (hydrodynamic) Fermi gas $\gamma = 2/3$ and the eigenfrequencies reduce to the results found in [Bru99, Amo99, Bar00].

For $n_r = 0$ the dispersion spectrum corresponds to the so-called surface modes. These modes have no radial nodes and with increasing l they become more localized near the surface of the cloud. From equation 3.29 it is obvious that these modes do not depend on the underlying equation of state. Of special interest is the $l = 1$ dipole mode, which corresponds to the center of mass motion of the system. Due to the harmonic confinement the oscillation frequency is the harmonic trap frequency. Because the center of mass motion and the internal degrees of freedom are separable for interactions that depend only on the relative coordinate of the particles, the mode is unaffected by two-body interactions. The dipole mode frequency ($\omega = \omega_0$) is the same for any system confined in a harmonic potential, independent of temperature and statistics [Pit03]. The fact that this mode is unaffected by interactions is very important for experiments. First, it enables the determination of the trapping frequencies to high accuracy by measuring the dipole frequency. Second, the frequency can be used to check the harmonicity of the trapping potential (for experimental details see section 6.2.1). The next higher surface mode is the quadrupole mode with $l = 2$ and $\omega = \sqrt{2}\omega_0$.

The comparison of the modes with the predictions for an ideal gas [Str96]

$$\omega/\omega_0 = (2n_r + l), \tag{3.30}$$

shows that the surface modes with $l > 1$ are systematically below the ideal gas predictions.

For the so-called compressional modes, which have $n_r = 1$, the lowest one is the monopole mode with $n_r = 1, l = 0$. From equation 3.29 the corresponding dispersions law reads

$$\omega^2/\omega_0^2 = 3\gamma + 2. \tag{3.31}$$

For a BEC in the Thomas-Fermi regime $\gamma = 1$ and the eigenfrequency amounts to $\omega = \sqrt{5}\,\omega_0$, while for a Fermi gas with $\gamma = 2/3$ the eigenfrequency is given by $\omega = 2\,\omega_0$. Because this mode is spherically symmetric with a radial velocity field having the same sign everywhere it is also referred to as the breathing mode.

Axially symmetric potential

The results of the isotropic harmonic potential can be generalized to anisotropic configurations with

$$V(x,y,z) = \frac{1}{2}m\omega_\perp^2 r^2 + \frac{1}{2}m\omega_\parallel^2 z^2 = \frac{1}{2}m\omega_\perp^2(r^2 + \lambda^2 z^2), \tag{3.32}$$

where $r^2 = x^2 + y^2$ and $\lambda = \omega_\parallel/\omega_\perp$ is the anisotropy parameter. In our measurements of the collective modes in the BEC-BCS crossover (see section 6.2) the anisotropy of the trapping potential is typically $\lambda \approx 0.03$.

In the isotropic case ($\lambda = 1$), the rotational symmetry ensures that the angular momentum l gives two good quantum numbers, i.e. l and m. For an axial symmetry only the axial component m of the angular moment l remains a good quantum number. However, the resulting dispersion relation will depend on m and explicit results are only available in some particular cases. For the low-lying collective modes it is still possible to start from a spherical base that is suitably modified to account for the cylindrical symmetry. The reduced symmetry gives rise to a coupling between some of the modes that, in the spherical trap, are characterized by different values of l [Str96, Amo99] (see also below).

The calculation in an axially symmetric trap leads to the following dispersion law for the surface excitations [Coz03]

$$\omega^2(l = 2, m = \pm 2) = 2\omega_\perp^2, \tag{3.33}$$

and

$$\omega^2(l = 2, m = \pm 1) = \omega_\perp^2 + \omega_\parallel^2. \tag{3.34}$$

As in the case of the isotropic harmonic potential, the frequencies of the surface modes are independent of the underlying equation of state.

This is contrasted by the $n_r = 0$, $l = 2$, $m = 0$ quadrupole surface mode which is, due to the axial symmetry of the external potential, coupled to the $n_r = 1$, $l = 0$, $m = 0$ monopole mode. Here the dispersion law of the two decoupled modes explicitly depends on the equation of state and is given by [Coz03]

$$\omega^2/\omega_\perp^2 = \gamma + 1 + \frac{\gamma+2}{2}\lambda^2 \pm \sqrt{(\gamma+2)^2\lambda^4/4 + (\gamma^2 - 3\gamma - 2)\lambda^2 + (\gamma+1)^2}. \tag{3.35}$$

For $\omega_\perp = \omega_\parallel = \omega_0$ one recovers the solutions for the quadrupole ($\omega/\omega_0 = \sqrt{2}$) and the monopole ($\omega^2/\omega_0^2 = 3\gamma + 2$) excitations in a spherical trap.

The explicit dependency of these collective mode frequencies on γ makes them perfectly suited to investigate the equation of state in the BEC-BCS crossover. In the following, several regimes of the dispersion spectrum given in equation 3.35 are discussed.

For an ideal gas $\gamma = 2/3$ and the dispersion law is identical to the predictions found in the following articles [Kag97, Gri97a, Amo99]. The same results apply to a Fermi

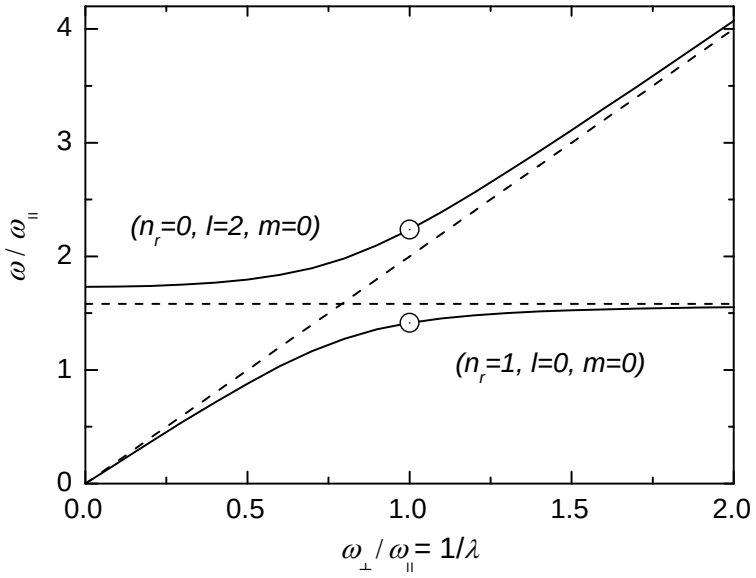

Figure 3.8: Mode frequency in units of $\omega_\parallel$ of the $n_r = 0, l = 2, m = 0$ and $n_r = 1, l = 0, m = 0$ modes calculated from equation 3.35 for a BEC in the Thomas-Fermi limit ($\gamma = 1$). The two frequencies for an isotropic trapping potential ($\omega_\perp/\omega_\parallel = 1$) are marked by the two circles. In the limit of very elongated traps ($\omega_\perp/\omega_\parallel \gg 1$) the frequencies approach $\omega/\omega_\parallel = \sqrt{5/2}$ and $\omega/\omega_\parallel = 2\omega_\perp/\omega_\parallel$, respectively (dashed lines).

gas in the superfluid state [Bar00]. Moreover, the same dispersion relation also applies to a strongly interacting, unitarity limited, BEC and Fermi gas because in both cases $\gamma = 2/3$, as shown in [Cow02] and [Hei01], respectively. On the other hand for a dilute, interacting BEC in the Thomas-Fermi limit $\gamma = 1$ and equation 3.35 reduces to the one found by S. Stringari *et al.* [Str96]. Figure 3.8 shows the two decoupled frequencies for a BEC as a function of the radial oscillation frequency ratio $\omega_\perp/\omega_\parallel = 1/\lambda$.

In our experiment the ratio between the radial and axial trap frequencies is typically $\omega_\perp/\omega_\parallel \approx 30$. In this limit of very elongated traps ($\omega_\perp \gg \omega_\parallel$) the dispersion law of the two decoupled modes correspond to a slow axial and a fast radial oscillation. The axial mode is characterized by an out-of-phase oscillation along the axial and radial direction. The radial mode, on the other hand, is primarily a radial breathing mode with a suppressed oscillation along the axial direction. These two modes are often referred to as the axial and radial breathing mode, respectively[7]. An illustration of these two modes is found in figure 6.5 in section 6.2, where we also describe our measurements of these two modes in the BEC-BCS crossover. The calculated dispersion law of the two modes is given by [Coz03]

$$\omega = \sqrt{(3\gamma + 2)/(\gamma + 1)}\,\omega_\parallel, \tag{3.36}$$

[7]Note that a well defined nomenclature of modes does not exist and different names for these modes might be used throughout the literature.

Table 3.2: Collective frequencies of the decoupled modes in a elongated trap, given by equation 3.37 and 3.36 for a gas obeying the hydrodynamic equations of motion with a polytropic index of $\gamma = 2/3$ and $\gamma = 1$, respectively.

	$\gamma = 2/3$	$\gamma = 1$
radial breathing mode	$\sqrt{10/3}\,\omega_\perp$	$2\,\omega_\perp$
axial breathing mode	$\sqrt{12/5}\,\omega_\parallel$	$\sqrt{5/2}\,\omega_\parallel$

for the axial breathing modes and

$$\omega = \sqrt{2(\gamma+1)}\,\omega_\perp, \tag{3.37}$$

for the radial breathing mode. Note that the radial mode reveals a much stronger dependence on the equation of state than the axial mode.

For a BEC with $\gamma = 1$ the solution of the axial breathing mode (equation 3.36) is given by $\omega/\omega_\parallel = \sqrt{5/2} = 1.581$, while the solution for the fast radial breathing mode (equation 3.37) amounts to $2\omega_\perp$, which is identical to the predicted frequency for an ideal gas [Str96]. The experimental investigation of a BEC in this limit yielded $\omega/\omega_\parallel = 1.569(4)$ for the low-lying mode [SK98] and $\omega/\omega_\perp \approx 2$ for the radial mode [Che02]. The measurements by F. Chevy *et al.* further demonstrated that the radial mode is only very weakly damped [Che02].

The above discussion shows that first of all, the predicted collective frequencies of a non superfluid Fermi gas in the hydrodynamic limit are the same as for a superfluid Fermi gas. The same collective frequencies are also predicted for any classical gas in the hydrodynamic limit, independent of the underlying statistics. The reason is that in all cases the equation of states has the same power law dependence with $\gamma = 2/3$. Moreover, as the unitarity limited quantum gas is predicted to have the same density dependence of the equation of state ($\mu \propto n^{2/3}$) it also obeys the same dispersion laws.

Conversely, a weakly interacting BEC in the Thomas-Fermi limit has an equation of state $\mu \propto n^1$ and the collective frequencies are expected to differ from the above cases. Table 3.2 summarizes the corresponding frequencies for an interacting BEC with $\gamma = 1$ and a gas with $\gamma = 2/3$ that obeys the hydrodynamic equations.

3.3.3 Collisional versus Collisionless dynamics

The collective modes frequencies of a gas that is described by the hydrodynamic equation of motion have been discussed in section 3.3.2. This description applies for a condensate and for a classical gas with a sufficiently large collision rate.

This section focuses on the description of the collective modes of a gas in the normal, non superfluid state. Of particular interest is the behavior of the quadrupole mode in an elongated trapping potential when the gas changes from a hydrodynamic to a collisionless gas. This situation was considered by D. Guery-Odelin *et al.* [GO99],

and here we summarize their results for the collective mode frequencies and damping rates.

In general, for temperatures T greater than the transition temperature T_c the thermal energy is large compared to the energy level spacing in the harmonic oscillator. The dynamics of such a gas are mainly effected by collisional effects, and due to the low density, mean field effects can be neglected in the derivation of the collective mode frequencies. For a gas in this regime the dynamics are well described by the Boltzmann equation [Pit03].

The Boltzmann equation exhibits two asymptotic regimes: the collisionless and the collisional or hydrodynamic regime. Both regimes are distinguished by the ratio of the collective frequency ω with respect to the relaxation time τ and correspond to $\omega\tau \gg 1$ and $\omega\tau \ll 1$, respectively.

Relaxation time of the quadrupole mode

For a gas in the classical regime the relaxation time of the quadrupole mode is given by [GO99]

$$\tau = \frac{5}{4}\frac{1}{\gamma_{coll}}, \tag{3.38}$$

where γ_{coll} is the classical collision rate. For a gas with thermal velocity $v_{\mathrm{th}} = \sqrt{8k_{\mathrm{B}}T/\pi m}$, central density $n(0)$, and a total scattering cross section σ, the collision rate is given by [Wu97]

$$\gamma_{\mathrm{coll}} = \frac{n(0)v_{\mathrm{th}}\sigma}{2}. \tag{3.39}$$

For a classical gas in a harmonic trap $v_{\mathrm{th}} \propto T^{1/2}$ and $n(0) \propto T^{-3/2}$, and consequently the collision rate decreases with increasing temperature.

In the classical limit the relaxation time and the collision rate are inversely proportional to each other (see above). However under conditions of quantum degeneracy the two quantities show a very different temperature dependence and are no longer proportional to each other [Vic00]. This behavior highlights the important role played by the underlying quantum statistics.

For degenerate fermions the collisions are quenched due to the Pauli exclusion principle and consequently at very low temperatures one expects the gas to be in the collisionless regime. As the author of [Vic00] shows, the relaxation time τ is proportional to $(T_{\mathrm{F}}/T)^2$. Thus in a Fermi gas the relaxation time diverges at zero temperature as a consequence of the Pauli principle and at temperatures $T \gg T_{\mathrm{F}}$ because the gas gets dilute. Consequently the Fermi gas is in both cases expected to be in the collisionless regime.

In contrast to the Fermi gas, the relaxation time for a Bose gas is predicted to decrease with respect to the classical trend when the critical temperature is approached [Vic00].

Intermediate regime

Starting from the Boltzmann equation, the general dispersion law for the quadrupole oscillation in an anisotropic harmonic trapping potential is given by [GO99]

$$(\omega^2 - 4\omega_\parallel^2)(\omega^2 - 4\omega_\perp^2) - \frac{i}{\omega\tau}\left(\omega^4 - \frac{2}{3}\omega^2(5\omega_\perp^2 + 4\omega_\parallel^2) + 8\omega_\perp^2\omega_\parallel^2\right) = 0. \tag{3.40}$$

The above dispersion relation was derived for a classical gas. However by including quantum statistical effects in the relaxation time τ the relation also holds for degenerate Fermi gases [Vic00].

The first term of equation 3.40 corresponds to the dispersion law of a purely collisionless regime ($\omega\tau \to \infty$). In this limit interactions are completely neglected and the eigenfrequencies coincide with the ones predicted for an ideal gas. The second term, multiplying $i/(\omega\tau)$, corresponds to the purely hydrodynamic case ($\omega\tau \to 0$). Note that this hydrodynamic dispersion law is identical to the one found from the hydrodynamic equations of irrotational superfluids (see equation 3.35 with $\gamma = 2/3$).

In the intermediate regime ($\omega\tau \approx 1$) equation 3.40 can be solved numerically for $\omega = \omega_{\text{real}} + i\Gamma$. Figure 3.9 shows the frequency ω_{real} and the damping rate Γ of the axial (radial) breathing mode as a function of $\omega_\parallel\tau$ ($\omega_\perp\tau$) for a cigar shaped trap. The chosen anisotropy corresponds to our experimental configuration ($\omega_\perp/\omega_\parallel = 31$). For the axial (radial) breathing mode frequency one observes a continuous decrease of the frequency with decreasing $\omega_\parallel\tau$ ($\omega_\perp\tau$) towards the hydrodynamic value of $\omega/\omega_\parallel = \sqrt{12/5}$ ($\omega/\omega_\perp = \sqrt{10/3}$) (see figure 3.9 left and right, respectively). For large $\omega_\parallel\tau$ ($\omega_\perp\tau$) the collisionless regime is reached and the frequency approaches $\omega/\omega_\parallel = 2$ ($\omega/\omega_\perp = 2$). A maximum damping rate is reached in the intermediate regime where $\omega_\parallel\tau \approx 0.4$ ($\omega_\perp\tau \approx 0.5$).

3.3.4 Mean field effects in Fermi gases

Because of the high density in Bose-Einstein condensates, interactions play a crucial role, not only in the equilibrium, but also in the behavior of the collective frequencies. Fermi gases however, are more dilute due to the Pauli exclusion principle and consequently the effects of interactions are expected to be much smaller. Moreover, for identical Fermions s-wave interactions are completely suppressed and one expects the gas to be in the collisionless regime. The study of the dynamics of such an ideal gas in time dependent traps is found in [Bru00].

In an ultracold two component Fermi gas, however, mean field effects may be present. In the following the influence of these interactions on the collective modes of a Fermi gas in the collisionless and hydrodynamic (superfluid) regime are described. A description of the influence of mean field effects to the dynamics in the regime between the hydrodynamic and the collisionless limit is found in reference [Ped03, Mas04].

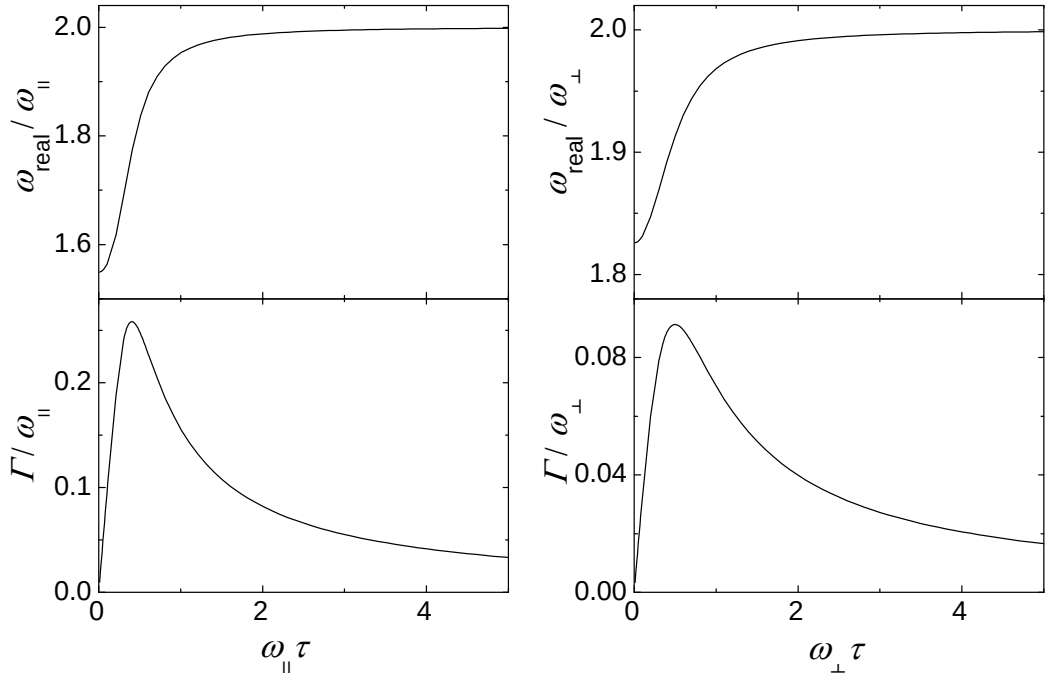

Figure 3.9: Real part and imaginary part of the axial (left) and radial breathing mode (right) of a classical gas confined in an axially symmetric trap ($\omega_\perp/\omega_\parallel = 31$). For $\omega_\parallel\tau \ll 1$ ($\omega_\perp\tau \ll 1$) the axial (radial) mode is in the hydrodynamic regime while for $\omega_\parallel\tau \gg 1$ ($\omega_\perp\tau \gg 1$) the collisionless regime is reached. For the axial (radial) breathing mode, the maximum damping rate Γ occurs in the intermediate regime at $\omega_\parallel\tau \approx 0.4$ ($\omega_\perp\tau \approx 0.5$).

Collisionless Fermi gas

In the collisionless regime the relaxation time of excitation is much larger than the characteristic period of motion ($\omega\tau \gg 1$) and consequently there is less than one scattering event per oscillation. In a homogenous system these collective excitations are referred to as zero sound.

Assuming a spin mixture of equal atom number and same trapping frequencies the collective frequencies can be calculated using a sum rule approach[8]. For an isotropic harmonic potential, the quadrupole mode frequency is given by [Vic99]

$$\omega_{\mathrm{Q}}^2 = 4\omega_{\mathrm{ho}}^2\left(1 - \frac{3}{4}\frac{E_{\mathrm{int}}}{E_{\mathrm{ho}}}\right), \tag{3.41}$$

while the frequency of the monopole mode amounts to

$$\omega_{\mathrm{M}}^2 = 4\omega_{\mathrm{ho}}^2\left(1 + \frac{3}{8}\frac{E_{\mathrm{int}}}{E_{\mathrm{ho}}}\right). \tag{3.42}$$

The results can be extended to axially symmetric traps if the interaction effects are smaller than the unperturbed splitting between the axial and radial frequencies. To first

[8] An introduction to this method is found in the textbook of L. Pitaevskii and S. Stringari [Pit03].

order in a the radial mode does not change with respect to the ideal gas case, while the axial mode becomes [Vic99]

$$\omega = 2\omega_{\mathrm{ho}}\left(1 - \frac{3}{16}\frac{E_{\mathrm{int}}}{E_{\mathrm{ho}}}\right). \tag{3.43}$$

For an interacting two component Fermi gas the quantity $E_{\mathrm{int}}/E_{\mathrm{ho}} \approx 0.3k_{\mathrm{F}}a$ is small (see equation 2.38) and thus one expects corrections of a few percent with respect to the ideal gas predictions.

Hydrodynamic and superfluid Fermi gases

As explained in section 3.3.1, the collective modes of gases that are described by the hydrodynamic equations, depend on the underlying equation of state.

For an interacting Fermi gas of two spin species with equal density $n/2$, the inclusion of mean field effects results in the equation of state [Men02]

$$\mu(n) = \frac{\hbar^2}{2m}(3\pi^2 n)^{2/3} + \frac{1}{2}gn, \tag{3.44}$$

where the coupling constant is $g = 4\pi\hbar^2 a/m$. The same equation of state also holds for a Fermi gas in the superfluid state. It should be noted, that the above equation of state neglects the effects of correlations, which become important for large values of the scattering length and affect in a different way the equation of state of the normal and superfluid phase [Men02].

Using a perturbative scheme the following correction to the radial breathing mode of a superfluid Fermi gas in an axially anisotropic trap is found [Str04a]

$$\omega = \sqrt{\frac{10}{3}}\omega_{\perp}\left(1 + \frac{3}{20}\frac{E_{\mathrm{int}}}{E_{\mathrm{ho}}}\right). \tag{3.45}$$

Note that because $a < 0$, the mean field correction ($E_{\mathrm{int}}/E_{\mathrm{ho}} \approx 0.3k_{\mathrm{F}}a$) is negative.

3.3.5 Beyond mean field corrections in a BEC

So far the investigation of the collective modes in a zero-temperature interacting BEC was done for a BEC in the Thomas-Fermi regime. As discussed in section 2.1.2 this approximation is well satisfied for a weakly interacting BEC with a sufficient large number of atoms. However, for large gas parameters $n|a|^3$ one expects corrections to the mean field predictions. These beyond mean field corrections lead to a modified equation of state and consequently to a change in the collective mode frequencies as described in the following.

The mean field Gross-Pitaevskii theory corresponds to the first approximation of Bogoliubov theory for uniform gases. The next order correction accounts for the change in the equation of state due to the occurrence of quantum correlations. The

corresponding correction to the chemical potential of a uniform gas was derived by Lee, Huang, and Yang and is given by [Lee57]

$$\mu(n) = gn\left(1 + \frac{32}{3\sqrt{\pi}}\sqrt{na^3}\right). \tag{3.46}$$

According to their theory, the first corrections to the mean field predictions are expected to behave like $\sqrt{na^3}$. For typical experimental parameters for the s-wave scattering length and the density at the center of the trap, the gas parameter is smaller than 10^{-4} and consequently the effects are on the order of 1% or less. Such corrections are too small to be observed in the density profile or the release energy. On the other hand they might be observable in the frequencies of the collective oscillations as they can be measured with much higher accuracy.

The corresponding frequency shifts can be derived by evaluating the hydrodynamic equations of superfluids (see above) with the equation of state given in equation 3.46 [Pit98]. The surface modes are independent of the equation of state and are unaffected by the beyond mean field corrections. Conversely, the compressional modes are sensitive to the equation of state and the calculated fractional shift for the lowest mode in a spherical harmonic potential (monopole mode) is given by

$$\frac{\delta\omega_M}{\omega_M} = \frac{63\sqrt{\pi}}{128}\sqrt{na^3}, \tag{3.47}$$

while the zeroth order dispersion relation for a BEC is given by $\omega_M = \sqrt{5}\omega_0$ (see above).

In case of axially deformed traps, the pure quadrupole modes are again uneffected by the beyond mean field effects. For the $n_r = 0, l = 2, m = 0$ quadrupole mode however, the coupling to the $n_r = 1, l = 0, m = 0$ monopole mode leads to a frequency shift that is given by [Pit98]

$$\frac{\delta\omega}{\omega} = \frac{63\sqrt{\pi}}{128}\sqrt{na^3}f_{\pm}(\lambda), \tag{3.48}$$

where

$$f_{\pm}(\lambda) = \frac{1}{2} \pm \frac{8 + \lambda^2}{6\sqrt{9\lambda^4 - 16\lambda^2 + 16}} \tag{3.49}$$

and λ is the anisotropy parameter of the trapping potential. The index $\pm$ refers to the lower $(-)$ and higher $(+)$ solution of dispersion law given in equation 3.35. In the limit of very elongated traps ($\lambda \ll 1$) one finds $f_- = 1/6$ and $f_+ = 5/6$. This shows again, that the slow axial mode in an elongated trap is less sensitive to the underlying equation of state than the fast radial mode.

3.3.6 Calculations in the BEC-BCS crossover

In the BEC-BCS crossover the system changes from the strong coupling molecular BEC limit into the weak coupling BCS limit. Because of the presence of the superfluid

order parameter the collective oscillations in the BEC-BCS crossover can be described by the hydrodynamic equations of superfluids.

As the quadrupole mode in an axially symmetric trapping potential directly depends on the underlying equation of state (see equation 3.35), this mode is ideally suited to explore the equation of state in the BEC-BCS crossover [Str04a, Hei04a, Hu04, Com04b, Com04a, Kim04b, Kim04a, Man04, Bul04].

In case of a polytropic equation of state the collective frequencies of a gas confined in a harmonic trap can be directly obtained from the polytropic index γ (see section 3.3.2). Assuming a polytropic equation of state for the gas in the BEC-BCS crossover an effective polytropic index $\bar{\gamma}$ can be obtained by averaging the density distribution of the harmonically trapped sample. This index is defined as the logarithmic derivative of the chemical potential [Hei04a, Bul04, Man04]

$$\bar{\gamma} = \frac{n}{\mu}\frac{\partial \mu}{\partial n}. \tag{3.50}$$

The collective modes can be calculated by replacing γ with the polytropic index $\bar{\gamma}$. Hence the problem of calculating the collective mode frequencies is reduced to the determination of the equation of state.

The effective polytropic index in the BEC-BCS crossover was, for example, calculated by H. Heiselberg [Hei04a] and H. Hu *et al.* [Hu04] from the microscopic mean field description introduced by A. Leggett [Leg80]. The calculated dependence of $\bar{\gamma}$ in the BEC-BCS crossover is shown as the solid line in the inset of figure 3.10 as a function of $1/k_{\mathrm{F}}a$ (data taken from reference [Hu04][9]). The effective polytropic index decreases from $\bar{\gamma} = 1$ in the strong coupling BEC limit ($1/k_{\mathrm{F}}a \gg 1$) to a minimum value of about $\bar{\gamma} = 0.6$ at $1/k_{\mathrm{F}}a \approx -0.5$ before it increases back to $\bar{\gamma} = 2/3$, expected for a superfluid Fermi gas in the BCS limit ($1/k_{\mathrm{F}}a \ll -1$). On resonance ($1/k_{\mathrm{F}}a = 0$) the gas is unitarity limited and $\bar{\gamma} = 2/3$.

From the analysis of the equation of state obtained from a recent quantum Monte Carlo calculation by A Astrakharchik *et al.* [Ast04] (see also section 2.3), N. Manini *et al.* [Man04] derived the predicted effective polytropic index in the BEC-BCS crossover (dashed line in the inset of figure 3.10). Conversely to the predicted monotonic decrease from the BEC limit with $\bar{\gamma} = 1$ to the unitarity limit with $\bar{\gamma} = 2/3$ (see above) the calculation predicts that $\bar{\gamma}$ first increases to values larger than 1 before it decreases to $\bar{\gamma} = 2/3$ obtained in the unitarity limit. This qualitative dependency was also predicted by H. Heiselberg's BEC approximation [Hei04a]. The reason for this different behavior with respect to the predictions by the mean field description of the crossover is found in the different contribution of higher order corrections to the chemical potential. In the mean field model of A. Leggett the corrections add negatively to the chemical potential, while in the BEC approximation they add positively [Hei04a] (see also section 3.3.5).

[9]Note that in reference [Hu04] the effective polytropic index and the collective mode frequencies are determined as a function of $a_{\mathrm{ho}}/N^{1/6}a = 1.70/k_{\mathrm{F}}a$, where k_{F} is the Fermi wave number at the trap center.

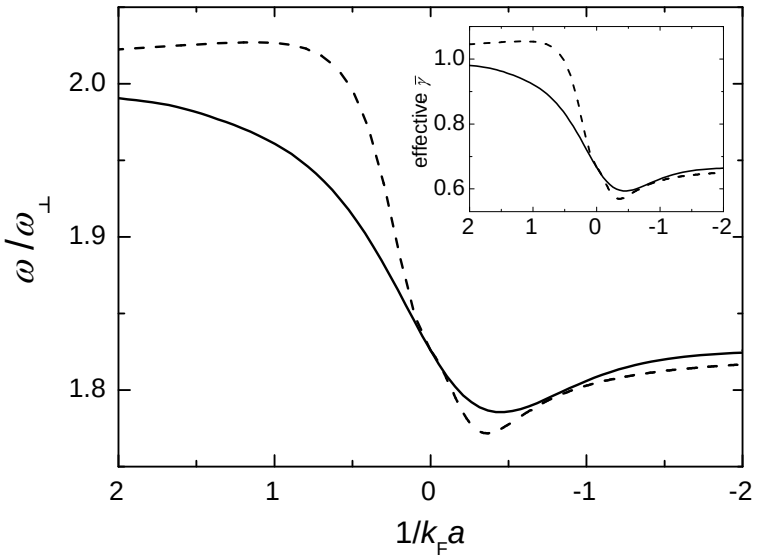

Figure 3.10: Predicted collective mode frequency of the radial quardrupole mode in an elongated trap in the BEC-BCS crossover. The solid line is the prediction of H. Hu *et al.* [Hu04] and is based on the mean field approach introduced by A. Leggett [Leg80]. The dashed line shows the predicted frequency by N. Manini *et al.* [Man04], which is based on the results from a recent Monte Carlo calculation by G. Astrakharchik *et al.* [Ast04]. The inset shows the effective polytropic index $\bar{\gamma}$ in the BEC-BCS crossover. The solid and dashed lines correspond to the prediction by H. Hu [Hu04] and N. Manini [Man04], respectively.

The behavior of the polytropic index in the BEC-BCS crossover directly shows up in the frequency of the radial and axial breathing mode. As an example we show in figure 3.10 the predicted dependency of the radial breathing mode in an elongated trap. The collective mode frequencies in the crossover are calculated from equation 3.37 and the effective polytropic index, which is shown in the inset of figure 3.10. The solid line corresponds to the prediction from the mean field model of reference [Hu04], while the dashed line is derived from a quantum Monte Carlo calculations [Man04]. The mean field description predicts a monotonically decreasing frequency from the dilute molecular BEC limit, with $\omega/\omega_\perp = 2$ towards $\omega/\omega_\perp = \sqrt{10/3}$ expected for a unitarity limited quantum gas [Hei04a, Hu04]. This is contrasted by the prediction from the quantum Monte Carlo calculation that predicts that the collective mode frequency first increases above the BEC limit ($\omega/\omega_\perp > 2$) before it decrease towards the value expected for a unitarity limited quantum gas. This qualitative dependency was previously suggested by S. Stringari [Str04a] and is also found in the calculations by H. Heiselberg [Hei04a].

The discussion of the axial mode frequency is found in section 6.2.4, where we compare the theoretical predictions of reference [Hu04] and [Man04] for the radial and axial breathing mode with our measurements in the BEC-BCS crossover.

Chapter 4

Experimental setup

Our experimental setup is described in detail in the recently published Ph.D. thesis of Selim Jochim [Joc04]. Therefore this chapter describes only briefly the main aspects of our apparatus. Further details are also found in the previous diploma thesis [Joc00, Els00, Mor01, Hen03, Rie04].

All our experiments are carried out in an ultra-high vacuum environment. In a first stage the atoms are trapped and precooled from a Zeeman slowed atomic beam using a standard magneto-optical trap (MOT). In a second stage we transfer the atoms into a far red detuned optical dipole trap. In this optical dipole trap an optical resonator is used to enhance the laser light intensity. This resonator enhanced optical dipole trap creates a deep trapping potential of large volume. It offers ideal conditions to load the atoms into a second far red detuned dipole trap that consists of a single focused Gaussian beam. The power of this dipole trap is precisely controlled and can be varied over more than four orders of magnitude. All the experiments presented in this thesis are performed in this dipole trap. In combination with a large scattering cross section that we obtain by tuning an external magnetic field to values close to the Feshbach resonance this optical dipole trap allows for a very efficient evaporative cooling of the atoms (see chapter 5).

4.1 Vacuum system and atomic beam

Our vacuum apparatus is sketched in figure 4.1. It consists of an oven chamber operating at a pressure of about 10^{-8} mbar and an ultra-high vacuum chamber with a pressure of below 10^{-10} mbar. Both chambers are connected by a 45 cm long slower tube which works as a differential pumping tube. The vacuum in the UHV cell and in the oven chamber is maintained by a 55 l/s and an 20 l/s ion pump, respectively.

The oven consists of a small hollow copper cube ($32 \times 22 \times 22\,\mathrm{mm}^3$) that is filled with about 0.2 g of ^{6}Li enriched to 95%. The gaseous ^{6}Li can escape from a 1 mm hole on the front side of the copper cube. In all our experiments the oven was operated at a temperature of 340° C.

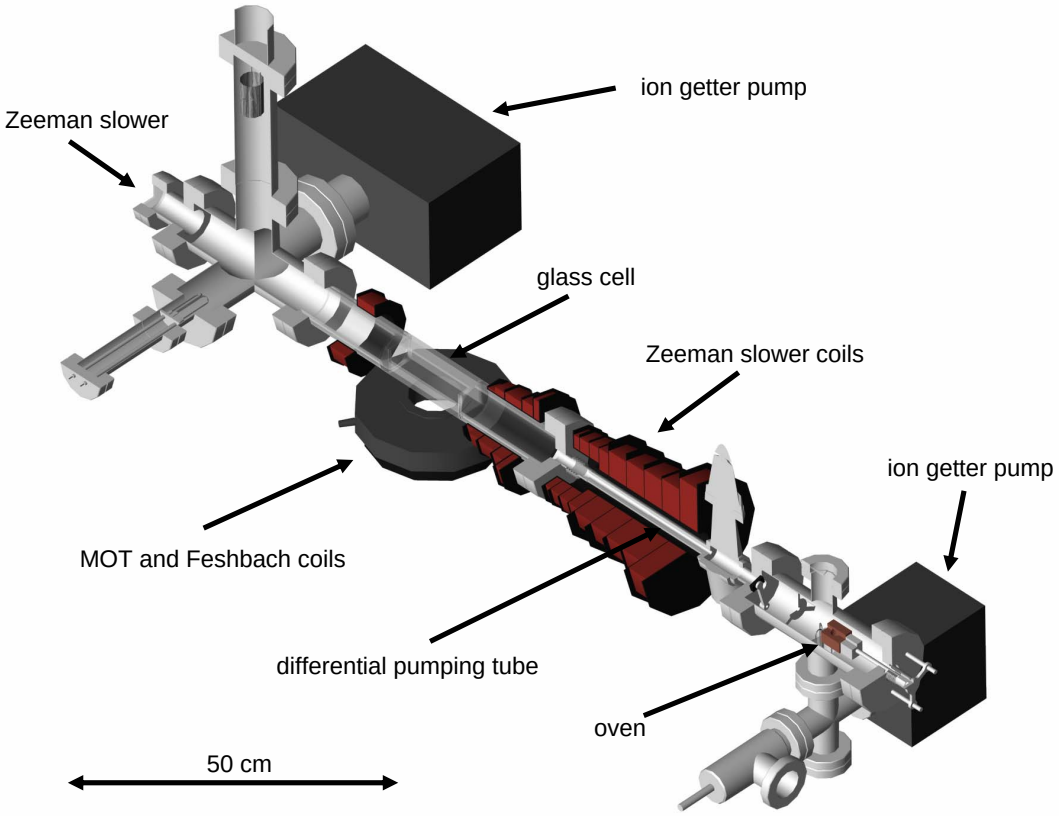

Figure 4.1: Overview of the vacuum chamber. All our experiments are performed inside the glass cell which is surrounded by the MOT and Feshbach coils.

The central part of our UHV chamber consists of a glass cell with the outer dimensions $4 \times 4 \times 12\,\mathrm{cm}^3$. It consists of 4 mm thick high purity fused silica that is not antireflection coated.

Figure 4.1 also shows the 45 cm long Zeeman slower tube. It is set up as a decreasing field Zeeman slower with a designed maximum capture velocity of 600 m/s. The necessary magnetic field is produced by 14 individual magnetic field coils with a maximum field of 560 G. The design of the coils is such that the corresponding magnetic field smoothly matches with the quadrupole field of the MOT [Joc00]. The laser light (see also next section) for the slowing beam enters the chamber through a sapphire viewport which in contrast to glass or quartz is resistent against lithium.

4.2 Magneto-optical trap and Zeeman slower

We load our MOT from the Zeeman slowed atoms. The whole laser system for trapping and cooling the atoms in the MOT is based on diode lasers. The main features of the laser system are described in the following. Further details are found in [Joc00, Rie04, Joc04].

For laser cooling of the ^{6}Li atoms we use the $D2$ line that connects the $2S_{1/2}$ ground state and the $2P_{3/2}$ excited state and has a transition wavelength of about 671 nm. For the operation of the MOT two laser frequencies are needed; one to drive the cooling transition from the $F = 3/2$ ground state and one for the repumping transition from the $F = 1/2$ ground state. For the Zeeman slower we use another laser frequency which is red detuned with respect to the cooling light.

The frequency reference is provided by saturation spectroscopy of ^{7}Li vapor produced in a heat pipe[1] that is operated at about 300° C. One grating stabilized laser is locked by frequency modulation to the ^{7}Li D1 line [Joc00]. This line is 698 MHz and 469 MHz blue detuned with respect to the D2 lines that are used for the cooling and repumping transitions, respectively.

A frequency offset locking technique [Sch99] is used to lock another laser with an offset frequency of 870 MHz to the red. This locking technique enables us to shift the laser frequency over a wide range of about ±100 MHz. To individually adjust the frequency for the cooling and repumping transition we split the laser beam into two beams and individually shift the frequencies by an acousto-optical modulator (AOM). Subsequently both laser frequencies are amplified by injection locked slave laser diodes that each provide an output power of about 20 mW.

The light for the Zeeman slower is obtained from the laser light that is adjusted to the cooling transition. Using an AOM we shift the frequency of this light by 65 MHz to the red. Afterwards the light is used to seed an injection locked slave laser. Experimentally it turned out that the loading rate of the MOT was optimized when the laser diode of this slave laser was modulated at about 40 MHz [Joc04]. The optimum value has to be carefully optimized and leads to loading rates of about 7×10^6 atoms/s when the trapping lasers are tuned about 4-5 natural linewidths[2] to the red of the resonance.

4.3 Optical dipole traps

To trap ultracold atoms and molecules independent of their internal state optical dipole traps are an ideal and versatile tool [Gri00]. These traps rely on the dispersive interaction of the induced atomic dipole moment with the intensity gradient of the laser light field. Because this optical dipole force is conservative it can be derived from a potential. Depending on the phase between the oscillation of the induced dipole and the incident light beam, the atoms experience a force towards the intensity minimum (out-of-phase oscillation) or intensity maximum (in phase osciallation). The corresponding potential is given by [Gri00]

$$U_{\mathrm{dip}}(\mathbf{r}) = -\frac{3\pi c^2}{2\omega_0^3}\left(\frac{\Gamma}{\omega_0 - \omega} + \frac{\Gamma}{\omega_0 + \omega}\right) I(\mathbf{r}), \tag{4.1}$$

[1] A detailed description of the heat pipe is found in [Joc04].

[2] For Lithium the natural linewidth amounts to 5.9 MHz.

and is negative (positve) if the light frequency ω is red (blue) detuned with respect to the atomic resonance frequency ω_0. Here Γ denotes the natural line width of the transition and $I(\mathbf{r})$ is the laser intensity profile. The other relevant quantity is the induced photon scattering rate which usually leads to heating of the particles in the trap. Because the photon scattering rate reduces faster with increasing detuning than the potential depth, it is advantageous to work at large detuning. Therefore, optical dipole traps usually use large detunings and high intensities to keep the scattering rate as low as possible at a certain potential depth [Gri00].

All the experiments presented in this thesis are performed in a optical dipole trap that is created by a single focused Gaussian beam. To efficiently load this dipole trap we use a second deep, large volume standing wave dipole trap. Both dipole traps employ laser light that is far red detuned with respect to the resonance frequency and thus provide a potential minimum at the intensity maximum.

4.3.1 Resonator enhanced optical dipole trap

This dipole trap is designed to allow a high transfer efficiency from the MOT into the dipole trap. The trap is based on the enhancement of the optical power density of a laser beam in an optical resonator. The resonator enhanced dipole trap fulfills the two main criteria: A trap depth that exceeds the mean kinetic energy of the atoms in the MOT and a reasonable overlap between the spread of the atoms in the MOT and the size of the dipole trap. A detailed description of this trap is found in [Els00, Mos01, Mor01, Joc04].

The resonator dipole trap features the 150 fold enhancement of an initially $\sim$1 W laser light at a wavelength of 1064 nm. This laser light is obtained from an ultrastable diode pumped Nd:YAG laser that emits 2 W (Mephisto 2000 by Innolight). The resonator geometry is a near confocal geometry with a distance between the two mirrors of 15.3 cm and a mirror curvature of 15 cm. The resulting waist is about 160 μm and the Rayleigh range stretches out to about 75 mm from the center of the resonator. Both resonator mirrors are outside the vacuum chamber. To minimize the optical losses at the glass cell, the symmetry axis of the resonator is aligned in Brewster's angle. A Hänsch Couillaud lock is employed to stabilize the resonator [Hän80]. To control and stabilize the intensity of the light in the resonator we monitor the transmitted light with a photodiode. The measured signal is used in a closed loop feedback system to stabilize the intensity using an acousto-optical modulator [Joc04].

The standing wave creates potentials with a maximum potential depth of about 1 mK. The separation between the individual potential wells is fixed by the wavelength of the laser and amounts to 532 nm. From the MOT we load[3] approximately 1500 individual wells with typically about 8×10^6 atoms.

[3]The exact timings of the transfer are found in [Joc04].

4.3.2 Focused beam dipole trap

This dipole trap is created by simply focusing a far red detuned laser beam with a Gaussian intensity profile. From the intensity distribution and equation 4.1 the trapping potential can be calculated. In the resulting cigar-shaped trapping potential the ratio between the axial ($\omega_\parallel$) and radial trap frequency ($\omega_\perp$) is fixed by the ratio between the waist of the focused beam w_0 and the emitted laser wavelength λ [Gri00]

$$\frac{\omega_\parallel}{\omega_\perp} = \sqrt{2}\pi\frac{w_0}{\lambda}. \tag{4.2}$$

In our case the laser light for the dipole trap is provided by a 15 W single mode Yb:YAG laser that emits at $\lambda = 1030\,\mathrm{nm}$ (VersaDisk by ELS). In order to have a sufficient axial confinement we designed the beam waist to be about $w_0 = 24\,\mu\mathrm{m}$. This beam waist results in a trap depth of about $U_{\mathrm{at}}/k_{\mathrm{B}} = 0.070\,\mu\mathrm{K} \times P/\mathrm{mW}$ as a function of the laser power P. Due to the two times larger polarizability of the $^6Li_2$ dimers the trap depth for the molecules is $U_{\mathrm{mol}} = 2U_{\mathrm{at}}$ [Joc03b]. The above scaling of the trap depth with the laser power will be used throughout this thesis. The calculated radial and axial trap frequencies are given by [Gri00]

$$\omega_\perp/2\pi = \frac{1}{\pi w_0}\sqrt{\frac{U_{\mathrm{at}}}{m}} = 130\,\mathrm{Hz} \times \sqrt{P/\,\mathrm{mW}} \tag{4.3}$$

$$\omega_\parallel/2\pi = \frac{\lambda}{\sqrt{2}\pi^2 w_0^2}\sqrt{\frac{U_{\mathrm{at}}}{m}} = 1.3\,\mathrm{Hz} \times \sqrt{P/\,\mathrm{mW}}. \tag{4.4}$$

Thus atoms and molecules have the same trap frequency. The maximum laser power of 10.5 W provides a trap depth of $U_{\mathrm{at}} \approx k_{\mathrm{B}} \times 750\,\mu\mathrm{K}$ with radial and axial trap frequencies of about $\omega_\perp/2\pi = 13\,\mathrm{kHz}$ and $\omega_\parallel/2\pi = 130\,\mathrm{Hz}$, respectively.

Setup

Our optical setup is shown in figure 4.2. The focused beam trap is installed under a relative angle of about 10° with respect the axis of the resonator enhanced dipole trap. This angle is the minimal attainable in our setup and is chosen to ensure a maximum spatial overlap with the resonator enhanced dipole trap. Therefore the tightly focused beam crosses our glass cell under an angle of about 46° which results in an astigmatism of several hundred micrometers. We compensate for this astigmatism by inserting a fused silica glass plate into the expanding beam (see figure 4.2). In a test setup we measured the beam waist to be about 23 μm and 25 μm in the vertical and horizontal plane, respectively [Rie04].

The main features of our dipole trap is the ability to precisely control the laser intensity over more than four orders of magnitude. This precise control of the optical trap depth is the key for a successful evaporative cooling of particles starting from almost 100 μK down to tens of nanokelvins. To control the trap laser power we measure

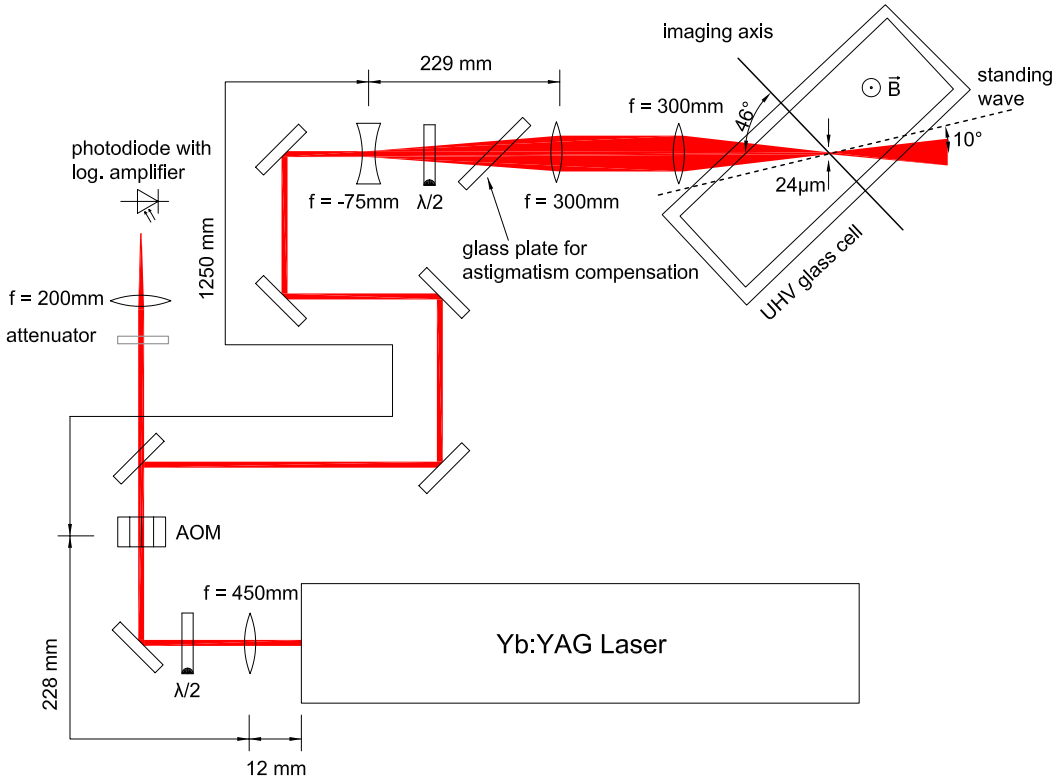

Figure 4.2: Setup of the focused beam dipole trap. The axis of the standing wave trap lies in the shown plane.

the laser intensity using a photodiode and employ a servo loop to stabilize the intensity using an AOM. To measure the photodiode current precisely and reliable over this large range we use a logarithmic amplifier that converts the the photodiode current into a logarithmic voltage[4].

Magnetic confinement

At low trapping laser power the trapping potential is no longer determined solely by the light intensity of the trapping laser but also by residual magnetic field gradients and gravity. These effects influence especially the weak axial confinement of the dipole trap.

In particular the large offset magnetic field that we apply to tune the interactions in our gas (see section 4.4) has a field curvature B'' that gives rise to an additional trapping potential

$$U_{\mathrm{mag}} = -\frac{1}{2}\mu B'' x^2 \tag{4.5}$$

in the axial direction x. In our case the magnetic moment μ of the atoms at high mag-

[4]Further details are found in [Joc04].

netic field is given by $\mu = \mu_B$. From the magnetic trapping potential the corresponding trap frequency is calculated to be

$$\omega_{mag} = \sqrt{\frac{\mu_B B''}{m}}. \tag{4.6}$$

The calculated curvature of the magnetic field in the horizontal plane is $B'' = -0.0255\,\mathrm{cm}^{-2} \times B$ and thus the magnetic trap frequency at a field of $B = 1000\,\mathrm{G}$ is about $\omega_{mag}/2\pi = 24.5\,\mathrm{Hz}$.

At very low laser power, gravity begins to tilt the trap significantly. We compensate for this by applying a magnetic field gradient that is on the order of one G/cm. This magnetic field gradient is experimentally optimized by minimizing the trap loss at very low trap depth.

Measured trap frequencies

Because the optical and magnetic trap are centered in the horizontal plane, the optical and magnetic trap frequencies can be added quadratically. Thus the resulting trap frequency is given by

$$\omega_{\parallel} = \sqrt{\omega_{mag}^2 + \omega_{opt}^2}. \tag{4.7}$$

To measure the axial and radial trap frequency we excited the dipole mode and measure the collective frequency as explained in detail in section 6.2. In a harmonic potential this collective mode oscillates with a frequency that corresponds to the trap frequency (see also section 3.3). From the axial dipole mode measurements performed at different magnetic field values and constant trapping laser power of $P = 34\,\mathrm{mW}$ we derive the following general dependency of the axial trap frequency on the magnetic field and laser power

$$\omega_z/2\pi = \sqrt{601(4)\,B/\mathrm{kG} + 0.3(1)\,P/\mathrm{mW}}\,\mathrm{Hz}, \tag{4.8}$$

where the values in brackets denote the error that we obtain from the fit. Measurements of the radial dipole mode at different laser intensity yield to [Rie04]

$$\omega_r/2\pi = 128(1)\mathrm{Hz} \times \sqrt{P/\mathrm{mW}}, \tag{4.9}$$

which is in good agreement with the calculated radial trap frequency (see equation 4.3)[5]. In the following we denote measured axial and radial trap frequencies by ω_z and ω_r, respectively and calculated trap frequencies by $\omega_{\parallel}$ and $\omega_{\perp}$, respectively.

[5] A comparison of equation 4.8 with equation 4.4, however, shows that the optical contribution in the axial direction is below the calculated value. The difference between the measured and calculated values might be due to a slight misalignment between the optical and magnetic trap in the horizontal plane. At high trapping laser powers equation 4.8 might therefore underestimate the axial trapping frequency. For trap laser powers below 100 mW, the difference is below 12%.

The expression for the axial trap frequency (equation 4.8) shows, that for trapping laser powers below $P \approx 50\,\mathrm{mW}$ the optical potential is much weaker than the magnetic field potential. In this case the dominant magnetic confinement provides a perfectly harmonic axial trapping potential.

Note that the measurements of the axial and radial dipole mode were performed during our investigation of the axial and radial collective mode frequencies in the BEC-BCS crossover (see section 6.2). In the Ph.D. thesis of Selim Jochim [Joc04] and in our publications [Joc03a, Bar04b] slightly different trap frequencies are given. The quoted values always correspond to our best knowledge of the system at the time the measurements were taken and we attribute the small changes in the numbers to tiny drifts in the alignment of the trap.

Transfer of the atoms from the standing wave

The timing for the transfer between the resonator enhanced dipole trap and the focused beam dipole trap was experimentally optimized. We ramp up the power in the focused beam trap within 2 s after switching off the MOT. After 1 s, we turn off the standing wave trap in a 1-s ramp. During the transfer of the atoms we apply a magnetic field of 300 G to achieve efficient collisional loading. It turned out that the exact timing is not critical and we typically load 3×10^6 atoms into the single beam dipole trap. However, test experiments where we tried to load the focused beam directly from the MOT resulted in a much lower number of atoms and showed that the intermediate step of loading the standing wave is crucial.

4.4 High magnetic field coils and auxiliary coils

In order to tune the scattering properties of our ^{6}Li gas over the full range of interest (see section 3.2) we use a pair of magnetic field coils that creates magnetic fields of up to 1470 G at a current of 200 A. The main features of our design are a small size, an efficient cooling and small Eddy currents. These requirements are met by using flat cooper wire from which we form two individual coils with a small gap between them. In the gap the cooling water flows. It is in contact with every winding and thus leads to an efficient cooling. Finally the water proof housing is made from PVC and avoids Eddy currents and in principle enables fast switching of the magnetic field. The technical detail of the coils are found in [Joc04, Hen03]. Reference [Joc04] also provides the technical details of our current stabilization which results in a stability of ±3 mA or 22 mG. This high stability is of particular importance for our radio-frequency spectroscopy measurements that are presented in section 6.3. Radio frequency spectroscopy of atoms is also used to calibrate our magnetic field as explained in section 6.3.1.

The space between the mount for the optical resonator and the large magnetic field coils contains a second pair of small coils. In contrast to the big coils these coils are not

water cooled and can be operates continuously with up to 500 mA. This results in a homogenous field of about 25 G or alternatively if operated in anti-Helmholtz configuration in a field gradient of about 8.5 G/cm. Moreover these coils can for short times < 1 s produce homogenous fields exceeding 300 G (or alternatively gradients > 100 G/cm).

In our experiments these coils are used in anti-Helmholtz configuration to compress the MOT during the transfer into the standing wave, to compensate for gravity and for residual magnetic field gradients in the vertical direction. Moreover these coils are used to excite the radial and axial dipole mode as described in section 6.2.1.

4.5 Diagnostic tools

To record the atomic and molecular number and density we employ two diagnostic tools; a calibrated photodiode, and a high field state selective absorption imaging system.

4.5.1 Fluorescence measurements

An important parameter to know in our experiments is the total number of particles. The simplest and most robust way to measure this quantity is to recapture the particles into the MOT and to measure their fluorescence.

We use a calibrated photodiode to detect the light that is scattered into a solid angle Ω. In combination with the rate of photons γ_{PD} hitting the photodiode and the photon scattering rate of the atoms in our MOT γ, the total number of atoms is determined by

$$N = \frac{\gamma_{\mathrm{PD}}}{\gamma\Omega}. \tag{4.10}$$

In our case the atom number calibration yields [Joc04]

$$N = 2.85 \times 10^7 \,\mathrm{atoms/V}, \tag{4.11}$$

with a relative uncertainty of about 50%.

Detection of molecules

To detect the number of molecules at a given magnetic field, we employ a technique that relies on the dissociation of the molecules by ramping the magnetic field across the Feshbach resonance [Reg03b]. We typically use a ramp speed of +6 G/ms to a magnetic field of 1200 G. This ramp shifts the bound level above the continuum and the molecules quickly dissociate. After this dissociation process we ramp the magnetic field down to zero with a ramp speed of −12 G/ms. This fast ramp speed avoids the molecule formation when crossing the Feshbach resonance and the region where $a > 0$. In addition to avoid molecule formation we heat the sample by abruptly turning on the full trapping laser power. This step turned out to be crucial as even while all molecules

might be dissociated during the ramp across the resonance, molecules could be formed again from a cold sample during the ramp back to zero magnetic field before detection. Care was also taken, that the heating of the sample did not lead to evaporative loss. This was done by minimizing the time for the magnetic field ramps so that the atoms would spend only negligible time in fields where the scattering length is large. After reaching zero magnetic field, we recapture the atoms in the MOT and measure the atom number as described above.

This measurement provides the total number of atoms $N_{\mathrm{tot}} = 2N_{\mathrm{mol}} + N_{\mathrm{at}}$, where N_{mol} and N_{at} denote the number of molecules and atoms, respectively. To obtain N_{at} we repeat the same measurement without the Feshbach dissociation ramp by immediately ramping down to zero magnetic field from the initial magnetic field. This ramp down to zero magnetic field increases the binding energy to a large value of about $k_{\mathrm{B}} \times 80\,\mathrm{mK}$ and the molecules are lost without leading to any fluorescence light in the MOT. The number of molecules is then obtained by taking the difference in atom numbers measured in the two subsequent runs with and without the dissociating Feshbach ramp.

4.5.2 Absorption imaging

To image our atoms and weakly bound molecules we use absorption images. The basic idea of this well established technique is to image the intensity profile of a resonant laser beam that has been partially absorbed in the atomic (or molecular) cloud onto a CCD camera [Ket99].

Assuming a laser beam travelling in the z direction, the column density of the particles is $\tilde{n}(x, y) = \int n(x, y, z)\, dz$, where $n(x, y, z)$ is the density of the particles. From the relative transmission and the absorption cross section σ the column density can be obtained by [Ket99]

$$\tilde{n}(x, y) = -\frac{1}{\sigma} \ln \frac{I}{I_0}. \tag{4.12}$$

High field imaging

To image the particles at high magnetic field in the vicinity of the Feshbach resonance we use a grating stabilized diode laser that is locked by a frequency offset locking technique to our reference laser. The setup enables us to tune the frequency of the imaging laser over a wide range of $\pm 1.8\,\mathrm{GHz}$. A detailed description of the setup is given in [Rie04].

To image the particles we use a closed σ^--transition from the $2S_{1/2}$ ground state to the $2P_{3/2}$ excited state ($|2S_{1/2}, m_J = -1/2, m_I\rangle \rightarrow |2P_{3/2}, m_J = -3/2, m_I\rangle$). Because the transition frequency depends on the orientation of the nuclear spin ($m_I = -1, 0, 1$), the imaging at high magnetic field also offers a state selective detection (see also appendix A). The magnetic moment of the excited and ground state amounts to $2\mu_{\mathrm{B}}$ and μ_{B}, respectively and therefore the transition frequency tunes with $-\mu_{\mathrm{B}} \approx -1.4\,\mathrm{MHz/G}$.

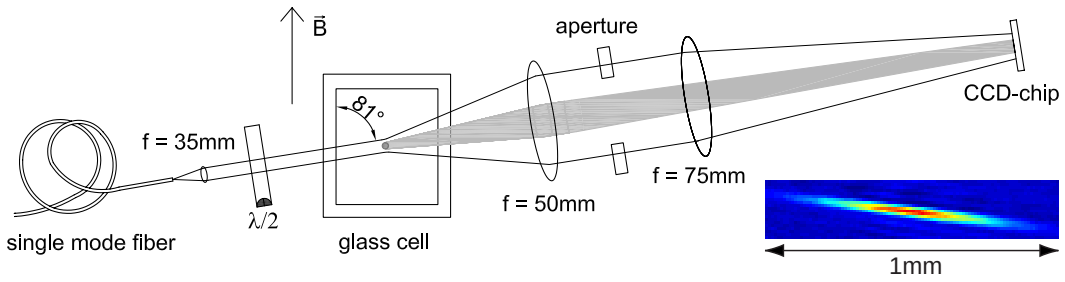

Figure 4.3: Optical setup of our imaging system. The total magnification of the system is 1.5. The image in the right corner shows a typical absorption image of the particles.

The magnetic field direction defines the quantization axis of the system. In our optical setup the imaging beam has an angle of $\alpha = 81°$ with respect to the quantization axis (see also figure 4.3). The polarization axis of our linear polarized imaging beam is perpendicular with respect to the direction of the magnetic field. For our typical imaging parameters with $I/I_0 \geq 0.5$ and our large angle of $\alpha = 81°$ the transmitted intensity is well approximated (error $< 1\%$) by the case of $\alpha = 90°$ [Joc04][6]. In this case, the absorption cross section is given by $\sigma = \sigma_0/2$, where $\sigma_0 = 3\lambda^2/2\pi$ is the absorption cross section for a two-level system.

Optical setup

The experimental setup of our imaging system is shown in figure 4.3. After the polarization maintaining fiber the beam is collimated by a lens ($f = 35\,\text{mm}$) to a diameter of about 0.8 mm. The beam power of ~0.3 mW corresponds to an intensity of about 0.6 mW/cm^2. This intensity is below the saturation intensity of ^{6}Li which amounts to 2.5 mW/cm^2. The imaging optics consist of two achromatic doublet lenses ($f = 50\,\text{mm}$ and $f = 75\,\text{mm}$). In combination with an maximum aperture defined by an iris diaphragm the calculated diffraction limit is 3.4 μm. In the experiment the imaging resolution is limited to about 10 μm due to lens abberations. The magnification of 1.5 was experimentally tested and leads in combination with the 7.5 μm pixel spacing of the CCD chip to a corresponding "pixel size" of 5 μm.

Image processing

Most of the measurements presented in this this thesis are obtained by in-situ imaging the cloud at high magnetic field. This technique is in favor over time-of-flight images because in our trap the axial magnetic confinement cannot be switched off without switching off the magnetic field. Therefore by switching off the optical dipole trap, the cloud is only released radially and quantitative information is hard to extract.

[6]The calculation of the transmitted intensity for an arbitrary angle α is found in the Ph.D. thesis of M. Gehm [Geh03a].

A typical in-situ image of the particles in the focused beam dipole trap is shown in the inset of figure 4.3. The 200 Pixel wide image represents a 1 mm range. While the radial cloud size is only a few pixels wide and cannot be accurately resolved by our imaging optics, the axial cloud size of typically 100 μm can be accurately measured. For the analysis of the axial density profiles we integrate the images in the vertical direction. To obtain the actual axial cloud size the viewing angle of 46° ± 1° between the axial trap direction and the imaging direction in the horizontal plane have to be taken into account. The resulting scaling factor is $1/\sin 46° = 1.39(2)$.

In principle the absorption images allow also the determination of the total particle number [Joc04]. In our case, however, the number calculated from the images is 4-8 times smaller than the number obtained from the fluorescence method. Because the fluorescence method is very robust and such low atom numbers are inconsistent with our measurements [Joc04], we calibrate the absorption images with the atom number obtained from the fluorescence measurements. The discrepancy between the two methods will be systematically investigated in the context of setting up a further imaging system (see chapter 7).

Imaging of weakly bound molecules

In the vicinity of the Feshbach resonance the binding energy of the molecules is extremely small. In this regime the molecules can be directly imaged by the same light that would be suited to image the atoms at the same magnetic field. This is possible as long as the shift of the transition frequency is smaller than the linewidth of the transition [Zwi03].

For ^{6}Li the natural linewidth amounts to $\Gamma/2\pi = 5.9$ MHz. To estimate the shift we note that due to the small binding energies the shift of the ground state is negligible[7]. The significant contribution stems from the shift of the excited state. The shift of the excited state can be estimated from the long range dipole potential that is given by [Wei99]

$$V_{\mathrm{exc}}(r) = f\hbar\Gamma\left(\frac{\lambda}{2\pi r}\right)^3, \tag{4.13}$$

where f is a constant on the order of unity and λ the wavenlength of the atomic transition. Assuming that the molecules absorb the light predominantly at the outer turning point R, the estimation shows that as long as the size of the molecules R is larger than ~100 nm the shift is below 1 MHz and the molecules can be imaged as if they were free atoms. Assuming a molecular size on the order of the atomic scattering length this corresponds to a magnetic field of about 720 G and is consistent with our observations.

[7] For example at 720 G the binding energy is about $k_{\mathrm{B}} \times 8\,\mu\mathrm{K} \approx h \times 170$ kHz.

Chapter 5

Bose-Einstein condensation of molecules

By the middle of the year 2003 a number of groups succeeded in the creation of ultracold weakly bound dimers that were formed by fermionic ^{40}K [Reg03b] atoms or as in our case from ^{6}Li atoms [Cub03, Str03, Joc03b].

Most of the groups employed an adiabatic magnetic field ramp across the Feshbach resonance to create the weakly bound molecules. Our approach however utilizes the enhanced three body recombination to dimers in the vicinity of the Feshbach resonance. The recombination leads to the formation of the very weakly bound molecular state that is associated with the Feshbach resonance. Because the binding energy can be tuned by the external magnetic field it can be chosen such that it is smaller than the trap depth to avoid loss of the dimers and at the same time is larger than the thermal energy of the sample so that the atom-molecule equilibrium favors the molecular state [Joc04].

Our experimental findings that the molecules can be formed efficiently from a thermal gas of fermionic atoms and the high stability of these molecules against inelastic decay are described in [Joc03b] and in the Ph.D. thesis of Selim Jochim [Joc04]. They immediately suggested that such molecules would be ideal candidates to form a molecular Bose-Einstein condensate [Joc03b, Joc03a]. This chapter briefly describes the Bose-Einstein condensation of more than 10^5 Li_2 molecules in our optical trap. Further details are found in [Joc03a, Joc04].

Our Bose-Einstein condensate is produced by evaporative cooling of an optically trapped ^{6}Li spin mixture of the two lowest spin states. We perform evaporative cooling at a constant magnetic field below the broad Feshbach resonance at 834 G. During the cooling process atoms are efficiently converted into dimers as the thermal energy of the atoms drops below the binding energy of the weakly bound molecular level. Further cooling of the sample results in the typical bimodal density distributions of the condensed and non-condensed particles that we observe by in-situ imaging of the molecules at high magnetic field. The long lifetime of more than 40 s allows us to produce pure molecular condensates with no noticeable thermal component.

Within a short time a number of groups were able to produce molecular condensates of fermionic ^{6}Li [Joc03a, Zwi03, Bou04, Hul04] and ^{40}K [Gre03]. The ability to tune the binding energy in these molecular condensates makes them ideally suited to experimentally investigate the crossover from a molecular BEC into a strongly interacting Fermi gas [Bar04b, Bou04, Reg04b, Zwi04, Kin04a, Bar04a, Chi04a, Gre04, Kin04b, Kin05]. Our experiments in this BEC-BCS crossover are described in detail in chapter 6.

5.1 Evaporation towards a molecular BEC

We perform evaporative cooling in the single beam focused dipole trap that is described in section 4.3.2. This trap is loaded from the resonator enhanced dipole trap which itself is loaded from the magneto-optical trap. This two-stage loading process of the focused beam trap results in typically 2×10^6 atoms at a temperature of about $80\,\mu$K. At the initial laser power of 10.5 W, the trap depth is $U_{\mathrm{at}}/k_{\mathrm{B}} \approx 750\,\mu$K and the peak number density and peak phase space density are calculated to be about $10^{14}\,\mathrm{cm}^{-3}$ and $\sim 5\times10^{-3}$, respectively. Together with the large elastic collision rate of about $5\times10^4\,\mathrm{s}^{-1}$ these starting conditions are ideally suited to perform evaporative cooling. We therefore ramp down the optical trapping potential in an exponential ramp with a $1/e$ time in the range of 0.23 and 0.46 s. During the evaporative cooling process the interactions are tuned by applying a constant external magnetic field. Tuning the magnetic field either above or below the Feshbach resonance at 834 G results in strikingly different results as described in the following.

5.1.1 Evaporation above the Feshbach resonance

In a fist series of experiments we performed evaporative cooling at a magnetic field of 1176 G. Here the interactions are described by a large, negative scattering length of about $-3000\,a_0$ and no weakly bound molecular state exists. The evaporation proceeds in a very similar way as that described in [Gra02, O'H02a]. The measured atom number N first follows a scaling law with the laser power P that is described by $N/N_0 = (P/P_0)^\alpha$ [O'H01] where $\alpha \approx 0.24$. In this regime the temperature of the gas is typically a factor of 10 below the trap depth [O'H01] and the elastic collision rate stays well above $10^4\,\mathrm{s}^{-1}$.

The crossover to Fermi degeneracy where the thermal energy $k_{\mathrm{B}}T$ reaches the Fermi energy E_{F} takes place at $P \approx 500\,$mW. Here the trap depth is $U_{\mathrm{at}}/k_{\mathrm{B}} \approx 35\,\mu$K. By further decreasing the trapping laser power, the axial confinement becomes dominated by the magnetic potential (see section 4.3.2). For small trapping laser powers ($P < 50\,$mW) the optical potential is much weaker than the magnetic field potential (see also 4.3.2). Consequently the axial confinement is determined by the magnetic field and the mean trap frequency $\bar{\omega} = (\omega_r^2\omega_z)^{1/3}$ scales as $\bar{\omega} \propto E_{\mathrm{F}} \propto U_{\mathrm{at}}^{1/3} \propto P^{1/3}$. Therefore the trap depth ($U_{\mathrm{at}} \propto P$) decreases faster than the Fermi energy and a thresh-

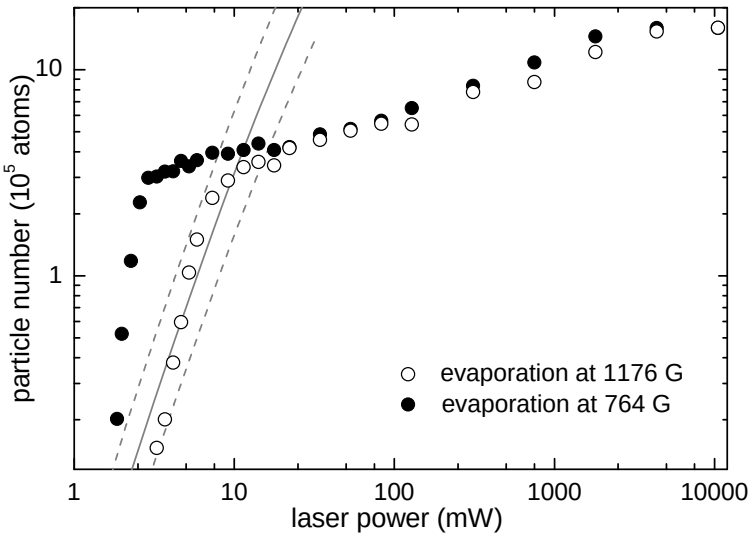

Figure 5.1: Evaporative cooling on both sides of the Feshbach resonance. We measure the number of trapped particles (the number of all atoms that are free or bound in molecules) as a function of the laser power P at the end of an exponential ramp $P(t) = 10.5\,\mathrm{W}\,\exp(-t/230\,\mathrm{ms})$. The trap depth for atoms is $U_{\mathrm{at}}/k_{\mathrm{B}} = P \times 70\,\mu\mathrm{K/W}$, whereas for molecules it is two times larger ($U_{\mathrm{mol}} = 2U_{\mathrm{at}}$). The measurements taken at 1176 G with $a < 0$ (○) show the spilling of a degenerate Fermi gas when the trap depth reaches the Fermi energy. The solid line shows the maximum of trapped atoms in a two-component Fermi gas according to a numerical calculation of the number of quantum states in our trap. The dashed lines indicate the corresponding uncertainty range due to the limited knowledge of the experimental parameters. The measurement at 764 G with $a > 0$ (•) exhibit a striking increase of the trapped particle number at low laser power, which is due to the formation of molecules.

old occurs when E_{F} reaches U_{at} and the trap is filled to the "rim". Further decreasing the trapping laser power then leads to a spilling of atoms out of the trap and thus a rapid decrease of the number of trapped atoms.

Our experimental data are presented in figure 5.1 (open symbols) and clearly show this spilling effect for a laser power $P < 10\,\mathrm{mW}$, which corresponds to a trap depth of $U_{\mathrm{at}}/k_{\mathrm{B}} < 720\,\mathrm{nK}$. Modelling the spilling curves provides an upper bound for the temperature of $k_{\mathrm{B}}T < 0.2\,E_{\mathrm{F}}$. In the regime of a completely filled shallow trap, the number of atoms in the two component spin mixture is given by two times the number of quantum states in the trap. A numerical calculation (dashed lines in figure 5.1) confirms this interpretation of our data.

5.1.2 Evaporation below the Feshbach resonance

We perform the same evaporative cooling procedure at a magnetic field of 764 G. Here a weakly bound molecular state exists and the scattering length is large and positive ($a \approx 4500\,a_0$). The binding energy of the dimers is calculated to be about $1.4\,\mu\mathrm{K}$. Com-

pared to the scattering length at 1176 G the value is on the same order of magnitude but has opposite sign.

In this regime atoms are converted into molecules when the temperature of the gas drops below the binding energy [Joc03b, Joc04]. To detect the molecules we dissociate them into atoms and recapture them in the MOT as described in section 4.5.1. The number of atoms that we measure after the dissociation process thus corresponds to the number of free atoms together with the number of atoms having formed molecules. It should be noted, that the heating of the sample by abruptly turning on the full trap laser power was also used during the measurements performed above the resonance.

Evaporation at 764 G initially processes in a very similar way as for the magnetic field above the resonance. However, below $P = 10\,\mathrm{mW}$ the measured atom number (filled symbols in figure 5.1) show a strikingly different behavior in comparison with the case of the degenerate Fermi gas. Down to a power level of $P = 3\,\mathrm{mW}$ ($U_{\mathrm{mol}}/k_{\mathrm{B}} \approx 420\,\mathrm{nK}$) the trap holds almost all particles and contains up to 20 times more atoms than it would be possible for fermions. Hence, the trapped sample can no longer be an atomic Fermi gas. The trap is filled with bosonic molecules in the weakly bound state. The lifetime of the molecular ensemble for which we measure about 20 s at a fixed trap depth of $U_{\mathrm{mol}}/k_{\mathrm{B}} \approx 500\,\mathrm{nK}$, exceeds the time scale of elastic collisions ($\sim 100\,\mu\mathrm{s}$) by several orders of magnitude. This highlights the fact that the molecular cloud exists in a thermal equilibrium state.

Formation of molecules during the evaporation

The formation of molecules during the evaporative cooling process can be understood in terms of a chemical atom-molecule equilibrium [Chi04b, Kok04]. Exothermal three-body recombination processes compete with dissociation by endothermal two-body processes. When the gas is cooled down, the equilibrium shifts to an increasing fraction of molecules. Because atom-atom, atom-molecule and molecule-molecule collisions have comparable scattering cross section near the resonance [Pet04] (see also section 3.2.4), evaporation continues at about the same speed. In the final stage of cooling, all the relevant energies, such as the thermal energy $k_{\mathrm{B}}T$ an the trap depth U_{at} and U_{mol}, are far below the binding energy $E = \hbar/ma^2$, so that in chemical equilibrium one is left with an essentially pure sample of molecules. This picture is confirmed by our radio-frequency spectroscopy measurements of the weakly bound molecules that we present in section 6.3.

Formation of a molecular BEC

The observation that a large number of $N_{\mathrm{mol}} \approx 1.5 \times 10^5$ molecules are confined in our very shallow, only 420 nK deep trap under thermal equilibrium conditions already shows that a molecular BEC is formed. The trap offers about 10 times more quantum states for dimers as compared to the case of atoms discussed before. A factor of 8 comes from the fact that the trap depth for the molecules is twice as large as

for the atoms and another factor of 1.24 is due to the lower magnetic confinement at 764 G. As we observe a factor of ∼20 more particles than for a degenerate atomic Fermi gas, the molecular gas is necessarily quantum degenerate. Because of the high elastic collision rates, which stay well above $10^3\,\mathrm{s}^{-1}$ even for very shallow traps, the sample is also thermalized. The temperature then must be a small fraction of the trap depth. According to standard evaporation theory [O'H01], we can typically assume $T \approx 0.1 U_{\mathrm{mol}}/k_{\mathrm{B}} \approx 40 - 50\,\mathrm{nK}$. This is well below the critical temperature for Bose-Einstein condensation, for which we calculate $T_{\mathrm{c}} = k_{\mathrm{B}}^{-1}\hbar\bar{\omega}(N_{\mathrm{mol}}/1.202)^{1/3} \approx 280\,\mathrm{nK}$ (see equation 2.7). As the condensate fraction is given by approximately $1 - (T/T_{\mathrm{c}})^3$, these arguments show that the molecular BEC must be almost pure.

5.2 Properties of the molecular BEC

In first experiments with the molecular BEC we studied its properties without imaging. These experiments allowed us to demonstrate the magnetic field dependent mean field potential and perform the first measurements of the collective oscillation in a molecular BEC. They are described in detail in [Joc03a, Joc04].

In this section we summarize the properties of the molecular BEC that are of particular relevance for our experiments in the BEC-BCS crossover, which we present in chapter 6.

5.2.1 Condensate fraction and temperature

To measure the condensate fraction, we adiabatically reduce the magnetic field from our production field of 764 G to 676 G in a 200 ms linear ramp after completion of the evaporation ramp. This reduces the scattering length a_{mol} and thus increases the visibility of the characteristic bimodal distribution. Based on the prediction $a_{\mathrm{mol}} = 0.6a$ [Pet04], the molecular scattering length at $B = 676\,\mathrm{G}$ is about $a_{\mathrm{mol}} = 700\,a_0$.

In figure 5.2 (a) we show a bimodal density profile observed in this way with $N_{\mathrm{mol}} = N/2 = 4 \times 10^5$ molecules remaining at a final laser power of 28 mW. A Gaussian fit to the thermal wings (dashed line) yields a temperature of $T = 430\,\mathrm{nK}$, which is a factor 9 below the calculated trap depth of about $U_{\mathrm{mol}} = 3.6\,\mu\mathrm{K}$. The calculated critical temperature for an ideal gas is $T_{\mathrm{c}} = k_{\mathrm{B}}^{-1}\hbar\bar{\omega}(N_{\mathrm{mol}}/1.202)^{1/3} \approx 640\,\mathrm{nK}$. Due to the interactions in our molecular BEC one expects a down shift of the critical temperature [Gio96] (see also section 2.1.2). The relevant quantity is the ratio

$$\eta = \frac{\mu(T=0)}{k_{\mathrm{B}}T_{\mathrm{c}}^0} \approx 1.57\left(N^{1/6}\frac{a}{a_{\mathrm{ho}}}\right)^{2/5}, \tag{5.1}$$

which in our case amounts to $\eta = 0.74$ and results in a predicted down shift of the critical temperature of about 20 % (see equation 2.25). However for large values of η on the order of one the critical temperature is difficult to get the shift right. A numerical calculation of S. Kokkelmans for our trap parameters and atom numbers yields a down

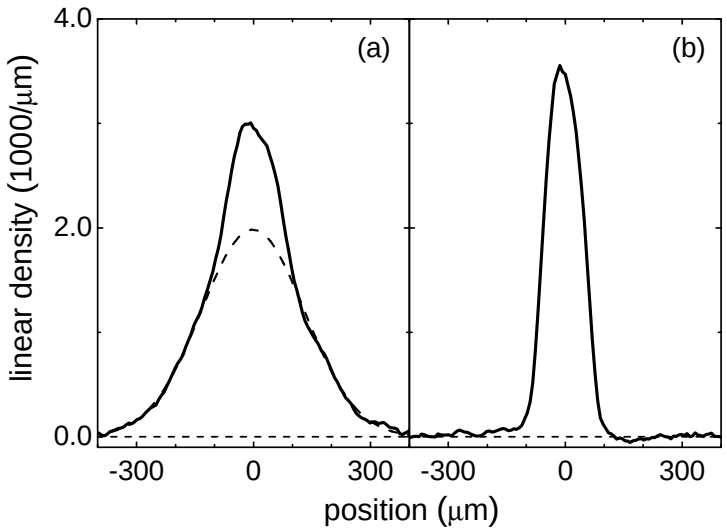

Figure 5.2: Axial density profiles of a partially condensed (a) and fully condensed (b) molecular cloud. The profiles are derived from averaging seven in situ images taken at a magnetic field of B=676 G after evaporation at the production field of 764 G. (a) When the evaporation ramp is stopped at a final laser power of 28 mW, the characteristic bimodal distribution is observed with 4×10^5 molecules and a condensate fraction of about 20%. (b) Full evaporation down to a final laser power of 3.8 mW results in an essentially pure molecular condensate with 2×10^5 molecules.

shift of 11 % for $a_{\mathrm{mol}} = 700\, a_0$ [Joc04]. The interactions are also expected to reduce the condensate fraction with respect to the ideal condensate. From equation 2.26 the condensate fraction for our parameters is estimated to be about 29%. This estimated value is in reasonable agreement with the observed condensate fraction of about 20%.

We obtain pure molecular condensates when we continue the evaporation process down to a final laser power of a few mW. Figure 5.2 (b) shows an essentially pure condensate of $N_{\mathrm{mol}} = 2 \times 10^5$ molecules obtained at a final trapping laser power of 3.8 mW where the trap depth is about $U_{\mathrm{mol}} = 530\,\mathrm{nK}$. The density profile is well fit by a Thomas-Fermi density distribution with a Thomas-Fermi radius $z_{\mathrm{TF}} = 105\,\mu\mathrm{m}$. The corresponding peak molecular density is $1.2 \times 10^{13}\,\mathrm{cm}^{-3}$. In the image a thermal component is not discernable. A careful analysis of axial density profiles is found in [Joc04]. The analysis provides a lower bound of 85(3)% for the condensate fraction and a temperature of 114(14) nK, corresponding to $T/T_{\mathrm{c}} = 0.42(5)$.

The chemical potential of the BEC is given by $\mu = \frac{1}{2} m_{\mathrm{mol}} \omega_z^2 z_{\mathrm{TF}}^2 = k_{\mathrm{B}} \times 130\,\mathrm{nK}$. The calculated chemical potential of $\mu = \frac{1}{2}(15\hbar^2 N_{\mathrm{mol}} \bar{\omega}^3 a_{\mathrm{mol}} \sqrt{m_{\mathrm{mol}}})^{2/5} = k_{\mathrm{B}} \times 160\,\mathrm{nK}$ is consistent with the observed value considering the experimental uncertainty. In particular the particle number is calibrated to within 50% through fluorescence imaging (see section 4.5.1).

5.2.2 Lifetime of the molecular condensate

The lifetime of the BEC is an important quantity since it determines the available time for a given experiment. We measure the lifetime of the BEC that we obtain after full evaporation down to a final laser power of 3.8 mW. After this evaporation ramp we adiabatically increase the laser power in a 200 ms exponential ramp to 34.4 mW. The compression increases the peak density of the condensate by a factor of 2.5. From the measured cloud size $z_{\mathrm{TF}} = 218\,\mu$m the peak molecular density can be estimated to be $n_{\mathrm{mol}} = (15/8\pi)(\omega_r/\omega_z)^2 N_{\mathrm{mol}}/z_{\mathrm{TF}}^3 = 1.0(5) \times 10^{13}\,\mathrm{cm}^{-3}$.

In this recompressed trap we measure a large lifetime of the BEC of 40 s at a magnetic field of 764 G. The loss rate due to two-body dimer-dimer collisions can be described by

$$\dot{N}_{\mathrm{mol}} = -G \int n^2(\mathbf{r})\, d\mathbf{r}, \tag{5.2}$$

where G is the loss rate coefficient for two-body collisions. Evaluation of the integral for a harmonically trapped BEC in the Thomas-Fermi limit yields [Söd99]

$$\dot{N}_{\mathrm{mol}} = -GcN_{\mathrm{mol}}^{2/5}, \tag{5.3}$$

with $c = (15^{2/5}/(14\pi))(m_{\mathrm{mol}}\bar{\omega}/(\hbar\sqrt{a_{\mathrm{mol}}})^{6/5}$. Under our experimental conditions $cN_{\mathrm{mol}}^{2/5} \approx 2.4 \times 10^{12}\,\mathrm{cm}^{-3}$ providing an upper bound for the binary loss rate coefficient for inelastic dimer-dimer collision of $G = 1 \times 10^{-14}\,\mathrm{cm}^3/\mathrm{s}$.

This value is consistent with previous measurements of G in thermal molecular gases [Cub03, Joc03b] taking into account a factor-of-2 suppression of binary collision loss in a condensate [Pet02] and the expected scaling of G with the scattering length [Pet04]. The value also agrees with the measurement performed in a molecular BEC at 770 G in the group of C. Salomon [Bou04].

5.2.3 Prospects for achieving a highly degenerate Fermi gas

Our measurements in the BEC-BCS crossover show that the conversion of the molecular BEC into a strongly interacting Fermi gas proceeds adiabatic and reversible (see section 6.1). In such an isentropic conversion the temperature of the gas will be reduced significantly while the molecules are converted into atoms and the thermal energy is distributed on twice as many particles.

This effect was studied in detail by L. Carr *et al.* for harmonically trapped particles [Car04]. In their analysis the entropy of a noninteracting Fermi gas is found to be

$$S_{\mathrm{F}} = k_{\mathrm{B}} N \pi^2 \left(\frac{T}{T_{\mathrm{F}}}\right), \tag{5.4}$$

while the entropy of a molecular BEC in the Thomas-Fermi limit is given by[Car04]

$$S_{\mathrm{BEC}} = k_{\mathrm{B}} N_{\mathrm{mol}} \left(\frac{T}{T_{\mathrm{c}}}\right)^3 \left(\frac{2\pi^4}{45\zeta(3)} + 3\frac{\mu_{\mathrm{mol}}}{k_{\mathrm{B}}T}\right). \tag{5.5}$$

The above result is accurate to within 10% for $k_B T/\mu_{mol} \geq 1/10$, a condition well fulfilled in our experiments. By equating both entropies the temperature of the Fermi gas can be estimated to be

$$\frac{T}{T_F} = \frac{1}{2\pi^2}\left(\frac{T}{T_c}\right)^3\left(\frac{2\pi^4}{45\zeta(3)} + 3\frac{\mu_{mol}}{k_B T}\right). \tag{5.6}$$

It should be noted that although presently no general theory exists one expects a similar temperature reduction when a molecular BEC is converted into a strongly interacting Fermi gas.

Our high condensate fraction of > 85(3)% suggest a very low entropy corresponding to an extremely low temperature in the Fermi gas. For the molecular condensate at 676 G we measure a temperature of $T = 114(14)$ nK corresponding to $T/T_c = 0.42(5)$, and a chemical potential of $\mu_{mol} = 125(6)$ nK [Joc04]. Using these numbers the temperature of the Fermi gas can be estimated to be $T/T_F = 0.026(10)$. At such low temperatures a Fermi gas with resonant interactions is predicted to be deep in the superfluid regime.

Chapter 6

Experiments in the BEC-BCS crossover

An intriguing property of some ultracold gases is the existence of a magnetically tunable scattering resonance. In such a Feshbach resonance, atoms couple to form diatomic molecules with a binding energy that can be controlled by the external magnetic field. This experimental knob is of particular interest when the molecules are formed from fermionic atoms, as it allows to continuously vary the coupling strength from the strong coupling BEC limit to the weak coupling BCS limit. This BEC-BCS crossover has been a subject of great theoretical interest for more than three decades [Eag69, Leg80, Noz85, Che04].

The first highlight in the experimental investigation of the BEC-BCS crossover in atomic Fermi gases was the creation of a molecular BEC [Joc03a, Gre03, Zwi03, Bou04, Hul04]. These molecular Bose-Einstein condensates now serve as an ideal starting point to experimentally investigate the crossover from a molecular condensate of tightly bound molecules to a BCS state of overlapping, strongly correlated pairs [Bar04b, Bou04, Reg04b, Zwi04, Kin04a, Bar04a, Chi04a, Gre04, Kin04b, Kin05]. The BEC-BCS crossover is closely related to resonance superfluidity [Hol01, Tim01, Oha02, Sta04] and the universal behavior of a Fermi gas with resonant interactions [Hei01, Ho04c]. The observation of the condensation of fermionic atom pairs close to the Feshbach resonance [Reg04b, Zwi04], measurements of collective oscillations [Kin04a, Bar04a, Kin04b], and the observation of the pairing gap in the strongly interacting Fermi gas [Chi04a], support the expected superfluidity at presently attainable temperatures in Fermi gases with resonant interactions.

Our experimental key to investigate the BEC-BCS crossover in fermionic ^{6}Li is the broad Feshbach resonance at a magnetic field of about 834 G [Bar04c]. For magnetic fields far below the Feshbach resonance we can realize the molecular BEC regime, where the molecules are formed by short range pairs [Joc03a]. With increasing magnetic field the interaction strength increases and the binding energy of the molecules is reduced. On resonance, at about 834 G, the scattering processes are unitarity limited and we obtain a universal quantum gas [Ho04c]. For magnetic fields above the res-

onance two-body physics no longer provides a bound molecular state and a strongly interacting Fermi gas of atoms is realized.

The starting point for all our experiments is a molecular Bose-Einstein condensate of well localized, tightly bound pairs [Joc03a]. In a first series of experiments we adiabatically convert the molecular BEC into a degenerate Fermi gas by changing the external magnetic field and analyze the density profile of the trapped cloud at different magnetic fields [Bar04b]. The observed crossover is smooth and reversible. The temperature in the Fermi gas regime can be estimated from the isentropic conversion and suggests that the system is in the superfluid state. This adiabatic and reversible crossover is the key ingredient of all further experiments that strongly support the existence of the superfluid phase.

To investigate the dynamics of the gas in the BEC-BCS crossover we excite low-lying collective modes in the axial and radial direction of our cigar shaped trapping potential [Bar04a]. The frequency and the damping of these modes is measured with high precision and can be compared with recently developed theoretical predictions in the BEC-BCS crossover [Str04a, Hei04a, Hu04, Com04b, Com04a, Kim04b, Kim04a, Man04, Bul04]. The modes in the axial direction show the expected behavior of a gas in the BEC-BCS crossover, with a particularly small damping rate in the vicinity of the Feshbach resonance. In contrast to the axial direction, the modes in the strongly confined radial direction show an abrupt change in the collective frequency at a magnetic field value that corresponds to a Fermi gas in the strongly interacting regime. The change in the frequency is accompanied by an extraordinary large damping rate. A possible explanation for this dramatic change in the excitation spectrum is that the magnetic field dependent pairing energy becomes similar to the collective excitation energy, which might lead to a breaking of the pairs due to the coupling to the collective mode.

A further strong support for the existence of the superfluid phase stems from the observation of a pairing gap in the strongly interacting Fermi gas regime [Chi04a]. In these experiments we employ radio-frequency spectroscopy to determine the pairing energy in the BEC-BCS crossover. In the BEC limit this energy is basically given by the binding energy of the molecules. The magnetic field dependent measurements show a smooth crossover from this two-body low density limit towards a density dependent many-body regime. The observed temperature dependence of the pairing gap in the strongly interacting Fermi gas regime is in agreement with theoretical expectations for a superfluid.

For a quantitative comparison of the experimental results with the theoretical predictions in BEC-BCS crossover, a precise knowledge of the magnetic field dependent scattering length is very important. Radio frequency spectroscopy of weakly bound molecules enables us to precisely measure the magnetic field dependent molecular level structure. This level structure unambiguously determines the scattering properties of the ultracold atoms. Fitting the corresponding experimental data with a multichannel quantum scattering calculation worked out in the theory group of Paul Julienne at the NIST, allows us to precisely determine the cold collision properties of ^{6}Li

[Bar04c]. In particular the magnetic field value of the broad Feshbach resonance is determined to be at $B_0 = 834.1(1.5)$ G.

This magnetic field value of the Feshbach resonance is used in the following description of our experiments in the BEC-BCS crossover. It should be noted that at the time of our publications [Bar04b, Bar04a, Chi04b] the resonance position was unknown to within 10 G. Therefore, the values given here might differ from the ones cited in our publications. Furthermore we analyzed all the experimental data again, including a careful investigation of errors. Some numbers changed within the given error and we will report these latest values, corresponding to our best knowledge of the system.

6.1 Smooth conversion from a molecular BEC into a degenerate Fermi gas

The tunability of interactions in our molecular BEC [Joc03b] provides a unique possibility to explore the BEC-BCS crossover. In this series of experiments we explore the BEC-BCS crossover by analyzing the axial density profiles of the trapped cloud at different magnetic fields.

It has been predicted by L. Carr *et al.* that an adiabatic passing of a pure molecular BEC over the resonance can lead to a superfluid Fermi gas [Car04]. The maximum available time for the magnetic field ramp across the resonance is set by the lifetime of the molecular BEC. The long lifetime of several 10 s, measured for our molecular BEC close to the Feshbach resonance (see section 5.2.2), allows us to use very slow magnetic field ramps. In section 6.1.1 we show that the magnetic field ramps we use to investigate the BEC-BCS crossover are adiabatic and reversible.

Employing these isentropic magnetic field ramps we record the spatial density profiles in the BEC-BCS crossover. Our measurement of the axial cloud size are presented in section 6.1.2 and show a smooth crossover from a molecular BEC to a strongly interacting Fermi gas of atoms. Furthermore, on the Feshbach resonance the scattering processes are unitarity limited and the measurements of the axial cloud size allow us to determine the universal parameter β [O'H02a].

Our experimental data have been quantitatively compared with the theoretical predictions for the BEC-BCS crossover by A. Perali *et al.* [Per04b]. In section 6.1.3 we briefly report on the main findings of this comparison before summarizing our results.

Experimental starting conditions and detection

The starting point for the experiments is an almost pure molecular BEC of about $N_{\mathrm{mol}} = 2 \times 10^5$ molecules at a magnetic field of 764 G and a trap laser power of 3.8 mW. At this magnetic field the molecular binding energy is $\sim k_{\mathrm{B}} \times 1.4\,\mu$K. Based on the predicted relation of $a_{\mathrm{mol}} = 0.6\,a$ [Pet03] and a calculated atomic scattering length

of about $a = 4500\,a_0$ [Bar04c], the scattering length for elastic molecule-molecule collisions is $a_{\mathrm{mol}} = 2700\,a_0$.

Before changing the magnetic field, we first adiabatically increase in a 200 ms exponential ramp the laser power from 3.8 mW to 34.4 mW. The higher power provides a trap depth of $\sim k_{\mathrm{B}} \times 2\,\mu$K for the atoms, which is roughly a factor of two above the Fermi energy. This avoids spilling of the gas at higher magnetic fields, where the repulsive mean field energy is larger [Joc03a]. The compression increases the peak density of the condensate by a factor of 2.5. The recompressed trap has an axial trap frequency of $\omega_z/2\pi = (0.6B/\,\mathrm{G} + 32)^{1/2}$ Hz and a radial trap frequency of $\omega_r/2\pi = 640$ Hz. From the measured cloud size $z_{\mathrm{TF}} = 218\,\mu$m the peak molecular density can be estimated (equation 2.22) to be $n_{\mathrm{mol}} = (15/8\pi)(\omega_r/\omega_z)^2 N_{\mathrm{mol}}/z_{TF}^3 = 1.0(5) \times 10^{13}\,\mathrm{cm}^{-3}$.

For detection we apply in situ absorption imaging to record the spatial density profiles of the trapped ensemble. As explained in section 4.5.2, in our cigar-shaped trap the radial cloud size is on the order of our imaging resolution of about $10\,\mu$m, while the axial cloud size of typically $\sim 100\,\mu$m can be accurately measured. We therefore obtain axial density distributions from images integrated radially.

6.1.1 Adiabatic and reversible crossover

To explore the crossover to a degenerate Fermi gas we apply slow magnetic field ramps. To ensure their adiabaticity we performed test experiments where we ramped the field linearly from the initial value of 764 G to 882 G and back to 764 G with variable ramp speed. These ramps convert the molecular BEC into a strongly interacting Fermi gas and vice versa. One therefore expects substantial changes in the cloud size. After the up-and-down ramp we observed axial oscillations of the ensemble at the quadrupole frequency (see also section 6.2). Being the lowest excitation mode of the system, this collective oscillation is sensitive to nonadiabaticity effects. In our test experiments we observed axial oscillations with relative amplitude of $> 5\%$ for ramp speeds above 1.2 G/ms. For ramp speeds of 0.6 G/ms and lower, the axial oscillation was no longer visible.

To check the reversibility of the crossover process, we ramped the field in a total time of 2 s from 764 G to 1176 G and down again to 764 G. This corresponds to ramp speeds of ± 0.41 G/ms. After the ramps an in situ image of the cloud was taken from which we determined the axial profile. In figure 6.1 this profile (•) is compared with the corresponding profile obtained after 2 s holding time at a fixed magnetic field of 764 G (○). The comparison does not show any significant deviation[1] and thus the conversion of the molecular BEC into a Fermi gas and back again is lossless and proceeds without noticeable increase of the entropy.

[1] For the given curves, the integrated absorption signal is 3% higher for the samples that are ramped to 1176 G and back. As this is within the fluctuations of our imaging system, we scale the corresponding density down by 3% for comparison.

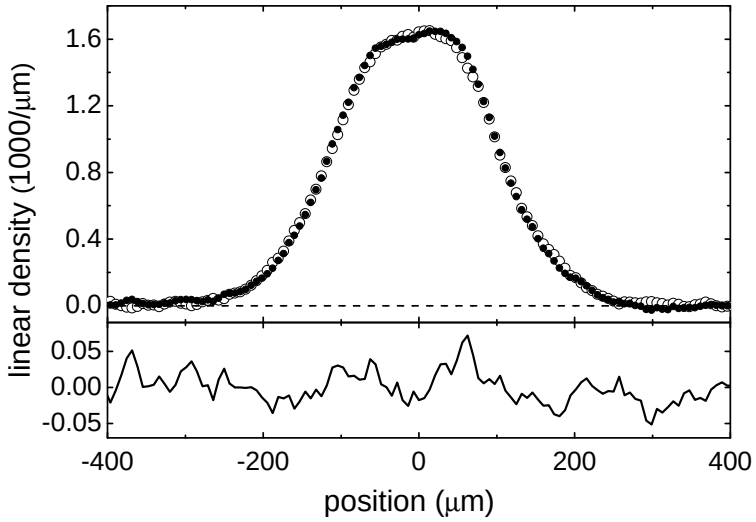

Figure 6.1: Axial profile of a molecular BEC at 764 G after its conversion into a Fermi gas at 1176 G and subsequent back-conversion (•). Two 1-s magnetic field ramps are applied in this reversible process. For reference the corresponding profile observed without the magnetic field ramp is shown (○). The density profiles are obtained by averaging over 50 images. The difference shown in the lower graph is consistent with the drifts of a residual interference pattern in the images.

6.1.2 Smooth crossover

To investigate the crossover, in situ images of the trapped gas are taken after a 1-s linear magnetic field ramp to final values between 740 and 1440 G.

To characterize the size of the trapped gas we determine the root-mean squared (rms) axial size z_{rms}. We therefore fit the density profile with a function

$$n(z) = n_0 \left(1 - \frac{z^2}{z_{\mathrm{a}}^2}\right)^{\alpha}, \tag{6.1}$$

where n_0, z_{a}, and $2 \leq \alpha \leq 2.5$ are free parameters. This function interpolates between the radially integrated density profile of a pure BEC in the Thomas-Fermi limit with $\alpha = 2$ and a zero-temperature, noninteracting or unitarity limited Fermi gas with $\alpha = 2.5$ [O'H02a]. These profiles are obtained by integrating equation 2.22 and equation 2.35, respectively. From the fitted values for z_{a} and α the rms axial cloud size is obtained by

$$z_{\mathrm{rms}} = z_{\mathrm{a}} / \sqrt{3 + 2\alpha}. \tag{6.2}$$

This rms size is related by $z_{\mathrm{rms}} = z_{\mathrm{TF}} / \sqrt{7}$ to the axial Thomas-Fermi radius z_{TF} of a pure BEC in the Thomas-Fermi limit and by $z_{\mathrm{rms}} = z_{\mathrm{TF}} / \sqrt{8}$ in the cases of zero-temperature noninteracting or unitarity limited Fermi gases.

In figure 6.2 (b) the measured axial cloud size is shown as a function of magnetic field. Figure 6.2 (a) shows for comparison the magnetic field dependence of the atomic

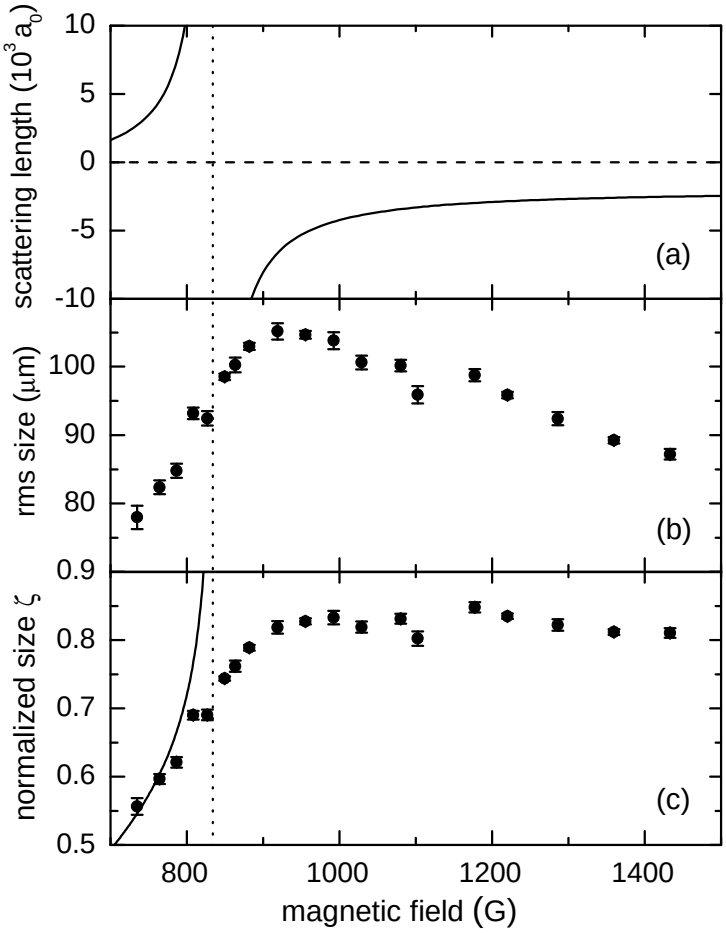

Figure 6.2: Axial cloud size measurements across the Feshbach resonance. In (a) the atomic scattering length a is shown, the resonance at 834 G is marked by the vertical dotted line. The data in (b) display the measured rms cloud sizes. In (c), the same data are plotted after normalization to a noninteracting Fermi gas. The solid line shows the expectation from BEC mean-field theory with $a_{\mathrm{mol}} = 0.6\,a$. In (b) and (c), the error bars show the statistical error of the size measurements from typically five individual images.

scattering length (see also section 3.2.3). The increase of the cloud size for fields up to 950 G is due to the crossover from the molecular BEC to the degenerate Fermi gas. For higher fields the axial cloud size of the Fermi gas shrinks with increasing B. Note that the axial magnetic confinement increases with increasing magnetic field ($\omega_z \propto \sqrt{B}$).

For the following discussion we remove the trap dependency by normalizing the observed size to the one expected for a noninteracting Fermi gas. Figure 6.2 (c) shows the normalized axial cloud size $\zeta = z_{\mathrm{rms}}/z_0$, where $z_0 = (E_{\mathrm{F}}/4m\omega_z^2)^{1/2}$ is the rms axial cloud size of a noninteracting zero-temperature Fermi gas. For $N = 4 \times 10^5$ atoms the Fermi energy $E_{\mathrm{F}} = \hbar^2 k_{\mathrm{F}}^2/2m = \hbar\bar{\omega}(3N)^{1/3}$ amounts to $k_{\mathrm{B}} \times 1.1\,\mu$K at 834 G, and the Fermi wave number k_{F} corresponds to a length scale of $1/k_{\mathrm{F}} = 3600\,a_0$.

For magnetic fields well below the resonance, the observed dependence of the

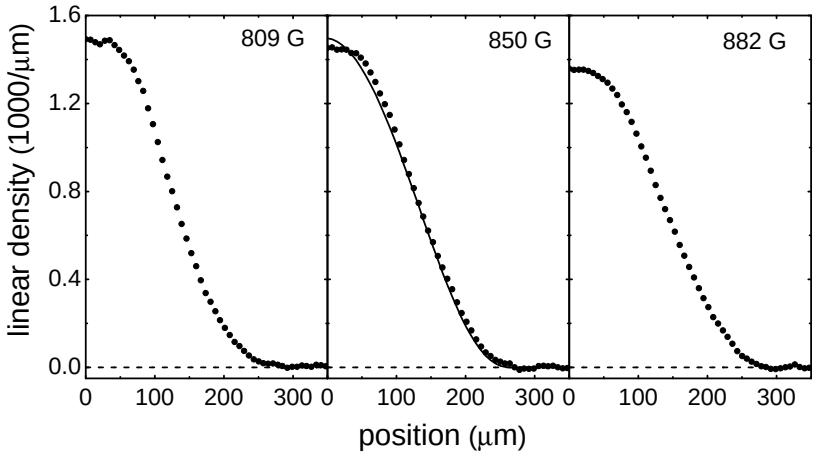

Figure 6.3: Axial density profiles near the Feshbach resonance. The rms cloud sizes are 93, 99 and 103 μm at 809, 850 and 882 G, respectively. For comparison, the image taken at 850 G is shown together with a fit by the expected density profile $\propto (1 - z^2/z_{\mathrm{TF}})^{5/2}$. The small fringes at the top of the profiles are due to a residual interference pattern in the images.

cloud size agrees with the expected behavior of a BEC in the Thomas-Fermi limit where the rms cloud size is given by $z_{\mathrm{rms}} = \sqrt{2\mu/(7m_{\mathrm{mol}}\omega_z^2)}$. With the chemical potential $\mu = \frac{1}{2}(15\hbar^2 N_{\mathrm{mol}}\bar{\omega}^3 a_{\mathrm{mol}}\sqrt{m_{\mathrm{mol}}})^{2/5}$ and the molecular binding energy $E_{\mathrm{b}} = \hbar^2/ma^2$ the normalized axial cloud size is given by

$$\zeta = 0.688(a_{\mathrm{mol}}/a)^{1/5}(E_{\mathrm{F}}/E_{\mathrm{b}})^{1/10} = 0.642(a_{\mathrm{mol}}/a)^{1/5}(k_{\mathrm{F}}a)^{1/5}. \tag{6.3}$$

The corresponding curve calculated with $a_{\mathrm{mol}}/a = 0.6$ is shown in Figure 6.2 (c) (solid line). The BEC limit provides a reasonable approximation up to ~775 G. Here the molecular gas parameter is $n_{\mathrm{mol}}a_{\mathrm{mol}}^3 \approx 0.046$. Using the relation $(n_{\mathrm{mol}}a_{\mathrm{mol}}^3)^{1/2} = 0.1298(k_{\mathrm{F}}a)^{6/5}$, the interaction strength can alternatively be expressed as $1/k_{\mathrm{F}}a \approx 0.7$.

The crossover from the molecular BEC to a degenerate Fermi gas is observed in the vicinity of the Feshbach resonance for fields between 775 and 950 G. Here the cloud size ζ smoothly increases with the magnetic field until it levels off at about 950 G where the interaction strength is characterized by $1/k_{\mathrm{F}}a \approx -0.7$. Our results suggest that the crossover occurs in the range of $-0.7 \lesssim (k_{\mathrm{F}}a)^{-1} \lesssim 0.7$, which corresponds to the strongly interacting regime.

Figure 6.3 shows axial density profiles near the Feshbach resonance at magnetic fields of 809, 850 and 882 G. To reduce imaging imperfections each profile is obtained by averaging and symmetrizing 50 images. The spatial profiles show the gradually increasing cloud size without any noticeable new features and further illustrate the smoothness of the crossover.

For magnetic fields above 950 G, the Fermi gas regime is reached and we observe an essentially constant normalized axial cloud size of $\zeta = 0.83 \pm 0.07$. In this regime the interaction parameter $1/k_{\mathrm{F}}a$ is calculated to vary between -0.7 and -1.2 at 950 and 1440 G, respectively. Based on the calculation of the ground state energy for an homo-

geneous, interacting Fermi gas, the normalized cloud size ζ can be estimated to vary between 0.92 and 0.94 at 950 and 1440 G, respectively [Hei01]. Our observed values are somewhat below this prediction. This discrepancy requires further investigation, a possible scenario could be a systematically lower atom number than expected (see also below).

Universal regime

On resonance the scattering processes are unitarity limited and a universal regime is realized (see section 2.2.3). Here the mean field is proportional to the Fermi energy $U_{\mathrm{MF}} = \beta E_{\mathrm{F}}$ and the shape of the Thomas-Fermi density distribution is preserved [O'H02a]. The zero-temperature spatial distribution then corresponds to that of a harmonic potential with scaled frequencies $\omega_i' = \omega_i/\sqrt{1+\beta}$ $(i = x, y, z)$ and the axial Thomas-Fermi radius of the trapped cloud is given by $z_{\mathrm{TF}} = \sqrt{2E_{\mathrm{F}}'/m\omega_z'^2}$, where $E_{\mathrm{F}}' = \hbar\bar{\omega}'(3N)^{1/3}$ is the Fermi energy including the mean field contribution [Geh03b]. The normalized cloud size can thus be written as $\zeta = (1+\beta)^{1/4}$.

The value for ζ at the resonance position of 834.1 G is found by an interpolation of the four neighboring values and amounts to $\zeta = 0.72 \pm 0.07$, giving $\beta = -0.73^{+0.12}_{-0.09}$. Here the total error range includes all statistic and systematic uncertainties, with the particle number giving the dominant contribution. Note that at the time of our previous publication [Bar04b] the exact resonance position was uncertain to within a few 10 G and assumed to be at ~850 G. This resulted in the slightly higher value of $\beta = -0.68^{+0.13}_{-0.10}$ reported in [Bar04b].

Our experimental results reveal a stronger interaction effect than recent measurements in the group of John Thomas that yielded $\beta = -0.49(4)$ at $B = 840$ G [Kin05] but agrees with $\beta \approx -0.64(15)$ obtained in the group of Christophe Salomon by measuring the release energy of a molecular BEC at $B = 820$ G [Bou04].

Our measured value of $\beta = -0.73^{+0.12}_{-0.09}$ agrees with theoretical predictions that range from $\beta \approx -0.7$ to $\beta \approx -0.3$. A detailed discussion of the theoretical predictions is found in section 2.2.3. The theoretical values are derived from energy expansions of zero-temperature Fermi gases [Bak99, Hei01, Ste00], from BEC-BCS crossover theories [Per04b] and from quantum Monte Carlo calculations [Car03, Ast04].

6.1.3 Comparison with theoretical predictions in the BEC-BCS crossover

The situation of our experiment was theoretically investigated by A. Perali *et al.* [Per04b]. In their analysis they compared our measured axial density profiles (shown in figure 6.3) and the behavior of the normalized axial cloud size as a function of magnetic field (figure 6.2 (c)) with the theoretical predictions in the BEC-BCS crossover and found a very good agreement.

At the time their calculation was carried out, the resonance position was uncertain to within some 10 G and their analysis showed that assuming the Feshbach resonance

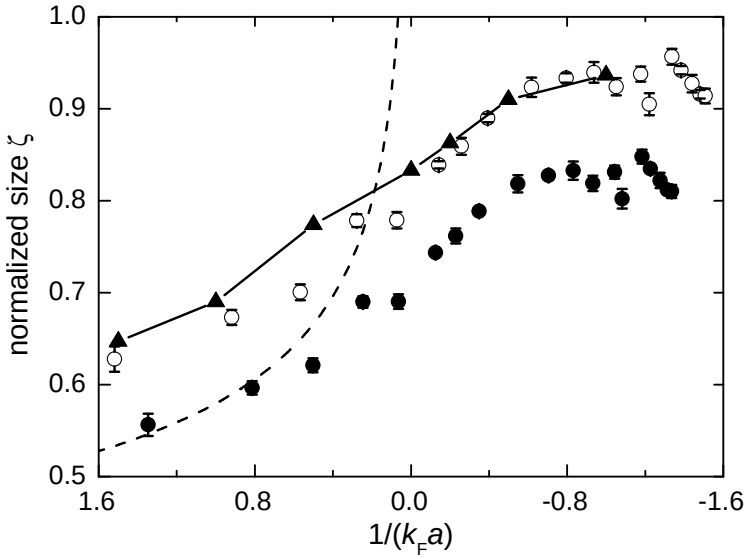

Figure 6.4: Comparison between the predicted (filled triangles) and the measured normalized axial cloud size in the BEC-BCS crossover, assuming $N = 4 \times 10^5$ (filled circles) and $N = 1.94 \times 10^5$ (open circles), respectively. The later value results in an optimal agreement between theory and experiment [Pie04a]. The dashed line shows the expectation from the BEC mean field theory. The strong coupling BEC limit is reached for $1/k_F a \gg 1$, while the weak coupling BCS limit is obtained for $1/k_F a \ll -1$.

at a field of 850 G (820 G) and an atom number of $N = 2.3 \times 10^5$ ($N = 1.65 \times 10^5$) the agreement between theory and experiment could be further optimized and become almost perfect. For the resonance at a field of 834.1 G, one expects an optimal agreement with $N \approx 1.94 \times 10^5$ atoms [Pie04a], a value that lies within our experimental uncertainty of ~50% for the calibration of our absolute atom number (see section 4.5). These values are assumed in figure 6.4, where we show the normalized axial cloud size (open symbols) in the BEC-BCS crossover together with the theoretical prediction (filled triangles). For comparison we also show the prediction from the BEC mean field theory (dashed line) assuming $a_{\mathrm{mol}}/a = 0.6$ (see equation 6.3) and our experimental data points with $N = 4 \times 10^5$ atoms (filled circles). The data are shown as a function of the interaction strength, expressed by $1/k_F a$ and the BEC limit is obtained for $1/k_F a \gg 1$, while the BCS limit is reached for $1/k_F a \ll -1$. The agreement between our experimental data and the theoretical prediction over the wide coupling range covered in our experiments is remarkable.

It should be noted that the prediction of A. Perali *et al.* (filled triangles in figure 6.4) assumes $a_{\mathrm{mol}}/a = 2$, which corresponds to the Born approximation of the dimer-dimer scattering length [Per04b]. Compared to the calculated dimer-dimer scattering length of $a_{\mathrm{mol}}/a = 0.6$ [Pet04], their theory overestimates the size of the cloud in the BEC limit by about 27% (see also figure 6.4). In this limit we find a better agreement between theory and experiment if we assume an atom number of $N = 4 \times 10^5$. In

contrast the measured cloud size on resonance and in the regime of an interacting Fermi gas agrees better with the theoretical prediction if we assume an atom number of $N = 1.94 \times 10^5$. Assuming the theoretical prediction to be correct, a possible scenario for the observed deviation is a decreasing radial confinement with increasing magnetic field. This effect could for example stem from anharmonicity effects of the radial trapping potential (see also the discussion of the radial dipole mode in section 6.2.1), but the estimated effects for a Gaussian beam are too small to explain the observed discrepancy. However, it may be possible that the Gaussian beam shows distortions for example due to a thermal lens effect.

6.1.4 Summary and Conclusion

Our measurements demonstrate the smooth crossover from a molecular BEC to a degenerate Fermi gas of atoms. On resonance we realize a universal quantum gas and the universal parameter is determined to be $\beta = -0.73^{+0.12}_{-0.09}$.

Since the conversion of the molecular BEC into an atomic Fermi gas is adiabatic and reversible, the temperature of the Fermi gas can be estimated from the conservation of the entropy [Car04] (see section 5.2.3). Our high condensate fraction of $> 85(3)\%$ suggests a very small entropy corresponding to an extremely low temperature in the Fermi gas limit of $T/T_\mathrm{F} < 0.03(1)$. In this scenario, superfluidity can be expected to extend from the molecular BEC regime into the interacting Fermi gas regime where $1/k_\mathrm{F}a \geq -1.4$.

Our experiment thus opens up intriguing possibilities to study atomic Cooper pairing and superfluidity in resonant quantum gases.

6.2 Collective excitations

To gain more insight into the physical behavior of the gas in the BEC-BCS crossover, the investigation of collective excitations provides a powerful method. In this section we present our measurements of fundamental collective excitation modes in the BEC-BCS crossover for various coupling strengths in the low temperature limit.

Detailed theoretical and experimental studies of collective oscillations in atomic Bose-Einstein condensates have proven important tools to characterize the behavior of these many-body systems[2]. The sensitivity of the collective modes to interaction effects and the ability to measure frequencies with high accuracy makes them perfectly suited to check theoretical predictions [Dal99a].

For a superfluid Fermi gas in the BEC-BCS crossover, a non trivial dependence of the collective frequencies was predicted by Stringari [Str04a]. The superfluidity implies a hydrodynamic behavior that causes substantial changes in the excitation spectrum with respect to the collisionless regime and in general very low damping rates.

[2] A brief summary of theoretical and experimental work prior to 2002 can be found in the article of F. Chevy *et al.* [Che02].

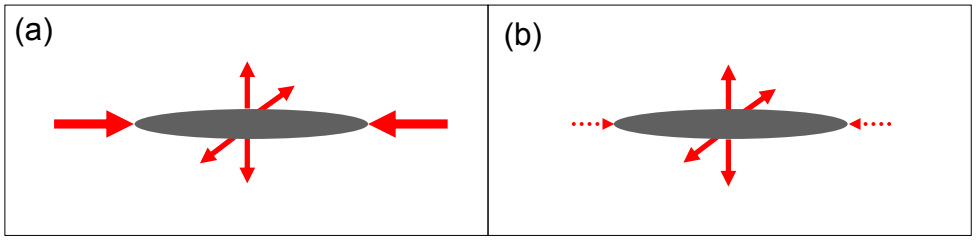

Figure 6.5: Illustration of the axial (a) and radial (b) breathing mode in our elongated trap. The slow axial mode consists of an out-of-phase oscillation in the axial and radial direction while the fast radial mode consists mainly of a radial oscillation of the cloud.

For strongly interacting Bose and Fermi gases however, collisions between the particles can result in a hydrodynamic behavior in the normal, non superfluid phase. Hence the interpretation of the collective modes in the BEC-BCS crossover in terms of superfluidity is not straightforward and needs careful investigation to identify the different regimes.

The lowest energy mode corresponds to the center of mass oscillation of the cloud. For a harmonic potential this "sloshing" or dipole mode is predicted to occur at the trap frequency and to be independent of statistics and interaction effects. Our measurements of the sloshing modes in the axial and radial direction are presented in section 6.2.1 and allow a very accurate determination of the trap frequencies.

The frequencies of the next higher modes, however, are expected to depend on the interactions and to deviate from the spectrum of an ideal gas, where the excitation frequencies are multiplies of the trap frequencies. In general the modes are classified by the number of radial nodes n, the total angular momentum l and its axial projection m. In our cigar shaped trap the quantum number l is no longer good and only the axial projection quantum number m is conserved. For a superfluid or hydrodynamic gas in an axially symmetric trap, the lowest $m = 0$ modes are coupled excitations of different symmetry, i.e a coupled monopole-quadrupole mode [Str96]. In our case of a very elongated trap, these modes correspond to a slow axial quadrupole mode and a fast radial monopole mode. The axial mode is characterized by an out-of-phase oscillation along the axial and radial direction, while the radial mode is primarily a radial breathing mode with a suppressed axial oscillation. These two modes are illustrated in figure 6.5 and are called the axial and radial breathing modes, respectively. A more detailed discussion of the collective dynamics in different regimes and trap configurations is found in section 3.3.

We use an excitation scheme that preserves the cylindrical symmetry of our elongated trap, and thus we expect to observe only $m = 0$ modes. Applying weak excitations, we measure the frequency and the damping rate of the axial and radial breathing modes for a degenerate gas in the BEC-BCS crossover. Our experimental results for the axial and radial mode are presented in section 6.2.2 and 6.2.3, respectively.

Our measurements show a very pronounced dependence of the collective breathing

modes on the magnetic field, i.e the interaction strength. In section 6.2.4 we compare our experimental findings with the most recent theoretical predictions in the BEC-BCS crossover. In this section we also briefly summarize and compare our results with similar measurements of the radial breathing mode that were carried out in the group of John Thomas at the Duke University [Kin04a, Kin04b].

Experimental starting conditions

The starting point for all the experiments is a cigar shaped molecular BEC at a magnetic field of 764 G and a laser power of 34 mW. To explore the collective excitations in the BEC-BCS crossover we first adiabatically ramp the magnetic field within 1 s from the initial value to fields between 676 and 1250 G. As shown in the previous section this ramp is isentropic and from the temperature in the BEC limit of $T/T_c = 0.42(5)$ we estimate the temperature in the noninteracting Fermi gas limit to be $T/T_F < 0.03$. With a total number of atoms $N \approx 4 \times 10^5$ (free atoms and atoms bound to molecules) and a geometrically averaged trap frequency at 834 G of $\bar{\omega} = (\omega_r^2 \omega_z)^{1/3} \approx 2\pi \times 230$ Hz, the Fermi energy for a noninteracting cloud amounts to $E_F = \hbar\bar{\omega}(3N)^{1/3} = k_B \times 1.2\,\mu$K.

6.2.1 Axial and radial dipole oscillations

We measure the axial and radial dipole mode frequency at various magnetic fields. The dipole mode corresponds to the center of mass motion of the system, which oscillates in a harmonic potential with the trap frequency. Because this sloshing mode is expected to be independent of statistics and two-body interactions, the measurements of the axial (radial) dipole mode frequency allows us to precisely characterize the axial (radial) trapping potential [Dal99a].

Axial dipole mode

To excite the axial dipole mode we apply for a 10 ms time interval an additional magnetic field gradient of about 18 G/cm in the vertical direction. This is done by using the small auxiliary coils that are also used to compensate for gravity and stray magnetic fields (see section 4.4). Because these coils and the axial direction of the optical dipole trap are not aligned perfectly perpendicular to each other, the effective potential is slightly tilted in the axial direction and the atoms are pushed to one side. At the same time the vertical potential becomes tilted and the particles spill out of the trap, limiting the maximal applicable field gradient [Joc03a]. After turning off the extra field gradient, the remaining particles begin to oscillate along the axial direction with the center of mass motion.

The axial oscillation is observed by in situ imaging the cloud after a variable hold time t at constant trap parameters. To determine the axial trap frequency ω_z, we fit a damped harmonic oscillation $c_z(t) = c_0 + a_z \exp(-\gamma_z t) \sin(\omega_z t + \phi_z)$ to the observed time

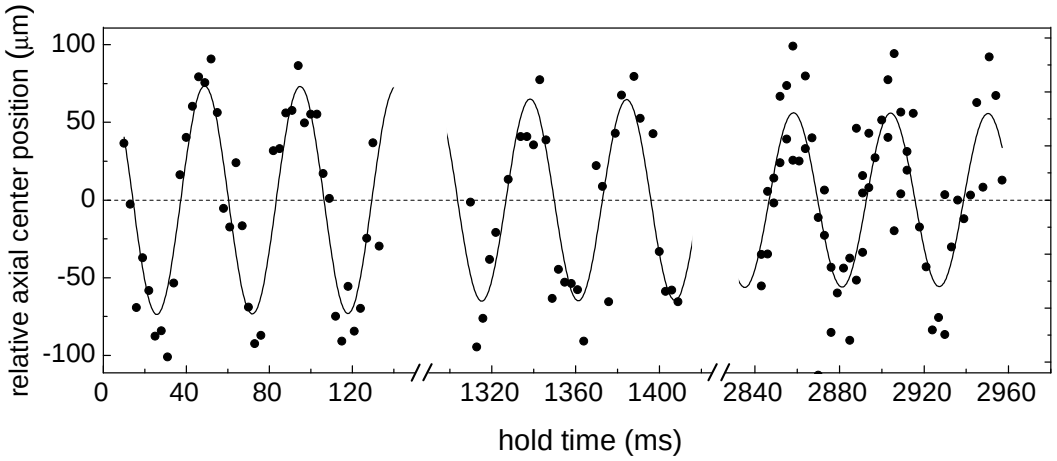

Figure 6.6: Oscillation of the axial dipole mode at a magnetic field of 764 G. The solid line shows a fit by a damped harmonic oscillation with a frequency of $\omega_z/2\pi = 21.71(2)$ Hz and a very low damping rate of $\gamma_z/\omega_z = 0.0007(7)$.

evolution of the axial center position, where γ_z is the damping rate and c_0, a_z and ϕ_z are additional fit parameters. A typical axial dipole oscillation is shown in figure 6.6.

The axial confinement at the given laser power of 34 mW stems mainly from the magnetic confinement, caused by the curvature of the of the Feshbach tuning field (see also section 4.3.2). Therefore the axial trapping potential is perfectly harmonic, and the dipole mode shows only very weak damping. This allows us to determine the axial trap frequency with a 10^{-3} precision. From the fit to the measurement at 764 G, shown in figure 6.6, we obtain a frequency of $\omega_z/2\pi = 21.71(2)$ Hz and the very low value $\gamma_z/\omega_z = 0.0007(7)$, corresponding to a $1/e$ damping time of about 10 s.

The magnetic field dependent axial trapping frequency $\omega_z(B)$ is derived from measurements of the dipole frequency at different magnetic fields [Rie04]. We fit the data with the function $\omega_z(B) = (\omega_{\mathrm{mag}}^2 B + \omega_{\mathrm{opt}}^2)^{1/2}$ that takes into account that the axial potential is a superposition of a magnetic and a (weak) optical potential with trap frequencies $\omega_{\mathrm{mag}}\sqrt{B}$ and ω_{opt}, respectively. From the fit we obtain

$$\omega_z(B) = 2\pi \times \sqrt{601(4)\, B/\mathrm{kG} + 11(4)}\,\mathrm{Hz}, \tag{6.4}$$

where the values in brackets denote the uncertainty from the fit.

Radial dipole mode

We excite the radial sloshing mode by a pulsed application of a vertical magnetic field gradient. Typically a gradient of 11.2 G/cm is applied for 0.1 ms. To detect the radial oscillation we turn off the trapping laser after a variable hold time t and image the cloud after usually 2 ms of expansion. From the image we determine the radial center position of the cloud and extract the radial dipole frequency ω_r by fitting the observed time evolution to a damped harmonic oscillation $c_r(t) = c_0 + a_r \exp(-\gamma_r t)\sin(\omega_r t + \phi_r)$,

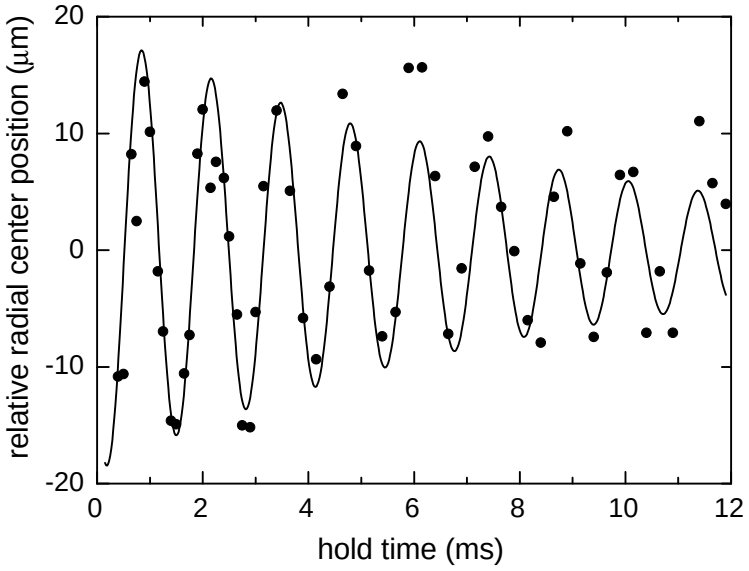

Figure 6.7: Oscillation of the radial dipole mode at a magnetic field of 764 G. The solid line shows a fit by a damped harmonic oscillation with a frequency of $\omega_r/2\pi = 760(5)$ Hz and a damping rate of $\gamma_r/\omega_r = 0.024(6)$.

where γ_r is the damping rate and c_0, a_r and ϕ_r are additional fit parameters. Figure 6.7 shows a typical radial dipole oscillation. From the corresponding fit (solid line) we obtain a frequency of $\omega_r/2\pi = 760(5)$ Hz and a damping rate of $\gamma_r/\omega_r = 0.024(6)$, which corresponds to a $1/e$ damping time of about 9 ms.

We attribute the observed damping of the radial dipole mode to anharmonic contributions to the radial trapping potential that stems from the Gaussian-shaped laser beam. The anharmonicity of this Gaussian-shaped radial potential also explains why with increasing magnetic field, and thus increasing radial cloud size, the measured sloshing mode frequency decreases (see figure 6.8). The expected lowest order anharmonicity correction was derived by S. Stringari [Str04b] and is given by (see also appendix B)

$$\omega_r = \omega_\perp \left(1 - \frac{m\,\omega_\parallel^2\, z_{\mathrm{rms}}^2}{U}\right). \tag{6.5}$$

Here U denotes the atomic trap depth, m the atomic mass, $\omega_\perp$ ($\omega_\parallel$) the radial (axial) trap frequency for the zero energy harmonic oscillator and z_{rms} the axial rms size of the trapped cloud[3].

To obtain the correction as a function of the magnetic field we use the in situ measurements of the cloud size discussed in the previous section and the corresponding axial trap frequency. Using an appropriate fit function with the right asymptotic behavior, we approximate the second term in equation 6.5. A further fit is then used to approximate the measured dependency of the radial dipole mode frequency on the

[3]Equation 6.5 holds for atoms and molecules. The later have $m_{\mathrm{mol}} = 2m$ and $U_{\mathrm{mol}} = 2U$.

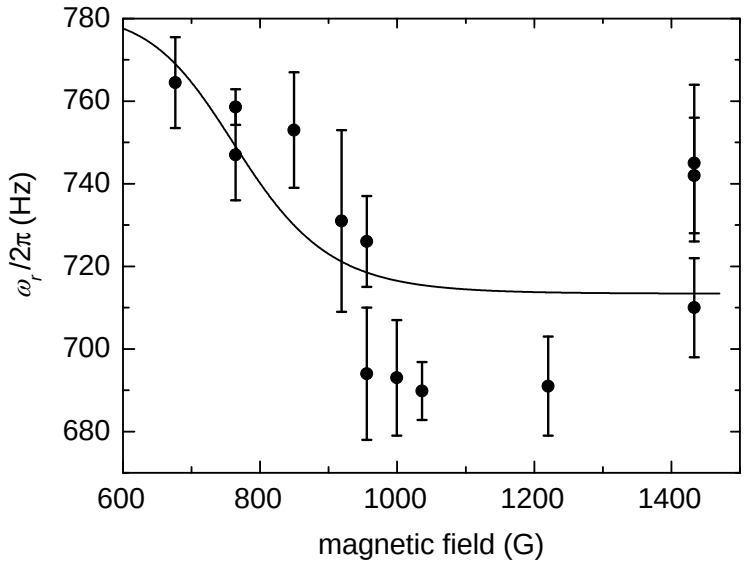

Figure 6.8: Measured radial dipole mode frequency at a constant laser power of 34 mW for different magnetic fields. With increasing magnetic field, i.e increasing cloud size, the dipole frequency decreases. The solid line shows the theoretical dependency of the dipole mode. Its shape is due to the lowest order anharmonicity correction given in equation 6.5 [Str04b].

magnetic field (solid line in figure 6.8). From this fit we obtain $\omega_\perp/2\pi = 781(3)$ Hz in the harmonic limit. As can be seen from the figure 6.8 the dipole frequency decreases from ~770 Hz at 675 G to ~715 Hz for fields above 1200 G. At the resonance position of 834.1 G the dipole frequency is about 735 Hz.

Note that these trap frequencies are slightly different than the ones given in the previous section. The quoted values always correspond to our best knowledge of the system at the time the measurements were taken. We attribute the small changes in the numbers to tiny drifts in the alignment of the trap.

6.2.2 Axial breathing mode

To excite the axial breathing mode at a given magnetic field, we increase the optical confinement in a 10 ms time interval by a factor of 1.5. The laser power is varied slow enough for the radial motion to follow adiabatically, but fast enough to induce axial oscillations. The relative amplitude of the resulting axial oscillation is kept small, typically ~10%. We observe the oscillation by in situ imaging after a variable hold time t at constant trap parameters. To determine the collective oscillation frequency Ω_z and the damping rate Γ_z we fit a damped harmonic oscillation $z(t) = z_0 + A_z \exp(-\Gamma_z t) \times \sin(\Omega_z t + \phi_z)$ to the observed time evolution of the cloud size, where z_0, A_z, and ϕ_z are additional fit parameters.

The measured oscillation frequencies and damping rates are shown in Figure 6.9. For a comparison to theory the data are normalized to the measured axial trap fre-

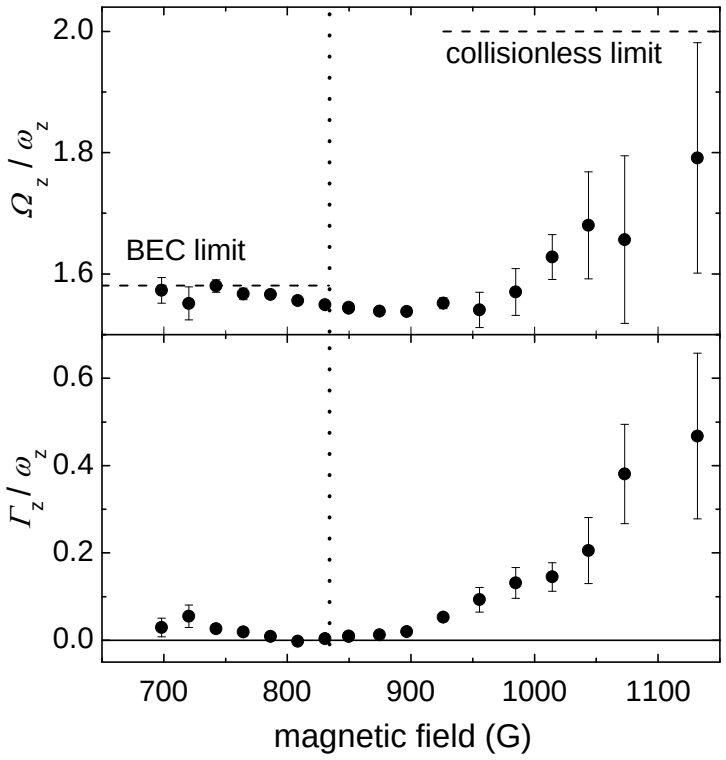

Figure 6.9: Measured frequency Ω_z and damping rate Γ_z of the axial breathing mode, normalized to the trap frequency ω_z. In the upper graph the dashed lines indicate the BEC limit of $\Omega_z/\omega_z = \sqrt{5/2}$ and the collisionless Fermi gas limit with $\Omega_z/\omega_z = 2$, respectively. The vertical dotted line indicates the resonance position at 834.1 G.

quency ω_z. In the BEC limit, obtained at low magnetic fields, the measured collective frequencies are in agreement with the expected $\Omega_z/\omega_z = \sqrt{5/2} = 1.581$ [Str96, Mew96]. With increasing magnetic field we observe a decrease in the collective excitation frequency until a minimum is reached at about 900 G. Here the interaction strength is $1/k_F a \approx -0.4$, corresponding to the strongly interacting Fermi gas regime. With further increasing magnetic field the interaction strength decreases and we observe a gradual increase of the collective excitation frequency towards $\Omega_z/\omega_z = 2$. This value is expected for a collisionless degenerate Fermi gas where the elastic collision rate is strongly reduced by Pauli blocking [Vic00]. Because of the large damping rate in the transition regime between the hydrodynamic and the collisionless behavior, the excitation frequencies cannot be determined with high accuracy. The observed axial damping is consistent with a gradual transition between the two regimes [Vic00] (see also section 3.3.3).

A zoom-in of the data for the resonance region between 750 and 900 G is shown in figure 6.10. The collective frequency that we measure on resonance at 834.1 G is in full agreement with the expected value for the unitarity limit ($\Omega_z/\omega_z = \sqrt{12/5} = 1.549$) [Str04a]. For the damping rate we observe a clear minimum at a magnetic field of

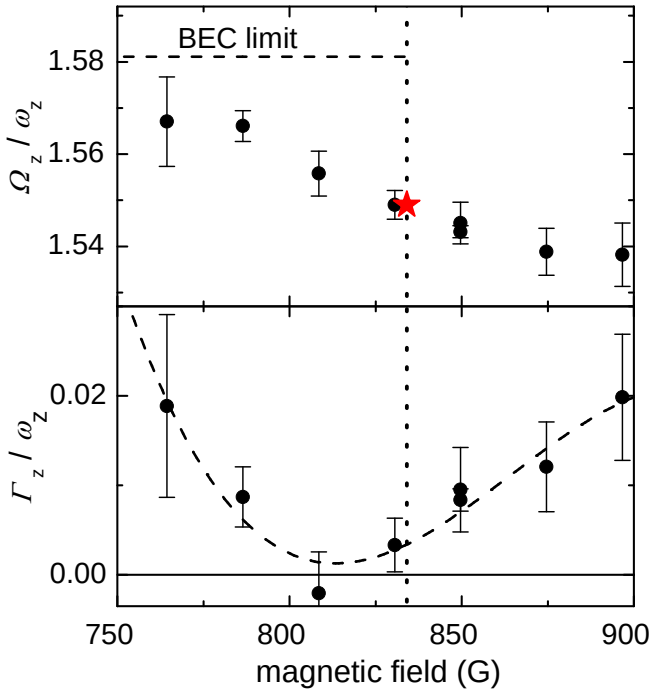

Figure 6.10: Zoom-in of the data shown in figure 6.9 for the resonance region. The star at 834.1 G marks the theoretical prediction $\Omega_z/\omega_z = \sqrt{12/5}$ for the unitarity limit. The dashed line in the lower graph is a third-order polynomial fit to the data to guide the eye.

about 815 G, which is close to the resonance position. It is interesting to note that this damping minimum coincides with the observation of a maximum fraction of condensed fermionic atom pairs observed by M. Zwierlein *et al.* [Zwi04]. For the minimum damping rate we obtain the very low value $\Gamma_z/\omega_z \approx 0.0015$, which corresponds to a $1/e$ damping time of ~5 s.

6.2.3 Radial breathing mode

To excite the radial breathing mode at a given magnetic field, we reduce the optical confinement for 50 μs, which is short compared to the radial oscillation period of about 1.3 ms. In this short interval the cloud slightly expands radially and then begins to oscillate when the optical confinement is switched back to the initial value. The amplitude of the excitation is adjusted such that the relative oscillation amplitude is ~10%. To detect the radial oscillation we turn off the trapping laser after various delay times t and measure the radial size $r(t)$ after 1.5 ms of expansion. The measured radial size $r(t)$ reflects the oscillation release energy. From the measured data, we extract the excitation frequency Ω_r and damping Γ_r by fitting the radial cloud size to $r(t) = r_0 + A_r \exp(-\Gamma_r t) \sin(\Omega_r t + \phi_\mathrm{r})$, where r_0, A_r and ϕ_r are additional fit parameters. Typical radial oscillation curves are shown in figure 6.11.

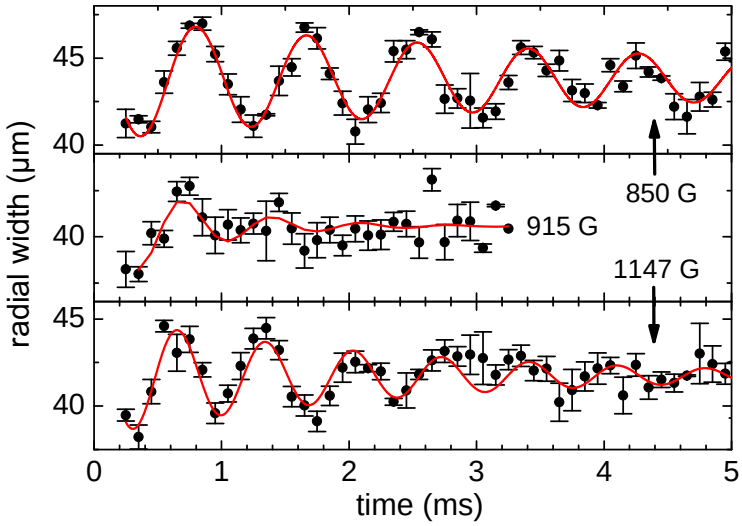

Figure 6.11: Oscillation of the radial breathing mode at different magnetic fields in the strongly interacting Fermi gas regime. The solid lines show fits by damped harmonic oscillations.

The magnetic-field dependence of the radial excitation frequency Ω_r and the damping rate Γ_r are shown in figure 6.12. The data are normalized to the measured frequency ω_r of the radial sloshing mode (see above). It was shown by S. Stringari that this normalization suppresses anharmonicity effects in the measured breathing mode to below 3% [Str04b].

For low magnetic fields the measured frequency approaches $\Omega_r/\omega_r = 2$, expected for the transverse breathing mode of an elongated Bose-Einstein condensate [Str96, Che02]. With increasing magnetic field we observe a large down-shift of the frequency. On resonance at $B = 834.1$ G we observe $\Omega_r/\omega_r = 1.63(2)$. For magnetic fields above the resonance the gas enters the strongly interacting Fermi gas regime and we observe a further decrease of the oscillation frequency until a maximum shift of more than 25% ($\Omega_r/\omega_r = 1.48(5)$) is reached at a magnetic field of 890 G. With further increasing field, i.e decreasing interaction strength, an abrupt change to $\Omega_r/\omega_r \approx 2$ is observed. For magnetic fields larger than 920 G our data are consistent with a Fermi gas in the collisionless regime.

The damping of the radial breathing mode is small in the BEC limit and reaches a minimum close to the Feshbach resonance (see inset in figure 6.12). The minimum damping rate of $\Gamma_r/\omega_r \approx 0.03$ corresponds to a $1/e$ damping time of ~7 ms. At a magnetic field of 910 G, where the abrupt change occurs, we observe very strong damping (see also the middle trace in figure 6.11).

To check our data on the radial breathing mode for systematic effects, we have performed further experiments presented in the next paragraph.

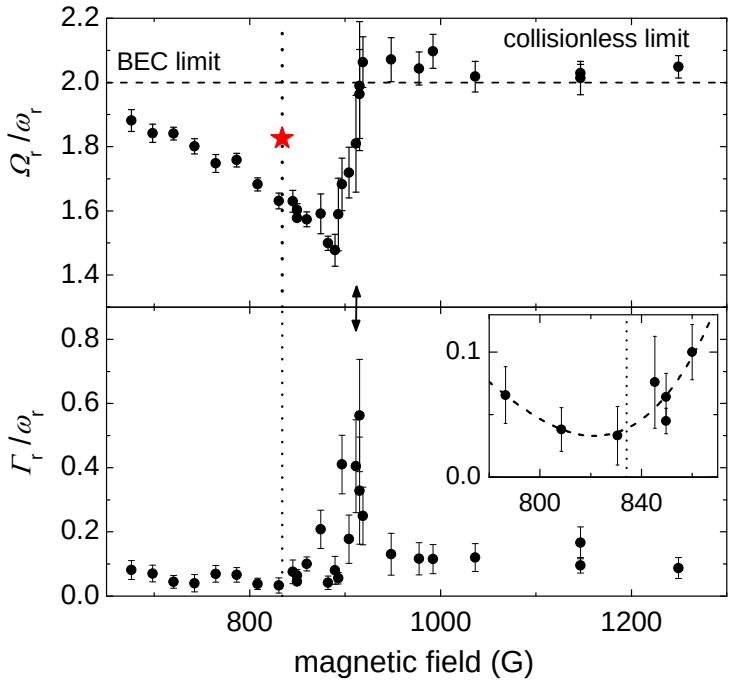

Figure 6.12: Measured frequency Ω_r and damping rate Γ_r of the radial breathing mode, normalized to the radial dipole mode frequency ω_r. In the upper graph, the dashed lines indicate the BEC limit of $\Omega_r/\omega_r = 2$ and the collisionless Fermi gas limit with $\Omega_r/\omega_r = 2$. The vertical dotted line indicates the resonance position at 834.1 G. The star indicates the theoretical expectation of $\Omega_r/\omega_r = \sqrt{10/3}$ in the unitarity limit. The abrupt change in the excitation frequency occurs at about 910 G and is accompanied by anomalously strong damping. The inset shows the damping rate in the resonance region with a second-order polynomial fit to guide the eye.

Investigation of systematic effects

We have repeated the above measurements after recompressing the trap by a factor of nine to a trapping laser power of 310 mW. In this trap the measured radial sloshing mode frequency is $\omega_r \approx 2\pi \times 2.3$ kHz. The measurements shown in figure 6.13 confirm all the previous observations in the shallower trap. In particular, the negative frequency shift and the sudden change in the collective frequency show up in essentially the same way. At resonance we find $\Omega_r/\omega_r = 1.68(2)$. Taking into account the small residual anharmonicity shift we can correct the measured value to $\Omega_r/\omega_r = 1.69(3)$, which is the value we would expect for a harmonic trap. As in the shallower trap we find a minimum of the damping rate in the resonance region. Furthermore the observed abrupt change in the collective frequency at about 910 G is again accompanied by a very large damping rate.

We have also checked that the frequency of the radial breathing mode does not depend on the way we prepare the ultracold gas. Direct evaporation at a fixed magnetic field of 867 G, without starting from a molecular BEC, leads to the same col-

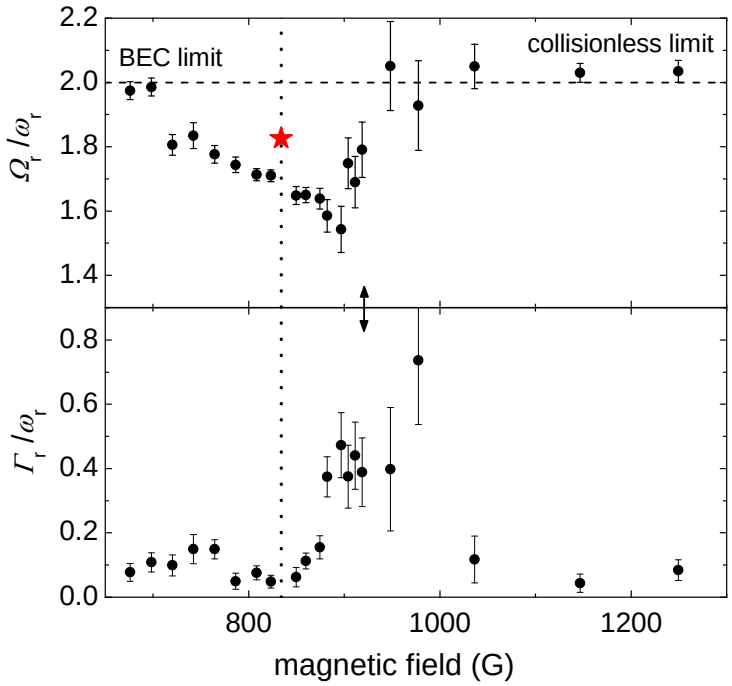

Figure 6.13: Measurements of the radial collective excitation frequency and damping rate in a nine times deeper trap ($\omega_r/2\pi \approx 2.3\,\mathrm{kHz}$). The data confirm all the observations in the shallower trap shown in figure 6.12.

lective frequency. Preliminary investigations of the collective excitations of the gas at higher temperature however, show a trend towards smaller frequency shifts in the radial breathing mode and to smoother changes of the collective frequency.

6.2.4 Comparison with theoretical predictions and related measurements

Our measurements were accompanied by a series of theoretical investigations of collective modes in the BEC-BCS crossover [Str04a, Hei04a, Hu04, Com04b, Com04a, Kim04b, Kim04a, Man04, Bul04].

These theoretical predictions are based on different approaches for the equation of state. In figure 6.14 we show our measured axial (upper graph) and radial (lower graph) breathing mode frequency as a function of the coupling strength, which is expressed by the dimensionless parameter $1/k_\mathrm{F}a$. In this notation the strong coupling BEC limit is obtained for $1/k_\mathrm{F}a \gg 1$, while the weak coupling BCS limit is obtained for $1/k_\mathrm{F}a \ll -1$. In the figure we compare our measurement to the predictions obtained from the mean field crossover theory introduced by A. Leggett [Leg80] and from a quantum Monte Carlo calculation that has been carried out by G. Astrakharchik *et al.* [Ast04] (see section 2.3). The shown calculations of the axial and radial collective mode frequencies in the BEC-BCS crossover were performed by H. Hu *et al.* [Hu04]

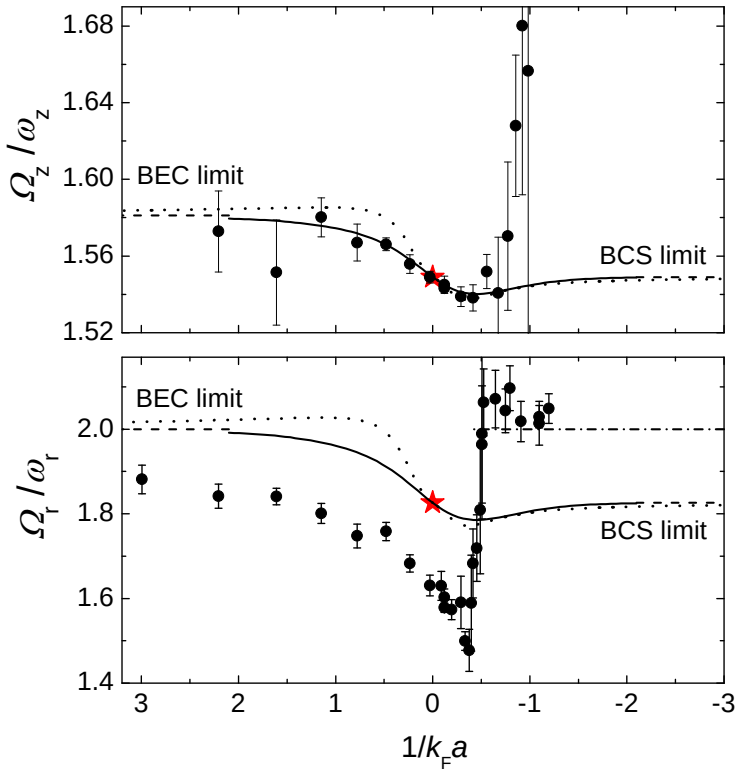

Figure 6.14: Comparison of our measured axial (upper graph) and radial (lower graph) collective mode frequency ratios with the predictions from H. Hu *et al.* [Hu04] (solid lines) and N. Manini *et al.* [Man04] (dotted lines). In the strong coupling limit ($1/k_F a \gg 1$) the frequencies approach the predicted frequency ratio for a molecular BEC in the Thomas-Fermi limit (left dashed lines). The stars mark the predicted frequency ratio for a unitarity limited gas realized on resonance ($1/k_F a = 0$). The same frequency ratio holds for a gas in the weak coupling BCS limit realized for $1/k_F a \ll -1$ (right dashed lines). The horizontal dashed-dotted line in the lower graph indicates the collisionless limit.

for the mean field model (solid lines) and by N. Manini *et al.* [Man04] for the case of the quantum Monte Carlo calculations (dotted lines). Further details of the calculations are found in section3.3.6.

In the following we discuss the main features of our measurements on the axial and radial breathing mode frequencies and compare them with theoretical predictions. The comparison is only qualitative and for a deeper understanding of the individual theoretical models the reader is referred to the cited publications and references therein. It should be noted that the theoretical predictions assume a hydrodynamic behavior of the gas. As explained in section 3.3.1 this hydrodynamic behavior is a general consequence of superfluidity but it also applies to a gas in the normal, non superfluid state, provided that the rate of collisions is large enough ($\omega\tau \ll 1$).

BEC limit: We begin our comparison in the strong coupling molecular BEC limit. As long as the gas is sufficiently dilute ($n_{\mathrm{mol}}a_{\mathrm{mol}}^3 \ll 1$), the collective mode frequencies can be derived from the hydrodynamic equations of superfluids (see section 3.3.1), with an equation of state given by $\mu(n) = gn$. For our cigar shaped molecular BEC, we obtain $\Omega_z/\omega_z = \sqrt{5/2}$ and $\Omega_r/\omega_r = 2$ for the axial and radial breathing mode frequency, respectively (see section 3.3.2).

The measured axial mode frequency agrees with the above theoretical prediction for $1/k_{\mathrm{F}}a > 1$. The measured radial frequency approaches this limit for large $1/k_{\mathrm{F}}a$. However, even at the largest coupling strength of $1/k_{\mathrm{F}}a \approx 3$, were the molecular gas parameter is relatively small ($n_{\mathrm{mol}}a_{\mathrm{mol}}^3 = 0.001$), we observe a substantial down shift with respect to the dilute BEC prediction.

Strongly interacting BEC With increasing interaction strength the binding energy of the molecules is reduced and the BEC-BCS crossover theory predicts a down shift of the collective excitation frequency [Hu04, Hei04a]. Our measurements of the radial and axial modes both show this predicted down shift.

On the other hand, for a strongly interacting BEC one expects corrections to the equation of state due to beyond mean field effects [Lee57]. From the modified equation of state the collective frequency is expected to increase with increasing interaction strength [Pit98] (see also section 3.3.5). Applying these predictions to a molecular BEC in the crossover regime, the collective frequency should follow $\delta\Omega_i/\Omega_i = c_i(n_{\mathrm{mol}}a_{\mathrm{mol}}^3)^{1/2}$ ($i = z, r$), where n_{mol} is the peak molecular number density. For our cigar shaped trap the numerical factors are $c_r = 5c_z = 0.727$. In contrast to this expectation we see a down-shift in both the radial and the axial direction. Using the above formula to fit our first four data points on the axial (radial) mode, we obtain $c_z = -0.05(3)$ ($c_r = -1.1(2)$).

Beyond mean field effects are included in the theory from reference [Man04] and consequently the calculation predicts an up-shift of the collective frequency from the value obtained in the dilute BEC limit (see dotted lines in figure 6.14). The same qualitative dependency is also predicted by the calculations of S. Stringari [Str04a], R. Combescot *et al.* [Com04a], and by H. Heiselberg's BEC approximation [Hei04a]. However, both our axial and radial collective mode frequencies do not show this behavior. In particular, the measured axial mode frequencies in the strongly interacting molecular BEC regime are found in excellent agreement with the theoretical prediction from the BEC-BCS crossover theory, which does not include beyond mean field corrections (see solid line in the upper graph of figure 6.14).

Unitarity limit: On resonance a universal gas is realized and the chemical potential is expected to have the same dependency on the density as in the ideal Fermi gas ($\mu \propto n^{2/3}$). From the hydrodynamic equations the corresponding frequency for the axial and radial mode is calculated to be $\Omega_z/\omega_z = \sqrt{12/5} = 1.549$ and $\Omega_r/\omega_r = \sqrt{10/3} = 1.826$, respectively [Str04a].

The measured axial collective frequency agrees very well with this prediction. On resonance we observe $\Omega_z/\omega_z = 1.548(3)$. For the radial mode, however, we obtain on resonance $\Omega_r/\omega_r = 1.69(3)$ for the harmonic trap limit, which is 8% below the predicted value. This downshift of the radial mode frequency is at present not understood and requires further investigations. Possible explanations for this observation are discussed further below.

Strongly interacting Fermi gas: Above the Feshbach resonance the calculation from the mean field theory [Hu04] predict a further decreasing collective excitation frequency until a minimum is reached at $1/k_F a \approx -0.45$. After this minimum the collective mode frequencies are expected to increase again towards the values predicted for a superfluid gas in the BCS limit. The prediction derived from quantum Monte Carlo calculation shows a very similar behavior, although the local minimum is a bit more pronounced. In the BCS limit one expects the same density dependence of the equation of state as in the case of an unitarity limited quantum gas. Consequently, the collective mode frequencies in the BCS limit are expected to be the same as the ones obtained on resonance [Str04a].

Up to $1/k_F a \approx -0.5$ our observation of the axial mode shows an excellent agreement with the theory. In particular, we observe a decreasing frequency that agrees very well with the prediction. For $1/k_F a \approx -0.5$ the measured frequency starts to deviate from the hydrodynamic prediction and approaches $\Omega_z/\omega_z = 2$ expected for a collisionless Fermi gas.

The behavior of the radial mode is strikingly different. Above resonance we also first observe a further decreasing collective frequency. However, at $1/k_F a \approx -0.5$ we observe an abrupt change in the radial excitation frequency towards $\Omega_r/\omega_r = 2$ expected for Fermi gas in the collisionless regime.

This dramatic change of the radial collective mode frequency and the large damping rate observed in the transition regime (see figure 6.12) are not expected for a normal (non superfluid) Fermi gas, where the collective frequency is predicted to vary smoothly from the hydrodynamic to the collisionless regime [Vic00] (see also section 3.3.3). In the transition regime the maximum damping rate of the radial mode is calculated to be $\Gamma_r/\omega_r = 0.09$ [GO99, Vic00]. Our measured damping rate of $\Gamma_r/\omega_r \approx 0.5$ is clearly inconsistent with this prediction for a gas in the normal (nonsuperfluid) hydrodynamic regime. For a transition from the superfluid to the normal, collisionless phase however, both the sudden change of the collective frequency and a strong damping are expected [Bar00].

A possible explanation for the observed sudden change in the radial mode at about 910 G can be obtained by comparing the radial oscillation energy with the pairing energy. A pair could break by coupling to the collective oscillation, which seems plausible for [Com04b, Hei04b]

$$\hbar\Omega_r \approx 2\Delta, \tag{6.6}$$

where 2Δ is the expected minimum single particle excitation energy and Δ is the zero

temperature BCS gap.

The minimum pairing energy can be estimated from our radio-frequency spectroscopy measurements[4] [Chi04a]. From our measurements at a magnetic field of ~910 G we obtain an effective pairing gap of $\Delta_{\mathrm{eff}}/h \approx 0.7\,\mathrm{kHz}$ (see section 6.3.4). The measured radial collective oscillation frequency at 910 G is about $\Omega_r/2\pi = 1.3\,\mathrm{Hz}$. These values are in reasonable agreement with the relation given in equation 6.6. The same holds for the measurements in the stronger compressed trap (see figure 6.13), where we observe the sudden change of the radial collective mode frequency at the same magnetic field. In this trap the radial collective frequency at 910 G is about $\Omega_r/2\pi = 3.9\,\mathrm{kHz}$, while the effective paring gap is approximately $\Delta_{\mathrm{eff}}/h \approx 2.2\,\mathrm{kHz}$.

It should be noted that in the regime of a strongly interacting Fermi gas, the ratio between the energy gap and the excitation energy is no longer small, indicating a possible breakdown of the hydrodynamic approximation [Men02]. It was pointed out by R. Combescot and X. Leyronas [Com04b] that this argument might explain the disagreement between our measurements and the theoretical predictions for the radial collective mode frequency on resonance. Note further that our results might have been influenced by a residual ellipticity of our trapping laser beam, which requires further investigations.

Measurements of the radial breathing mode at Duke University

The group of J. Thomas studied, parallel to our measurements, the radial breathing mode in the resonance region [Kin04a]. Their measurements showed much weaker frequency shifts than observed in our measurements and the collective frequencies reported in the magnetic field range from 770 to 910 G are close to the hydrodynamic predictions. Their measurements also showed a decreasing damping rate with decreasing temperature.

To investigate the discrepancy between the two experiments J. Kinast *et al.* later extended the investigation to the magnetic field range from 750 to 1114 G [Kin04b]. Over the magnetic field range from 770 to 910 G these measurements confirmed their former results. For fields near 1080 G they observed a sharp increase in frequency and damping rate which is in qualitative agreement with our observed transition at a field of 910 G.

The reason for the different behavior of the collective excitation frequency on the magnetic field is at the moment not fully understood. One reason might be the higher axial trapping frequency in the experiment of J. Kinast *et al.* resulting in a larger ratio of the Fermi energy to the radial trap frequency than in our case. As the pairing energy is proportional to the Fermi energy and exponentially depends on coupling strength $1/k_{\mathrm{F}}a$, this tends to shift the effect of coupling the collective modes to in-gap excitations to higher magnetic fields. Consequently, they observe the abrupt transition at a higher magnetic field. The same mechanism might also affect the collective mode

[4] The corresponding measurements are presented in detail in the next section.

frequency at unitarity.

6.2.5 Summary and Conclusion

Our measurements demonstrate that the collective modes of a degenerate Fermi gas in the BEC-BCS crossover show a pronounced dependence on the coupling strength and thus provide valuable information on the physical behavior of the system.

Our measurements of the axial breathing mode agree very well with the theoretical expectations for a gas in the BEC-BCS crossover. In particular, our measurements in the unitarity limited quantum gas confirm the theoretical expectation. For magnetic fields somewhat below the resonance we measure a very low damping rate of the axial oscillation, which may be seen as a strong piece of evidence for superfluidity.

The measurements of the radial breathing mode show a very strong dependence on the coupling strength that cannot be explained on the basis of available theoretical models. In particular, the observed down shift on resonance is larger than predicted. The most striking feature however, is the observed abrupt change of the radial collective frequency at a magnetic field of ∼910 G ($1/k_{\mathrm{F}}a \approx -0.5$), which is accompanied by very strong damping. The observation supports an interpretation in terms of a transition from a hydrodynamic to a collisionless phase. A superfluid scenario for the hydrodynamic phase seems plausible in view of current theories on resonance superfluidity [Hol01, Mil02, Chi02, Oha02] and the very low temperatures provided by the molecular BEC [Car04].

These measurements are the first step to understand the dynamics of a degenerate Fermi gas in the BEC-BCS crossover. In particular the behavior of the radial collective mode requires further investigations, which we plan to perform after upgrading our diagnostic tools and implementing additional excitation schemes as discussed in the outlook in chapter 7.

6.3 Observation of the pairing gap by radio-frequency spectroscopy

Radio-frequency (rf) spectroscopy was introduced as a powerful and sensitive tool to study interaction effects in ultracold Fermi gases [Reg03a, Gup03, Reg03b]. In ^{40}K this technique was used to directly measure the mean field interaction energy [Reg03a], to detect ultracold $^{40}K_2$ molecules and to determine their binding energies [Reg03b]. In atomic ^{6}Li rf spectroscopy has been applied to study interaction effects for magnetic fields up to 750 G [Gup03]. One important observation was the absence of mean-field shifts in the strongly interacting regime. This effect can be attributed to the fact, that in the relevant magnetic field range, all s-wave scattering processes between the ^{6}Li atoms in the involved states are simultaneously unitarity limited. This property of ^{6}Li is very favorable for rf spectroscopy because it suppresses shifts and broadening

by mean-field effects. The potential of the rf spectroscopy to observe a pairing gap in a strongly interacting Fermi gas was already pointed out in the first experimental application of this sensitive method in ^{40}K [Reg03a].

Offering an excellent energy resolution spectroscopic approaches were proposed to observe the pairing gap in a superfluid Fermi gas [Tör00, Bru01b, Kin04d]. The basic idea of these schemes is to create a population transfer from a superfluid to a normal phase. The transfer can for example be obtained by an rf-field, that couples one hyperfine state for which the atoms are paired to a hyperfine state that does not lead to a superfluid phase. The population transfer requires breaking the pairs, and the extra energy for this pair breaking process has to be provided by the rf-field. Measurements of the change in the atomic population of the superfluid phase as a function of the applied radio-frequency thus provide information about the energy of the pairing gap.

In our case the pairs consist of one atom in the internal state $|1\rangle$ and one atom in the state $|2\rangle$. To probe the system we drive rf-transitions at ~80 MHz from state $|2\rangle$ into the empty state $|3\rangle$. Using state selective absorption imaging we monitor the loss of particles in state $|2\rangle$ as a function of the applied rf. While unpaired atoms show a resonant loss at a frequency corresponding to the energy difference between the two atomic states $|1\rangle$ and $|2\rangle$, the transition frequency for paired atoms occurs at a higher frequency as energy is required to break the pairs. Radio frequency spectroscopy of unpaired atoms serves as a frequency standard for our measurements of paired atoms and allows us to calibrate our magnetic field as explained in section 6.3.1.

In a first series of experiments we applied radio-frequency spectroscopy to pairs in the low density molecular regime. In this strong coupling limit the localized pairs are molecules. As shown in section 6.3.2 these molecules show a characteristic broad dissociation lineshape, from which we can determine the molecular binding energy. Furthermore we can drive rf transitions between different molecular states to determine their energy splitting. These measurements performed at various magnetic field values in combination with a multi-channel quantum scattering calculation worked out in the group of Paul Julienne at NIST, allow us to extract the interaction parameters of ultracold ^{6}Li atoms with unpresented precision [Bar04c].

The high energy resolution of our radio-frequency spectroscopy technique allows us to observe the pairing gap in the BEC-BCS crossover. Our rf spectra taken for different degrees of cooling and for various coupling strengths are shown in section 6.3.3. We observe the pairing gap for magnetic fields up to ~900 G, clearly beyond the Feshbach resonance. To quantitatively analyze the crossover from the two-body molecular regime to the many-body regime, we measure the dependence of the pairing gap on the Fermi energy and temperature as shown in section 6.3.4. In this section we also present radio-frequency spectra showing the universal behavior of a unitarity limited quantum gas obtained at a magnetic field of 837 G.

The situation of our experiment was theoretically analyzed in the group of Päivi Törmä [Kin04c] for the case of resonant two-body interactions. The theoretically predicted radio-frequency spectra presented in section 6.3.5 are in agreement with our measured spectra. Following the argument given in J. Kinnunen *et al.* [Kin04c] our

results strongly suggest that a resonance superfluid is formed in the central region of the trap.

Preparation of the quantum gas and thermometry

Our experimental approach facilitates the preparation of the quantum gas in various regimes with controlled temperature, Fermi energy and interaction strength.

The final laser power of the evaporation ramp allows us to control the temperature T. Through compressing the trap after the cooling process by increasing the trap laser power, we are able to vary the Fermi energy E_F. After this preparation at 764 G, we slowly change the magnetic field within typically 1 s to tune the interaction strength.

The radial and axial trap frequencies are given by (see section 4.3.2)

$$\omega_r/2\pi = 128(1)\,\mathrm{Hz} \times \sqrt{P/\mathrm{mW}} \tag{6.7}$$

$$\omega_z/2\pi = \sqrt{601(4)\,B/\mathrm{kG} + 0.3(1)\,P/\mathrm{mW}}\,\mathrm{Hz}. \tag{6.8}$$

From the trap frequencies and the measured number N of paired and unpaired atoms the Fermi energy for a noninteracting gas is determined by $E_F = \hbar\bar{\omega}(3N)^{1/3}$ where $\bar{\omega} = (\omega_r^2\omega_z)^{1/3}$.

Because we do not have a reliable method to determine the temperature T of the deeply degenerate, strongly interacting Fermi gas, we characterize the system by the temperature T' measured after an adiabatic and reversible conversion of the gas into the BEC limit. The temperature T' is determined at a magnetic field of 676 G by fitting a bimodal distribution to in situ images of the trapped, partially condensed cloud as described in section 5.2.1.

For the full evaporation, we observe a condensate fraction of above 85(3)% and we determine an upper limit for the temperature $T'/T_c = 0.42(5)$ where T_c is the critical temperature for a noninteracting molecular BEC (section 5.2.1). We rewrite this temperature in terms of the Fermi energy for a two component Fermi gas in a harmonic trap using the relation $T_c = 0.518\,T_F$ [Oha03] and obtain $T'/T_F < 0.22(3)$.

As mentioned already a general theory for the relation between the true temperature T in the crossover region and our observable T' is presently not available. Following the arguments presented in section 5.2.3 we however expect a substantial temperature reduction when the molecular BEC is converted into a strongly interacting gas with resonant interactions.

6.3.1 Relevant atomic states and rf spectroscopy of atoms

The Zeeman shift of the $2S_{1/2}$ ground state manifold of ^{6}Li is shown in figure 6.15 (left). The states are denoted with increasing energy by $|1\rangle, |2\rangle, \ldots |6\rangle$ (details to the notation are found in appendix A). Within the magnetic field range investigated in our experiments the electronic and nuclear spin decouple and the system is in the Paschen-Back regime. In this regime the atomic states are characterized by the quantum numbers of the electronic spin S, the nuclear spin I and their orientation with respect to

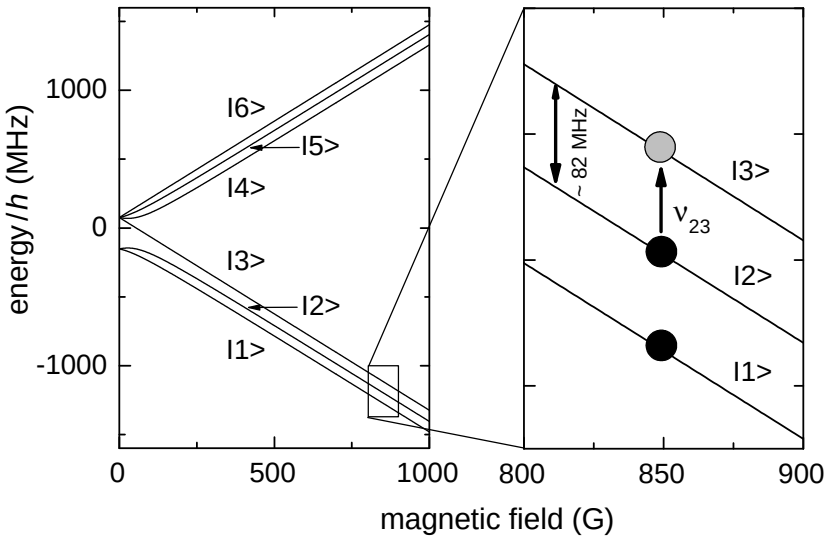

Figure 6.15: Hyperfine ground state manifold of ^{6}Li in an external magnetic field. The states are denoted with increasing energy by $|1\rangle, |2\rangle, \ldots |6\rangle$ (left). We drive rf transitions from the state $|2\rangle$ to the empty state $|3\rangle$ and monitor the loss in state $|2\rangle$ by state selective absorption imaging. In the magnetic field range of interest the system is in the Paschen-Back regime and the transition frequency ν_{23} is about 82 MHz (right).

the external magnetic field, denoted by the quantum number m_S and m_I, respectively. For ^{6}Li the electronic spin is $S = 1/2$ and the orientation can either be $m_S = +1/2$ or $m_S = -1/2$ corresponding to low and high field seeking states with a magnetic moment of $\sim\mu_\mathrm{B}$, respectively. The orientation of the nuclear spin $I = 1$ leads to a splitting of the two electronic states in triplets of states corresponding to $m_I = 1, 0, -1$ as seen in figure 6.15.

In principle one can drive transitions between the ^{6}Li ground states using either electromagnetic fields in the radio-frequency or microwave regime. The corresponding transitions are accompanied by a change of the nuclear ($\Delta m_I = \pm 1$) or the electronic spin ($\Delta m_S = \pm 1$), respectively. Because the nuclear magnetic moment couples much weaker than the electronic magnetic moment to the electromagnetic field the strength of both transitions is very different making it more easy to drive microwave transition. The sensitivity of both transitions to the stability of the external magnetic field is also strikingly different. While in the microwave transition the electronic spin state is changed, which corresponds to a change in the magnetic moment of about $\Delta\mu = \pm 2\mu_\mathrm{B}$, the rf transition conserves the electronic spin state and the magnetic moment is only slightly changed. Consequently the microwave transitions are much more sensitive to the stability of the external magnetic field. Taking our magnetic field stability of about 20 mG the maximum attainable resolution of the microwave transition is limited to about $2\mu_\mathrm{B}\Delta B \approx 50\,\mathrm{kHz}$. Using rf transitions on the other hand we were able to observe narrow spectroscopic signals of about 200 Hz. Only this high resolution of

the radio-frequency transitions makes the observation of the pairing gap possible (see section 6.3.3).

For our experiments the relevant states are the three lowest sublevels $|1\rangle$, $|2\rangle$ and $|3\rangle$. In the Paschen-Back regime these states correspond to $m_S = -1/2$ and $m_I = 1, 0, -1$, respectively (figure 6.15, right). We drive transitions between the state $|2\rangle$ and $|3\rangle$ using a weak rf pulse of typically 1 s duration and monitor the loss of atoms in state $|2\rangle$ employing state selective absorption imaging. In all measurements we individually adjust the rf power to obtain a maximum loss of about 40%. This value is chosen as a compromise between a good signal to noise ratio and a minimum perturbation of the system. To avoid broadening effects the rf power is generally weak and applied to the sample for a long time. In the magnetic field range investigated in our experiments the transition frequency ν_{23} for a noninteracting atomic ^{6}Li gas is about 82 MHz.

Rf spectroscopy of unpaired atoms

Radio-frequency spectroscopy of unpaired, thermal atoms at $T \approx 6T_F$ ($T_F = 19\,\mu$K) serves as a reference and allows us to calibrate our magnetic field. Figure 6.16 shows a typical rf spectrum obtained at a magnetic field of ~837 G. The spectrum shows the narrow atomic transition line with a linewidth of below 1 kHz that enables us to determine the center position to within a few 100 Hz. This high resolution corresponds to an intrinsic sensitivity to interaction effects on the scale of 5 nK. Based on the Breit-Rabi formula [Bre31] and the ^{6}Li parameters given in the appendix, this allows us to calibrate our magnetic field to an accuracy of a few 10 mG. Within our statistical uncertainty, we do not observe any density-dependent frequency shifts of the transition frequency. The absence of mean-field effects in the strongly interacting regime was also observed in the rf spectroscopic investigation of atomic ^{6}Li by S. Gupta *et al.* [Gup03] and can be attributed to the fact that in this regime the s-wave interactions between the atoms in the states $|1\rangle$, $|2\rangle$ and $|3\rangle$ are simultaneously unitarity limited (see figure 3.4 and 3.6 in section 3.2.3). The saturation of mean field effects in the vicinity of a Feshbach resonance was also observed in the rf spectroscopy in atomic ^{40}K [Reg03a].

6.3.2 Rf spectroscopy of weakly bound molecules

So far our initial sample contained unpaired atoms in the internal states $|1\rangle$ and $|2\rangle$. Two atoms in this spin configuration are said to be in the scattering channel (1,2). Consequently after an rf-transition that transfers one of the atoms from state $|2\rangle$ into the state $|3\rangle$ the two atoms are in the scattering channel (1,3).

For atoms in the scattering channel (1,2) a broad Feshbach resonance exists at a magnetic field of about 834 G (see section 3.2.3). For magnetic fields tuned below the resonance atoms in the (1,2) channel can form weakly bound molecules as described in section 3.2.4. A similar Feshbach resonance occurs for atoms in the (1,3) scattering channel at a magnetic field of 690 G. Analogous to the (1,2) channel the

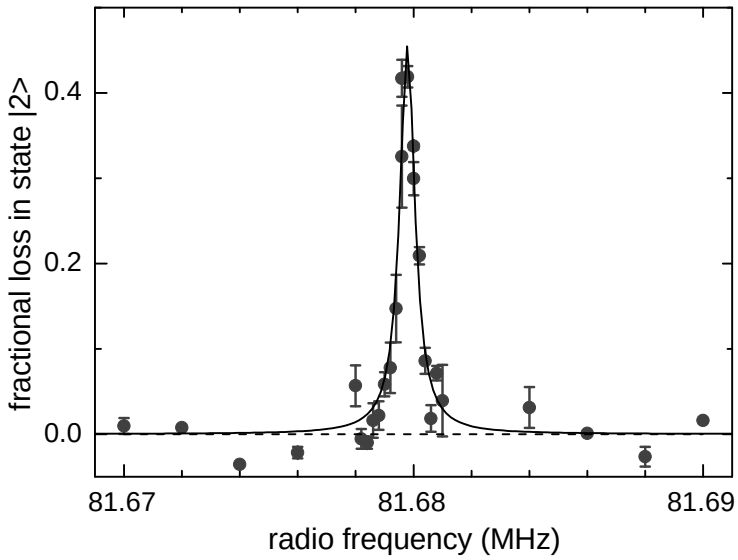

Figure 6.16: Rf-spectroscopy signal of an unpaired "hot" thermal sample at $T \approx 6T_F$ ($T_F = 19\,\mu$K). The fractional loss in state $|2\rangle$ is measured as a function of the radio-frequency. From a Lorentzian fit (solid line) we determine the linewidth to be 640(20) Hz and the center frequency to be at 81.6798(2) MHz. Based on the Breit-Rabi formula this allows us to determined the magnetic field to be 836.92(4) G.

(1,3) channel provides a weakly bound molecular level for magnetic fields below this resonance field. In figure 6.17 we show the magnetic field dependent energy level structure for the two channels (1,2) and (1,3). For purely atomic samples (dotted lines) the frequency difference between the two channels corresponds to the magnetic field dependent atomic transition frequency ν_{23}.

Starting with molecules created in the (1,2) channel we drive a rf transition to the (1,3) channel. This rf transition can dissociate the molecule into two free atoms (bound-free transition) or, for magnetic fields below 690 G, can drive the transition between the molecular states in the (1,2) and the (1,3) channel (bound-bound transition) (see figure 6.17). In both cases the rf excitation results in a loss of molecules in the (1,2) channel which we detect by state selective absorption imaging.

Bound-free transition

For weakly bound molecules with a binding energy E_b formed by an atom in state $|1\rangle$ and an atom in state $|2\rangle$, the rf can dissociate the molecule into two atoms (one in state $|1\rangle$ and one in state $|3\rangle$), if the threshold condition $h\nu_{rf} > h\nu_{23} + E_b$ is fulfilled. Above threshold, the rf-induced dissociation produces two atoms with a total kinetic energy of $2E_k$. In the center of mass system, where the molecule is at rest, the energy conservation reads

$$h\nu_{rf} = h\nu_{23} + E_b + 2E_k. \tag{6.9}$$

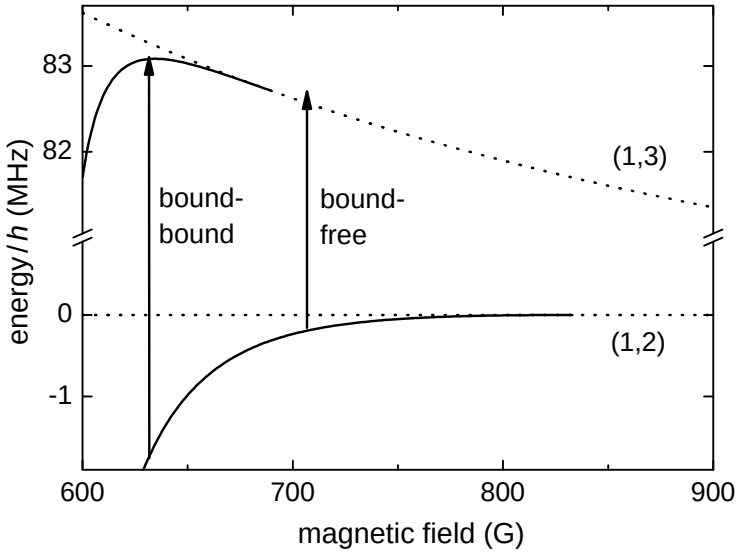

Figure 6.17: Energy level structure near the $^6Li_2$ dissociation threshold as a function of magnetic field. The threshold energy of the (1,3) scattering channel (upper dotted line) is plotted relative to the (1,2) threshold (lower dotted line). The molecular state (lower solid line) in the (1,2) channel exists below the Feshbach resonance at ~834 G. Another molecular state (upper solid line) exists in the (1,3) channel below the resonance at ~690 G. The bound-bound and the bound-free transition are illustrated by the arrows.

Typical molecular lineshapes are shown in figure 6.18. As a clear signature of the pairing process, we observe the transition spectrum at higher frequencies with respect to the pure atomic transition frequency (vertical dotted lines in figure 6.18). The temperature in these samples is $T'/T_F < 0.22$ ($T_F = 1.2\,\mu$K), which we realize with a deep evaporative cooling ramp down to an optical trap with a laser power of $P = 3.8$ mW. In such a cold sample all atoms are paired and the atomic transition frequencies are determined from independent measurements with unpaired atoms. By employing a weaker evaporative cooling process, we are also able to create samples that simultaneously contain unpaired and paired atoms. The rf spectra of such samples show the characteristic double peak structure from the unpaired and paired atoms (see figure 6.20 middle row) and are further described in the next section where we present our rf spectroscopy measurements in the BEC-BCS crossover.

The sharp onset of the fractional loss shown in figure 6.18 corresponds to the threshold condition given in equation 6.9. The full rf spectrum can be understood in terms of the Franck-Condon overlap of the molecular wave function with the wave function in the dissociation channel. The wave function of the molecules is essentially determined by the the scattering length a (or the corresponding binding energy $E_b \approx \hbar^2/ma^2$). The wave function of the dissocitation channel (1,3) depends on the kinetic energy E_k and the scattering length a_{13}. This dissociation channel exhibits a broad Feshbach resonance at 690 G which significantly affects the dissociation line-

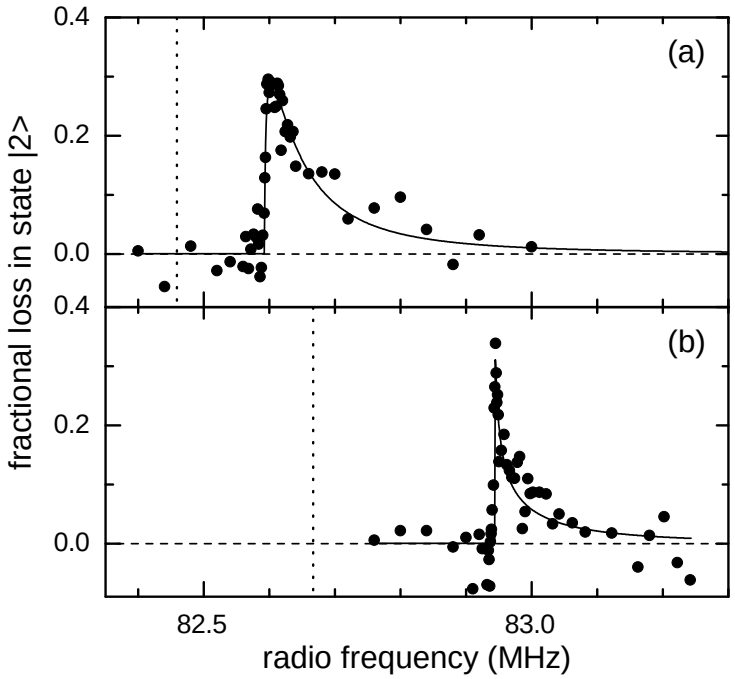

Figure 6.18: Bound-free rf spectra at a magnetic field of 720.13(4) G (a) and 694.83(4) G (b). The fractional loss in state $|2\rangle$ is measured as a function of the applied radio-frequency. The solid lines are the fit based on equation 6.10. The atomic transition frequencies, which are measured independently, are indicated by the vertical dashed lines.

shape [Chi05].

In the range of magnetic field we investigate, a_{13} is much larger than the range of the van der Waals potential of $r_c \approx 30\,a_0$. In this case the lineshape function $P(E)$ is well approximated by [Chi05]

$$P(E) \propto \frac{(E - E_b)^{1/2}}{E^2(E + E' - E_b)}, \tag{6.10}$$

where $E = h\nu_{rf} - h\nu_{23}$ and $E' = \hbar^2/ma_{13}^2$.

Assuming an exponential decay of the particle number we fit $(1 - e^{\alpha P(E)})$ to the loss signal, where α depends on the rf power. The fit of this function to the experimental data is shown in figure 6.18 as the solid lines. From the fit we determine the dissociation threshold and thus the molecular binding energy[5]. From the two bound-free rf spectra shown in figure 6.18 in combination with the independent measurement of the atomic transition frequencies (not shown) we determine the binding energy to be $E_b = h \times 134(2)$ kHz at a magnetic field of 720.13(4) G and $E_b = h \times 277(2)$ kHz at 694.83(4) G.

[5]From the fit we also obtain E' which could in principle be used to determine interaction parameters of ^{6}Li as described below. Because in the magnetic field range investigated in this experiment, the value of $E' \ll E_b$, the fits yield large uncertainties for E' and the values are therefore not taken into account.

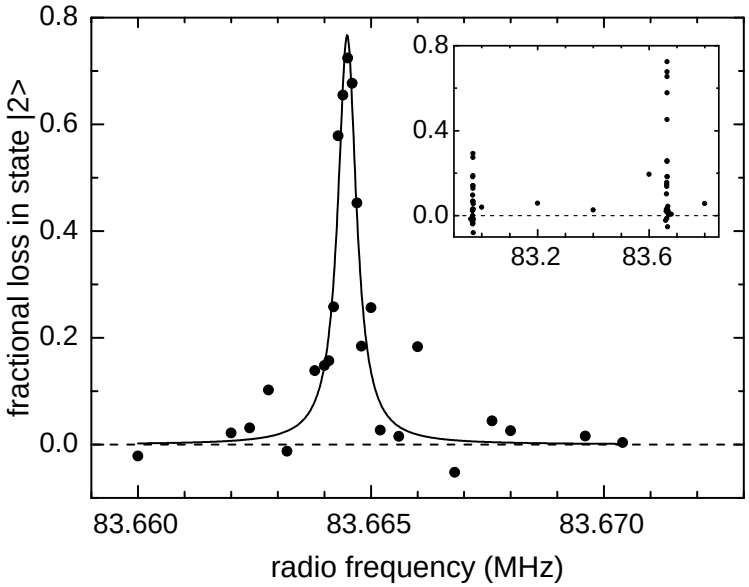

Figure 6.19: Rf spectrum of the bound-bound transition at 661.44(2) G. The fractional loss in state $|2\rangle$ shows a narrow resonance at the bound-bound transition frequency. From a Lorentzian fit (solid line) we determine the center frequency to be 83.6645(3) MHz. The inset shows the whole rf spectrum that includes the fractional loss from the unpaired atoms. The later signal is used to calibrate the magnetic field based on the Breit-Rabi formula.

Bound-bound transition

A weakly bound molecular state in the (1,3) channel exists for magnetic fields below the corresponding Feshbach resonance at about ~690 G. At these magnetic fields ($B < 690$ G), we can drive the rf transition between the (1,2) and (1,3) molecular states (see figure 6.17). The transition frequency of this bound-bound transition is given by the energy difference of the two molecular states. To avoid possible systematic shifts at these lower magnetic fields [Gup03], we prepare a thermal mixture of atoms and molecules at a temperature of $T' \approx T_F$ ($T_F = 2.5\,\mu$K) by a controlled heating method (see section 6.3.4 for details).

A typical bound-bound transition signal at a magnetic field of 661 G is shown in figure 6.19. The resonance frequency of the narrow bound-bound transitions is determined from a fit by a Lorentzian profile. The coexistence of atoms and molecules in the (1,2) channel allows us to simultaneously determine the molecular and atomic transition frequencies (see inset in figure 6.19). From an individual fit to the atomic transition frequency (not shown) we determine the magnetic field using the Breit-Rabi formula.

It should be noted that for magnetic fields below the Feshbach resonance in the (1,3) channel the bound-free transition is much weaker. For a detailed description of the evolution of the rf spectrum when the magnetic field is tuned through the resonance we refer to the article by Cheng Chin and Paul Julienne [Chi05].

Precise determination of the ultracold ^{6}Li collision parameters

The molecular level structure near the collision threshold unambiguously determines the scattering properties of ultracold atoms. As we have seen in the previous sections we can precisely measure this level structure by rf spectroscopy measurements on weakly bound molecules. By fitting the corresponding experimental data with a multi-channel quantum scattering calculation, we were able to obtain a full characterization of the two-body scattering properties. This work is a collaboration with the theory group of Paul Julienne at NIST and is published in [Bar04c]. In this section we report on the main findings.

The precise knowledge of the magnetic field dependent scattering length is important for a quantitative comparison of the experimental results with the predictions of the crossover theory. Of particular importance is the value of the Feshbach resonance in the (1,2) channel, as it determines the magnetic field value where the strongly interacting quantum gas is expected to show a universal behavior [Hei01, Ho04b]. At the time our measurement were carried out, the resonance position was expected to be in the range of magnetic fields between 822 G and 834 G [Sch04]. This range is given from the observation of the controlled dissociation of $^6Li_2$ dimers at 822 G and studies of systematical effects that suggest the upper bound of 834 G. Previous measurement explored the Feshbach resonance in ^{6}Li by measuring inelastic decay [Die02], elastic collisions [O'H02b, Joc02] and the interaction energy [Bou03], but could not locate the exact resonance position to within a range between 800 and 850 G.

The experimental data used to calculate the magnetic filed dependent scattering length of the (1,2), (1,3) and (2,3) channels are summarized in table 6.1. The upper two rows refer to measurements of the bound-bound transition at magnetic fields of 661 G (see figure 6.19) and 676 G, respectively. The lower two rows refer to measurements of the bound-free transition at magnetic fields of 695 G and 720 G, respectively (see figure 6.18). The calculated values for the correspond transition frequency are reported in the last column of the table. They are determined by fitting the experimental data to a multi-channel quantum scattering model.

Because of the high precision of the measured transition frequencies, a careful analysis of systematic effects is necessary. Possible systematic shifts include differential light shifts of the two molecular states and density dependent many-body shifts. In order to characterize these possible systematic errors, we experimentally investigated these shifts by varying the trap depth of the optical potential. In a deeper trap, both the differential light shifts and mean field shifts are expected to increase. We repeated the bound-bound and the bound-free rf spectroscopy in traps with different laser power P between 3.8 mW and 310 mW. Furthermore we repeated the measurements of the unpaired atom-atom transition in traps with different laser power ranging from 10.5 W down to 0.2 W. In all cases we did not see systematic shifts within our statistical uncertainty. The measurements show that these systematic shifts do not exceed the uncertainties given in table 6.1.

Using our experimental data listed in table 6.1 the group of Paul Julienne deter-

Table 6.1: Comparison between our experimental and theoretical results. The magnetic field B is determined from the measured atomic transition frequency ν_{23}. The molecular transition frequency f_{mol} refers to the resonance peak for bound-bound transitions (upper two rows) or to the dissociation threshold position for molecular bound-free transitions (lower two rows). The theoretical values are from the multi-channel quantum scattering calculation that has be carried out in the group of Paul Julienne. The values in parentheses indicate 1σ uncertainties.

ν_{23} (MHz)	B (G)	f_{mol} (MHz)	
		experiment	theory
82.96808(20)	661.436(20)	83.6645(3)	83.6640(10)
82.83184(30)	676.090(30)	83.2966(5)	83.2973(10)
82.66686(30)	694.826(40)	82.9438(20)	82.9419(13)
82.45906(30)	720.131(40)	82.5928(20)	82.5910(13)

mined the singlet and triple scattering length by fitting the data to a multi-channel quantum scattering model [Sto88]. Using the same interaction potential model as described in [O'H02b], they varied the singlet and triplet scattering lengths by making small variations to the inner wall of the potential to fit our measured binding energy and energy differences. Once the values for the singlet and triplet scattering length are specified, all other scattering and bound state properties, including the position of the Feshbach resonances, are determined.

Fitting the experimental data, the singlet and triplet scattering length are determined to be $a_{\mathrm{s}} = 45.167(8)\,a_0$ and $a_{\mathrm{t}} = -2140(18)\,a_0$, respectively. The uncertainty includes both the uncertainty in the in the measured value of the magnetic field and the uncertainty in the rf spectrum. These values agree within the uncertainties with previous determinations $a_s = 45.1591(16)\,a_0$ [Sch04] and $a_t = -2160(250)\,a_0$ [Abr97].

The calculated positions for the broad s-wave resonances for the (1,2), (1,3) and (2,3) channels are 834.1(1.5) G, 690.4(5) G and 811.2(1.0) G, respectively. The calculated scattering lengths for the three different scattering channels are shown in section 3.2.3. These very precise values for the magnetic field dependent scattering lengths in ^{6}Li are used throughout this thesis and allow us to fully characterize the interaction strength between the particles in the BEC-BCS crossover.

6.3.3 Rf spectra in the crossover

In this section we employ rf spectroscopy in the BEC-BCS crossover. Our measurements cover the range from weakly bound molecules in the BEC limit to the BCS side of the Feshbach resonance where no weakly bound molecular level exists. The rf transition is again driven between the (1,2) and the (1,3) channel by employing a weak rf pulse of 1 s with an individually adjusted power to obtain a maximum loss of about 40%. We introduce the rf detuning as the difference between the applied rf ν_{rf} and the

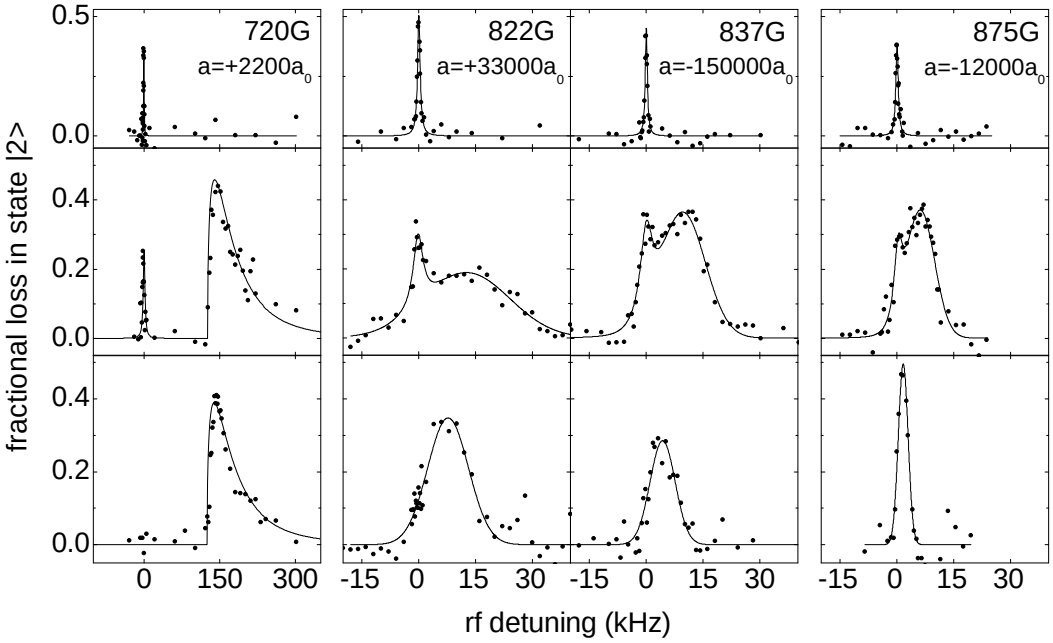

Figure 6.20: Rf spectra for various magnetic fields and different degrees of evaporative cooling. The rf detuning is given relative to the atomic transition $|2\rangle \rightarrow |3\rangle$. The molecular limit is realized for $B = 720\,\mathrm{G}$ (first column). The resonance region is studied for $B = 822$ and $B = 837\,\mathrm{G}$ (second and third column). The BCS side of the crossover is explored at 875 G (fourth column). The top row shows the signal of unpaired atoms at $T'/T_\mathrm{F} \approx 6$ ($T_\mathrm{F} = 19\,\mu\mathrm{K}$). The middle row shows a mixture of paired and unpaired atoms at $T'/T_\mathrm{F} = 0.5$ ($T_\mathrm{F} = 3.4\,\mu\mathrm{K}$). The bottom row shows the signal of paired atoms at $T'/T_\mathrm{F} < 0.22$ ($T_\mathrm{F} = 1.2\,\mu\mathrm{K}$). The solid lines are introduced to guide the eye.

atomic resonance frequency δ_rf ($\Delta = \nu_\mathrm{rf} - \nu_{23}$).

Figure 6.20 shows the rf spectra in the crossover regime at different temperatures for various interaction strengths. The molecular regime is realized for a magnetic field of 720 G. Here the scattering length is about $+2200\,a_0$ and the molecular binding energy amounts to $E_\mathrm{b} \approx h\times 135\,\mathrm{kHz} = k_\mathrm{B}\times 6.5\,\mu\mathrm{K}$. For the resonance region we examined two different magnetic fields of 822 G ($a \approx +33000\,a_0$) and 837 G ($a \approx -150000\,a_0$), respectively[6]. The data at 875 G explore the regime beyond the resonance where the scattering length is large and negative ($a = -12000\,a_0$).

The spectra in the top row of figure 6.20 are taken in a "hot" thermal sample with a temperature $T'/T_\mathrm{F} = 6$, where $T_\mathrm{F} = 19\,\mu\mathrm{K}$. These spectra of unpaired atoms show the narrow atomic transition line and serve as a frequency reference (see section 6.3.1).

The middle row shows rf spectra taken after moderate evaporative cooling down to a final laser power of $P = 200\,\mathrm{mW}$. The temperature in these samples amounts to $T'/T_\mathrm{F} = 0.5$ ($T_\mathrm{F} = 3.4\,\mu\mathrm{K}$). Already at this early stage of our evaporation process

[6] At the time the measurements were carried out, the exact resonance position was unknown to within 10 G and the two values were considered as the lower and upper bounds.

we observe a clear double-peak structure as a result of the coexistence of unpaired and paired atoms. In the molecular regime the sharp atomic peak is well separated from the broad molecular dissociation signal (see also the discussion in the previous section). With increasing magnetic, i.e decreasing binding energy, the peaks approach each other and begin to overlap. In the resonance region ($B = 822\,\mathrm{G}$ and $B = 837\,\mathrm{G}$) we still observe a relatively narrow atomic peak at the original position together with a broader pair signal. For magnetic fields beyond the resonance we can resolve the double peak structure up to ~900 G.

The spectra in the bottom row of figure 6.20 are obtained after deep evaporative cooling down to a final laser power of 3.8 mW. In these samples with $T'/T_\mathrm{F} < 0.22$ ($T_\mathrm{F} = 1.2\,\mu\mathrm{K}$) we observe the disappearance of the narrow atomic peak, showing that all atoms are paired. In the BEC limit the dissociation lineshape from the pairs is identical to the one observed in the trap at higher temperature and Fermi energy. Here the localized pairs form molecules with a size much smaller than the mean interparticle spacing and the dissociation signal is independent of the density. In the resonance region ($B = 822\,\mathrm{G}$ and $B = 837\,\mathrm{G}$) however, the pairing signal shows a clear dependence on the density, which becomes even more pronounced beyond the resonance at 875 G. We attribute this to the fact that the size of the pairs becomes comparable to or larger than the interparticle spacing. This argument is supported by the narrow width of the pair signal in this regime. This indicates a pair localization in momentum space to well below the Fermi momentum $\hbar k_\mathrm{F} = \sqrt{2mE_\mathrm{F}}$ and thus a pair size exceeding the interparticle spacing.

Spectral signatures of pairing have been theoretically considered [Tör00, Bru01b, Kin04d, Büc04, Die04, Kin04c]. A clear signature of the pairing process is the emergence of a double peak structure in the spectral response. The double-peak structure is a direct consequence of the coexistence of unpaired and paired atoms. Because energy is required for pair breaking, the pair related signal is located at higher frequency than the signal from the unpaired atoms. To understand the spectra, both the homogeneous line shape of the pair signal [Kin04d, Die04] and the inhomogeneous line broadening due to the density distribution in the harmonic trap need to be taken into account [Kin04c]. As an effect of inhomogeneity, pairing due to many-body effects takes place predominantly in the central high-density region of the trap and unpaired atoms mostly populate the outer region of the trap where the density is low [Kin04c, Bul03a, Per04a]. In addition to the homogeneous width of the pair breaking signal the spectral component of the pairs thus shows a large inhomogeneous broadening. In the two-body molecular regime the effects of the inhomogeneous density distribution are negligible and the line shape shows the typical molecular lineshape described in section 6.3.2. For the unpaired atoms the homogenous width is narrow and the effects of inhomogeneity are negligible (see also section 6.3.1). These arguments explain why the rf spectra show in general a relatively narrow peak from the unpaired atoms together with a broader peak attributed to the pairs.

6.3.4 Exploring the pairing gap

In this section we present our measurements that investigate the pairing gap in more detail.

For the following discussion we define the effective pairing gap $\Delta\nu$ as the frequency difference between the maximum of the paired signal and the bare atomic resonance position. According to this definition the effective pairing gap $\Delta\nu$ in the low density molecular limit is directly given by the maximum of the molecular dissociation signal. From the lineshape function $P(E)$ (see equation 6.10) the signal maximum is calculated to be $h\Delta\nu = \zeta E_\mathrm{b}$, where ζ depends on the ratio E_b/E' and varies between the two limits $\zeta = 1$ and $\zeta = 4/3$ for $E' \ll E_\mathrm{b}$ and $E' \gg E_\mathrm{b}$, respectively.

Pairing gap in the crossover regime

To qualitatively investigate the crossover from the two-body molecular regime to the many-body regime, we measure the pairing energy in a magnetic field range between 720 and 905 G. The measurements are performed after deep evaporative cooling to $T'/T_\mathrm{F} < 0.22$ for two different Fermi temperatures, $T_\mathrm{F} = 1.2\,\mu$K and $T_\mathrm{F} = 3.8\,\mu$K. These two different Fermi energies are obtained by recompressing the trap to different laser powers of $P = 34.4$ mW and $P = 932$ mW, respectively. Figure 6.21 shows the measured pairing gap $\Delta\nu$ for the two Fermi temperatures as a function of the magnetic field. In the low density molecular limit $\Delta\nu$ can be calculated on the basis of the lineshape function given in equation 6.10 and the most recent data for the scattering length a and a_{13} [Bar04c] (solid line in figure 6.21). For low magnetic field the pairing gap simply reflects the molecular binding energy. With increasing magnetic field, in the BEC-BCS crossover, the pairing gap shows an increasing deviation from this low density molecular limit and evolves into a density dependent many-body regime where $h\Delta\nu < E_\mathrm{F}$.

A comparison of the pairing energies at the two different Fermi energies provides further insight into the nature of the pairs. Figure 6.21 shows the ratio of the pairing gap measured at the two Fermi energies. In the BEC limit the pairing energy is solely determined by the binding energy and does not depend on the Fermi energy, i.e. the density. In the BEC-BCS crossover the pairing energy becomes density dependent. On resonance a universal regime is realized and the Fermi energy is the only relevant energy scale. In the vicinity of the resonance at 837 G we indeed observe the effective pairing gap to increase linearly with the Fermi energy. We find a corresponding relation $h\Delta\nu \approx 0.2E_\mathrm{F}$ (see also the discussion below). Beyond the resonance the system is expected to change from a resonant to a BCS-type behavior. Here we find the the pairing energy to depend more strongly on the Fermi energy and the corresponding gap ratio further increases. We interpret this observation in terms of the increasing BCS character of the pairing for which an exponential dependence $h\Delta\nu \propto E_\mathrm{F} \exp(-\pi/2k_\mathrm{F}|a|)$ is expected (see section 2.2.2).

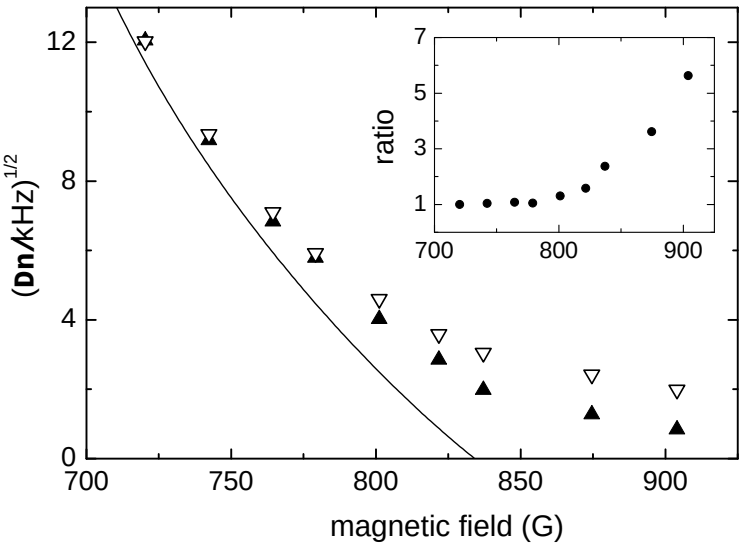

Figure 6.21: Measurements of the effective pairing gap in the BEC-BCS crossover after deep evaporative cooling at two different Fermi temperatures, $T_F = 1.2\,\mu$K (solid symbols) and $T_F = 3.8\,\mu$K (open symbols). The low density limit for the effective pairing gap is shown by the solid line and is essentially given by the molecular binding energy. The ratio of the two measured pairing gaps at the two different Fermi energies is shown in the inset.

Temperature dependence of the pairing gap

To study the temperature dependence of the pairing gap in the strongly interacting Fermi gas, we apply a controlled heating method that allows us to keep all other parameters of the sample constant. After production of a pure molecular BEC with $T'/T_F < 0.22$ in the usual way, we first adiabatically increase the trap laser power to $P = 34\,$mW and then apply an adiabatic magnetic field ramp to $B = 837\,$G. This results in a Fermi temperature of $T_F = 1.2\,\mu$K. We then increase the trap laser power by a factor of nine (T_F increases to $T_F = 2.5\,\mu$K) using exponential ramps of different duration. For fast ramps, this recompression is nonadiabatic and increases the entropy. By variation of the ramp time we investigate a range from our lowest temperatures of $T'/T_F < 0.22\,$K to $T'/T_F = 0.8$. The emergence of the pairing gap (marked by the arrow) with decreasing temperature is clearly visible in the rf spectra shown in figure 6.22.

The marked increase of the pairing gap with decreasing temperature is in agreement with theoretical expectations for the pairing gap energy [Che04]. In figure 6.23 we show the measured pairing gap as a function of the entropy per particle calculated from the measured temperature T'/T_F [Car04]. The figure indicates that the gap emerges below an entropy per particle of $S \approx 15k_B$. For our deep evaporative cooling the entropy is $S \approx 0.2k_B$, which is more than a factor of 10 below the value where the gap first appears.

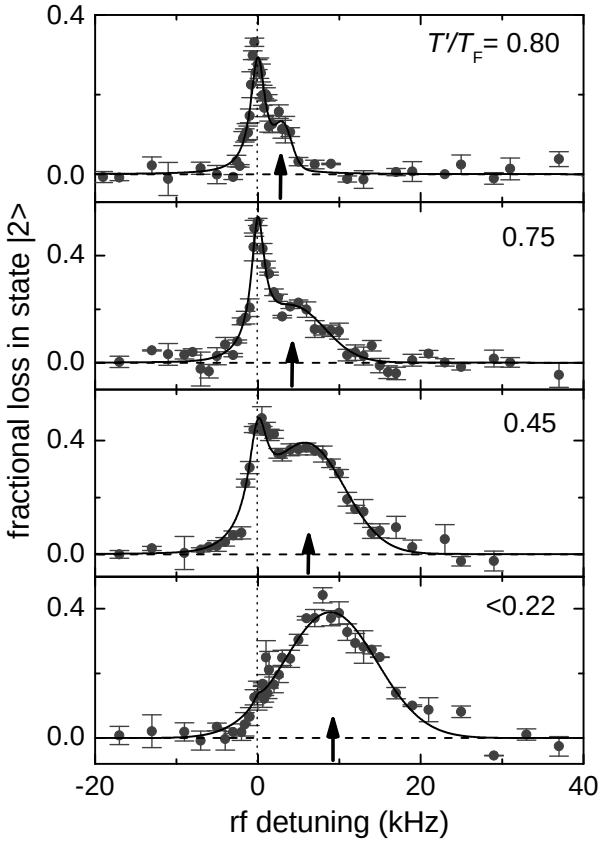

Figure 6.22: Rf spectra at 837 G and $T_F = 2.5\,\mu$K for different temperature T' adjusted by controlled heating. The solid lines are fits to guide the eye, using a Lorentzian curve for the atom peak and a Gaussian curve for the pair signal. The vertical dotted line marks the atomic transition line and the arrow indicates the effective pairing gap $\Delta\nu$.

Rf spectra of a universal quantum gas

On resonance the scattering cross section is unitarity limited and a universal quantum gas is realized [Ho04c]. As discussed in section 2.2.3 and 6.1.2 the only relevant energy scale in such a gas is the Fermi energy and the mean field potential as well as the pairing gap become proportional to the Fermi energy with different proportionality constants [Hei01].

Our measurements of the effective pairing gap at 837 G show the expected linear dependency of the pairing gap on the Fermi energy. From our experimental data we obtain $\gamma \approx 0.1$ where $\gamma = \Delta/E_F$. The theoretical calculations for a uniform system predict a somewhat stronger scaling. For example the BEC-BCS theory for a homogeneous gas predicts $\gamma = 0.53$ [Per04b]. A very similar value of $\gamma \approx 0.54$ has been predicted from a quantum Monte Carlo study [Car03]. An estimate can also be obtained by extrapolating the gap equation (see equation 2.39) for a uniform gas to $ak_F \to \pm\infty$ which results in $\gamma = 0.49$ [Gor61].

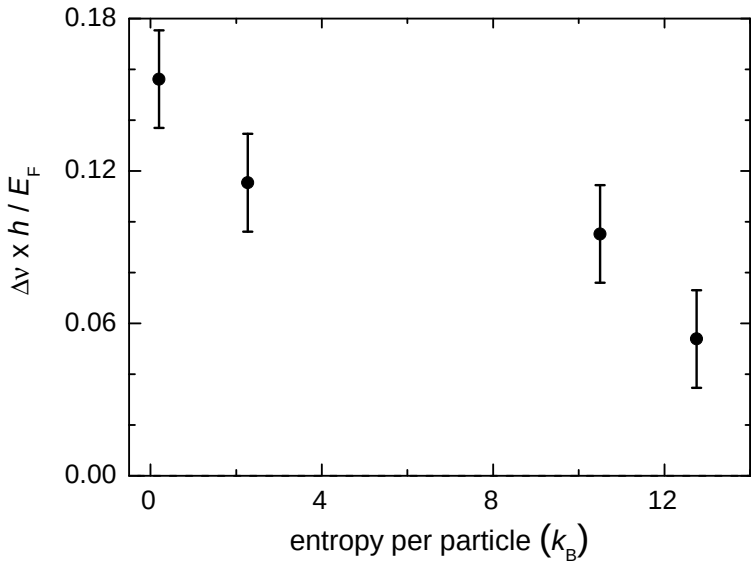

Figure 6.23: Effective pairing gap at a magnetic field of 837 G as a function of the calculated entropy per particle. The lowest entropy of $S \approx 0.2k_B$ reached after deep evaporative cooling, is more than a factor of 10 below the value were the pairing gap emerges.

To further investigate the unitarity limited quantum gas we compare rf spectra of a universal gas realized at 837 G. The spectra are measured at different Fermi energies ranging from $E_F = k_B \times 1.2\,\mu$K up to $E_F = k_B \times 3.8\,\mu$K. Starting point for these experiments is a molecular BEC obtained after full evaporation down to a final laser power of 3.8 mW ($T'/T_F < 0.22$). In a first step we vary the Fermi energy by adiabatically increasing the trap laser power to an intensity of up to ∼1 W which corresponds to a Fermi temperature of $T_F = 3.8\,\mu$K. Following this, we adiabatically change the magnetic field from the production field at 764 G to $B = 837$ G.

In figure 6.24 we present four rf spectra taken at four different Fermi energies in the range from $E_F = k_B \times 1.2\,\mu$K to $E_F = k_B \times 3.8\,\mu$K. The rf detuning of each spectrum is normalized to the corresponding Fermi energy and the maximum fractional loss in each spectrum is normalized to one. The spectra scale with the Fermi energy as predicted for a universal quantum gas. The rf spectrum taken in the strongest recompressed trap at $P = 910$ mW ($T_F = 3.8\,\mu$K), indicates small derivations from the universal lineshape, which we attribute to heating effects in the optical dipole trap. In fact, as we have seen in the previous section, the pairing gap decreases with increasing temperature (see figure 6.22). This argument is further supported by the observation of a small atomic peak in the corresponding spectrum.

Our measurements at 837 G show the expected universal behavior and confirm that the pairing process on resonance is a many-body effect. The measurements presented here are the first experimental investigation of the universal behavior of a unitarity limited quantum gas and more quantitative investigations will follow [Alt].

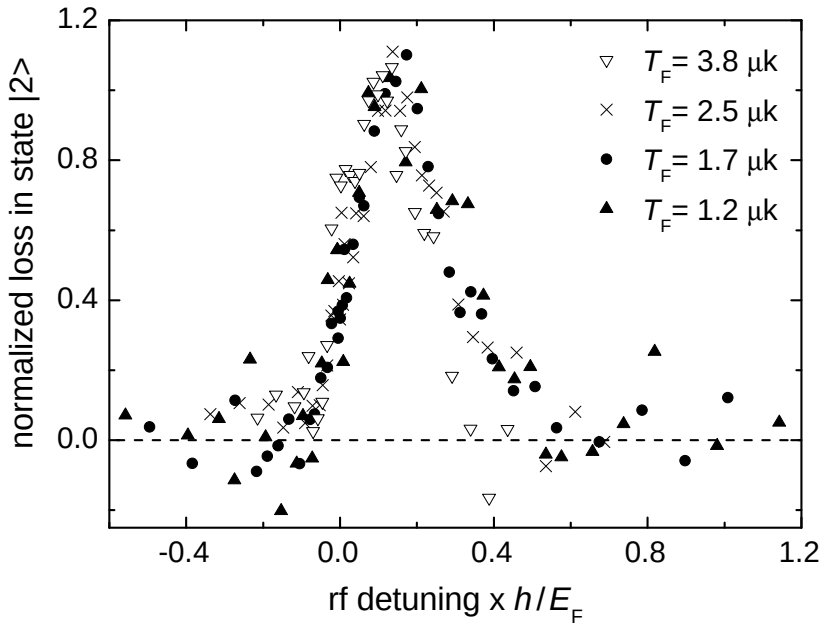

Figure 6.24: Universal rf spectra of atom pairs at $B = 837\,\mathrm{G}$ measured at four different Fermi energies $E_\mathrm{F}/k_\mathrm{B} = 1.2, 1.7, 2.5$ and $3.8\,\mu\mathrm{K}$, respectively. The rf detuning of the individual spectrum is normalized to E_F/h where E_F is the corresponding Fermi energy. In each spectrum the maximum fractional loss in state $|2\rangle$ is set to one.

6.3.5 Comparison with calculated rf spectra of fermionic superfluids

The conditions of our experiment were theoretically analyzed in the group of P. Törmä for the case of resonant two-body interactions [Kin04c]. They calculated the response defined as $I(\delta) = <\dot{N}_3>$, where N_3 is the number of atoms in state $|3\rangle$ and δ is the rf detuning. For details of the calculation we refer to the corresponding article of J. Kinnunen *et al.* [Kin04c].

The calculated rf spectra are in qualitative agreement with our experimental results and demonstrate how a double peak structure emerges as the gas is cooled below $T'/T_\mathrm{F} \approx 0.5$ and how the atomic peak disappears with further decreasing temperature (figure 6.25). A quantitative comparison, however, shows some discrepancies. For our lowest temperatures we observe a shift of the pair peak of about $0.2\,E_\mathrm{F}$ which is similar to $0.3\,E_\mathrm{F}$ obtained from the calculations for $T < 0.1\,T_\mathrm{F}$. The width of the pair signal is determined by the gap and amounts to $0.3\,E_\mathrm{F}$ and $0.4\,E_\mathrm{F}$ from our measurement and from the calculations, respectively. To estimate the experimental uncertainty, we note, that the largest contribution arises from the calibration of the atom number (see section 4.5). The 50% uncertainty in N results in an uncertainty of the Fermi energy of about 17%, which is smaller than the difference between the theoretical predictions and our experimental results.

The calculation predicts a critical temperature in the center of the trap of $T_c \approx 0.3 T_\mathrm{F}$

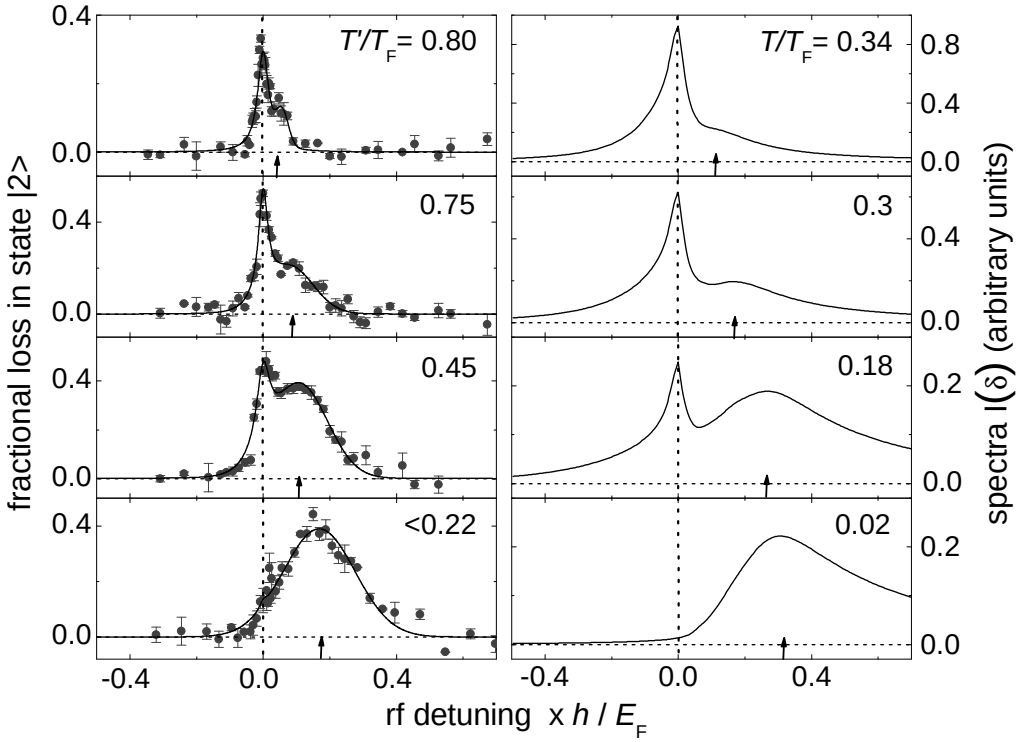

Figure 6.25: Comparison between our measured (left) and the calculated rf spectra by J. Kinnunen *et al.* using the parameters of our experiment [Kin04c] (right). The calculated spectra show the emergence of the gap (marked by the arrow) and the disappearance of the free-atom peak with decreasing temperature. The calculated critical temperature in the trap center is $T_c \approx 0.3$. Our observation of the disappearance of the free atom signal at $T'/T_\mathrm{F} \leq 0.22$ corresponds to a temperature that according to the calculation is well below the critical temperature for a phase-transition to a superfluid.

and they estimate that in our case T_c is in the range of $0.2 < T_c/T_\mathrm{F} < 0.25$. As already mentioned our temperature T' is determined in the BEC limit and the actual temperature T is expected to be reduced as a result of entropy conservation during the adiabatic passage to the unitarity limit. As shown by J. Kinnunen [Kin04c], this argument is consistent with the observation that in the calculated spectra the pair signal appears at $T \approx 0.35\,T_\mathrm{F}$ and is clearly visible $T \approx 0.2\,T_\mathrm{F}$ while in our experiment it appears at the higher BEC limit temperatures $T' \approx 0.8\,T_\mathrm{F}$ and is clearly visible at $T' \approx 0.75\,T_\mathrm{F}$. According to the calculation the atomic peak disappears at temperatures well below the critical temperature for a phase-transition to a superfluid. A recent theoretical study of the BCS-BEC crossover at finite temperature for trapped fermions predicts the phase transition to occur at a temperature only ∼30% below the temperature where pair formation sets in [Per04a].

6.3.6 Summary and conclusion

Applying radio-frequency spectroscopy on ultracold, weakly bound molecules allows us to precisely determine the molecular binding energies and the energy splitting between two molecular states. In combination with a multi-channel quantum Monte Carlo calculation employed by the theory group of Paul Julienne this allowed us to precisely determine the ultracold scattering properties of ^{6}Li.

The high energy resolution of the radio-frequency spectroscopy measurements enabled us to observe the pairing gap in a strongly interacting Fermi gas. The rf spectra taken in the BEC-BCS crossover show a smooth change from the two-body molecular regime to the many-body regime. The observed temperature dependence of the pairing gap in the strongly interacting Fermi gas regime is in agreement with theoretical expectations. Furthermore the pairing gap of a unitarity limited quantum gas is observed to scale with the Fermi energy and shows the predicted universal behavior.

Our measured rf spectra for a strongly interacting Fermi gas are found to be in agreement with theoretical predictions considering resonant two-body interactions. We observe the pairing in the strongly interacting regime already after moderate evaporative cooling. With much deeper cooling the signal of the unpaired atoms disappears from our spectra which shows that the pairing takes place also in the outer region of the trap where the density and the Fermi energy are low. Thus our result strongly suggests that in the central region of our trap a resonance superfluid is formed.

Chapter 7

Outlook

Our experiments provide firm evidence for the superfluidity in a strongly interacting Fermi gas. However, the direct observation of the superfluidity has not yet been achieved and is the major goal of further experiments. The study of rotational phenomena, in particular the investigation of quantized vortices, offers unique access to probe superfluidity in experiments in the BEC-BCS crossover.

Vortices

A direct consequence of superfluidity is that the system cannot rotate as a normal fluid. In contrast to a normal fluid, which in thermal equilibrium will rotate like a solid body, a superfluid will not circulate unless the frequency is larger than some critical frequency. Moreover, when the superfluid does circulate it can only do so by forming vortices in which the condensate density goes to zero and for which the circulation of the velocity field evaluated over a closed contour around the vortex core is quantized [Pit03]. Therefore the observation of quantized vortices presents a direct and unambiguous evidence for superfluidity. Quantized vortices were observed in superconductors [Tin66], superfluid liquid helium [Don91] and in atomic Bose-Einstein condensates [Mat99, Mad00a, AS01, Hod01].

Our approach to produce a vortex will be the creation of an elliptic potential that rotates in the radial plane in order to create the necessary angular momentum for the formation of a vortex. The rotating potential will be created by a fast spatial modulation of our optical dipole potential. To spatially modulate the optical potential we will use acousto-optical modulators. By fast modulation, with modulation frequencies large compared to the radial trap frequency, we can "write" time averaged motional potentials.

To detect the vortices a further imaging system is currently being installed along the symmetry axis of the trap, which is defined by the propagation direction of the trapping laser beam. Similar to the experiments performed with atomic BECs at the ENS in Paris, we will detect the vortex using time-of-flight images at high magnetic field after releasing it from the optical dipole trap [Mad00a] (see also figure 7.1).

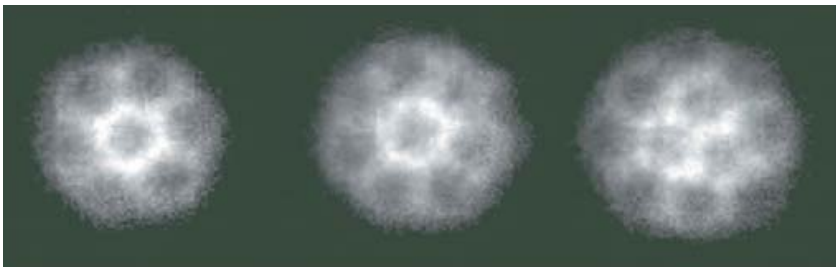

Figure 7.1: Vortices observed in a rotating atomic BEC at the ENS in Paris [Mad00b] with a trap geometry that is similar to our system. In our experiment we plan to use vortices created in the molecular BEC regime to probe the superfluidity in the BEC-BCS crossover.

In the molecular BEC regime the creation and detection of the vortices should be rather straightforward as the macroscopic behavior of the gas should be essentially the same as in case of an atomic BEC. The density of the condensate in the center of the vortex is zero and the region near the axis of the vortex where the density is significantly influenced is on the order of the healing length $\xi = 1/\sqrt{8\pi na}$ [Pit03]. In the molecular BEC regime the healing length will be very similar to the value in the experiments at the ENS ($\xi = 0.2\,\mu$m) [Mad00a]. Furthermore, their trap geometry is similar to our system and we therefore expect a similar visibility of the vortex as displayed in figure 7.1. However, in the strongly interacting regime we expect a loss of visibility due to the shrinking of the healing length down to the value of the Fermi wave number $1/k_{\mathrm{F}}$ [Bul03b].

In a first series of experiments we plan to create vortices in the molecular BEC regime. After the creation we will convert the system into the strongly interacting regime with variable coupling strength and then back convert into the BEC regime to detect the survival of the vortices. An intriguing question is at which coupling strength the superfluidity breaks down, and whether this point corresponds to the observed break down of the hydrodynamic description in our collective mode measurements.

New and refined collective mode measurements

The new axial imaging system will provide better knowledge of the radial trap frequency. We therefore plan to further investigate the radial breathing mode that showed an apparent break down of the hydrodynamic description on the BCS side of the resonance.

Moreover the new acousto-optical modulators will allow us to excite higher radial modes and thus opens up new possibilities to study radial collective modes in the BEC-BCS crossover. In particular we plan to excite the radial quadrupole mode. While the radial breathing mode is a radial monopole (or compressional) mode, the radial quardupole mode is a radial surface mode and is therefore insensitive to the underlying equation of state. The investigation of this mode will thus provide information about the hydrodynamicity of the system. Of particular interest is the investigation of this

mode in the transition region from hydrodynamic to collisionless behavior.

Due to the predicted low visibility of the vortex in the strongly interacting regime the direct detection of vortices in time of flight measurements will be difficult (see above). However the existence of the vortex could be revealed by measurements of the angular momentum through the splitting of the quadrupole frequencies in the presence of the vortex [Zam98, Bru01c]. The use of such a surface-wave spectroscopy has already been demonstrated experimentally in atomic BECs [Che00, Hal01a, Hal01b].

Extension of the pairing gap measurements in the BCS regime

We plan to further investigate the pairing gap on the BCS side of the resonance. Of particular interest is the region where we observe the abrupt transition from a hydrodynamic to a collisionless behavior in the collective mode spectrum. This region will be investigated by simultaneously investigating the rf-spectrum and the collective mode frequency and will allow us to check our hypothesis that the change in the spectrum is related to pair breaking.

Moreover the acousto-optical scanning system will potentially allow us to create box-like potentials. In such a potential the inhomogeneity is reduced with respect to the harmonic potential and consequently the pairing gap will emerge in a much more pronounced way. We hope to perform quantitative studies of the pairing gap in these box-like potentials.

Interference and Diffraction experiments

To gain more insight into the properties of a deeply degenerate Fermi gas in the BEC-BCS crossover we plan to investigate the matter-wave interference pattern. Such matter-wave interference patterns were observed in atomic BECs and allow to test macroscopic first order coherence properties [And97]. Similar to the recent atom interferometry with a BEC [Shi04], we hope to use our acousto-optical modulation system to smoothly convert our single well potential into a double well potential. As in reference [Shi04] the two condensates will then be released from the trap and overlap during the expansion.

On a longer time scale we plan to examine Bragg diffraction [Ste99] of the gas in the BEC-BCS crossover. The observation of the fringe spacing in the crossover will provide us with a new possibility to distinguish between paired and unpaired atoms. Similar to experiments with atomic BECs, we plan to perform Bragg diffraction on a stationary cloud with a pulsed standing wave [Ovc99].

Optical lattices

A strongly interacting Fermi gas in a three dimensional optical lattice will open the door to a widely unexplored field. In bosonic systems experiments in optical lattices

are well established [And98, Gre02]. Such optical lattices represent an ideal environment to model solid-state systems and to study related many-body quantum phenomena. For example fermionic atoms in an optical lattice are predicted to undergo a phase transition to a superfluid state at a dramatically increased transition temperature [Hof02]. The experimental investigation of Fermi gases in optical lattices has just begun [Mod03, Stö04] and many more fascinating experiments can be expected within the near future.

Appendix A

Atomic level structure of ^{6}Li

Most of the properties of ^{6}Li are determined from the single $2S_{1/2}$ valence electron. The coupling of the electron spin with the nuclear spin of $I = 1/2$ results in a hyperfine splitting of the ground state into states with total angular momentum $F = 1/2$ and $F = 3/2$, respectively. The states are split by $\Delta E_0 = 228.2052590\,\mathrm{MHz}$ [Van89].

The first excited state of ^{6}Li is split by the $\mathbf{L}\cdot\mathbf{S}$ coupling of the angular momentum $\mathbf{L}$ and the electronic spin $\mathbf{S}$. The two states $2P_{1/2}$ and $2P_{3/2}$ states are split by about 10 GHz. For laser cooling we use the $D2$ line that connects the $2S_{1/2}$ ground state and the $2P_{3/2}$ excited state and has a transition wavelength of 670.78 nm [Van89]. In contrast to the ground state, the hyperfine splitting of the excited state is smaller than half the natural linewidth of 5.9 MHz and different lines are thus unresolved. This is important for the operation of the MOT as explained in detail in [Joc00, Joc04].

Applying an external magnetic field B results in the Zeeman shift of the ground and excited states (see figure A.1). For the ground state, the magnetic field dependent energies of the hyperfine states can be calculated by the Breit-Rabi formula [Bre31]

$$E(B, m_F) = -\frac{1}{6}\Delta E_0 + m_F g_I \mu_\mathrm{B} B \pm \frac{\Delta E_0}{2}\left(1 + \frac{2}{3} m_F x + x^2\right)^{1/2}, \tag{A.1}$$

where $x = (g_J - g_I)\mu_\mathrm{B} B/\Delta E_0$ with $g_J = 2.002301$ and $g_I = 0.447654 \times 10^{-3}$ [Van89]. For states with total angular momentum of $F = 3/2$ and $F = 1/2$ the + and − sign have to be used, respectively. In the high magnetic field range ($B \gg 100$) the nuclear and the electronic spin decouple and the atom is in the Paschen-Back regime. Depending on the orientation of the electronic spin, the atoms are either high field seekers ($m_s = 1/2$) or low field seekers ($m_s = -1/2$) with a magnetic moment of about μ_B. The nuclear spin $I = 1$ ($m_I = -1, 0, 1$) leads to a splitting of the electronic states by approximately 80 MHz. A convenient notation of the different states is to label them with $|1\rangle, |2\rangle \ldots |6\rangle$ in order of increasing energy (see figure A.1).

In the magnetic field range of relevance for this experiment the magnetic field dependent energy splitting of the excited state is given by [Geh03a]

$$\Delta E = \frac{\mu_\mathrm{B}}{\hbar}(g_J m_J + g_I M_I)B. \tag{A.2}$$

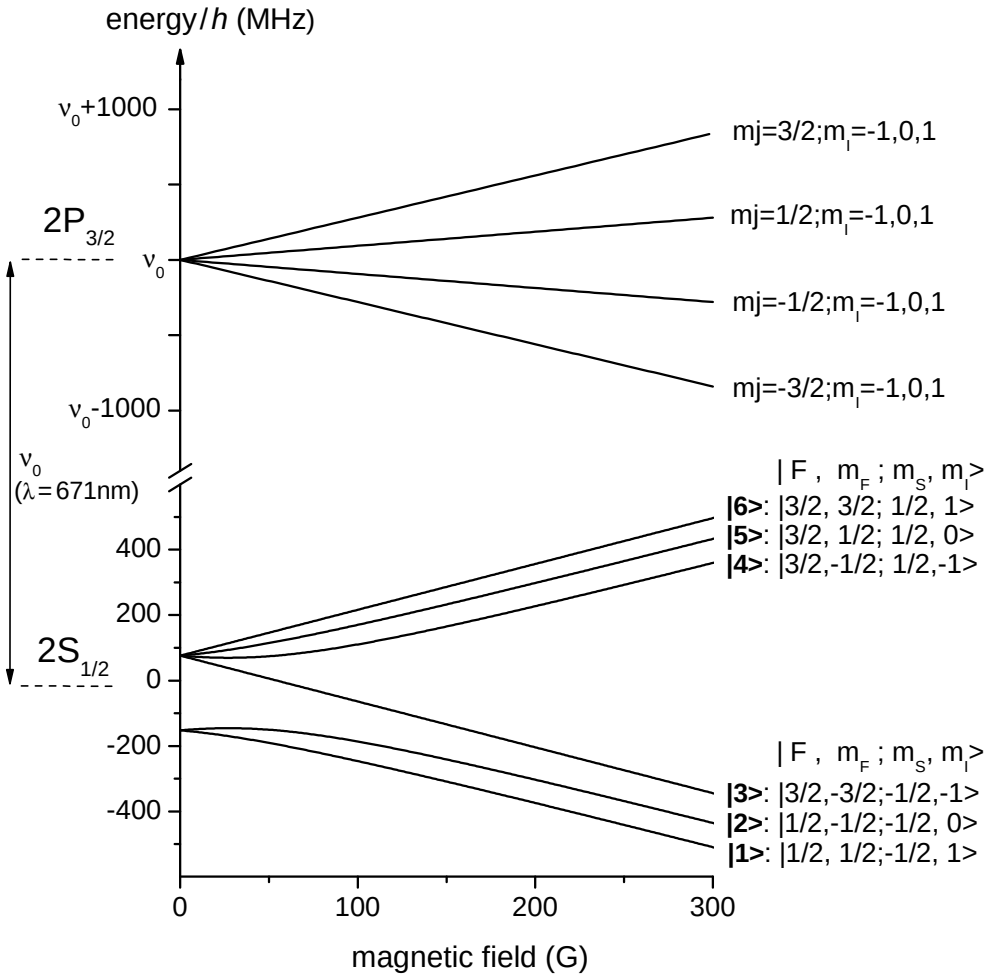

Figure A.1: Magnetic field dependent energy level structure of the $2S_{1/2}$ ground state and the $2P_{3/2}$ excited state of ^{6}Li. In the excited state the hyperfine contribution and the nuclear contribution have been neglected as their effects are only relevant on scales below the linewidth of the optical transition at $\lambda = 671$ nm of 5.9 MHz. As a result each line in the excited state is three fold degenerate.

The corresponding states are arranged into spectroscopic triplets. Since the electronic g-factor of the excited state $g_J = 1.3335$ [Ari77] is much larger then the nuclear g-factor g_I, the nuclear contribution can be neglected at large magnetic field and the energies are well approximated by

$$\Delta E = \mu_B g_J m_J B/\hbar. \tag{A.3}$$

In our experiments we use the closed σ^--transition from the $2S_{1/2}, m_J = -1/2, m_I$ state to the $2P_{3/2}, m_J = -3/2, m_I$ excited state ($m_I = -1, 0, 1$) to image the atoms at high magnetic field. Here the splitting between the different hyperfine ground states is about 80 MHz and allows for a state selective detection of the different hyperfine states.

Appendix B

Non linear corrections to the collective frequencies

The scaling of the lowest-order anharmonicity corrections in our cigar shaped trap was derived for us by Sandro Stringari [Str04b]. Here we briefly report on the results of his analysis.

The starting point of his analysis is the following radial potential with

$$V_{\mathrm{ext}}(r) = -V_0 \exp\left(-m\omega_\perp^2 r^2/2V_0\right) \tag{B.1}$$

in addition to a harmonic potential in the axial direction z with trapping frequency $\omega_\parallel$. In the above equation V_0 denotes the potential depth in the center of the trap and $\omega_\perp$ is the radial trap frequency. Expanding the radial potential to 4-th power in r leads to

$$V_{\mathrm{ext}}(r) = -V_0 + \frac{1}{2}m\omega_\perp^2 r^2 - \frac{1}{8V_0}m^2\omega_\perp^4 r^4 \tag{B.2}$$

Radial dipole mode

The frequency of the dipole mode is obtained by $\omega_{\mathrm{D}}^2 = \frac{1}{m}<\partial_r^2 r^2 V_{\mathrm{ext}}>$ and thus

$$\omega_{\mathrm{D}} = \omega_\perp\left(1 - \frac{1}{2}\frac{m\omega_\perp^2 <r^2>}{V_0}\right) \tag{B.3}$$

This expression is expected to be valid up to the first non harmonic correction [Str04b]. Using the relation $\omega_\perp^2 <r^2> = 2\omega_\parallel^2 <z^2>$ the term responsible for the anharmonicity effect can be directly determined by in situ measurements of $<z^2>$.

Radial breathing mode

From a scaling ansatz in the radial direction one finds analytic results, which are expected to be exact for an elongated trap and up to first non harmonic corrections in the external potential. The results for the three relevant cases of a molecular BEC, a unitarity limited quantum gas and an ideal Fermi gas are:

- molecular BEC

$$\omega_{\text{breath}} = 2\omega_\perp \left(1 - \frac{7}{12}\frac{m\omega_\perp^2 <r^2>}{V_0}\right) \tag{B.4}$$

- unitarity limited quantum gas

$$\omega_{\text{breath}} = \sqrt{\frac{10}{3}}\omega_\perp \left(1 - \frac{16}{25}\frac{m\omega_\perp^2 <r^2>}{V_0}\right) \tag{B.5}$$

- ideal Fermi gas

$$\omega_{\text{breath}} = 2\omega_\perp \left(1 - \frac{3}{5}\frac{m\omega_\perp^2 <r^2>}{V_0}\right) \tag{B.6}$$

In the derivation of the above equations the following relations have been used that are obtained using Thomas-Fermi profiles: in the BEC $<r^4>/(<r^2>)^2 = 14/9$ and in the unitarity and ideal Fermi gas limit $<r^4>/(<r^2>)^2 = 8/5$.

The value of the ratio $m\omega_\perp^2 <r^2>/V_0$ varies in the different regimes. In the unitarity limit one finds $m\omega_\perp^2 <r^2>/V_0 = \frac{1}{2}(1+\beta)^{1/2} E_{\text{F}}$ where $E_{\text{F}} = \hbar\omega_{\text{ho}}(3N)^{1/3}$ is the Fermi energy of a noninteracting Fermi gas with N atoms and β is the universal parameter (see section 2.2.3).

Appendix C

Magnetic Field Control of Elastic Scattering in a Cold Gas of Fermionic Lithium Atoms

Magnetic Field Control of Elastic Scattering in a Cold Gas of Fermionic Lithium Atoms

S. Jochim, M. Bartenstein, G. Hendl, J. Hecker Denschlag, and R. Grimm
Institut für Experimentalphysik, Universität Innsbruck, Technikerstrasse 25, 6020 Innsbruck, Austria

A. Mosk
FOM instituut voor plasmafysica Rijnhuizen, P.O. Box 1207, 3430 BE Nieuwegein, The Netherlands

M. Weidemüller
Max-Planck-Institut für Kernphysik, Postfach 103980, 69029 Heidelberg, Germany
(Received 24 July 2002; published 18 December 2002)

We study elastic collisions in an optically trapped spin mixture of fermionic lithium atoms in the presence of magnetic fields up to 1.5 kG by measuring evaporative loss. Our experiments confirm the expected magnetic tunability of the scattering length by showing the main features of elastic scattering according to recent calculations. We measure the zero crossing of the scattering length at 530(3) G which is associated with a predicted Feshbach resonance at ~850 G. Beyond the resonance we observe the expected large cross section in the triplet scattering regime.

DOI: 10.1103/PhysRevLett.89.273202 PACS numbers: 34.50.–s, 05.30.Fk, 32.80.Pj, 39.25.+k

In an ultracold atomic gas, the *s*-wave scattering length characterizes the elastic interactions and has a profound effect on the physical behavior. The scattering length can be conveniently tuned by using a magnetic field when a Feshbach resonance is present. For bosonic atoms, such resonances have been observed [1–3], and they have found particular applications for attainment and manipulation of a Bose-Einstein condensate in ^{85}Rb [4,5] and for the production of bright solitons in bosonic ^{7}Li [6,7].

For fermionic gases, Feshbach resonances in *s*-wave scattering of atoms in different spin states are of great interest to experimentally explore the rich physics of paired fermionic gases [8–11]. For obtaining superfluidity in a Cooper-paired gas, magnetic tuning allows one to raise the critical temperature [8] from values far below the Fermi temperature into a region that seems accessible with current experimental methods. With resonantly tuned interactions the fermionic superfluid is predicted [9,10] to perform a crossover from a superfluid of weakly coupled Cooper pairs to a Bose-Einstein condensate of strongly coupled molecules. Feshbach tuning also offers a possible way to detect this molecular coupling through oscillations induced by magnetic-field transients [10] analogous to a recent observation with coupled bosonic atoms [5]. Experimental control of different pairing regimes thus represents an intriguing prospect of a fermionic gas with magnetically tuned interactions.

A narrow Feshbach resonance between two different spin states of fermionic ^{40}K was recently observed by Loftus *et al.* [12]. The other fermionic species currently used in several experiments, ^{6}Li, is predicted to a show a Feshbach resonance with strong modifications of *s*-wave interactions in a very wide magnetic-field range [13–15]. At relatively small fields, this dependence was recently used by Granade *et al.* to obtain a sufficient scattering cross section for the all-optical production of a degenerate Fermi gas of lithium [16].

In this Letter, we experimentally explore the magnetic tunability of elastic scattering in an optically trapped spin mixture of fermionic lithium atoms in high magnetic fields up to 1.5 kG. Our results verify the expected dependence of *s*-wave interactions in the whole magnetic-field range of interest [13–15]. As a particular feature associated with the predicted Feshbach resonance [13], we observe the zero crossing of the scattering length at a field of 530 G. The exact location of this feature is of great interest as a sensitive input parameter to better constrain the uncertainty in the molecular potentials for more accurate theoretical calculations of the scattering properties of ^{6}Li. Our measurements of elastic collisions are based on evaporation out of an optical dipole trap.

The scattering properties in different spin mixtures of fermionic lithium atoms were theoretically investigated by Houbiers *et al.* [13], Kokkelmans *et al.* [14], and Venturi and Williams [15]. Magnetic tunability, of particular interest for Cooper pairing in a Fermi gas [8,9], was predicted for the stable combination of the two lowest states $|1\rangle$ and $|2\rangle$; at low magnetic field these states correspond to $F = 1/2$, $m_F = +1/2$, and $m_F = -1/2$, respectively. Most prominently, a broad Feshbach resonance at ~850 G is expected to mark the transition from the low-field scattering regime to the high-field region. As a precursor of the Feshbach resonance, the *s*-wave scattering length a crosses zero in the range between 500 and 550 G. Beyond the resonance, scattering in higher fields is dominated by the triplet potential with a very large and negative scattering length of $-2200a_0$, where a_0 is the Bohr radius. The available theoretical data [13–15] show the same behavior for $a(B)$ within some variations due to the limited knowledge of the

molecular interaction parameters. Figure 1(a) illustrates these predictions for the scattering length $a(B)$ by a corresponding model curve that approximates the results of Refs. [13–15].

In a cold gas at finite temperature the cross section for elastic scattering of nonidentical particles is unitarity limited to a maximum value of $\sigma_{\max} = 4\pi/k^2$, where $k = mv/(2\hbar)$ is the wave number corresponding to a relative velocity v and a reduced mass $m/2$. Taking into account the B-field dependent scattering length $a(B)$ and the unitarity limit, the resulting B-field dependent cross section can be written as $\sigma = 4\pi a^2/(1 + k^2a^2)$. For the considered $|1\rangle - |2\rangle$ spin mixture of ^{6}Li the expected behavior of the cross section is shown in Fig. 1(b) for the example of a wave number $k = (300a_0)^{-1}$ close to our experimental conditions. Most notably, as a consequence of the unitarity limit in combination with the very large scattering length for high magnetic fields, the Feshbach resonance does not appear as a pronounced feature in the cross section. The zero crossing of the scattering length, however, leads to a vanishing scattering cross section and thus shows up as a manifestation of the resonance.

Our dipole trap [17] makes use of the enhancement of the laser intensity inside a linear optical resonator to create a large and deep trapping volume for lithium atoms. The power provided by a 2-W Nd:YAG laser (Innolight Mephisto-2000) at a wavelength of 1064 nm is enhanced by a factor of 120 to create a far red-detuned 1D optical lattice trap with an axial period of 532 nm and a transverse $1/e$ radius of 115 μm. The maximum trap depth is of the order of 1 mK. To vary the trap depth the resonator-internal power is servo-controlled by an acousto-optical modulator in the incident laser beam. From a standard magneto-optical trap (MOT) operated with diode lasers we typically transfer 5×10^5 ^{6}Li atoms into roughly 1000 individual wells at a temperature of

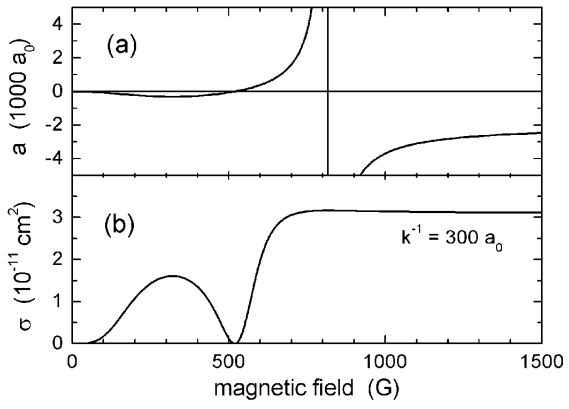

FIG. 1. (a) Model curve approximating the results of [13–15] for the s-wave scattering length of ^{6}Li atoms in the two lowest spin states versus magnetic field. (b) Corresponding behavior of the scattering cross section at a finite collision energy with a relative wave number of $k = (300a_0)^{-1}$.

$\sim$400 μK. The resulting peak density is $\sim 1.5 \times 10^{11}$ cm^{-3}. By extinguishing the repumping light of the MOT 1 ms before the main trapping light is turned off, all atoms are pumped into the two states $|1\rangle$ and $|2\rangle$ to create a 50-50 spin mixture [16].

The magnetic field is produced by a pair of water-cooled coils outside of the glass vacuum cell of the trap. At a maximum continuous operation current of 200 A the coils produce a magnetic field of 1.5 kG with a curvature of only 75 G/cm^2 along the symmetry axis; the corresponding power dissipation is 6 kW. The setup allows for a maximum ramp speed of 5 G/ms within the full range. The magnetic field is calibrated by radio-frequency induced transitions from $|2\rangle$ to the state that at $B = 0$ corresponds to $F = 3/2$, $m_F = +1/2$. The latter is unstable against inelastic collisions with $|2\rangle$ which leads to easily detectable loss. With a fit to the Breit-Rabi formula we obtain a calibration of the magnetic field to better than 1 G over the full range.

The basic idea of our measurements is to observe elastic collisions through evaporative loss at a variable magnetic field [18]. The method is particularly well suited for measuring the position of a resonance by locating the corresponding zero crossing of the scattering length. With this sensitive experimental input for theoretical calculations, as is readily available in our case [13–15], precise knowledge of the magnetic-field dependent scattering length can be obtained. Our dipole trap is loaded under conditions where the effective temperature T of a truncated Boltzmann distribution [19] is only slightly below the trap depth U. A strongly nonthermal distribution is thus created with a small truncation parameter $\eta = U/k_BT \approx 2$. The thermal relaxation resulting from elastic collisions then leads to rapid evaporative loss and cooling of the sample, i.e., an increase of η. The trap depth can be kept constant to study plain evaporation or, alternatively, ramped down to force the evaporation process.

In a series of plain evaporation experiments performed at a constant trap depth of 750 μK we measure evaporative loss over the maximum accessible range of magnetic fields up to 1.5 kG. After a fixed holding time the remaining atoms are retrapped into the MOT and their number is measured via the fluorescence signal by a calibrated photodiode. The signal is recorded after holding times of 1 and 3 s corresponding to the time scale of evaporation. These holding times are short compared with the rest-gas limited lifetime of 30 s. Figure 2 shows the result of 1000 different measurements obtained in an acquisition time of 6 h. The data points are taken in a random sequence for 31 magnetic field values equally distributed over the full range. Data points for 1 and 3 s are recorded alternatingly. This way of data taking ensures that the signal is not influenced by residual long-term drifts of the experimental conditions.

The observed evaporation loss in Fig. 2 shows a pronounced dependence on the magnetic field, which we

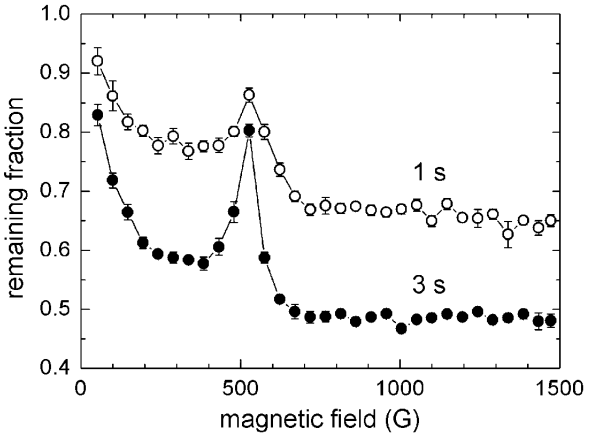

FIG. 2. Evaporative loss measurements over the full magnetic field range. The data points show the measured number of atoms remaining in the trap after 1 s (∘) and 3 s (•) of plain evaporation at a constant trap depth of 750 μK.

compare with the expected cross section for elastic collisions ejecting atoms out of the trap. Figure 1(b) displays the cross section for $k = (300a_0)^{-1}$, which corresponds to a collision energy of about half the trap depth and thus to the relevant energies for evaporating collisions. After being very small at low magnetic fields, the observed loss increases for fields up to ~350 G where the expected local maximum of evaporation shows up. The loss then decreases and disappears at about 530 G in agreement with the predicted zero crossing of the scattering length. Here the slight observed loss in the 1 s curve is explained by the finite ramp time of the magnetic field. In the 100 ms ramping time some evaporation does already take place. At 530 G the decrease of the trapped atom number between 1 and 3 s is fully explained by rest-gas losses without any further evaporation. For higher magnetic fields evaporative loss rapidly rises until it levels off at about 700 G. Up to the maximum attainable value of 1.5 kG high evaporation loss is observed. A slight decrease of the atom number for fields exceeding 1 kG occurs which we attribute to technical reasons; we observe an increasing noise for currents higher than ~130 A in the error signal of the resonator lock. The relatively large and constant evaporative loss for fields exceeding 700 G is consistent with the predicted behavior of the cross section.

The evaporative cooling effect is confirmed by measuring the change of the truncation parameter η after 3 s of trapping at selected values of the magnetic field. For thermometry we turn off the magnetic field to avoid further elastic collisions and adiabatically lower the trap depth in a 1-s exponential ramp. The fraction of remaining atoms as a function of the relative depth then provides a good measure of η. At the zero crossing at 530 G we observe only a slight increase of η to a value of 2.3(3) which is explained by the unavoidable evaporation during the magnetic-field ramps. At 340 G close to the local maximum of $|a|$ we find an increase of η to 4.2(3) as a clear evidence of evaporative cooling. At 720 G, i.e., in the case of a large positive scattering length, a higher value of 5.5(4) is measured showing deeper evaporative cooling. Essentially the same η of 5.3(4) is obtained at $B = 1290$ G where scattering takes place in the triplet-dominated regime with a very large negative scattering length.

We measure the minimum-loss feature in a closer range of magnetic fields to precisely determine the value of the magnetic field at which the zero crossing of scattering length occurs. The main data points in Fig. 3 are obtained with 500 individual measurements at a holding time of 3 s with the magnetic field randomly varied between 30 values in an interval between 370 and 670 G; the data shown in the inset are obtained with 1000 measurements in the very narrow range between 520 and 544 G. The results allow us to determine the B field for minimum evaporative loss, and thus the zero crossing of the scattering length to 530(3) G [20].

Forced evaporation measurements provide complementary data to plain evaporation and allow us to rule out a significant role of inelastic collisions. When the trap depth is ramped down, elastic collisions reduce trap loss in contrast to increased loss at constant trap depth. This can be understood by the spilling loss of energetic particles [19]: Without elastic collisions the most energetic particles are spilled out of the trap when its depth is reduced. With elastic collisions the evaporative cooling effect decreases the temperature and thus reduces the spilling loss.

In our forced evaporation measurements we reduce the trap depth in 10 s to 20% of its initial value in an exponential ramp and measure the number of remaining atoms; the results are displayed in Fig. 4. A minimum

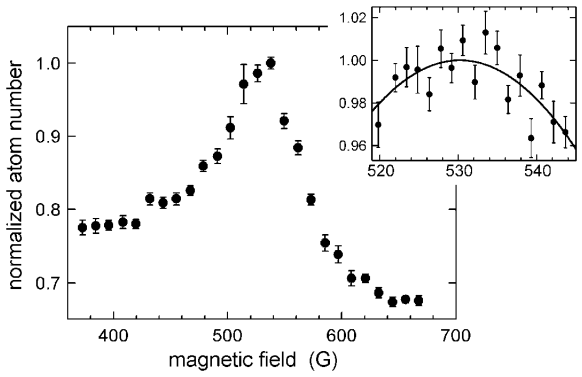

FIG. 3. Measurements on plain evaporation in magnetic fields close to the zero crossing of the scattering length under the same conditions as in Fig. 2 for a holding time of 3 s. Here the number of remaining atoms is normalized to the observed maximum value. The inset shows a series of measurements in a very narrow range around the maximum at 530(3) G together with a parabolic fit.

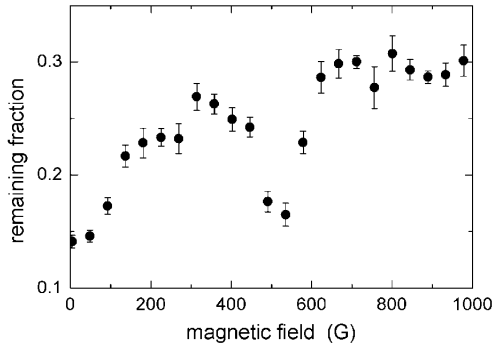

FIG. 4. Fraction of atoms remaining after forced evaporation versus applied magnetic field. The trap depth is ramped down exponentially in 10 s to 20% of the initial value.

number of atoms is now measured at 0 and 530 G instead of the maximum observed with constant trap depth. The largest number of atoms is observed in the high-field region above 650 G as expected for the large scattering cross section.

On a Feshbach resonance, enhanced inelastic loss can occur as a result of three-body collisions [1] or, if the system has internal energy, as a result of two-body decay [3]. For fermions, three-body processes are symmetry forbidden at ultralow energies when only s-wave collisions are involved. In a spin mixture at nonzero magnetic field, two-body decay is energetically possible (in our case with an energy release of $k_B \times 3.5$ mK) but involves higher partial waves and relies on weak dipolar coupling. Consequently, inelastic loss can be expected to be weak in our experiments. Indeed, our data do not show any indication of inelastic loss even at the very center of the Feshbach resonance.

At much higher densities ($\sim 10^{13}$ cm^{-3}) as compared to our conditions ($\sim 10^{11}$ cm^{-3}), a recent experiment [21] has revealed inelastic loss with a maximum at 680 G. As our results support the predicted position of the s-wave resonance at $\sim$850 G, the explanation for the inelastic feature cannot be attributed to the Feshbach resonance in a simple way. The experiment [21] also provided evidence for a two-body nature of the underlying process with a rate constant of 2×10^{-12} cm^3/s measured at $\sim 20\ \mu$K. At a higher temperature of $\sim 100\ \mu$K we derive an upper bound for the two-body rate constant of 1×10^{-12} cm^3/s, whereas for a process involving higher partial waves one would expect the rate to increase with temperature. For three-body collisions our densities are too low to provide useful constraints. Obviously, inelastic loss in the fermionic spin mixture is an interesting problem that deserves more attention.

In conclusion, our measurements confirm the predicted magnetic tunability of the s-wave scattering length in a spin mixture of fermionic lithium atoms in the whole magnetic-field range of experimental interest. The observed zero crossing of the scattering length at 530(3) G together with the large cross section observed for higher fields provides clear evidence of the predicted Feshbach resonance. Moreover, it enables more precise calculations of the ^{6}Li scattering properties. The resonance itself is masked by unitarity-limited scattering and requires much deeper evaporative cooling for a direct observation. The fact that we do not see any significant effect of inelastic loss highlights the fact that the extremely large positive and negative scattering lengths attainable with fermionic lithium offer intriguing new possibilities for experiments on interacting Fermi gases.

We thank R. G. Hulet and H. Stoof for very useful discussions and V. Venturi for valuable input. Support by the Austrian Science Fund (FWF) within Project No. P15115 and SFB15 and by the Institut für Quanteninformation GesmbH is gratefully acknowledged.

Shortly before submission of the present Letter we learned about the measurements of the group of J. E. Thomas on the zero crossing of the scattering length which agree with our data.

[1] S. Inouye *et al.*, Nature (London) **392**, 151 (1998).
[2] P. Courteille *et al.*, Phys. Rev. Lett. **81**, 69 (1998).
[3] V. Vuletić, A. J. Kerman, C. Chin, and S. Chu, Phys. Rev. Lett. **82**, 1406 (1999).
[4] S. Cornish *et al.*, Phys. Rev. Lett. **85**, 1795 (2000).
[5] E. A. Donley, N. R. Claussen, S. T. Thompson, and C. E. Wieman, Nature (London) **417**, 529 (2002).
[6] L. Khaykovich *et al.*, Science **296**, 1290 (2002).
[7] K. Strecker, G. Partridge, A. Truscott, and R. Hulet, Nature (London) **417**, 150 (2002).
[8] H. T. C. Stoof, M. Houbiers, C. Sackett, and R. Hulet, Phys. Rev. Lett. **76**, 10 (1996).
[9] M. Holland, S. Kokkelmans, M. Chiofalo, and R. Walser, Phys. Rev. Lett. **87**, 120406 (2001).
[10] E. Timmermans, K. Furuya, P.W. Milonni, and A. K. Kerman, Phys. Lett. A **285**, 228 (2001).
[11] M. L. Chiofalo, S. J. J. M. F. Kokkelmans, J. L. Milstein, and M. J. Holland, Phys. Rev. Lett. **88**, 090402 (2002).
[12] T. Loftus *et al.*, Phys. Rev. Lett. **88**, 173201 (2002).
[13] M. Houbiers, H. T. C. Stoof, W. McAlexander, and R. Hulet, Phys. Rev. A **57**, R1497 (1998).
[14] S. Kokkelmans *et al.*, Phys. Rev. A **65**, 053617 (2002).
[15] V. Venturi and C. Williams (private communication).
[16] S. Granade, M. Gehm, K. O'Hara, and J. Thomas, Phys. Rev. Lett. **88**, 120405 (2002).
[17] A. Mosk *et al.*, Opt. Lett. **26**, 1837 (2001).
[18] C. Chin, V. Vuletić, A. J. Kerman, and S. Chu, Phys. Rev. Lett. **85**, 2717 (2000).
[19] O. J. Luiten, M. W. Reynolds, and J. T. M. Walraven, Phys. Rev. A **53**, 381 (1996).
[20] A finite collision energy E_C leads to a shift of $+0.7G \times E_C/(k_B \times 100\ \mu\text{K})$ [15], which for our data stays within the error.
[21] K. Dieckmann *et al.*, cond-mat/0207046v2.

Appendix D

Pure Gas of Optically Trapped Molecules Created from Fermionic Atoms

Pure Gas of Optically Trapped Molecules Created from Fermionic Atoms

S. Jochim, M. Bartenstein, A. Altmeyer, G. Hendl, C. Chin, J. Hecker Denschlag, and R. Grimm
Institut für Experimentalphysik, Universität Innsbruck, Technikerstraße 25, 6020 Innsbruck, Austria
(Received 5 August 2003; published 8 December 2003)

We report on the production of a pure sample of up to 3×10^5 optically trapped molecules from a Fermi gas of ^{6}Li atoms. The dimers are formed by three-body recombination near a Feshbach resonance. For purification, a Stern-Gerlach selection technique is used that efficiently removes all trapped atoms from the atom-molecule mixture. The behavior of the purified molecular sample shows a striking dependence on the applied magnetic field. For very weakly bound molecules near the Feshbach resonance, the gas exhibits a remarkable stability with respect to collisional decay.

DOI: 10.1103/PhysRevLett.91.240402 PACS numbers: 03.75.Ss, 05.30.Fk, 32.80.Pj, 33.80.Ps

The formation of composite bosons by pairing of fermions is the key to many intriguing phenomena in physics, with superfluidity and superconductivity being prominent examples. In ultracold atomic gases, pairs of fermionic atoms can be combined to form bosonic molecules [1,2] or possibly Cooper pairs [3]. The pairing changes the properties of the gas, highlighted by the prospect of a molecular Bose-Einstein condensate or a Cooper-paired superfluid. The interatomic interactions play a crucial role for the nature of the pairing process. The ability to control the interaction via magnetically tuned Feshbach resonances [4–6] opens up exciting possibilities for experiments on ultracold fermionic gases, e.g., exploring superfluidity in different pairing regimes [7–10].

The formation of molecules near Feshbach resonances in ultracold gases has been reported for bosons [11–14] and fermions [1,2]. In the experiments [1,2,11,12], the molecules coexist with the atoms in a strongly interacting mixture. A generic feature of a Feshbach resonance is the existence of a bound molecular state with a magnetic moment that differs from that of the unbound atom pair. The binding energy thus depends on the magnetic field, and a properly chosen field can resonantly couple colliding atoms into the molecular state. The inherent difference in magnetic moments facilitates a Stern-Gerlach selection of molecules and atoms. Two recent experiments [13,14] demonstrate the separation of the molecular from the atomic cloud in free space.

In this Letter, we report the creation of a pure sample of up to 3×10^5 optically trapped molecules from a fermionic gas of ^{6}Li atoms. After the production of an atom-molecule mixture via three-body collisions, a Stern-Gerlach purification scheme efficiently removes all trapped atoms, while leaving all molecules trapped. This allows us to investigate the intriguing behavior of the pure molecular sample, which strongly depends on the magnetic field.

The lithium isotope ^{6}Li is one of the two prime candidates in current experiments exploring the physics of fermionic quantum gases [15–19], the other one being ^{40}K [1,20]. A spin mixture composed of the lowest two sublevels in the hyperfine manifold of the electronic ground state is stable against two-body decay and exhibits wide magnetic tunability of s-wave interactions via a broad Feshbach resonance at about 850 G [21]. A calculation of the corresponding scattering length a as a function of the magnetic field [22] is shown in Fig. 1(a) [23]. The large cross section for elastic scattering near the resonance can be used for efficient evaporative cooling, in particular, above the resonance at negative scattering length where inelastic loss is negligible [16]. In the region of positive scattering length below the resonance, loss features have been observed [24]. At large positive a, a weakly bound molecular level exists with a binding energy approximately given by $\hbar/(ma^2)$, where $\hbar$ is Planck's constant and m denotes the atomic mass. For the region of interest, Fig. 1(b) shows this binding energy as calculated from the scattering length data [25].

The starting point of our experiments is a sample of 2.5×10^6 ^{6}Li atoms in a standing-wave optical dipole trap realized with a Nd:YAG laser at a wavelength of 1064 nm [19,26]. The 50-50 spin mixture in the lowest two spin states is spread over ~1500 individual lattice sites of the standing-wave trap. In the central region of the trap, a single site contains typically 1800 atoms. The

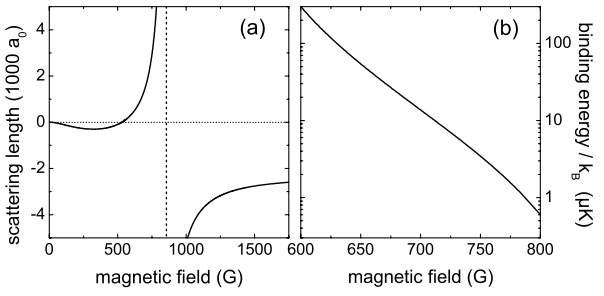

FIG. 1. (a) Magnetic-field dependence of the s-wave scattering length a in the ^{6}Li spin mixture. An additional, narrow Feshbach resonance near 550 G [22] is omitted in the plot. (b) Binding energy of the weakly bound molecular level in the region of large positive a.

axial and radial trap frequencies are 260 kHz and 390 Hz, respectively. The trap depth is $k_B \times 27\ \mu$K with k_B denoting Boltzmann's constant. At a temperature of 2.5 μK, peak values for the number density and phase-space density are 3×10^{12} cm^{-3} and 0.04 [27,28], respectively. The ultracold gas is prepared by forced evaporative cooling after loading the optical trap at an initial depth of $\sim$1 mK with 8×10^6 atoms from a magneto-optical trap (MOT). The evaporation is performed by ramping down the light intensity in 1 s at a magnetic field of 1200 G. The evaporation initially proceeds with very high efficiency similarly to [16,29], but finally loses its efficiency when the tightly confining lattice potential does not support more than one or two quantum states.

We form molecules in the weakly bound level at a field of 690 G, where we find optimum production rates at a large positive scattering length of $a = +1300a_0$. Here a_0 denotes Bohr's radius. To reach the production field of 690 G, we quickly ramp from the evaporation field of 1200 G down to this value with a speed of -7.5 G/ms. In contrast to other experiments with fermionic atoms [1,2], the molecule formation during this ramp is negligible and the molecules are predominantly formed after the ramp at the fixed production field.

The molecules are detected by dissociating them into atoms [1,2,13,14] and measuring their fluorescence. For this purpose, we apply a ramp across the Feshbach resonance to fields of typically 1200 G (speed $+6$ G/ms). This brings the weakly bound level above the scattering continuum and the molecules quickly dissociate. The dissociation turns out to be insensitive to variations of the ramp speed and the final field. After the dissociation ramp, we immediately ramp down to zero magnetic field. The ramp speed of -12 G/ms is fast enough to avoid molecule formation when crossing the region of positive scattering length. After reaching zero magnetic field, we recapture all atoms into the MOT. Their number is then determined by measuring the emitted fluorescence intensity using a calibrated photodiode [27]. This measurement provides the total atom number $2N_{\mathrm{mol}} + N_{\mathrm{at}}$, where N_{mol} and N_{at} denote the number of molecules and atoms after the production phase, respectively. To determine N_{at}, we repeat the same measurement without the Feshbach dissociation ramp by immediately ramping down to zero from the production field. The ramp down to zero magnetic field increases the binding energy to a large value of about $k_B \times 80$ mK and the molecules are lost without leading to any fluorescence light in the MOT. The number of molecules N_{mol} is then obtained by taking the difference in atom numbers measured in two subsequent runs with and without the dissociating Feshbach ramp.

The creation of molecules from the atomic gas is demonstrated in Fig. 2 for the optimum production field of 690 G. The time evolution of the measured numbers $2N_{\mathrm{mol}} + N_{\mathrm{at}}$ and N_{at} is shown together with the corresponding number of molecules $2N_{\mathrm{mol}}$. We attribute the molecule formation to three-body recombination into the

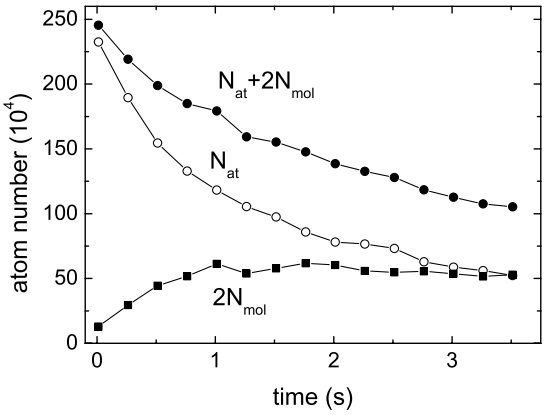

FIG. 2. Formation of molecules at a fixed magnetic field of 690 G. The measured numbers $N_{\mathrm{at}} + 2N_{\mathrm{mol}}$ and N_{at} are plotted as a function of time together with the resulting number of molecules $2N_{\mathrm{mol}}$.

weakly bound state [30,31]. Two-body processes cannot lead to bound dimers as a third particle is required for energy and momentum conservation. The three-body molecule formation process can be modeled with the differential equation $\dot{N}_{\mathrm{mol}}/N_{\mathrm{at}} = M_3\langle n_{\mathrm{at}}^2\rangle$, where $\langle n_{\mathrm{at}}^2\rangle$ denotes the mean quadratic density of the atoms. From the initial molecule formation rate of $\dot{N}_{\mathrm{mol}} = 3.5 \times 10^5$ s^{-1}, we thus derive a three-body formation coefficient of $M_3 = 1 \times 10^{-25}$ cm^6/s^{-1} [27]. The maximum number of 3×10^5 molecules is reached after about 1 s. For longer times, the fraction of atoms forming molecules approaches a value of $\sim$50%.

At the optimum production field of 690 G, the molecular binding energy amounts to $\sim k_B \times 18\ \mu$K, which is in between the thermal energy of $k_B \times 2.5\ \mu$K and the trap depth of $k_B \times 27\ \mu$K for the atoms. For the molecules, the trap depth is a factor of 2 higher because of the 2 times larger polarizability. We have verified this fact by measuring the trap frequencies for atoms and molecules to be equal within the experimental uncertainty of a few percent. After a three-body recombination event both the atom and the molecule remain trapped. We believe that the recombination heat is cooled away by a evaporation of atoms out of the trap. Evaporative loss of molecules is strongly suppressed because of the higher trap depth.

To purify the created molecules we use a Stern-Gerlach selection technique. We apply a magnetic field gradient perpendicular to the standing-wave axis. This pulls particles out of the trap for which the magnetic force is larger than the trapping force. In order to be able to apply large enough field gradients, we lower the trap depth to $k_B \times 19\ \mu$K while applying the gradient for about 10 ms. Figure 3 demonstrates such a purification at 568 G. While all the atoms are lost above $B'_{\mathrm{at}} = 17$ G/cm, the molecules start getting spilled at 20 G/cm, and are lost completely above $B'_{\mathrm{mol}} = 32.5$ G/cm. This means that, under suitable conditions, we can remove all the atoms while keeping the molecule number constant.

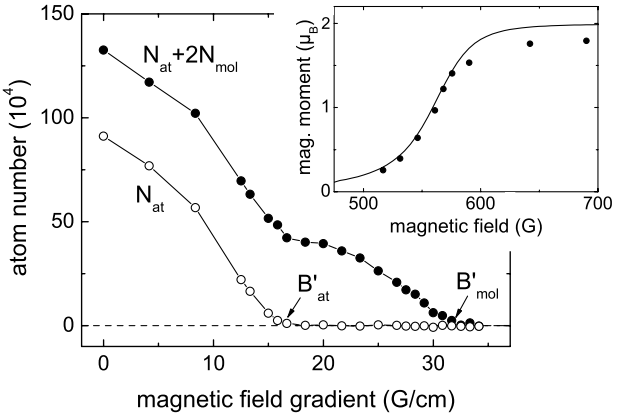

FIG. 3. Stern-Gerlach selection by applying a magnetic field gradient to the trapped atom-molecule mixture at 568 G and a trap depth of $k_B \times 19$ μK. Marked are the two gradients where all the atoms and all the molecules are lost. The inset shows the magnetic moment of the molecules estimated from the Stern-Gerlach selection at different magnetic fields together with the theoretical calculation.

The magnetic moment of the molecules μ_{mol} can be estimated to be $\mu_{mol} = 2\mu_{at}B'_{mol}/B'_{at}$, where μ_{at} is the magnetic moment of one free atom. At high magnetic field, μ_{at} equals Bohr's magneton μ_B. The inset of Fig. 3 shows the magnetic moments of the molecules determined at various magnetic fields. The data agree well with the magnetic field dependence calculated from theory (solid curve). We attribute the systematic deviation to slightly different trap parameters for atoms and molecules.

Starting with a pure molecular sample, we study its stability against inelastic molecule-molecule collisions. Corresponding decay curves are displayed in Fig. 4 for two different magnetic fields. At 546 G a rapid nonexponential decay is observed as a clear signature of inelastic molecule-molecule collisions. From the initial decay rate we derive a two-body loss coefficient of 5×10^{-11} cm^3/s [27]. At 690 G, the observed behavior is strikingly different. The molecular sample shows a nearly exponential decay with a time constant as long as ~10 s. As similar lifetimes are observed for trapped atom samples under conditions where trapped molecules cannot be created, the observed molecular lifetime can be fully attributed to one-body effects such as heating in the optical trap. For a loss rate coefficient at 690 G our data provide an upper limit of 3×10^{-13} cm^3/s [27], which is surprisingly low for inelastic collisions in a molecular system with many open exit channels.

The data at 690 G show another interesting collisional effect. Atoms reappear after purification of the molecular cloud, see (○) in Fig. 4. For long storage times (~15 s), an atom-molecule mixture is reestablished with a similar fraction of molecules as observed in the initial formation process at the same magnetic field (see Fig. 2). Collisions producing atoms from molecules are endoergic in nature as kinetic energy is required to provide the dissociation energy. The increasing atom fraction does not lead to any increased loss. This shows that the gas is remarkably stable both against molecule-molecule and atom-molecule collisions.

The dependence of the molecular decay on the magnetic field is shown in Fig. 5. Here we store the initially pure gas of 1.8×10^5 molecules at a variable magnetic field for a fixed holding time of 1 s before we measure the number of remaining molecules and atoms. A sharp transition occurs around 650 G. For fields below ~600 G, where the binding energy is relatively large ($> k_B \times$ 100 μK), the observed decay is very fast and no atoms are found to reappear. Here inelastic collisions apparently lead to a rapid vibrational quenching. Furthermore, the kinetic energy of the molecules cannot provide the necessary energy for collisional dissociation. Consequently, we do not observe any atoms reappearing.

For fields above ~680 G, a completely different behavior is observed. In this regime, no significant loss occurs in the total number $2N_{mol} + N_{at}$. However, an increasing atom fraction is observed as a result of collisional dissociation of the molecules. Here the binding energy

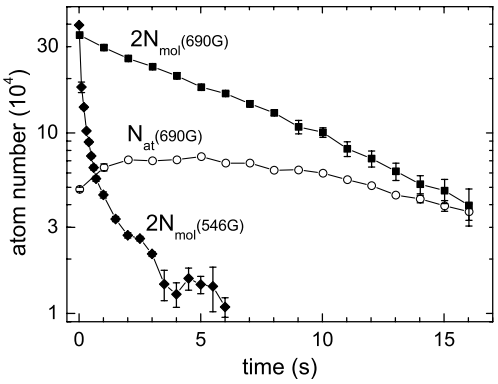

FIG. 4. Time evolution of an initially pure sample of molecules at 546 G (◆) and at 690 G (■). At 690 G, atoms are observed to reappear (○).

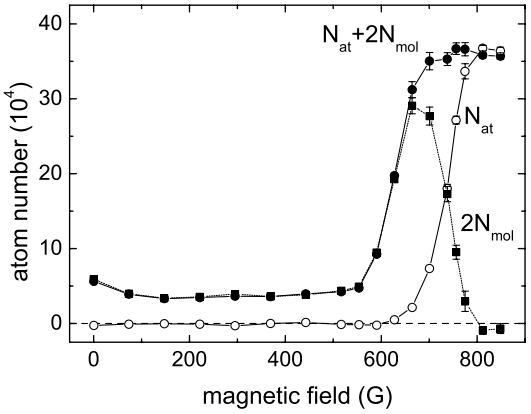

FIG. 5. Remaining number of atoms N_{at}, $N_{at} + 2N_{mol}$ and $2N_{mol}$ after a 1-s hold time at variable magnetic field starting with a pure molecular sample.

approaches the thermal energy and the sample tends towards a thermal atom-molecule equilibrium. Close to the Feshbach resonance, where the binding energy becomes comparable to thermal energy, the atomic fraction dominates in the atom-molecule mixture.

In conclusion we have produced an ultracold, pure molecular gas of ^{6}Li dimers in an optical dipole trap. Close to the Feshbach resonance, where the molecular binding energy is small, there is a strong coupling of the atomic gas and the molecules. Three-body collisions between atoms form molecules and collisions break up molecules to produce atoms. Our observations show that this exchange between atomic and molecular fraction can be nearly lossless. The long molecular lifetime along with a large elastic collision rate between the particles opens up great perspectives for further evaporative cooling of the molecular gas to Bose-Einstein condensation. Given the maximum molecule number of 3×10^5 and a temperature of about 2.5 μK, we reach a phase-space density of 0.01, only a factor of 4 lower than our initial atomic phase-space density. The molecular sample may be further cooled to condensation by efficient evaporation. Out of a mixture of atoms and molecules, mainly atoms will evaporate because they are more weakly trapped than the molecules. The gas is cooled further when molecules break up into atoms since this is an endoergic process. Once quantum degeneracy is accomplished it will be very interesting to cross the Feshbach resonance in order to observe the transition to a strongly interacting superfluid Fermi gas [7–10].

We thank G. Shlyapnikov for very stimulating discussions and V. Venturi for providing us with theoretical data on the scattering length and binding energy. We gratefully acknowledge support by the Austrian Science Fund (FWF) within SFB 15 (project part 15) and by the European Union in the frame of the Cold Molecules TMR Network under Contract No. HPRN-CT-2002-00290.

Note added.—After submission of the present Letter, molecule formation in ^{6}Li using the narrow Feshbach resonance at 543 G was reported by Hulet's group [32].

[1] C. A. Regal, C. Ticknor, J. L. Bohn, and D. S. Jin, Nature (London) **424**, 47 (2003).
[2] J. Cubizolles, T. Bourdel, S. J. J. M. F. Kokkelmans, G. V. Shlyapnikov, and C. Salomon, preceding Letter, Phys. Rev. Lett. **91**, 240401 (2003).
[3] H. T. C. Stoof, M. Houbiers, C. Sackett, and R. Hulet, Phys. Rev. Lett. **76**, 10 (1996).
[4] H. Feshbach, Ann. Phys. (Leipzig) **19**, 287 (1962).
[5] S. Inouye, M. Andrews, J. Stenger, H.-J. Miesner, D. Stamper-Kurn, and W. Ketterle, Nature (London) **392**, 151 (1998).
[6] T. Loftus, C. Regal, C. Ticknor, J. Bohn, and D. Jin, Phys. Rev. Lett. **88**, 173201 (2002).
[7] M. Holland, S. J J. M. F. Kokkelmans, M. Chiofalo, and R. Walser, Phys. Rev. Lett. **87**, 120406 (2001).
[8] E. Timmermans, K. Furuya, P. W. Milonni, and A. K. Kerman, Phys. Lett. A **285**, 228 (2001).
[9] M. L. Chiofalo, S. J. J. M. F. Kokkelmans, J. L. Milstein, and M. J. Holland, Phys. Rev. Lett. **88**, 090402 (2002).
[10] Y. Ohashi and A. Griffin, Phys. Rev. Lett. **89**, 130402 (2002).
[11] E. A. Donley, N. R. Claussen, S. T. Thompson, and C. E. Wieman, Nature (London) **417**, 529 (2002).
[12] C. Chin, A. J. Kerman, V. Vuletić, and S. Chu, Phys. Rev. Lett. **90**, 033201 (2003).
[13] J. Herbig, T. Kraemer, M. Mark, T. Weber, C. Chin, H.-C. Nägerl, and R. Grimm, Science **301**, 1510 (2003).
[14] S. Dürr, T. Volz, A. Marte, and G. Rempe, cond-mat/0307440.
[15] A. G. Truscott, K. E. Strecker, W. I. McAlexander, G. B. Partridge, and R. G. Hulet, Science **291**, 2570 (2001).
[16] K. O'Hara, S. Hemmer, M. Gehm, S. Granade, and J. Thomas, Science **298**, 2179 (2002).
[17] T. Bourdel, J. Cubizolles, L. Khaykovich, K. M. F. Magalhães, S. J. J. M. F. Kokkelmans, G. Shlyapnikov, and C. Salomon, Phys. Rev. Lett. **91**, 020402 (2003).
[18] S. Gupta, Z. Hadzibabic, M. Zwierlein, C. Stan, K. Dieckmann, C. H. Schunck, E. G. M. van Kempten, B. J. Verhaar, and W. Ketterle, Science **300**, 1723 (2003).
[19] S. Jochim, M. Bartenstein, G. Hendl, J. Hecker Denschlag, R. Grimm, A. Mosk, and M. Weidemüller, Phys. Rev. Lett. **89**, 273202 (2002).
[20] G. Modugno, G. Roati, F. Riboli, F. Ferlaino, R. J. Brecha, and M. Inguscio, Science **297**, 2240 (2002).
[21] M. Houbiers, H. T. C. Stoof, W. McAlexander, and R. Hulet, Phys. Rev. A **57**, R1497 (1998).
[22] K. O'Hara, S. Hemmer, S. Granade, M. Gehm, J. Thomas, V. Venturi, E. Tiesinga, and C. Williams, Phys. Rev. A **66**, 041401(R) (2002).
[23] The exact resonance position is uncertain within a few 10 G [17], whereas the location of the zero-crossing has been determined to 529 G within 3 G [19,22].
[24] K. Dieckmann, C. Stan, S. Gupta, Z. Hadzibabic, C. Schunck, and W. Ketterle, Phys. Rev. Lett. **89**, 203201 (2002).
[25] From the scattering length data [22], we calculate the binding energy $\hbar^2/[m(a-\bar{a})^2]$ including a correction with $\bar{a} = 29.8a_0$ for lithium. See G. Gribakin and V. Flambaum, Phys. Rev. A **48**, 546 (1993).
[26] A. Mosk, S. Jochim, H. Moritz, T. Elsässer, M. Weidemüller, and R. Grimm, Opt. Lett. **26**, 1837 (2001).
[27] With fluorescence detection, we can determine the absolute atom number only within a factor of 2. All the derived quantities are subject to this systematic error.
[28] With a ground-state population of 99% in the tightly confined direction, each lattice site contains a quasi-2D gas. This fact is taken into account in our calculations of number and phase-space densities.
[29] S. R. Granade, M. E. Gehm, K. M. O'Hara, and J. E. Thomas, Phys. Rev. Lett. **88**, 120405 (2002).
[30] H. Suno, B. D. Esry, and C. H. Greene, Phys. Rev. Lett. **90**, 053202 (2003).
[31] D. Petrov, Phys. Rev. A **67**, 010703(R) (2003).
[32] K. E. Strecker, G. B. Partridge, and R. G. Hulet, Phys. Rev. Lett. **91**, 080406 (2003).

Appendix E

Bose-Einstein Condensation of Molecules

Bose-Einstein Condensation of Molecules

S. Jochim,[1] M. Bartenstein,[1] A. Altmeyer,[1] G. Hendl,[1] S. Riedl,[1] C. Chin,[1] J. Hecker Denschlag,[1] R. Grimm[1,2]*

We report on the Bose-Einstein condensation of more than 10^5 Li_2 molecules in an optical trap starting from a spin mixture of fermionic lithium atoms. During forced evaporative cooling, the molecules are formed by three-body recombination near a Feshbach resonance and finally condense in a long-lived thermal equilibrium state. We measured the characteristic frequency of a collective excitation mode and demonstrated the magnetic field–dependent mean field by controlled condensate spilling.

Since the first experiments on Bose-Einstein condensation (BEC) in ultracold atomic gases in 1995 (*1*–*3*), atoms of eight chemical elements have been condensed. BEC of more complex objects such as molecules or Cooper-paired atoms will open up many new avenues of research because they offer new degrees of freedom. An intriguing example is the fundamental change in quantum statistics when paired fermions form composite bosons. Recent experiments have demonstrated the formation of molecules in ultracold atomic gases of bosons (*4*–*9*) and fermions (*10*–*13*). Experiments starting with atomic BEC show the creation of molecular clouds at the threshold to quantum degeneracy (*7*) or clearly in that regime (*9*), but not in a thermal equilibrium state. In most of these experiments, weakly bound dimers are produced via magnetically tuned Feshbach resonances (*14*). Such a scattering resonance occurs when a free colliding atom pair energetically coincides with a bound molecular state. On the side of the resonance where the energy of the molecular level is below the dissociation limit, a weakly bound dimer state exists. The experiments indicate an important difference between weakly bound dimers composed of bosonic and of fermionic atoms. Dimers of bosons show a quick decay via inelastic atom-molecule or molecule-molecule collisions (*9*), so that quantum-degenerate molecular clouds can only be created in a transient regime. In contrast, the dimers of fermions exhibit a remarkable stability (*11*–*13*, *15*). Such molecular gases have been observed with lifetimes far longer than the time scales for elastic collisions and thermalization. This fact has been explained by a fermionic suppression of vibrational quenching in molecule collisions (*16*). Their stability allows us to use bosonic molecules composed of fermionic atoms to achieve molecular BEC in thermal equilibrium.

Our experiment is based on evaporative cooling of an optically trapped mixture of fermionic ^{6}Li atoms in the two lowest spin states (*11*–*13*, *17*–*21*). During the cooling process, a large number of bosonic dimers are formed by three-body recombination and finally condense into a molecular BEC. The spin mixture exhibits a broad Feshbach resonance at a magnetic field of about 850 G (*18*, *19*, *22*, *23*), which leads to a pronounced magnetic field dependence of the scattering length a (Fig. 1) that characterizes the s-wave interactions. Dimers in a single weakly bound state can be formed in the range of large positive a with a binding energy of $\hbar^2/(ma^2)$, where $\hbar$ is Planck's constant h divided by 2π and m is the mass of a ^{6}Li atom. This has been observed in magnetic field–dependent loss features (*24*) and changes in the interaction energy of the gas (*21*). Two recent experiments have directly demonstrated the presence of these molecules and investigated some of their properties (*12*, *13*). For negative scattering length, no weakly bound dimer state exists. For negative scattering length, where a weakly bound dimer state does not exist, the ^{6}Li gas exhibits a remarkable stability against collisional decay, and deeply degenerate Fermi gases have been created (*20*).

Our optical dipole trap is realized with a single Gaussian laser beam at a wavelength of 1030 nm, which is focused to a waist of 23 μm. At the full power of $P_0 = 10.5$ W, the radial and axial oscillation frequencies are $\Omega_r/2\pi = 14.5$ kHz and $\Omega_z/2\pi = 140$ Hz, respectively, and the atom trap is $U_0 \approx k_B \times 800$ μK deep (k_B denotes Boltzmann's constant). When the power P is reduced to a relative value $p = P/P_0$, the optical trap frequencies follow $p^{1/2}\Omega_i (i = r, z)$ and the trap depth for the atoms is $U_{at} = pU_0$. Our magnetic field B used for Feshbach tuning exhibits a curvature that gives rise to an additional contribution to the trapping potential. For the tight radial confinement of the optical trap, this effect is negligibly small. For the weak axis, however, a magnetic trapping effect becomes important with decreasing p. Taking this into account, the axial trap frequency is given by $\omega_z = \sqrt{p\Omega_z^2 + \omega_m^2}$. Here $\omega_m/2\pi = 24.5$ Hz $\times \sqrt{B/\mathrm{kG}}$ is the magnetic contribution, which is precisely known for our coils. For weak traps with $p \ll 0.03$ ($U_{at}/k_B \ll 25$ μK), the magnetic contribution dominates, and the axial confinement is harmonic with a corresponding frequency known on the percent level. In this regime, the mean trap frequency is given by $\bar{\omega} = (p\Omega_r^2\omega_m)^{1/3}$. For the weakly bound ^{6}Li dimers, all external forces are twice the ones on the individual atoms. Thus, the molecular trap is two times deeper than the atom trap ($U_{mol} = 2U_{at}$), and the trap frequencies are identical. Gravity is compensated for by a magnetic field gradient of 1.1 G/cm.

We start the evaporation process with $\sim 1.5 \times 10^6$ atoms at a temperature of ~ 80 μK, a peak number density of $\sim 10^{14}$ cm^{-3}, and a peak phase-space density of $\sim 5 \times 10^{-3}$. The mean elastic collision rate is as high as $\sim 5 \times 10^4$ s^{-1}. These excellent starting conditions are obtained by a two-stage loading process. The atoms are loaded into the dipole trap from another deep, large-volume standing wave trap (*25*), which itself is loaded from a magneto-optical trap. Forced evaporative cooling is then performed by reducing the trap power (*17*, *20*). We use a simple exponential ramp with a relative power $p(t) = \exp(-t/\tau)$, where the time constant $\tau = 0.23$ s is experimentally optimized. A feedback system allows us to precisely control the laser power to levels well below $p = 10^{-4}$.

BEC of weakly bound molecules occurs when we perform evaporative cooling at a large positive scattering length of $a \approx +3500a_0$, where a_0 is Bohr's radius. In this case, the evaporation process shows a strikingly different behavior in comparison with the corresponding situation at large negative scattering length, where no dimers can be produced.

First we discuss the creation of a degenerate Fermi gas without the possibility of molecule formation at a magnetic field of 1176 G, where $a \approx -3500a_0$ (*23*). Here the evaporation pro-

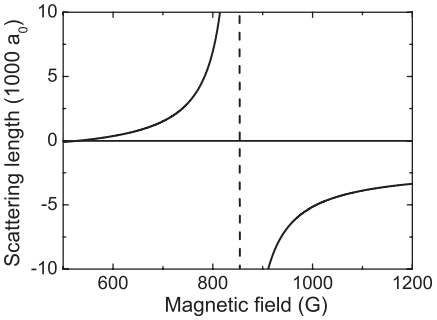

Fig. 1. Feshbach resonance at ~850 G in a mixture of the two lowest spin states of ^{6}Li (*18*). The s-wave scattering length a is plotted as a function of the magnetic field B.

[1]Institut für Experimentalphysik, Universität Innsbruck, Technikerstraβe 25, 6020 Innsbruck, Austria. [2]Institut für Quantenoptik und Quanteninformation, Österreichische Akademie der Wissenschaften, 6020 Innsbruck, Austria.

*To whom correspondence should be addressed. E-mail: rudolf.grimm@uibk.ac.at

ceeds in a very similar way as that described in (*17*, *20*). The measured atom number N (*26*) first follows a scaling law $N/N_0 = p^{\alpha}$ (*27*), with $\alpha \approx 0.25$. In this regime, the temperature of the gas is typically a factor of 10 below the trap depth (*27*), and the elastic collision rate stays well above 10^4 s^{-1}. The crossover to Fermi degeneracy, where the thermal energy $k_B T$ reaches the Fermi energy $E_F = \hbar\,\bar{\omega}\,(3N)^{1/3}$, takes place at $p \approx 0.05$ ($U_{at}/k_B \approx 40$ μK). By further decreasing p, the trap depth $U_{at} \propto p$ decreases faster than the Fermi energy $E_F \propto p^{1/3}$. A threshold occurs when E_F reaches U_{at} and the trap is filled up to the "rim." Further decrease of p then leads to a spilling of atoms out of the trap and thus to a rapid decrease of N with p. Our data (Fig. 2) clearly show this spilling effect for $p < 1 \times 10^{-3}$ ($U_{at}/k_B < 800$ nK). Modeling the spilling curves provides us with an upper bound of $k_B T < 0.2 E_F$ for the temperature in terms of the Fermi energy. In the regime of a completely filled shallow trap, the number of atoms in the two-component spin mixture is given by two times the number of quantum states in the trap. A numerical calculation, shown in Fig. 2, confirms this interpretation of our data.

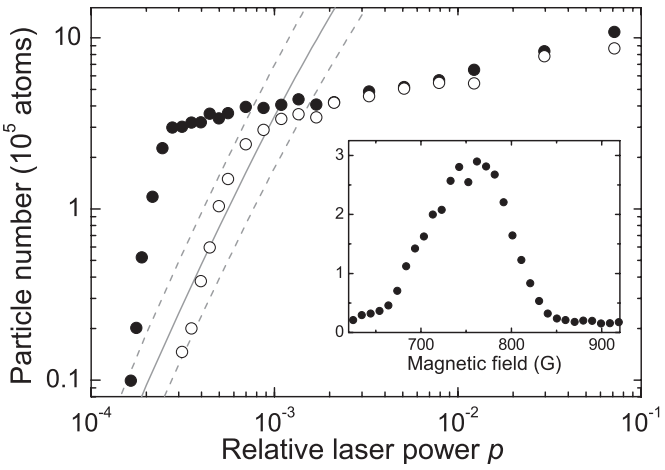

Fig. 2. Evaporative cooling results obtained on both sides of the Feshbach resonance. We measure the number of trapped particles (the number of all atoms that are free or bound in long-range dimers) as a function of the relative laser power p at the end of an exponential evaporation ramp $p(t) = \exp(-t/230\ \text{ms})$. The trap depth for atoms is $U_{at}/k_B = p \times 800$ μK, whereas for molecules it is two times larger ($U_{mol} = 2U_{at}$). The measurements taken at 1176 G with negative scattering length $a \approx -3500 a_0$ (open circles) show the spilling of a degenerate Fermi gas when the trap depth reaches the Fermi energy. The solid line shows the maximum number of trapped atoms in a two-component Fermi gas according to a numerical calculation of the number of quantum states in our trap. The dashed lines indicate the corresponding uncertainty range due to the limited knowledge of the experimental parameters. The measurements at 764 G with positive scattering length $a \approx +3500 a_0$ (solid circles) exhibit a striking increase of the trapped particle number at low values of p, which is due to the formation of molecules. The inset shows the optimum production of molecules in the magnetic field range where a weakly bound level exists. Here the total number of particles is measured for various magnetic fields at a fixed final ramp power $p = 2.8 \times 10^{-4}$ ($U_{mol}/k_B \approx 440$ nK).

The same evaporation procedure is performed at a magnetic field of 764 G, where the scattering length $a \approx +3500 a_0$ (*23*) has essentially the same magnitude but opposite sign. Here the weakly bound dimers have a binding energy of ~2 μK, and their formation has been observed in several experiments (*12*, *13*, *21*). In order to detect the molecules, we dissociate them and measure the number of resulting atoms (*26*). For this purpose, we abruptly turn on the full trap power, which strongly heats the sample and leads to collisional dissociation. In order to ensure that we dissociate all molecules, we also apply a magnetic field ramp across the Feshbach resonance (*13*). The number of atoms measured after the dissociation process thus yields the number of free atoms together with atoms having formed molecules.

Below $p = 1 \times 10^{-3}$ the measured atom numbers (solid circles in Fig. 2) show a striking difference in comparison with the case of the degenerate Fermi gas. Down to a power level of $p = 3 \times 10^{-4}$ ($U_{mol}/k_B \approx 480$ nK), the trap holds almost all particles and contains up to 20 times more atoms than would be possible for fermions. Hence, the trapped sample can no longer be an atomic Fermi gas. The trap is filled with bosonic molecules in the weakly bound state (*28*). The lifetime of the molecular ensemble, for which we measure about 20 s at a fixed trap depth of $U_{mol}/k_B \approx 560$ nK, exceeds the time scale of elastic collisions (~100 μs) by several orders of magnitude. This highlights the fact that the molecular cloud exists in a thermal equilibrium state.

The formation of molecules during the evaporative cooling process can be understood in terms of a chemical atom-molecule equilibrium (*29*, *30*). Exothermal three-body recombination processes compete with dissociation by endothermal two-body processes. When the gas is cooled down, the equilibrium shifts to an increasing fraction of molecules. Because atom-atom, atom-molecule, and molecule-molecule collisions have comparable cross sections near the resonance (*16*), evaporation continues at about the same speed. In the final stage of cooling, all relevant energies, such as the thermal energy $k_B T$ and the trap depths U_{at} and U_{mol}, are far below the binding energy $\hbar^2/(ma^2)$, so that in chemical equilibrium one is left with an essentially pure sample of molecules. The fact that the binding energy of ~2 μK at our optimized magnetic field of 764 G is a few times larger than the final trap depth (inset, Fig. 1) fits well into this picture.

The observation that a large number of $N_{mol} \approx 1.5 \times 10^5$ molecules is confined in our very shallow, only 480 nK deep trap under thermal equilibrium conditions already shows that a molecular BEC is formed. The trap offers about 10 times more quantum states for dimers as compared to the case of atoms discussed before (*31*). Because we observe a factor of ~20 more particles than for the degenerate atomic Fermi gas, the molecular gas is necessarily quantum degenerate. Because of the high elastic collision rates, which stay well above 10^3 s^{-1} even for very shallow traps, the sample is also thermalized. The temperature then is a small fraction of the trap depth. According to standard evaporation theory (*27*), we can typically assume $T \approx 0.1\ U_{mol}/k_B \approx 50$ nK. This is well below the critical temperature for BEC, for which we calculate $T_C = \hbar\,\bar{\omega}\,k_B^{-1}\,(N_{mol}/1.202)^{1/3} = 280$ nK. Because the condensate fraction is given by $1 - (T/T_C)^3$, these arguments show that the molecular BEC must be almost pure.

To investigate the molecular condensate, we have studied a characteristic collective excitation mode (*32*, *33*). For a cigar-shaped sample in the Thomas-Fermi limit, well fulfilled in our experiment, such a quadrupolar mode is expected at a frequency of $\sqrt{5/2}\,\omega_z = 2\pi \times 33.8$ Hz. We perform our measurement at $p = 3.5 \times 10^{-4}$ ($U_{mol}/k_B \approx 560$ nK) with a trapped sample of ~10^5 molecules. We apply a sinusoidal modulation to the magnetic field with an amplitude of 3.5 G to modulate the molecular scattering length $a_m \propto a$ (*16*) with a relative amplitude of about 5%. After 2 s of continuous excitation, we measure the remaining number of particles in the trap. The resonance manifests itself in a sharp dip in the number of particles (Fig. 3). The observed resonance frequency of 33.6 Hz is in remarkable agreement with the expectation. We point out that a noncondensed gas deep in the hydrodynamic regime would show a similar frequency of 33.2 Hz (*34*), but thermalization in our shallow trap excludes this scenario (*35*). The measured collective excitation frequency rules out a gas in the collisionless regime, which would show its resonant loss at $2\omega_z = 2\pi \times 42.8$ Hz, and thus again confirms the thermalization of the sample. The observed narrow resonance width of ~1 Hz shows a very low damping rate and is consistent with an almost pure BEC (*33*, *36*).

An essential property of a BEC is its mean field potential $U_{MF} = 4\pi n a_m \hbar^2/(2m)$ resulting

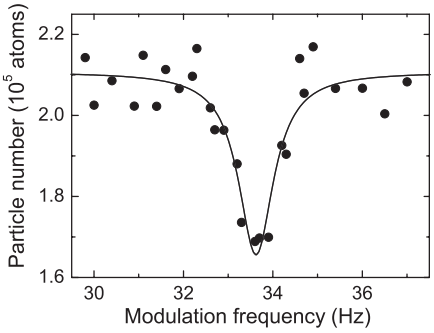

Fig. 3. Resonance of a collective excitation mode at $\sqrt{5/2}\,\omega_z$. The oscillation is excited by magnetic modulation of the molecular BEC mean field. The solid curve shows a Lorentzian fit to the data.

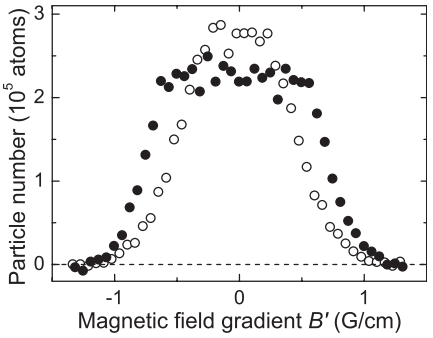

Fig. 4. Controlled spilling of the BEC by application of a magnetic field gradient B'. This variable gradient is applied in addition to the constant gradient of 1.1 G/cm that we use for gravity compensation. The data are taken at the two different magnetic fields $B_1 = 772$ G (open circles) and $B_2 = 731$ G (solid circles), where the mean field of the BEC is different by a factor of ~2.

from *s*-wave interactions; here n denotes the molecular density. For our molecular BEC with large positive a_m, the mean field is repulsive and thus stabilizes the BEC against collapse and decay. In a trap of finite depth, however, the mean field repulsion limits the maximum number of trappable molecules. When the chemical potential μ reaches the trap depth, a similar spilling effect is expected as we see for the Fermi gas, but for weaker traps. The decrease of our molecular signal (Fig. 2) below $p = 3 \times 10^{-4}$ ($U_{mol}/k_B \approx 480$ nK) may be explained by such a spilling effect.

We used spilling in a controlled way to demonstrate the mean field of the molecular BEC and to investigate its dependence on the magnetic field. After producing the BEC at a magnetic field of $B_1 = 772$ G and $p = 3.5 \times 10^{-4}$ ($U_{mol}/k_B \approx 560$ nK), we adiabatically tilt the vertical trapping potential by application of a magnetic field gradient B' that is smoothly ramped up within 50 ms. The number of remaining particles as a function of the applied field gradient (Fig. 4) shows the loss of molecules resulting from the reduced trap depth. When the magnetic field is kept at the evaporation field of $B_1 = 772$ G, where $a = 4100a_0$ (*23*), even very weak gradients lead to loss (open circles in Fig. 4). This indicates that the chemical potential is close to the potential depth, so that the trap is full. The chemical potential can be lowered by reducing the scattering length. For this purpose, we ramp the magnetic field to a smaller value. A spilling curve taken at $B_2 = 731$ G, where $a = 2200a_0$ (*23*), indeed shows a markedly different behavior (solid circles in Fig. 4). Here small gradients do not lead to any loss and the curve thus shows a flat top. For gradients $|B'|$ exceeding 0.65 G/cm, molecules get spilled until everything is lost at $|B'| = 1.3$ G/cm. The sharp onset of the spilling confirms the essentially pure nature of the BEC.

A comparison of the two spilling curves in Fig. 4 provides us with information on the ratio of the scattering lengths a_m at the two magnetic fields B_1 and B_2. In the spilling region above $|B'| = 0.65$ G/cm, the trap is full in both cases, and the trapped particle number is inversely proportional to a_m. Comparing the two spilling curves in that region, we obtain a scattering length ratio of $a_m(B_1)/a_m(B_2) = 2.4(2)$. This factor is indeed close to the factor of 1.9 (*23*) expected from the proportionality of atomic and molecular scattering lengths $a_m \propto a$ (*16*) and the dependence of a shown in Fig. 1. This observation demonstrates the mean field of the molecular BEC together with its magnetic tunability.

The ability to control interactions in a Bose condensed ensemble of paired fermionic atoms has many exciting prospects (*37*, *38*). It opens up unique ways to cool a fermionic gas far below the Fermi temperature (*39*) and to study different regimes of superfluidity (*40*–*43*). The experimental exploration of the strongly interacting crossover regime between a BEC-like and a Cooper-paired phase is a particular challenge and promises more insight into the physical mechanisms underlying superconductivity.

References and Notes

1. M. Anderson, J. Ensher, M. Matthews, C. Wieman, E. Cornell, *Science* **269**, 198 (1995).
2. K. Davis *et al.*, *Phys. Rev. Lett.* **75**, 3969 (1995).
3. C. Bradley, C. Sackett, J. Tollett, R. Hulet, *Phys. Rev. Lett.* **75**, 1687 (1995).
4. R. Wynar, R. S. Freeland, D. J. Han, C. Ryu, D. J. Heinzen, *Science* **287**, 1016 (2000).
5. E. A. Donley, N. R. Claussen, S. T. Thompson, C. E. Wieman, *Nature* **417**, 529 (2002).
6. C. Chin, A. J. Kerman, V. Vuletić, S. Chu, *Phys. Rev. Lett.* **90**, 033201 (2003).
7. J. Herbig *et al.*, *Science* **301**, 1510 (2003); published online 21 August 2003 (10.1126/science.1088876).
8. S. Dürr, T. Volz, A. Marte, G. Rempe, preprint available at http://arxiv.org/abs/cond-mat/0307440.
9. K. Xu, *et al.* preprint available at http://arxiv.org/abs/cond-mat/0310027.
10. C. A. Regal, C. Ticknor, J. L. Bohn, D. S. Jin, *Nature* **424**, 47 (2003).
11. K. E. Strecker, G. B. Partridge, R. G. Hulet, *Phys. Rev. Lett.* **91**, 080406 (2003).
12. J. Cubizolles, T. Bourdel, S. J. J. M. F. Kokkelmans, G. V. Shlyapnikov, C. Salomon, preprint available at http://arxiv.org/abs/cond-mat/0308018.
13. S. Jochim *et al.*, *Phys. Rev. Lett.*, in press (preprint available at http://arxiv.org/abs/cond-mat/0308095).
14. S. Inouye *et al.*, *Nature* **392**, 151 (1998).
15. C. A. Regal, M. Greiner, D. S. Jin, preprint available at http://arxiv.org/abs/cond-mat/0308606.
16. D. S. Petrov, C. Salomon, G. V. Shlyapnikov, preprint available at http://arxiv.org/abs/cond-mat/0309010.
17. S. Granade, M. E. Gehm, K. M. O'Hara, J. E. Thomas, *Phys. Rev. Lett.* **88**, 120405 (2002).
18. K. M. O'Hara *et al.*, *Phys. Rev. A* **66**, 041401 (2002).
19. S. Jochim *et al.*, *Phys. Rev. Lett.* **89**, 273202 (2002).
20. K. M. O'Hara, S. L. Hemmer, M. E. Gehm, S. R. Granade, J. E. Thomas, *Science* **298**, 2179 (2002); published online 7 November 2002 (10.1126/science.1079107).
21. T. Bourdel *et al.*, *Phys. Rev. Lett.* **91**, 020402 (2003).
22. M. Houbiers, H. T. C. Stoof, W. McAlexander, R. Hulet, *Phys. Rev. A* **57**, R1497 (1998).
23. The position of the Feshbach resonance is known to within a few tens of Gauss. All numbers given for the scattering lengths and binding energies are subject to a corresponding systematic error.
24. K. Dieckmann *et al.*, *Phys. Rev. Lett.* **89**, 203201 (2002).
25. A. Mosk *et al.*, *Opt. Lett.* **26**, 1837 (2001).
26. We measure the atom number via fluorescence detection after recapture into a magneto-optical trap. In order to avoid molecule formation and loss when the Feshbach tuning field is ramped down before detection, we heat the sample by abruptly turning on the full laser power of the optical dipole trap. At low phase-space densities, the thermal gas is not affected by the downward Feshbach ramp (*13*).
27. K. M. O'Hara, M. E. Gehm, S. R. Granade, J. E. Thomas, *Phys. Rev. A* **64**, 051403 (2001).
28. We know that only the weakly bound state is populated, because the release of binding energy in a three-body process would otherwise lead to immediate trap loss. Moreover, our dissociation-based detection is sensitive only to molecules in this state.
29. C. Chin, R. Grimm, preprint available at http://arxiv.org/abs/cond-mat/0309078.
30. S. J. J. M. F. Kokkelmans, G. V. Shlyapnikov, C. Salomon, preprint available at http://arxiv.org/abs/cond-mat/0308384.
31. For the harmonically approximated trap with same frequencies and twice the depth, the molecules have eight times more quantum states than the atoms. The lower ω_z at 764 G as compared to 1176 G gives another factor of 1.24.
32. S. Stringari, *Phys. Rev. Lett.* **77**, 2360 (1996).
33. D. M. Stamper-Kurn, H.-J. Miesner, S. Inouye, M. R. Andrews, W. Ketterle, *Phys. Rev. Lett.* **81**, 500 (1998).
34. D. Guéry-Odelin, F. Zambelli, J. Dalibard, S. Stringari, *Phys. Rev. A* **60**, 4851 (1999).
35. A noncondensed ensemble in the hydrodynamic regime, where the elastic collision rate exceeds all other time scales, would rapidly cool down by evaporation to temperatures far below the trap depth and thus form a BEC.
36. D. S. Jin, M. R. Matthews, J. R. Ensher, C. E. Wieman, E. A. Cornell, *Phys. Rev. Lett.* **78**, 764 (1997).
37. L. Pitaevskii, S. Stringari, *Science* **298**, 2144 (2002).
38. A. Cho, *Science* **301**, 750 (2003).
39. L. D. Carr, G. V. Shlyapnikov, Y. Castin, preprint available at http://arxiv.org/abs/cond-mat/0308306.
40. H. T .C. Stoof, M. Houbiers, C. Sackett, R. Hulet, *Phys. Rev. Lett.* **76**, 10 (1996).
41. M. Holland, S. J. J. M. F. Kokkelmans, M. L. Chiofalo, R. Walser, *Phys. Rev. Lett.* **87**, 120406 (2001).
42. E. Timmermans, K. Furuya, P. W. Milonni, A. K. Kerman, *Phys. Lett. A* **285**, 228 (2001).
43. Y. Ohashi, A. Griffin, *Phys. Rev. Lett.* **89**, 130402 (2002).

44. We thank P. Zoller for very useful discussions and for stimulating the measurement of the collective excitation frequency. We acknowledge support by the Austrian Science Fund (FWF) within Spezialforschungsbereich 15 (project part 15) and by the European Union through the Cold Molecules Training and Mobility of Researchers Network under contract no. HPRN-CT-2002-00290. C.C. is a Lise-Meitner fellow of the FWF.

3 November 2003; accepted 11 November 2003
Published online 13 November 2003;
10.1126/science.1093280
Include this information when citing this paper.

Appendix F

Crossover from a Molecular Bose-Einstein Condensate to a Degenerate Fermi Gas

Crossover from a Molecular Bose-Einstein Condensate to a Degenerate Fermi Gas

M. Bartenstein,[1] A. Altmeyer,[1] S. Riedl,[1] S. Jochim,[1] C. Chin,[1] J. Hecker Denschlag,[1] and R. Grimm[1,2]

[1]*Institut für Experimentalphysik, Universität Innsbruck, Technikerstraße 25, 6020 Innsbruck, Austria*

[2]*Institut für Quantenoptik und Quanteninformation, Österreichische Akademie der Wissenschaften, 6020 Innsbruck, Austria*

(Received 8 January 2004; revised manuscript received 2 February 2004; published 23 March 2004)

We demonstrate a reversible conversion of a $^6Li_2$ molecular Bose-Einstein condensate to a degenerate Fermi gas of atoms by adiabatically crossing a Feshbach resonance. By optical *in situ* imaging, we observe a smooth change of the cloud size in the crossover regime. On the Feshbach resonance, the ensemble is strongly interacting and the measured cloud size is 75(7)% of the one of a noninteracting zero-temperature Fermi gas. The high condensate fraction of more than 90% and the adiabatic crossover suggest our Fermi gas to be cold enough to form a superfluid.

DOI: 10.1103/PhysRevLett.92.120401 PACS numbers: 03.75.Mn, 05.30.Fk, 32.80.Pj, 34.50.–s

Bose-Einstein condensation (BEC) of molecules formed by fermionic atoms was recently demonstrated [1–4]. The tunability of interactions in such systems provides a unique possibility to explore the Bose-Einstein condensate to Bardeen-Cooper-Schrieffer (BEC-BCS) crossover [5], an intriguing interplay between the superfluidity of bosons and Cooper pairing of fermions. While the BEC and BCS limits are both well understood, the crossover takes place in a strongly interacting regime, which represents a challenge for many-body theory.

Feshbach resonances [6] play a central role to control two-body interaction and have been used for conversion between fermionic atoms and bosonic molecules [7–10]. They are also the experimental key to investigate phenomena related to the BEC-BCS crossover. For example, it has been predicted in Ref. [11] that a pure molecular BEC can be converted into a superfluid Fermi gas by an adiabatic passage over the Feshbach resonance. Moreover, in the crossover regime where the interactions are unitarity limited, a universal behavior is expected [12,13]. Ultracold gases in that regime may provide new insights into other strongly interacting systems such as high-T_c superconductors, ^{3}He superfluids, and neutron stars.

A spin mixture of ^{6}Li atoms in the lowest two hyperfine sublevels is an excellent system to investigate the crossover [14,15] based on a broad Feshbach resonance at a magnetic field of $B = 850$ G [16–18]. An efficient formation of ultracold molecules has been realized by three-body recombination [10,19], or by sweeping the magnetic field across the resonance [8]. The long lifetime of the molecules permits efficient evaporation [1,8,10] and facilitates slow, adiabatic changes of the system.

In this work, we explore the regime where the BEC-BCS crossover is expected by analyzing the density profiles of the trapped cloud at different magnetic fields. Our experimental setup is described in Ref. [1]. We load 2×10^6 precooled ^{6}Li atoms into a single focused-beam dipole trap, which is generated by a 10 W Yb:YAG laser operating at a wavelength of 1030 nm. We evaporatively cool the cloud by exponentially lowering the trap depth with a time constant of 460 ms. The radial and axial trap frequencies are $\omega_r/2\pi = 110\ \mathrm{Hz}(P/\mathrm{mW})^{1/2}$ and $\omega_z/2\pi = (600B/\mathrm{kG} + 0.94P/\mathrm{mW})^{1/2}$ Hz, respectively, where P is the laser power. The curvature of the magnetic field that we use for Feshbach tuning results in a magnetic contribution to the axial trapping. In the low power range where the molecular BEC is formed ($P < 50$ mW), the axial confinement is predominantly magnetic. During the whole evaporation process, the magnetic field is kept at $B = 764$ G. At this field the molecular binding energy is $\sim k_B \times 2\ \mu$K, where k_B is Boltzmann's constant. For the scattering length of elastic molecule-molecule collisions, we expect $a_{\mathrm{mol}} = 2200a_0$, based on the predicted relation of $a_{\mathrm{mol}} = 0.6a$ [20] and an atomic scattering length of $a = 3500a_0$ [17]. Here a_0 is Bohr's radius. Using radio-frequency spectroscopy which allows us to distinguish signals from atoms and molecules [7], we observe a complete atom to molecule conversion when the thermal energy of the particles is reduced to values well below the molecular binding energy.

For detection we apply *in situ* absorption imaging to record spatial density profiles of the trapped ensemble. To image at high magnetic fields, we illuminate the cloud for 20 μs with a probe beam (intensity 0.5 mW/cm^2) tuned to the atomic $|2S_{1/2}, m_J = -1/2, m_I = 0\rangle \rightarrow |2P_{3/2}, m_J' = -3/2, m_I' = 0\rangle$ transition. The probe beam dissociates the molecules and is used to image the resulting atom cloud [3]. Compared to the absorption imaging of unbound atoms, we found that the detection efficiency of the molecules approaches 100% at fields higher than 750 G and ~50% at 650 G. The difference is due to the Franck-Condon wave function overlap, which favors fields closer to the resonance where the interatomic separation in the molecular state is larger. In our cigar-shaped trap, the radial cloud size is on the order of our imaging resolution of 10 μm, while the axial cloud size of typically ~100 μm can be accurately measured. We therefore obtain axial density distributions from images integrated radially.

To measure the condensate fraction, we adiabatically reduce the magnetic field from 764 to 676 G in a 200-ms linear ramp after completion of the evaporation ramp. This reduces the scattering length $a_{\rm mol}$ and thus increases the visibility of the characteristic bimodal distribution. Figure 1(a) shows a bimodal profile observed in this way with $N_{\rm mol} = N/2 = 4 \times 10^5$ molecules remaining at a final evaporation ramp power of 28 mW. A Gaussian fit to the thermal wings (dashed line) yields a temperature of $T = 430$ nK, which is a factor of 7.5 below the calculated trap depth of 3.2 μK. The observed condensate fraction of $\sim$20% is consistent with $1 - (T/T_c)^3$, where $T_c = 0.8 k_B^{-1} \hbar \bar{\omega} (N_{\rm mol}/1.202)^{1/3} = 500$ nK is the critical temperature, $\bar{\omega} = (\omega_r^2 \omega_z)^{1/3}$ is the mean vibration frequency, and the factor of 0.8 takes into account the $\sim$20% downshift in T_c due to interactions [21].

We obtain pure molecular condensates when we continue the evaporation process down to final power levels of a few mW. Figure 1(b) shows an essentially pure condensate of $N_{\rm mol} = 2.0 \times 10^5$ molecules obtained at a final power of 3.8 mW, where the trap depth is 450 nK. The density profile is well fit by a Thomas-Fermi density distribution $\propto (1 - z^2/z_{\rm TF}^2)^2$ with a radius $z_{\rm TF} = 105$ μm. The corresponding peak molecular density is 1.2×10^{13} cm^{-3}. In the image a thermal component is not discernable. A careful analysis of the profile provides us with a lower bound of 90% for the condensate fraction. For the chemical potential of the BEC, we obtain $\mu = \frac{1}{2} m_{\rm mol} \omega_z^2 z_{\rm TF}^2 = k_B \times 130$ nK. Here $m_{\rm mol} = 2m$ is the mass of the ^{6}Li dimer. Based on the prediction $a_{\rm mol} = 0.6a = 650 a_0$, the calculated chemical potential of $\frac{1}{2}(15\hbar^2 N_{\rm mol} \bar{\omega}^3 a_{\rm mol} \sqrt{m_{\rm mol}})^{2/5} = k_B \times 155$ nK is consistent with the observed value of $k_B \times 130$ nK considering the experimental uncertainty. In particular, the particle number is calibrated to within a factor of 1.5 through fluorescence imaging [10].

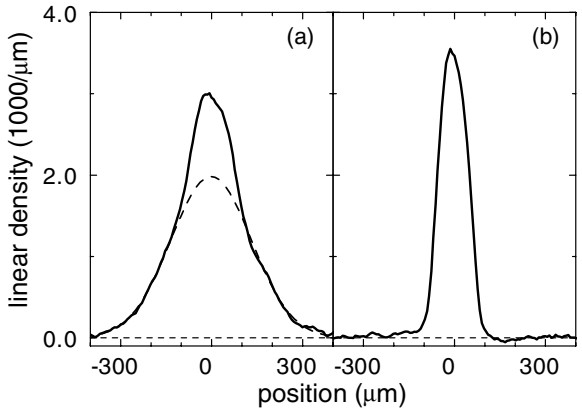

FIG. 1. Axial density profiles of a partially condensed (a) and fully condensed (b) molecular cloud. The profiles are derived from averaging seven *in situ* images taken at a magnetic field of $B = 676$ G after evaporation at the production field of 764 G. (a) When the evaporation ramp is stopped with 4×10^5 molecules at a final laser power of 28 mW, a characteristic bimodal distribution is observed with a condensate fraction of $\sim$20%. The dashed curve shows Gaussian fit to the thermal fraction. (b) At a final laser power of 3.8 mW, an essentially pure condensate of 2×10^5 molecules is obtained.

The pure molecular BEC at 764 G serves as our starting point for exploring the crossover to the degenerate Fermi gas. Before we change the magnetic field, we first adiabatically increase the trap power from 3.8 to 35 mW in a 200-ms exponential ramp. The higher power provides a trap depth of $\sim k_B \times 2$ μK for the atoms, which is roughly a factor of 2 above the Fermi energy, and avoids spilling of the Fermi gas produced at magnetic fields above the resonance [1]. The compression increases the peak density of the condensate by a factor of 2.5. All further experiments reported here are performed in the recompressed trap with $\omega_r/2\pi = 640$ Hz and $\omega_z/2\pi = (600 B/\text{kG} + 32)^{1/2}$ Hz.

We measure the lifetime of the BEC in the compressed trap at 764 G to be 40 s. The peak molecular density is estimated to be $n_{\rm mol} = (15/8\pi)(\omega_r/\omega_z)^2 N_{\rm mol}/z_{\rm TF}^3 = 1.0(5) \times 10^{13}$ cm^{-3}. This provides an upper bound for the binary loss coefficient of 1×10^{-14} cm^3/s, and is consistent with previous measurements in thermal molecular gases [8,10] together with the predicted scattering length scaling [20] and the factor-of-2 suppression of binary collision loss in a condensate.

For exploring the crossover to a Fermi gas we apply slow magnetic-field ramps. To ensure their adiabaticity, we performed several test experiments. In one series of measurements we ramped up the field from 764 to 882 G and back to 764 G with variable ramp speed. This converts the molecular BEC into a strongly interacting Fermi gas and vice versa. Therefore substantial changes are expected in the cloud size. After the up-and-down ramp, we observe an axial oscillation of the ensemble at the quadrupolar excitation frequency [1,22]. This collective oscillation is the lowest excitation mode of the system and is thus sensitive to nonadiabaticity effects. We observe axial oscillations with relative amplitudes of $>$ 5% for ramp speeds above 1.2 G/ms. For ramp speeds of 0.6 G/ms and lower, the axial oscillation was no longer visible.

We also checked the reversibility of the crossover process by linearly ramping up the magnetic field from 764 to 1176 G and down again to 764 G within 2 s (ramp speed of ± 0.41 G/ms). In Fig. 2, we compare the axial profile taken after this ramp (●) with the corresponding profile obtained after 2 s at fixed magnetic field (○). The comparison does not show any significant deviation. This highlights that the conversion into a Fermi gas and its back-conversion into a molecular BEC are lossless and proceed without noticeable increase of the entropy.

To investigate the spatial profile of the trapped gas in different regimes, we start with the molecular BEC at 764 G and change the magnetic field in 1-s linear ramps to final values between 740 and 1440 G. Images are then taken at the final ramp field. To characterize the size of

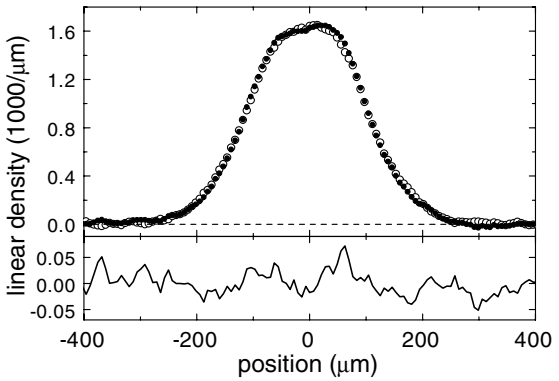

FIG. 2. Axial profile of a molecular BEC at 764 G (●) after its conversion into a Fermi gas at 1176 G and subsequent back conversion. Two 1-s magnetic field ramps are applied in this reversible process. For reference we show the corresponding profile observed without the magnetic field ramp (○). The density profiles are obtained by averaging over 50 images. The difference shown in the lower graph is consistent with the drifts of a residual interference pattern in the images.

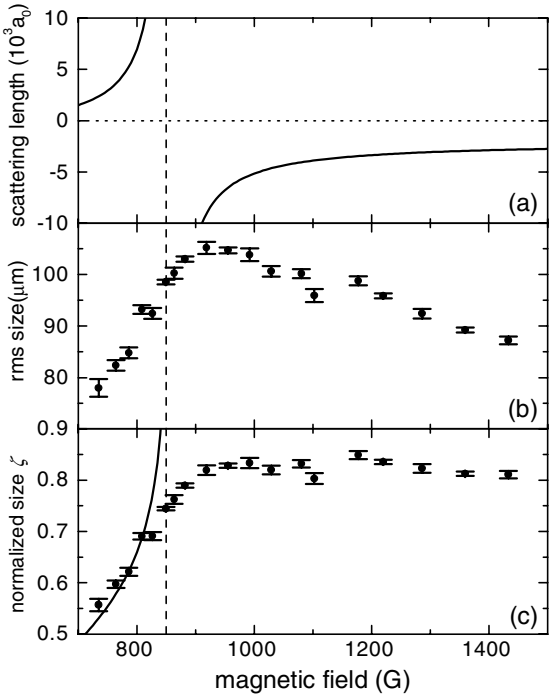

FIG. 3. Axial cloud size measurements across the Feshbach resonance. In (a) the atomic scattering length a is shown according to [17]; the resonance at 850 G is marked by the vertical dashed line. The data in (b) display the measured rms cloud sizes. In (c), the same data are plotted after normalization to a noninteracting Fermi gas. The solid line shows the expectation from BEC mean-field theory with $a_{\mathrm{mol}} = 0.6a$. In (b) and (c), the error bars show the statistical error of the size measurements from typically five individual images.

the trapped gas, we determine the root-mean-squared axial size z_{rms}. This rms size is related to the axial radius z_{TF} by $z_{\mathrm{rms}} = z_{\mathrm{TF}}/\sqrt{7}$ in the case of a pure BEC in the Thomas-Fermi limit and by $z_{\mathrm{rms}} = z_{\mathrm{TF}}/\sqrt{8}$ in the cases of zero-temperature noninteracting or strongly interacting Fermi gases [23].

Figure 3(b) shows how the measured axial size z_{rms} changes with the magnetic field. For comparison, Fig. 3(a) displays the magnetic-field dependence of the atomic scattering length a. Up to 950 G, an increase in z_{rms} is due to the crossover from the molecular BEC to the degenerate Fermi gas. For higher magnetic fields, the axial cloud size of the Fermi gas shrinks with B as the axial magnetic confinement increases ($\omega_z \propto \sqrt{B}$).

For the following discussions, we normalize the observed size to the one expected for a noninteracting Fermi gas. In particular, this removes the explicit trap dependence. In Fig. 3(c), we show the normalized axial size $\zeta = z_{\mathrm{rms}}/z_0$, where $z_0 = (E_F/4m\omega_z^2)^{1/2}$ is the rms axial size of a noninteracting zero-temperature Fermi gas with $N = 4 \times 10^5$ atoms. The Fermi energy $E_F = \hbar^2 k_F^2/2m = \hbar\bar{\omega}(3N)^{1/3}$ amounts to $k_B \times 1.1\ \mu$K at 850 G, and the Fermi wave number k_F corresponds to a length scale of $k_F^{-1} = 3600 a_0$.

Below the Feshbach resonance, the observed dependence of the cloud size agrees well with the mean-field behavior of a BEC in the Thomas-Fermi limit. In this regime, the normalized size is given by $\zeta = 0.688(a_{\mathrm{mol}}/a)^{1/5}(E_F/E_b)^{1/10}$, where $E_b = \hbar^2/ma^2$ is the molecular binding energy. Figure 3(c) shows the corresponding curve (solid line) calculated with $a_{\mathrm{mol}}/a = 0.6$ [20]. This BEC limit provides a reasonable approximation up to ~800 G; here the molecular gas interaction parameter is $n_{\mathrm{mol}} a_{\mathrm{mol}}^3 \approx 0.08$. Alternatively, the interaction strength can be expressed as $k_F a \approx 1.9$.

The crossover to the Fermi gas is observed in the vicinity of the Feshbach resonance between 800 and 950 G; here ζ smoothly increases with the magnetic field until it levels off at 950 G, where the interaction strength is characterized by $k_F a \approx -1.9$. Our results suggest that the crossover occurs within the range of $-0.5 \lesssim (k_F a)^{-1} \lesssim 0.5$, which corresponds to the strongly interacting regime. The smoothness of the crossover is further illustrated in Fig. 4. Here the spatial profiles near the resonance show the gradually increasing cloud size without any noticeable new features.

On resonance a universal regime is realized [12–14], where scattering is fully governed by unitarity and the scattering length drops out of the description. Here the normalized cloud size can be written as $\zeta = (1 + \beta)^{1/4}$, where β parametrizes the mean-field contribution to the chemical potential in terms of the local Fermi energy [14]. At 850 G our measured value of $\zeta = 0.75 \pm 0.07$ provides $\beta = -0.68^{+0.13}_{-0.10}$. Here the total error range includes all statistic and systematic uncertainties with the particle number giving the dominant contribution. Note that the uncertainty in the Feshbach resonance position is not included in the errors [18]. Our experimental results reveal a stronger interaction effect than previous measurements that yielded $\beta = -0.26(7)$ at $T = 0.15T_F$ [14]

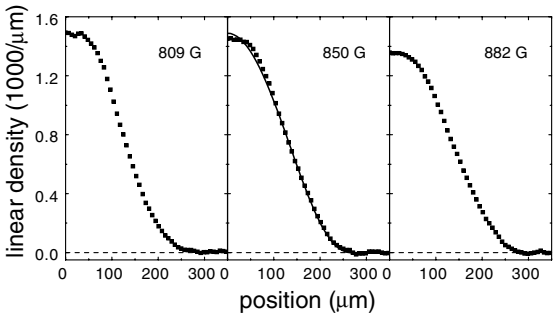

FIG. 4. Observed axial density profiles near the Feshbach resonance, averaged over 50 images and symmetrized to reduce imaging imperfections. The rms cloud sizes are 93, 99, and 103 μm at $B = 809$, 850, and 882 G, respectively. For comparison, the on-resonance data at 850 G are shown together with a fit by the expected profile $\propto (1 - z^2/z_{\mathrm{TF}}^2)^{5/2}$. The small deviation near the top is due to a residual interference pattern in the images.

and $\beta \approx -0.3$ at $T = 0.6T_F$ [15]. Our value of β lies within the range of the theoretical predictions for a zero-temperature Fermi gas: -0.67 [12,24], -0.43 [24], and, in particular, $-0.56(1)$ from a recent quantum Monte Carlo calculation [25].

Beyond the Feshbach resonance, in the Fermi gas regime above 950 G, we observe an essentially constant normalized cloud size of $\zeta = 0.83 \pm 0.07$. In this regime, the interaction parameter $k_F a$ is calculated to vary between -2 (at 950 G) and -0.8 (at 1440 G), which allows us to estimate ζ to vary between 0.90 and 0.95 based on the interaction energy calculations in Ref. [12]. Our observed values are somewhat below this expectation, which requires further investigation.

In summary, we have demonstrated the smooth crossover from a molecular condensate of ^{6}Li dimers to an atomic Fermi gas. Since the conversion is adiabatic and reversible, the temperature of the Fermi gas can be estimated from the conservation of entropy [11]. Our high condensate fraction of $> 90\%$ suggests a very small entropy which in the Fermi gas limit corresponds to an extremely low temperature of $k_B T < 0.04 E_F$. In this scenario, superfluidity can be expected to extend from the molecular BEC regime into the strongly interacting Fermi gas regime above the Feshbach resonance where $k_F a \lesssim -0.8$. Our experiment thus opens up intriguing possibilities to study atomic Cooper pairing and superfluidity in resonant quantum gases.

We thank G.V. Shlyapnikov, W. Zwerger, and S. Stringari and his group for very useful discussions. We acknowledge support by the Austrian Science Fund (FWF) within SFB 15 (project part 15) and by the European Union in the frame of the Cold Molecules TMR Network under Contract No. HPRN-CT-2002-00290. C. C. thanks the FWF for financial support.

[1] S. Jochim *et al.*, Science **302**, 2101 (2003); published online 13 November 2003 (www.sciencemag.org/cgi/content/abstract/1093280v1).
[2] M. Greiner, C. A. Regal, and D. S. Jin, Nature (London) **426**, 537 (2003).
[3] M. Zwierlein *et al.*, Phys. Rev. Lett. **91**, 250401 (2003).
[4] T. Bourdel *et al.*, cond-mat/0403091.
[5] A. J. Leggett, in *Modern Trends in the Theory of Condensed Matter*, edited by A. Pekalski and R. Przystawa (Springer-Verlag, Berlin, 1980); P. Nozières and S. Schmitt-Rink, J. Low Temp. Phys. **59**, 195 (1985); M. Drechsler and W. Zwerger, Ann. Phys. (Leipzig) **1**, 15 (1992); E. Timmermans, K. Furuya, P.W. Milonni, and A. K. Kerman, Phys. Lett. A **285**, 228 (2001); M. Holland, S. J. M. F. Kokkelmans, M. L. Chiofalo, and R. Walser, Phys. Rev. Lett. **87**, 120406 (2001); Y. Ohashi and A. Griffin, Phys. Rev. Lett. **89**, 130402 (2002); R. Combescot, Phys. Rev. Lett. **91**, 120401 (2003); A. Perali, P. Pieri, and G. C. Strinati, Phys. Rev. A **68**, 031601(R) (2003); J. Stajic *et al.*, cond-mat/0309329.
[6] E. Tiesinga, B. J. Verhaar, and H. T. C. Stoof, Phys. Rev. A **47**, 4114 (1993); S. Inouye *et al.*, Nature (London) **392**, 151 (1998).
[7] C. A. Regal, C. Ticknor, J. L. Bohn, and D. S. Jin, Nature (London) **424**, 47 (2003).
[8] J. Cubizolles *et al.*, Phys. Rev. Lett. **91**, 240401 (2003).
[9] K. E. Strecker, G. B. Partridge, and R. G. Hulet, Phys. Rev. Lett. **91**, 080406 (2003).
[10] S. Jochim *et al.*, Phys. Rev. Lett. **91**, 240402 (2003).
[11] L. D. Carr, G.V. Shlyapnikov, and Y. Castin, cond-mat/0308306.
[12] H. Heiselberg, Phys. Rev. A **63**, 043606 (2001).
[13] T.-L. Ho, Phys. Rev. Lett. **92**, 090402 (2004).
[14] K. M. O'Hara *et al.*, Science **298**, 2179 (2002); M. E. Gehm *et al.*, Phys. Rev. A **68**, 011401 (2003).
[15] T. Bourdel *et al.*, Phys. Rev. Lett. **91**, 020402 (2003).
[16] M. Houbiers, H. T. C. Stoof, W. McAlexander, and R. Hulet, Phys. Rev. A **57**, R1497 (1998).
[17] K. M. O'Hara *et al.*, Phys. Rev. A **66**, 041401(R) (2002).
[18] The resonance position is uncertain within a few 10 G.
[19] C. Chin and R. Grimm, cond-mat/0309078.
[20] D. S. Petrov, C. Salomon, and G.V. Shlyapnikov, cond-mat/0309010.
[21] S. Giorgini, L. P. Pitaevskii, and S. Stringari, Phys. Rev. A **54**, R4633 (1996).
[22] S. Stringari, Phys. Rev. Lett. **77**, 2360 (1996).
[23] We fit the density profiles with the function $\rho(z) = \rho_0(1 - z^2/z_{\mathrm{r}}^2)^{\alpha}$, where ρ_0, z_r, and $2 \leq \alpha \leq 2.5$ are free parameters. This function interpolates between the density profile of a pure BEC in the Thomas-Fermi limit with $\alpha = 2$ and a zero-temperature noninteracting or strongly interacting Fermi gas with $\alpha = 2.5$. The rms cloud size z_{rms} is obtained from z_{r} and α by $z_{\mathrm{rms}} = z_{\mathrm{r}}/\sqrt{3 + 2\alpha}$.
[24] G. A. Baker, Phys. Rev. C **60**, 054311 (1999).
[25] J. Carlson, S.-Y. Chang, V. R. Pandharipande, and K. E. Schmidt, Phys. Rev. Lett. **91**, 050401 (2003).

Appendix G

Collective Excitations of a Degenerate Gas at the BEC-BCS Crossover

Collective Excitations of a Degenerate Gas at the BEC-BCS Crossover

M. Bartenstein,[1] A. Altmeyer,[1] S. Riedl,[1] S. Jochim,[1] C. Chin,[1] J. Hecker Denschlag,[1] and R. Grimm[1,2]
[1]*Institut für Experimentalphysik, Universität Innsbruck, Technikerstraße 25, 6020 Innsbruck, Austria*
[2]*Institut für Quantenoptik und Quanteninformation, Österreichische Akademie der Wissenschaften, 6020 Innsbruck, Austria*
(Received 29 March 2004; published 19 May 2004)

We study collective excitation modes of a fermionic gas of ^{6}Li atoms in the BEC-BCS crossover regime. While measurements of the axial compression mode in the cigar-shaped trap close to a Feshbach resonance confirm theoretical expectations, the radial compression mode shows surprising features. In the strongly interacting molecular BEC regime, we observe a negative frequency shift with increasing coupling strength. In the regime of a strongly interacting Fermi gas, an abrupt change in the collective excitation frequency occurs, which may be a signature for a transition from a superfluid to a collisionless phase.

DOI: 10.1103/PhysRevLett.92.203201 PACS numbers: 34.50.–s, 05.30.Fk, 32.80.Pj, 39.25.+k

The crossover from a Bose-Einstein condensate (BEC) to a Bardeen-Cooper-Schrieffer (BCS) superfluid has for decades attracted considerable attention in many-body theory [1]. Bose-Einstein condensates of molecules formed by fermionic atoms of ^{6}Li and ^{40}K [2–5] provide a unique system to experimentally explore this BEC-BCS crossover. In such ultracold gases magnetically tuned scattering resonances, known as Feshbach resonances, allow one to control and vary the interaction strength over a very broad range. Recent experiments have entered the crossover regime and yield results on the interaction strength by measuring the cloud size [6] and expansion energy [5]. Moreover, two experiments [7,8] have demonstrated the condensed nature of fermionic atom pairs in the crossover regime.

Important questions are related to superfluidity in the crossover regime [9]. When a molecular BEC is converted into an ultracold Fermi gas [6], one can expect ultralow temperatures and superfluidity to extend far into the Fermi gas regime [10]. Detection tools to probe superfluidity in this regime are therefore requested. The investigation of collective excitation modes [11] is well established as a powerful method to gain insight into the physical behavior of ultracold quantum gases in different regimes of Bose [12] and Fermi gases [13]. A recent paper [14] points out an interesting dependence of the collective frequencies in the BEC-BCS crossover of a superfluid Fermi gas. Superfluidity implies a hydrodynamic behavior which can cause substantial changes in the excitation spectrum and in general very low damping rates. However, in the crossover regime the strong interaction between the particles also results in hydrodynamic behavior in the normal, nonsuperfluid phase. Therefore the interpretation of collective modes in the BEC-BCS crossover in terms of superfluidity is not straightforward and needs careful investigation to identify the different regimes.

In this Letter, we report on measurements of fundamental collective excitation modes in the BEC-BCS crossover for various coupling strengths in the low-temperature limit. In Ref. [2], we have already presented a first measurement of the collective excitation of a molecular BEC in the limit of strong coupling. As described previously [2,6], we work with a spin mixture of ^{6}Li atoms in the two lowest internal states. For exploring different interaction regimes, we use a broad Feshbach resonance, the position of which we determined to 837(5) G [15]. The different interaction regimes can be characterized by the coupling parameter $1/(k_F a)$, where a represents the atom-atom scattering length and k_F is the Fermi wave number. Well below the Feshbach resonance ($B < 700$ G), we can realize the molecular BEC regime with $1/(k_F a) \gg 1$. On resonance, we obtain the unitarity-limited regime of a universal fermionic quantum gas with $1/(k_F a) = 0$ [16]. An interacting Fermi gas of atoms is realized beyond the resonance where $1/(k_F a) < 0$.

The starting point of our experiments is a cigar-shaped molecular BEC produced by evaporative cooling in an optical dipole trap in the same way as described in Ref. [6]. Radially the sample is confined by a 35-mW laser beam (wavelength 1030 nm) focused to a waist of 25 μm. The radial vibration frequency is $\omega_r \approx 2\pi \times 750$ Hz. The axial vibration frequency is $\omega_z = 2\pi \times (601 B/\mathrm{kG} + 11)^{1/2}$ Hz, where the predominant contribution stems from magnetic confinement caused by the curvature of the Feshbach tuning field B, and a very small additional contribution arises from the weak axial optical trapping force.

For exploring collective excitations in the BEC-BCS crossover regime, we ramp the magnetic field from the evaporation field of 764 G, where the molecular BEC is formed, to fields between 676 and 1250 G within 1 s. In previous work [6], we have shown that the conversion to an atomic Fermi gas proceeds in an adiabatic and reversible way, i.e., without increase of entropy. From the condensate fraction in the BEC limit, for which we measure more than 90% [6], we can give upper bounds for the temperature in both the BEC limit and the noninteracting Fermi gas limit of $T < 0.46 T_{\mathrm{BEC}}$ and $T < 0.03 T_F$ [10], respectively. Here T_{BEC} (T_F) denotes the

critical temperature (Fermi temperature). With a total number of atoms $N \approx 4 \times 10^5$ (free atoms and atoms bound to molecules) and a geometrically averaged trap frequency at 837 G of $\bar{\omega} = (\omega_r^2 \omega_z)^{1/3} \approx 2\pi \times 230\,\mathrm{Hz}$, we calculate a Fermi energy $E_F = \hbar^2 k_F^2/2m = \hbar\bar{\omega}(3N)^{1/3} = k_B \times 1.2\ \mu\mathrm{K}$ for a noninteracting cloud, where m is the mass of an atom and k_B is Boltzmann's constant.

To excite the *axial* compression mode at a given magnetic field, we increase the optical confinement in a 10-ms time interval by a factor of 1.5. The laser power is varied slow enough for the radial motion to follow adiabatically, but fast enough to induce axial oscillations. The relative amplitude of the resulting axial oscillation is kept small, typically $\sim$10%. We observe the oscillation by *in situ* imaging of the cloud [6] after a variable hold time t at constant trap parameters. To determine the collective oscillation frequency Ω_z and the damping rate Γ_z, we fit a damped harmonic oscillation $z(t) = z_0 + A_z \exp(-\Gamma_z t) \times \sin(\Omega_z t + \phi_z)$ to the observed time evolution of the cloud size, where z_0, A_z, and ϕ_z are additional fit parameters.

The measured oscillation frequencies and damping rates are shown in Fig. 1. The data are normalized to the axial trap frequency ω_z, as determined by excitation of the axial sloshing mode. We point out that the axial confinement is harmonic because of the dominant magnetic trapping, and we can measure ω_z with a 10^{-3} precision. In the BEC limit, the measured collective frequencies are in agreement with the expected $\Omega_z/\omega_z = \sqrt{5/2} = 1.581$ [11,17]. With increasing magnetic field, we observe a decrease in the collective excitation frequency until a minimum is reached at about 900 G, i.e., in the regime of a strongly interacting Fermi gas where $1/(k_F a) \approx -0.5$. With further increasing magnetic field and decreasing interaction strength, we then observe a gradual increase of the collective frequency toward $\Omega_z/\omega_z = 2$. The latter value is expected for a collisionless degenerate Fermi gas, where the elastic collision rate is strongly reduced by Pauli blocking. Because of the large damping rates in the transition regime between hydrodynamic and collisionless behavior, the excitation frequencies cannot be determined with high accuracy. The observed axial damping is consistent with a gradual transition between these two regimes [18].

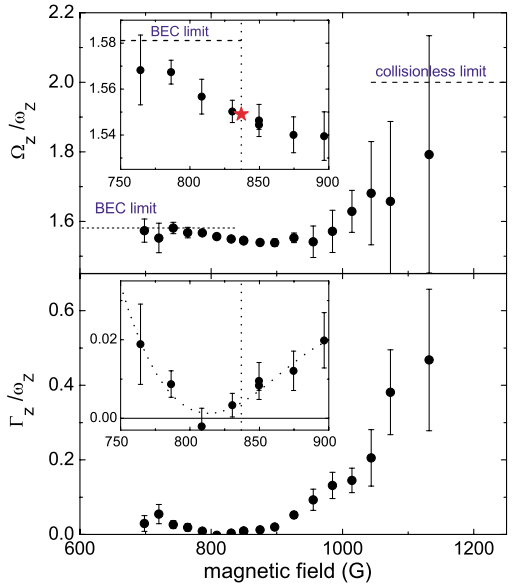

FIG. 1 (color online). Measured frequency Ω_z and damping rate Γ_z of the axial compression mode, normalized to the trap frequency ω_z. In the upper graph, the dashed lines indicate the BEC limit of $\Omega_z/\omega_z = \sqrt{5/2}$ and the collisionless Fermi gas limit with $\Omega_z/\omega_z = 2$. The insets show the data in the resonance region. Here the vertical dotted line indicates the resonance position at 837(5) G. The star marks the theoretical prediction of $\Omega_z/\omega_z = \sqrt{12/5}$ in the unitarity limit. In the lower inset, the dotted line is a third-order polynomial fit to the data.

The insets of Fig. 1 show a zoom-in of the data for the resonance region between 750 and 900 G. The collective frequency that we measure on resonance exhibits the small 2% down-shift expected for the unitarity limit ($\Omega_z/\omega_z = \sqrt{12/5} = 1.549$) [14]. For the damping rate, we observe a clear minimum at a magnetic field of 815(10) G, which is close to the resonance position. It is interesting to note that this damping minimum coincides with the recent observation of a maximum fraction of condensed fermionic atom pairs in Ref. [18]. For the minimum damping rate, we obtain the very low value of $\Gamma_z/\omega_z \approx 0.0015$, which corresponds to a $1/e$ damping time of $\sim$5 s.

To excite the *radial* compression mode, we reduce the optical confinement for 50 μs, which is short compared with the radial oscillation period of 1.3 ms. In this short interval the cloud slightly expands radially, and then begins to oscillate when the trap is switched back to the initial laser power. The relative oscillation amplitude is $\sim$10%. To detect the radial oscillation, we turn off the trapping laser after various delay times t and measure the radial size $r(t)$ after 1.5 ms of expansion. The measured radial size $r(t)$ reflects the oscillating release energy. From the corresponding experimental data, we extract the excitation frequency Ω_r and damping Γ_r by fitting the radial cloud size to $r(t) = r_0 + A_r \exp(-\Gamma_r t) \sin(\Omega_r t + \phi_r)$, where r_0, A_r, and ϕ_r are additional fit parameters. Typical radial oscillation curves are shown in Fig. 2.

The magnetic-field dependence of the radial excitation frequency Ω_r and the damping rate Γ_r is shown in Fig. 3. Here we normalize the data to the trap frequency ω_r, which we obtain by measuring the radial sloshing mode at the given magnetic field [19]. This normalization suppresses anharmonicity effects in the measured compression mode frequency to below 3% [21]. For low magnetic fields, the measured frequency ratio approaches the BEC limit [11,22] ($\Omega_r/\omega_r = 2$). With increasing magnetic field, i.e., increasing interaction strength, we observe a large down-shift of the frequency. On resonance ($B =$ 837 G), we observe $\Omega_r/\omega_r = 1.62(2)$. Above resonance, i.e., with the gas entering the strongly interacting Fermi

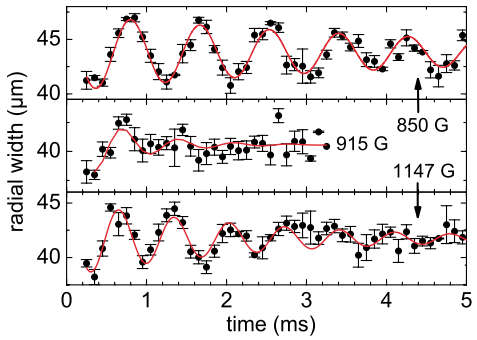

FIG. 2 (color online). Oscillations of the radial compression mode at different magnetic fields in the strongly interacting Fermi gas regime. The solid lines show fits by damped harmonic oscillations.

gas regime, the oscillation frequency further decreases until a maximum shift of almost 30% [$\Omega_r/\omega_r = 1.42(5)$] is reached at $B = 890$ G. With further increasing magnetic field, i.e., decreasing interaction strength, an abrupt change to $\Omega_r/\omega_r \approx 2$ is observed. For $B > 920$ G our data are consistent with a Fermi gas in the collisionless regime. The damping of the radial compression mode is small in the BEC limit and reaches a minimum close to the unitarity regime. At $B = 910$ G, where the abrupt change occurs, we observe very strong damping (see also middle trace in Fig. 2).

We have performed further experiments to check our data on the radial compression mode for systematic effects. We have repeated the measurements after recompressing the trap to 9 times higher trap laser power

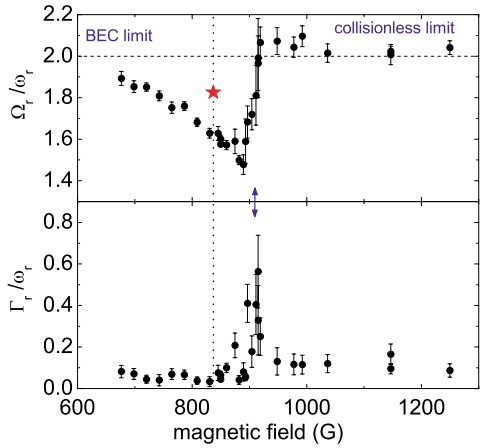

FIG. 3 (color online). Measured frequency Ω_r and damping rate Γ_r of the radial compression mode, normalized to the trap frequency (sloshing mode frequency) ω_r. In the upper graph, the dashed line indicates $\Omega_r/\omega_r = 2$, which corresponds to both the BEC limit and the collisionless Fermi gas limit. The vertical dotted line marks the resonance position at 837(5) G. The star indicates the theoretical expectation of $\Omega_r/\omega_r = \sqrt{10/3}$ in the unitarity limit. A striking change in the excitation frequency occurs at ~910 G (arrow) and is accompanied by anomalously strong damping.

($\omega_r \approx 2.4$ kHz). The corresponding data confirm all our observations in the shallower trap. In particular, the negative frequency shift and the sudden change in the collective frequency show up in essentially the same way. The recompressed trap also allows us to eliminate a small residual anharmonicity shift from our measurement of the collective frequency at 837 G, and we obtain $\Omega_r/\omega_r = 1.67(3)$ for the harmonic trap limit. We have also checked that the frequency of the compression mode in the resonance region does not depend on the way we prepare the ultracold gas. Direct evaporation at a fixed magnetic field, without starting from a molecular BEC, leads to the same collective frequency. Preliminary measurements at higher temperatures, however, show a trend towards smaller frequency shifts in the radial compression mode and to smoother changes of the collective frequency.

Our measurements on the radial compression mode show *three surprises*. The corresponding features, which we discuss in the following, cannot be explained on the basis of available theoretical models and suggest new physics in the BEC-BCS crossover regime.

Surprise one.—For a strongly interacting BEC, Ref. [23] has predicted up-shifts of the collective frequencies with increasing coupling strength based on beyond mean-field theory corrections [24]. Applying these predictions to a molecular BEC in the crossover regime, the collective excitation frequencies should follow $\delta\Omega_i/\Omega_i = c_i\sqrt{n_m a_m^3}$ ($i = z, r$), where n_m is the peak molecular number density and $a_m = 0.6a$ [25] is the molecule-molecule scattering length. For our highly elongated trap geometry, the numerical factors are $c_r = 5c_z = 0.727$. In contrast to these expectations, we observe a strong frequency down-shift in the radial direction. Using the above formula to fit the first four data points, we obtain a negative coefficient of $c_r = -1.2(3)$. For the axial oscillation we obtain $c_z = -0.04(5)$. Note that a substantial down-shift in radial direction is observed even at the low magnetic field of 676 G where the molecular gas parameter is relatively small ($n_m a_m^3 = 0.001$). Apparently, the beyond mean-field theory of a BEC is not adequate to describe the transition from a molecular BEC to a strongly interacting gas in the BEC-BCS crossover.

Surprise two.—The universal character of the strongly interacting quantum gas on resonance suggests a simple equation of state for which one expects $\Omega_z/\omega_z = \sqrt{12/5} = 1.549$ and $\Omega_r/\omega_r = \sqrt{10/3} = 1.826$ for the collective excitation frequencies [14]. While our measurements confirm the predicted axial frequency, we obtain a different frequency in the radial direction of $\Omega_r/\omega_r = 1.67(3)$.

Surprise three.—The abrupt change of the excitation frequency and the large damping rate are not expected in a normal degenerate Fermi gas, where the collective excitation frequency is expected to vary smoothly from the hydrodynamic regime to the collisionless one. Furthermore, for the damping rate of the radial mode in the

transition regime, a maximum value of $\Gamma_r/\omega_r = 0.09$ is calculated in Ref. [18]. Our measured damping rate of $\Gamma_r/\omega_r \approx 0.5$ is clearly inconsistent with this prediction for the normal (nonsuperfluid) hydrodynamic regime. However, both the sudden change of the collective frequency and a strong damping are expected for a transition from the superfluid to the normal phase [26].

In conclusion, our experiments demonstrate that the collective modes of a degenerate gas in the BEC-BCS crossover region show a pronounced dependence on the coupling strength and thus provide valuable information on the physical behavior of the system. For the axial compression mode, the frequency shift observed in the unitarity limit confirms theoretical expectations. However, the radial compression mode reveals a surprising behavior. In the strongly interacting BEC regime, the observed frequency shifts have an opposite sign as compared to expectations from beyond mean-field theory and the frequency shift on resonance is even larger than expected. The most striking feature is an abrupt change of the radial collective frequency in the regime of a strongly attractive Fermi gas where $1/(k_F a) \approx -0.5$. The transition is accompanied by very strong damping. The observation supports an interpretation in terms of a transition from a hydrodynamic to a collisionless phase. A superfluid scenario for the hydrodynamic case seems plausible in view of current theories on resonance superfluidity [9] and the very low temperatures provided by the molecular BEC [10]. A definite answer, however, to the sensitive question of superfluidity requires further careful investigations, e.g., on the temperature dependence of the phase transition.

We warmly thank S. Stringari for stimulating this work and for many useful discussions. We also thank W. Zwerger and M. Baranov for very useful discussions. We acknowledge support by the Austrian Science Fund (FWF) within SFB 15 (project part 15) and by the European Union in the frame of the Cold Molecules TMR Network under Contract No. HPRN-CT-2002-00290. C. C. thanks the FWF for financial support.

Note added.—A recent paper by John Thomas' group [27] reports on measurements of the radial compression mode in the resonance region, which show much weaker frequency shifts than we observe. This apparent discrepancy needs further investigation.

[1] A. J. Leggett, in *Modern Trends in the Theory of Condensed Matter*, edited by A. Pekalski and R. Przystawa (Springer-Verlag, Berlin, 1980); P. Nozières and S. Schmitt-Rink, J. Low Temp. Phys. **59**, 195 (1985); E. Timmermans, K. Furuya, P.W. Milonni, and A. K. Kerman, Phys. Lett. A **285**, 228 (2001); J. N. Milstein, S. J. J. M. F. Kokkelmans, and M. J. Holland, Phys. Rev. A **66**, 043604 (2002); Y. Ohashi and A. Griffin, Phys. Rev. Lett. **89**, 130402 (2002); R. Combescot, Phys. Rev. Lett. **91**, 120401 (2003); A. Perali, P. Pieri, and G. C. Strinati, Phys. Rev. A **68**, 031601(R) (2003); J. Stajic *et al.*, cond-mat/0309329.
[2] S. Jochim *et al.*, Science **302**, 2101 (2003).
[3] M. Greiner, C. A. Regal, and D. S. Jin, Nature (London) **426**, 537 (2003).
[4] M.W. Zwierlein *et al.*, Phys. Rev. Lett. **91**, 250401 (2003).
[5] T. Bourdel *et al.*, cond-mat/0403091.
[6] M. Bartenstein *et al.*, Phys. Rev. Lett. **92**, 120401 (2004).
[7] C. A. Regal, M. Greiner, and D. S. Jin, Phys. Rev. Lett. **92**, 040403 (2004).
[8] M.W. Zwierlein *et al.*, Phys. Rev. Lett. **92**, 120403 (2004).
[9] M. Holland *et al.*, Phys. Rev. Lett. **87**, 120406 (2001).
[10] L. D. Carr, G.V. Shlyapnikov, and Y. Castin, Phys. Rev. Lett. **92**, 150404 (2004).
[11] S. Stringari, Phys. Rev. Lett. **77**, 2360 (1996).
[12] L. Pitaevski and S. Stringari, *Bose-Einstein Condensation* (Clarendon, Oxford, 2003), and references therein.
[13] G. M. Bruun and C.W. Clark, Phys. Rev. Lett. **83**, 5415 (1999); G. M. Bruun and B. R. Mottelson, Phys. Rev. Lett. **87**, 270403 (2001); A. Minguzzi and M. P. Tosi, Phys. Rev. A **63**, 023609 (2001).
[14] S. Stringari, Europhys. Lett. **65**, 749 (2004).
[15] We determined the resonance position by measuring the molecular binding energy using radio-frequency spectroscopy as introduced in C. A. Regal, C. Ticknor, J. L. Bohn, and D. S. Jin, Nature (London) **424**, 47 (2003).
[16] H. Heiselberg, Phys. Rev. A **63**, 043606 (2001).
[17] M.-O. Mewes *et al.*, Phys. Rev. Lett. **77**, 988 (1996).
[18] L. Vichi, J. Low Temp. Phys. **121**, 177 (2000).
[19] We excite the radial sloshing mode by pulsed application of a vertical magnetic gradient. With increasing magnetic field and, thus, increasing radial cloud size, the anharmonicity of the Gaussian-shaped radial potential leads to a decrease of the sloshing mode frequency. For $\omega_r/2\pi$, we observe a corresponding decrease from 765 Hz at 676 G to 710 Hz at magnetic fields above 1.2 kG; at 837 G we obtain 740 Hz. Our measurements of the sloshing mode frequency agree well with an expected scaling of the lowest-order anharmonicity correction with the squared cloud size [20].
[20] S. Stringari (private communication).
[21] The anharmonicity corrections to frequencies of both the compression mode (Ω_r) and the sloshing mode (ω_r) scale in the same way with the increasing cloud size with a slightly larger prefactor for the compression mode [20]. Our normalization Ω_r/ω_r reduces the anharmonicity effect by typically a factor of 5.
[22] F. Chevy *et al.*, Phys. Rev. Lett. **88**, 250402 (2002).
[23] L. Pitaevski and S. Stringari, Phys. Rev. Lett. **81**, 4541 (1998).
[24] T. D. Lee, K.W. Huang, and C. N. Yang, Phys. Rev. **106**, 1135 (1957).
[25] D. S. Petrov, C. Salomon, and G.V. Shlyapnikov, cond-mat/0309010.
[26] M. A. Baranov and D. S. Petrov, Phys. Rev. A **62**, 041601 (2000).
[27] J. Kinast *et al.*, Phys. Rev. Lett. **92**, 150402 (2004).

Appendix H

Observation of the Pairing Gap in a Strongly Interacting Fermi Gas

16. A. vanOtterlo *et al.*, *Phys. Rev. B* **52**, 16176 (1995).
17. G. Schmid, S. Todo, M. Troyer, A. Dorneich, *Phys. Rev. Lett.* **88**, 167208 (2002).
18. A. Görlitz, *Phys. Rev. Lett.* **87**, 130402 (2001).
19. M. Greiner, I. Bloch, O. Mandel, T. W. Hänsch, T. Esslinger, *Appl. Phys. B* **73**, 769 (2001).
20. M. T. DePue, C. McCormick, S. L. Winoto, S. Oliver, D. S. Weiss, *Phys. Rev. Lett.* **82**, 2262 (1999).
21. B. L. Tolra *et al.*, *Phys. Rev. Lett.* **92**, 190401 (2004).
22. H. Moritz, T. Söferle, M. Köhl, T. Esslinger, *Phys. Rev. Lett.* **91**, 250402 (2003).
23. T. Söferle, H. Moritz, C. Schori, M. Köhl, T. Esslinger, *Phys. Rev. Lett.* **92**, 130403 (2004).
24. B. Paredes *et al.*, *Nature* **429**, 277 (2004).
25. V. Dunjko, V. Lorent, M. Olshanii, *Phys. Rev. Lett.* **86**, 5413 (2001).
26. M. Greiner, O. Mandel, T. Esslinger, T. W. Hänsch, I. Bloch, *Nature* **415**, 39 (2002).
27. T. Kinoshita, T. Wenger, D. S. Weiss, in preparation.
28. D. J. Han, M. T. DePue, D. S. Weiss, *Phys. Rev. A* **63**, 023405 (2001).
29. M. T. DePue, S. L. Winoto, D. J. Han, D. S. Weiss, *Opt. Commun.* **180**, 73 (2000).
30. S. L. Winoto, M. T. DePue, N. E. Bramall, D. S. Weiss, *Phys. Rev A*, **59**, R19 (1999).
31. We thank M. Olshanii, K. Gibble, and J. Banavar for useful discussions and V. Dunjko for providing us with the exact 1D Bose gas theory curves. This work was supported by the NSF grant no. PHY-0137477.

Supporting Online Material
www.sciencemag.org/cgi/content/full/1100700/DC1
SOM Text
Table S1

25 May 2004; accepted 20 July 2004
Published online 29 July 2004;
10.1126/science.1100700
Include this information when citing this paper.

Observation of the Pairing Gap in a Strongly Interacting Fermi Gas

C. Chin,[1] M. Bartenstein,[1] A. Altmeyer,[1] S. Riedl,[1] S. Jochim,[1] J. Hecker Denschlag,[1] R. Grimm[1,2]*

We studied fermionic pairing in an ultracold two-component gas of ^{6}Li atoms by observing an energy gap in the radio-frequency excitation spectra. With control of the two-body interactions through a Feshbach resonance, we demonstrated the dependence of the pairing gap on coupling strength, temperature, and Fermi energy. The appearance of an energy gap with moderate evaporative cooling suggests that our full evaporation brought the strongly interacting system deep into a superfluid state.

The spectroscopic observation of a pairing gap in the 1950s marked an important experimental breakthrough in research on superconductivity (*1*). The gap measurements provided a key to investigating the paired nature of the particles responsible for the frictionless current in metals at very low temperatures. The ground-breaking Bardeen-Cooper-Schrieffer (BCS) theory, developed at about the same time, showed that two electrons in the degenerate Fermi sea can be coupled by an effectively attractive interaction and will form a delocalized, composite particle with bosonic character. BCS theory predicted that the gap in the low-temperature limit is proportional to the critical temperature T_c for the phase transition, in agreement with the experimental measurements. In general, the physics of superconductivity and superfluidity go far beyond the weak-coupling limit of BCS theory. In the limit of strong coupling, paired fermions form localized bosons, and the system can undergo Bose-Einstein condensation (BEC). The BCS limit and the BEC limit are connected by a smooth BCS-BEC crossover, which has been a subject of great theoretical interest for more than three decades (*2*–*5*). The formation of pairs generally represents a key ingredient of superfluidity in fermionic systems, and the gap energy is a central quantity to characterize the pairing regime.

The rapid progress in experiments with ultracold degenerate Fermi gases (*6*) has opened up a unique testing ground to study phenomena related to pairing and superfluidity at densities typically a billion times below the ones in usual condensed-matter systems. In cold-atom experiments, magnetically tuned scattering resonances (Feshbach resonances) serve as a powerful tool to control the two-body coupling strength in the gas (*7*). On the basis of such a resonance, a strongly interacting degenerate Fermi gas was recently realized (*8*). A major breakthrough then followed, with the creation of Bose-Einstein condensates of molecular dimers composed of fermionic atoms (*9*–*13*), which corresponds to the realization of a BEC-type superfluid in the strong coupling limit. By variation of the coupling strength, subsequent experiments (*12*, *14*–*18*) began to explore the crossover to a BCS-type system. This BEC-BCS crossover is closely linked to the predicted "resonance superfluidity" (*19*–*22*) and a "universal" behavior of a Fermi gas with resonant interactions (*23*, *24*). The observation of the condensation of atom pairs (*15*, *16*) and measurements of collective oscillations (*17*, *18*) support the expected superfluidity at presently attainable temperatures in Fermi gases with resonant interactions.

We prepared our ultracold gas of fermionic ^{6}Li atoms in a balanced spin-mixture of the two lowest sub-states $|1\rangle$ and $|2\rangle$ of the electronic $1s^2 2s$ ground state, employing methods of laser cooling and trapping and subsequent evaporative cooling (*9*). A magnetic field B in the range between 650 to 950 G was applied for Feshbach tuning through a broad resonance centered at the field $B_0 \approx 830$ G. In this high-field range, the three lowest atomic levels form a triplet of states $|1\rangle$, $|2\rangle$, and $|3\rangle$, essentially differing by the orientation of the nuclear spin ($m_I = 1, 0, -1$, where m_I is the nuclear magnetic quantum number). In the resonance region with $B < B_0$, the s-wave scattering length a for collisions between atoms in states $|1\rangle$ and $|2\rangle$ is positive. Here, two-body physics supports a weakly bound molecular state with a binding energy $E_b = \hbar^2/(ma^2)$, where $\hbar$ is Planck's constant h divided by 2π and m is the atomic mass. Molecules formed in this state can undergo BEC (*9*–*13*). At $B = B_0$, the two-body interaction is resonant ($a \rightarrow \pm\infty$), corresponding to a vanishing binding energy of the molecular state. Beyond the resonance ($B > B_0$), the scattering length is negative ($a < 0$), which leads to an effective attraction. Here, two-body physics does not support a weakly bound molecular level, and pairing can only occur because of many-body effects.

Our experimental approach (*9*, *14*) facilitated preparation of the quantum gas in various regimes with controlled temperature, Fermi energy, and interaction strength. We performed evaporative cooling under conditions (*25*) in which an essentially pure molecular Bose-Einstein condensate containing $N = 4 \times 10^5$ paired atoms could be created as a starting point for the experiments. The final laser power of the evaporation ramp allowed us to vary the temperature T. The Fermi energy E_F (Fermi temperature $T_F = E_F/k_B$, with Boltzmann's constant k_B) was controlled by a recompression of the gas, which we performed by increasing the trap laser power after the cooling process (*25*). We then varied the interaction strength by slowly changing the magnetic field to the desired final value. The adiabatic changes applied to the gas after evaporative cooling proceeded with conserved entropy (*14*). Lacking a reliable method to determine the temperature T of a deeply degenerate, strongly interacting Fermi gas in a direct way, we characterized the system by the temperature T' measured after an isentropic conversion into the BEC limit (*25*). For

[1]Institut für Experimentalphysik, Universität Innsbruck, Technikerstraße 25, 6020 Innsbruck, Austria. [2]Institut für Quantenoptik und Quanteninformation, Österreichische Akademie der Wissenschaften, 6020 Innsbruck, Austria.

*To whom correspondence should be addressed. E-mail: rudolf.grimm@uibk.ac.at

a deeply degenerate Fermi gas, the true temperature T is substantially below our observable T' (*25*, *26*), but a general theory for this relation is not yet available.

Radio-frequency (RF) spectroscopy has been introduced as a powerful tool to study interaction effects in ultracold Fermi gases (*27*–*29*). Molecular binding energies have been measured for ^{40}K atoms (*29*), for which the potential of the method to observe fermionic pairing gap energies has also been pointed out. RF spectroscopy has been applied to ^{6}Li atoms to study interaction effects up to magnetic fields of 750 G (*28*). One important observation was the absence of mean-field shifts in the strongly interacting regime. This effect can be attributed to the fact that, in the relevant magnetic-field range, all s-wave scattering processes between ^{6}Li atoms in the states $|1\rangle$, $|2\rangle$, and $|3\rangle$ are simultaneously unitarity-limited. This property of ^{6}Li is very favorable for RF spectroscopy because it suppresses shifts and broadening by mean-field effects.

We drove RF transitions from state $|2\rangle$ to the empty state $|3\rangle$ at ~80 MHz and monitored the loss of atoms in state $|2\rangle$ after weak excitation by a 1-s RF pulse, using state-selective absorption imaging (*14*). Our experiment was optimized to obtain a resolution of ~100 Hz, corresponding to an intrinsic sensitivity to interaction effects on the scale of ~5 nK, which is more than two orders of magnitude below the typical Fermi temperatures.

We recorded RF spectra for different degrees of cooling and in various coupling regimes (Fig. 1). We realized the molecular regime at $B = 720$ G ($a = +120$ nm). For the resonance region, we examined two different magnetic fields, because the precise resonance location B_0 is not exactly known. Our two values $B = 822$ G (*16*) and 837 G (*13*, *18*) may be considered as lower and upper bounds for B_0. We also studied the regime beyond the resonance with a large negative scattering length at $B = 875$ G ($a \approx -600$ nm). Spectra taken in a "hot" thermal sample at $T \approx 6T_F$ (where $T_F = 15$ μK) show the narrow atomic $|2\rangle \rightarrow |3\rangle$ transition line (Fig. 1, top) and serve as a frequency reference. We present our spectra as a function of the RF offset with respect to the bare atomic transition frequency.

Spectral signatures of pairing have been theoretically considered (*30*–*34*). A clear signature of the pairing process is the emergence of a double-peak structure in the spectral response as a result of the coexistence of unpaired and paired atoms. The pair-related peak is located at a higher frequency than the unpaired-atoms signal, because energy is required for pair breaking. For understanding of the spectra, both the homogeneous line shape of the pair signal (*31*, *33*) and the inhomogeneous line broadening due to the density distribution in the harmonic trap need to be taken into account (*34*). As an effect of inhomogeneity, fermionic pairing due to many-body effects takes place predominantly in the central high-density region of the trap, and unpaired atoms mostly populate the outer region of the trap where the density is low (*34*–*36*). The spectral component corresponding to the pairs thus shows a large inhomogeneous broadening in addition to the homogeneous width of the pair-breaking signal. For the unpaired atoms, the homogeneous line is narrow and the effects of inhomogeneity and mean-field shifts are negligible. These arguments explain why the RF spectra in general show a relatively sharp peak for the unpaired atoms together with a broader peak attributed to the pairs.

We observed clear double-peak structures already at $T'/T_F = 0.5$, which we obtained with moderate evaporative cooling down to a laser power of $P = 200$ mW (Fig. 1, middle, $T_F = 3.4$ μK). In the molecular regime $B = 720$ G, the sharp atomic peak was well separated from the broad dissociation signal (*29*), which showed a molecular binding energy of $E_b = h \times 130$ kHz $= k_B \times 6.2$ μK. For $B \rightarrow B_0$, the peaks began to overlap. In the resonance region [822 G and 837 G (Fig. 1)], we still observed a relatively narrow atomic peak at the original position together with a pair signal. For magnetic fields beyond the resonance, we could resolve the double-peak structure for fields up to ~900 G.

For $T'/T_F < 0.2$, realized with a deep evaporative cooling ramp down to an optical trap power of $P = 3.8$ mW, we observed the disappearance of the narrow atomic peak in the RF spectra (Fig. 1, bottom, $T_F = 1.2$ μK). This shows that essentially all atoms were paired. In the BEC limit (720 G), the dissociation line shape is identical to the one observed in the trap at higher temperature and Fermi energy. Here the localized pairs are molecules with a size much smaller than the mean interparticle spacing, and the dissociation signal is independent of the density. In the resonance region [822 G and 837 G (Fig. 1)], the pairing signal shows a clear dependence on density (Fermi energy), which becomes even more pronounced beyond the resonance (875 G). We attribute this to the fact that the size of the pairs becomes comparable to or larger than the interparticle spacing. In addition, the narrow width of the pair signal in this regime (Fig. 1, bottom, $B = 875$ G) indicates a pair localization in momentum space to well below the Fermi momentum $\hbar k_F = \sqrt{2mE_F}$ and thus a pair size exceeding the interparticle spacing.

To quantitatively investigate the crossover from the two-body molecular regime to the fermionic many-body regime, we measured the pairing energy in a range between 720 and 905 G. The measurements were performed after deep evaporative cooling ($T'/T_F < 0.2$) for two different Fermi temperatures, $T_F = 1.2$ μK and $T_F = 3.6$ μK (Fig. 2). As an effective pairing gap, we defined $\Delta\nu$ as the frequency difference between the pair-signal maximum and the bare atomic resonance. In the BEC limit, the effec-

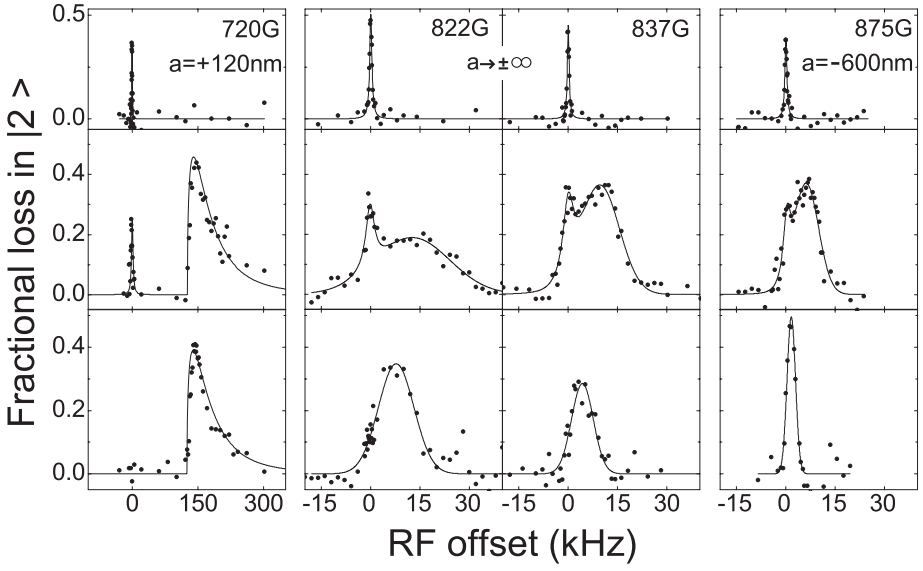

Fig. 1. RF spectra for various magnetic fields and different degrees of evaporative cooling. The RF offset ($k_B \times 1$ μK $\cong h \times 20.8$ kHz) is given relative to the atomic transition $|2\rangle \rightarrow |3\rangle$. The molecular limit is realized for $B = 720$ G (first column). The resonance regime is studied for $B = 822$ G and $B = 837$ G (second and third columns). The data at 875 G (fourth column) explore the crossover on the BCS side. Top row, signals of unpaired atoms at $T' \approx 6T_F$ ($T_F = 15$ μK); middle row, signals for a mixture of unpaired and paired atoms at $T' = 0.5T_F$ ($T_F = 3.4$ μK); bottom row, signals for paired atoms at $T' < 0.2T_F$ ($T_F = 1.2$ μK). The true temperature T of the atomic Fermi gas is below the temperature T', which we measured in the BEC limit. The solid lines are introduced to guide the eye.

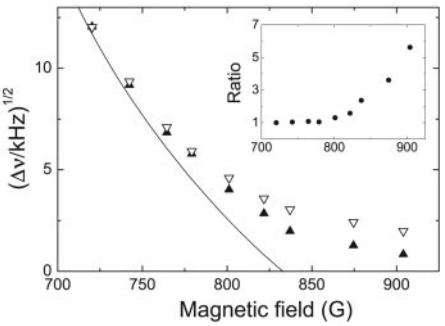

Fig. 2. Measurements of the effective pairing gap $\Delta\nu$ as a function of the magnetic field B for deep evaporative cooling and two different Fermi temperatures, T_F = 1.2 μK (solid symbols) and 3.6 μK (open symbols). The solid line shows $\Delta\nu$ for the low-density limit, where it is essentially given by the molecular binding energy (*25*). Inset: The ratio of the effective pairing gaps measured at the two different Fermi energies.

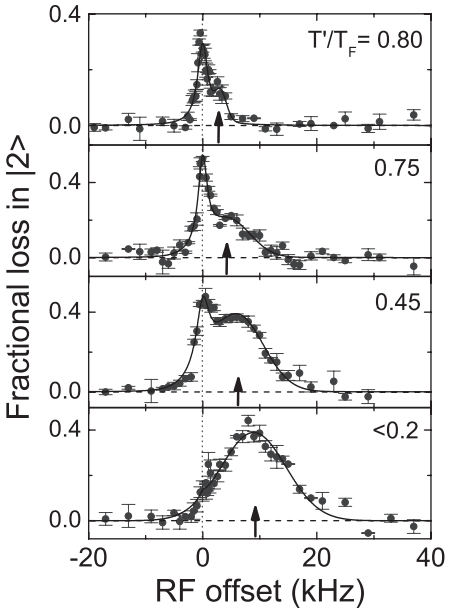

Fig. 3. RF spectra measured at B = 837 G and T_F = 2.5 μK for different temperatures T' adjusted by controlled heating. The solid lines are fits to guide the eye, using a Lorentzian curve for the atom peak and a Gaussian curve for the pair signal. The vertical dotted line marks the atomic transition, and the arrows indicate the effective pairing gap $\Delta\nu$.

tive pairing gap $\Delta\nu$ simply reflects the molecular binding energy E_b (Fig. 2, solid line) (*25*). With an increasing magnetic field, in the BEC-BCS crossover, $\Delta\nu$ shows an increasing deviation from this low-density molecular limit and smoothly evolves into a density-dependent many-body regime where $h\Delta\nu < E_F$.

A comparison of the pairing energies at the two different Fermi energies (Fig. 2, inset) provides further insight into the nature of the pairs. In the BEC limit, $\Delta\nu$ is solely determined by E_b and thus does not depend on E_F. In the universal regime on resonance, E_F is the only energy scale, and we indeed observed the effective pairing gap $\Delta\nu$ to increase linearly with the Fermi energy. We found a corresponding relation $h\Delta\nu \approx 0.2\ E_F$. Beyond the resonance, where the system is expected to change from a resonant to a BCS-type behavior, $\Delta\nu$ was found to depend more strongly on the Fermi energy and the observed gap ratio further increased. We interpret this in terms of the increasing BCS character of pairing, for which an exponential dependence $h\Delta\nu/E_F \propto \exp(-\pi/2k_F|a|)$ is expected.

In a further series of measurements (Fig. 3), we applied a controlled heating method to study the temperature dependence of the gap in a way that allowed us to keep all other parameters constant. After production of a pure molecular Bose-Einstein condensate ($T' < 0.2T_F$) in the usual way, we adiabatically changed the conditions to B = 837 G and T_F = 1.2 μK. We then increased the trap laser power by a factor of nine (T_F increased to 2.5 μK), using exponential ramps of different durations. For fast ramps, this recompression was nonadiabatic and increased the entropy. By variation of the ramp time, we explored a range from our lowest temperatures up to $T'/T_F = 0.8$. The emergence of the gap with decreasing temperature is clearly visible in the RF spectra (Fig. 3). The marked increase of $\Delta\nu$ for decreasing temperature is in good agreement with theoretical expectations for the pairing gap energy (*5*).

The conditions of our experiment were theoretically analyzed for the case of resonant two-body interaction (*34*). The calculated RF spectra are in agreement with our experimental results and demonstrate how a double-peak structure emerges as the gas is cooled below $T/T_F \approx 0.5$ and how the atomic peak disappears with further decreasing temperature. In particular, the work clarifies the role of the "pseudo-gap" regime (*5*, *22*), in which pairs are formed before superfluidity is reached. According to the calculated spectra, the atomic peak disappears at temperatures well below the critical temperature for the phase-transition to a superfluid. A recent theoretical study of the BCS-BEC crossover at finite temperature (*36*) predicted the phase-transition to a superfluid to occur at a temperature that on resonance is only ~30% below the point where pair formation sets in.

We have observed fermionic pairing already after moderate evaporative cooling. With much deeper cooling applied, the unpaired atom signal disappeared from our spectra. This observation shows that pairing takes place even in the outer region of the trapped gas where the density and the local Fermi energy are low. Our results thus strongly suggest that a resonance superfluid is formed in the central region of the trap (*34*). Together with the observations of resonance condensation of fermionic pairs (*15*, *16*) and weak damping of collective excitations (*17*, *18*), our observation of the pairing gap provides a strong case for superfluidity in experiments on resonantly interacting Fermi gases.

References and Notes

1. M. Tinkham, *Introduction to Superconductivity* (McGraw-Hill, New York, ed. 2, 1996).
2. D. M. Eagles, *Phys. Rev.* **186**, 456 (1969).
3. A. J. Leggett, in *Modern Trends in the Theory of Condensed Matter*, A. Pekalski, R. Przystawa, Eds. (Springer-Verlag, Berlin, 1980), pp. 13–27.
4. P. Nozières, S. Schmitt-Rink, *J. Low Temp. Phys.* **59**, 195 (1985).
5. Q. Chen, J. Stajic, S. Tan, K. Levin, in preparation (available at http://arxiv.org/abs/cond-mat/0404274).
6. A. Cho, *Science* **301**, 750 (2003).
7. S. Inouye *et al.*, *Nature* **392**, 151 (1998).
8. K. M. O'Hara, S. L. Hemmer, M. E. Gehm, S. R. Granade, J. E. Thomas, *Science* **298**, 2179 (2002); published online 7 Nov 2002 (10.1126/science.1079107).
9. S. Jochim *et al.*, *Science* **302**, 2101 (2003); published online 13 November 2003 (10.1126/science.1093280).
10. M. Greiner, C. A. Regal, D. S. Jin, *Nature* **426**, 537 (2003).
11. M. W. Zwierlein *et al.*, *Phys. Rev. Lett.* **91**, 250401 (2003).
12. T. Bourdel *et al.*, *Phys. Rev. Lett.* **93**, 050401 (2004).
13. R. Hulet, paper presented at the Kauli Institute for Theoretical Physics Conference on Quantum Gases, Santa Barbara, CA, 10 to 14 May 2004.
14. M. Bartenstein *et al.*, *Phys. Rev. Lett.* **92**, 120401 (2004).
15. C. A. Regal, M. Greiner, D. S. Jin, *Phys. Rev. Lett.* **92**, 040403 (2004).
16. M. W. Zwierlein *et al.*, *Phys. Rev. Lett.* **92**, 120403 (2004).
17. J. Kinast, S. L. Hemmer, M. E. Gehm, A. Turlapov, J. E. Thomas, *Phys. Rev. Lett.* **92**, 150402 (2004).
18. M. Bartenstein *et al.*, *Phys. Rev. Lett.* **92**, 203201 (2004).
19. M. Holland, S. J. J. M. F. Kokkelmans, M. L. Chiofalo, R. Walser, *Phys. Rev. Lett.* **87**, 120406 (2001).
20. E. Timmermans, K. Furuya, P. W. Milonni, A. K. Kerman, *Phys. Lett. A* **285**, 228 (2001).
21. Y. Ohashi, A. Griffin, *Phys. Rev. Lett.* **89**, 130402 (2002).
22. J. Stajic *et al.*, *Phys. Rev. A.* **69**, 063610 (2004).
23. H. Heiselberg, *Phys. Rev. A.* **63**, 043606 (2001).
24. T.-L. Ho, *Phys. Rev. Lett.* **92**, 090402 (2004).
25. Materials and methods are available as supporting material on *Science* Online.
26. L. D. Carr, G. V. Shlyapnikov, Y. Castin, *Phys. Rev. Lett.* **92**, 150404 (2004).
27. C. Regal, D. Jin, *Phys. Rev. Lett.* **90**, 230404 (2003).
28. S. Gupta *et al.*, *Science* **300**, 1723 (2003); published online 8 May 2003 (10.1126/science.1085335).
29. C. A. Regal, C. Ticknor, J. L. Bohn, D. S. Jin, *Nature* **424**, 47 (2003).
30. P. Törmä, P. Zoller, *Phys. Rev. Lett.* **85**, 487 (2000).
31. J. Kinnunen, M. Rodriguez, P. Törmä, *Phys. Rev. Lett.* **92**, 230403 (2004).
32. H. P. Büchler, P. Zoller, W. Zwerger, in preparation (available at http://arxiv.org/abs/cond-mat/0404116).
33. R. B. Diener, T.-L. Ho, in preparation (available at http://arxiv.org/abs/cond-mat/0405174).
34. J. Kinnunen, M. Rodriguez, P. Törmä, *Science* **305**, 1131; published online 22 July 2004 (10.1126/science.1100782).
35. A. Bulgac, in preparation (available at http://arxiv.org/abs/cond-mat/0309358).
36. A. Perali, P. Pieri, L. Pisani, G. C. Strinati, *Phys. Rev. Lett.* **92**, 220404 (2004).

37. We thank P. Törmä for a stimulating exchange of results and very useful discussions and W. Zwerger and H. P. Büchler for many stimulating discussions. Supported by the Austrian Science Fund (FWF) within spezial forschungsbereich 15 (project part 15) and by the European Union in the frame of the Cold Molecules Training and Mobility of Researchers Network under contract no. HPRN-CT-2002-00290. C.C. is a Lise-Meitner research fellow of the FWF.

Supporting Online Material
www.sciencemag.org/cgi/content/full/1100818/DC1
Materials and Methods
References and Notes

27 May 2004; accepted 13 July 2004
Published online 22 July 2004;
10.1126/science.1100818
Include this information when citing this paper.

Appendix I

Precise determination of ^{6}Li cold collision parameters by radio-frequency spectroscopy on weakly bound molecules

Precise determination of ^{6}Li cold collision parameters by radio-frequency spectroscopy on weakly bound molecules

M. Bartenstein[1], A. Altmeyer[1], S. Riedl[1], R. Geursen[1], S. Jochim[1], C. Chin[1], J. Hecker Denschlag[1], and R. Grimm[1,2]
[1]*Institut für Experimentalphysik, Universität Innsbruck, Technikerstraße 25, 6020 Innsbruck, Austria*
[2]*Institut für Quantenoptik und Quanteninformation, Österreichische Akademie der Wissenschaften, 6020 Innsbruck, Austria*

A. Simoni, E. Tiesinga, C. J. Williams, and P. S. Julienne
Atomic Physics Division, National Institute of Standards and Technology 100 Bureau Drive Stop 8423, Gaithersburg, Maryland 20899
(Dated: August 31, 2004)

We employ radio-frequency spectroscopy on weakly bound $^6Li_2$ molecules to precisely determine the molecular binding energies and the energy splittings between molecular states for different magnetic fields. These measurements allow us to extract the interaction parameters of ultracold ^{6}Li atoms based on a multi-channel quantum scattering model. We determine the singlet and triplet scattering lengths to be $a_s = 45.167(8)a_0$ and $a_t = -2140(18)a_0$ ($1\ a_0 = 0.0529177$ nm), and the positions of the broad Feshbach resonances in the energetically lowest three $s-$wave scattering channels to be 83.41(15) mT, 69.04(5) mT, and 81.12(10) mT.

PACS numbers: 34.50.-s, 05.30.Jp, 32.80.Pj, 67.40.Hf

Molecular level structure near a collision threshold uniquely determines the scattering properties of ultracold atoms. When a molecular state is tuned near the scattering threshold, the atomic scattering amplitude can be resonantly altered. Magnetically tuned Feshbach resonances [1] in ultracold fermionic gases have recently led to ground-breaking observations, including the condensation of molecules [2, 3, 4, 5, 6] and the studies of the crossover physics from a molecular Bose-Einstein condensate to atomic Cooper pairs in the Bardeen-Cooper-Schrieffer state (BEC-BCS crossover) [5, 7, 8]. These studies are of general importance in physics as the ultracold Fermi gas provides a unique model system for other strongly interacting fermionic systems [9].

In spin mixtures of ^{6}Li atoms, a broad Feshbach resonance in the energetically lowest s-wave channel [10] allows for precise interaction tuning. This, together with the extraordinary stability of the system against inelastic decay [2, 11], makes ^{6}Li the prime candidate for BEC-BCS crossover studies. Precise knowledge of the magnetic-field dependent scattering properties is crucial for a quantitative comparison of the experimental results with crossover theories. Of particular importance is the precise value of the magnetic field where the $s-$wave scattering diverges. At this unique point, the strongly interacting fermionic quantum gas is expected to exhibit universal properties [12]. Previous experiments explored the ^{6}Li resonance by measuring inelastic decay [13], elastic collisions [14, 15], and the interaction energy [16], but could only locate the exact resonance point to within a range between 80 mT and 85 mT.

An ultracold gas of weakly bound molecules is an excellent starting point to explore the molecular energy structure near threshold [17]. Improved knowledge on the exact ^{6}Li resonance position was recently obtained in an experiment that observed the controlled dissociation of weakly bound $^6Li_2$ molecules induced by magnetic field ramps [18]. These measurements provided a lower bound of 82.2 mT for the resonance position. Studies of systematic effects suggested an upper bound of 83.4 mT. Within this range, however, we observe the physical behavior of the ultracold gas still exhibits a substantial dependence on the magnetic field [8]. In this Letter, we apply radio-frequency (rf) spectroscopy [17, 19] on weakly bound molecules to precisely determine the interaction parameters of cold ^{6}Li atoms. Together with a multi-channel quantum scattering model, we obtain a full characterization of the two-body scattering properties, essential for BEC-BCS crossover physics.

The relevant atomic states are the lowest three sublevels in the ^{6}Li ground state manifold, denoted by $|1\rangle$, $|2\rangle$ and $|3\rangle$. Within the magnetic field range investigated in this experiment, these levels form a triplet of states, essentially differing by the orientation of the nuclear spin ($m_I = 1, 0, -1$). Figure 1 shows the energy level structure of the two scattering channels $|1\rangle+|2\rangle$ and $|1\rangle + |3\rangle$, denoted by $(1, 2)$ and $(1, 3)$, respectively. The broad Feshbach resonance occurs in the $(1, 2)$ channel near 83 mT. When the magnetic field is tuned below the resonance, atoms in the $(1, 2)$ channel can form weakly bound molecules [20]. For the $(1, 3)$ channel, a similar Feshbach resonance [19] occurs near 69 mT.

Starting with molecules formed in the $(1, 2)$ channel, we drive the rf transition to the $(1, 3)$ channel at various magnetic field values B. The rf excitation can dissociate a molecule into two free atoms (bound-free transition; see Fig. 1) [17] or, for $B < 69$ mT, it can also drive the transition between the molecular states in the $(1, 2)$ and $(1, 3)$ channels (bound-bound transition). In both processes, the rf excitation results in loss of molecules in the $(1, 2)$ channel. This loss constitutes our experimental signal. We perform measurements at different magnetic

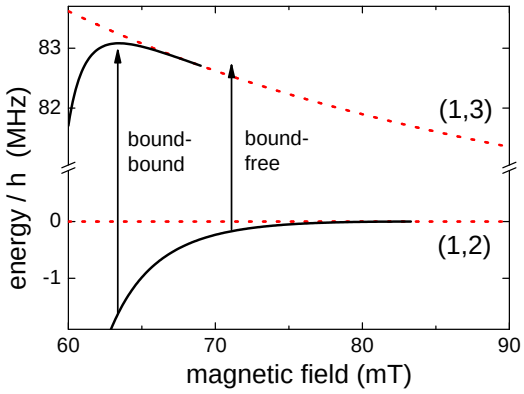

FIG. 1: Energy level structure near the Li_2 dissociation threshold as a function of magnetic field B. The threshold energy of the $(1,3)$ scattering channel (upper dotted line) is plotted relative to the $(1,2)$ threshold (lower dotted line). In the $(1,2)$ channel, a molecular state (lower solid line) exists below the Feshbach resonance at ~ 83 mT. In the $(1,3)$ channel, another molecular state (upper solid line) exists below the resonance at ~ 69 mT. The bound-free and bound-bound transitions of molecules in the $(1,2)$ channel are illustrated by the arrows.

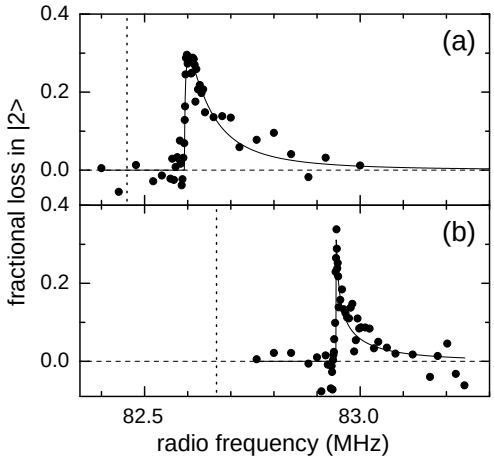

FIG. 2: Bound-free rf spectra at 72.013(4) mT (a) and 69.483(4) mT (b). Fractional loss in state $|2\rangle$ is measured as a function of the radio frequency. The solid lines are the fit based on Eq. (1). The atomic transition frequencies, which are measured independently, are indicated by the vertical dashed lines.

fields for both the bound-free and the bound-bound transitions.

Our experimental procedure is similar to Ref. [8]. We start with a pure condensate of typically 2×10^5 molecules at a magnetic field of 76.4 mT [2]. The condensate is confined in a weak optical trap, where the peak molecular density is near 10^{13} cm^{-3}. We then linearly ramp the magnetic field to a specific value between 66 mT and 72 mT in typically 200 ms. After the ramp, we apply a single rf pulse for 200 ms with its frequency tuned close to the atomic transition $|2\rangle$ to $|3\rangle$. Following the rf pulse, we apply state-selective absorption imaging, which is sensitive to free atoms in state $|2\rangle$ and molecules in the $(1,2)$ channel.

To precisely determine the magnetic field, we employ rf spectroscopy on thermal atoms with temperature $T = 6T_F$, where T_F is the Fermi temperature. Here, the rf transition energy corresponds to the internal energy difference between the states $|2\rangle$ and $|3\rangle$, hf_0, where h is Planck's constant. This energy is magnetic field dependent and the transition frequency is about 83 MHz in the magnetic field range we study. The measured transition has a narrow linewidth of less than 1 kHz, and the center position can be determined to within a few 100 Hz. This high resolution allows us to calibrate our magnetic field to an accuracy of a few μT based on the Breit-Rabi formula and the ^{6}Li parameters given in [21]. Within our statistical uncertainty, we do not observe any density-dependent frequency shifts [19].

For bound-free transitions, the molecules in the $(1,2)$ channel make a transition to the $(1,3)$ scattering continuum. The excitation rate from a stationary molecule to an atomic scattering state with kinetic energy $2E_k$ is determined by the Franck-Condon factor between the bound and free wavefunctions [22]. From energy conservation, $2E_k$ is related to the rf transition energy hf by $hf = hf_0 + E_b + 2E_k$, where E_b is the binding energy of the molecules in the $(1,2)$ channel. The variation of the Franck-Condon factor with atomic kinetic energy leads to a broad and asymmetric dissociation lineshape [22].

Rf dissociation spectra at 72.0 mT and 69.5 mT are shown in Fig. 2. An important feature of the spectra is the sharp rising edge on the low frequency side. This threshold corresponds to the dissociation of a molecule into two atoms with zero relative momentum. Therefore, the position of the edge relative to the atomic transition directly indicates the molecular binding energy.

We determine the dissociation threshold and thus the molecular binding energy by fitting the full lineshape. The lineshape function [22] depends on both the $(1,2)$ molecular binding energy E_b and the scattering length a_{13} in the $(1,3)$ channel. In the range of magnetic fields we investigate, a_{13} is much larger than the interaction range of the van der Waals potential of $\sim 30a_0$. The lineshape function $P(E)$ is then well approximated by [22]

$$P(E) \propto E^{-2}(E - E_b)^{1/2}(E - E_b + E')^{-1}\,, \qquad (1)$$

where $E = hf - hf_0$ and $E' = \hbar^2/ma_{13}^2$. From the fits to the experimental data [23], we determine the threshold positions, given in Table I. Together with the atomic transition frequencies, we conclude that the molecular binding energies are $E_b = h \times 134(2)$ kHz at 72.013(4) mT and $E_b = h \times 277(2)$ kHz at 69.483(4) mT.

For magnetic field $B < 69$ mT, we can drive the rf transition between the $(1,2)$ and $(1,3)$ molecular states. Here, the resonance frequency is given by the energy

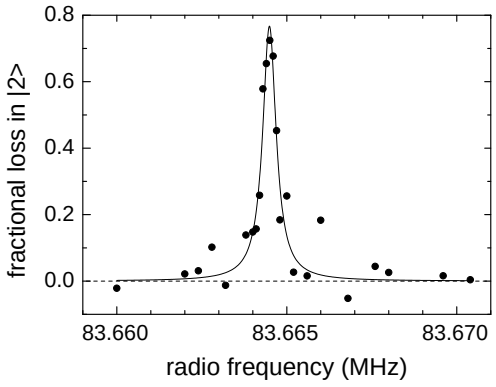

FIG. 3: Bound-bound rf spectrum at 66.144(2) mT. The fractional population loss in state $|2\rangle$ shows a narrow resonance. We determine the center position to be 83.6645(3) MHz from a Lorentzian fit (solid line).

TABLE I: Comparison of measured and calculated transition frequencies. Magnetic field values in the second column are derived from the atomic transition positions in the first column. We report the measured peak resonance frequencies for the atomic and molecular bound-bound transitions and the transition threshold positions for molecular bound-free transitions. The theory values are from the multi-channel quantum scattering calculation. Values in parentheses indicate one σ uncertainties.

Atoms (MHz)	B (mT)	Molecules (MHz)	Theory (MHz)
82.96808(20)	66.1436(20)	83.6645(3)[a]	83.6640(10)
82.83184(30)	67.6090(30)	83.2966(5)[a]	83.2973(10)
82.66686(30)	69.4826(40)	82.9438(20)[b]	82.9419(13)
82.45906(30)	72.0131(40)	82.5928(20)[b]	82.5910(13)

[a] bound-bound transition frequency.

[b] bound-free transition threshold.

difference of the two molecular states. To avoid possible systematic mean-field shifts at these lower magnetic fields [19], we prepare a thermal mixture of atoms and molecules with temperature $T \approx T_{\rm F}$ by a controlled heating method [8]. Rf spectroscopy is performed at 67.6 mT and 66.1 mT. The bound-bound transition signal at 66.1 mT is shown in Fig. 3. By fitting the narrow transition line with a Lorentzian profile, we determine the resonance frequency, see Table I. Notably, below the resonance in the $(1,3)$ channel at $\sim$69 mT, the bound-free transition is much weaker due to a Fano-type interference effect [22].

Because of the high precision of the measured transition frequencies, a careful analysis of systematic effects is necessary. Possible systematic shifts include differential light shifts of the two molecular states and density-dependent many-body shifts. In order to characterize these possible systematic errors, we experimentally investigate these shifts by varying the trap depth of the optical potential. In a deeper trap, both the differential light shifts and mean-field shifts are expected to increase. We repeat the bound-free and bound-bound rf spectroscopy in traps with different laser powers P between 3.8 mW and 310 mW. We do not see systematic shifts within our statistical uncertainty. The measurements show that these systematic shifts do not exceed the uncertainties given in Table I.

Given the measured data summarized in Table I, it is possible to predict the location of the scattering resonances in the $(1,2)$, $(1,3)$ and $(2,3)$ channels if we have an accurate theoretical model of the collision. We use a standard multi-channel model for the interaction of two ^{2}S atoms with nuclear spin [24] to calculate the scattering lengths and bound state energies for these channels. It is only necessary to include s-waves in the basis set, since we find that there is a negligible change within the experimental uncertainties if we also include higher partial waves in the basis set. The interaction potential model is the same as described in Ref. [14]. It uses a combination of Rydberg-Klein-Rees and *ab initio* potentials for the singlet ($^1\Sigma_g^+$) and triplet ($^3\Sigma_u^+$) states at short range, and joins them smoothly onto long range potentials based on the exchange [25] and van der Waals dispersion energy [26], the lead term of which is $C_6 = 1393.39(16)$ au (1 au $= 9.57344 \times 10^{-26}$ J nm^6). As in Ref. [14], the singlet $^1\Sigma_g^+$ and triplet $^3\Sigma_u^+$ scattering lengths, a_s and a_t respectively, are varied by making small variations to the inner wall of the potential. Once a_s and a_t are specified, all other scattering and bound state properties for all channels of two ^{6}Li atoms are uniquely determined, including the positions of the resonances. Consequently, varying a_s and a_t to fit the binding energies and energy differences from rf spectroscopy determines the values of these two free parameters.

Fitting the data of the present experiment determines $a_s = 45.167(8)a_0$ and $a_t = -2140(18)a_0$. The uncertainty includes both the uncertainty in the measured value of the magnetic field and the uncertainty in the rf measurements. Our scattering lengths agree within the uncertainties with previous determinations: $a_s = 45.1591(16)a_0$ [18] and $a_t = -2160(250)a_0$ [27]. Table I shows a comparison of the measured and best fit calculated energies. The calculated positions of the broad $s-$wave resonances for the $(1,2)$, $(1,3)$, and $(2,3)$ channels are 83.41(15) mT, 69.04(5) mT, and 81.12(10) mT respectively.

Figure 4 shows the scattering lengths calculated for several different channels in the magnetic field range of interest to BEC-BCS crossover experiments. We find that the formula $a = a_b[1+\Delta(B-B_0)^{-1}][1+\alpha(B-B_0)]$ fits the calculated scattering lengths to better than 99% over the range of 60 to 120 mT. This expression includes the standard Feshbach resonance term [28] with the background scattering length a_b, resonance position B_0 and resonance width Δ, and a leading-order correction parameterized by α. The respective values for a_b, B_0, Δ, and α are $-1405a_0$, 83.4149 mT, 30.0 mT, and 0.0040 mT^{-1} for channel $(1,2)$, $-1727a_0$, 69.043 mT, 12.23 mT,

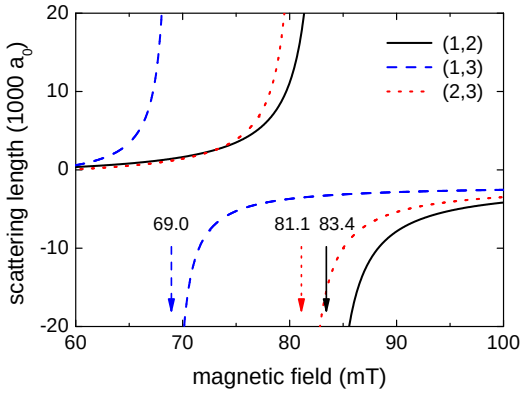

FIG. 4: Scattering lengths versus magnetic field from multi-channel quantum scattering calculations for the $(1,2)$, $(1,3)$, and $(2,3)$ scattering channels. The arrows indicate the resonance positions.

and 0.0020 mT^{-1} for channel $(1,3)$, and $-1490a_0$, 81.122 mT, 22.23 mT, and 0.00395 mT^{-1} for channel $(2,3)$.

The $(1,3)$ channel molecular bound state can decay to the $(1,2)$ channel by a very weak spin-dipolar coupling. We have used the methods of Ref. [29] to calculate the two-body lifetime of the $(1,3)$ bound state due to pre-dissociation to the $(1,2)$ channel, and find that it is very long, greater than 10 s at 60.0 mT, increasing to 1000 s at 68.5 mT very close to resonance. However, $(1,3)$ molecules might be quenched by collisions with $|2\rangle$ atoms or $(1,2)$ channel molecules, since with three different spin states involved in the collision, there would be no fermionic suppression of collision rates according to the mechanism of Ref. [11].

In conclusion, radio-frequency spectroscopy on ultracold, weakly bound molecules allowed us to precisely determine the molecular binding energies and the energy splittings between two molecular states for different magnetic fields. Based on the measured data and a multi-channel quantum scattering model, we determine the scattering lengths as a function of magnetic field and the Feshbach resonance positions in the lowest three channels with unprecedented precision. With this data, we can fully characterize the interaction strength between particles in the BEC-BCS crossover regime for future experiments based on ^{6}Li atoms.

We acknowledge support by the Austrian Science Fund (FWF) within SFB 15 (project part 15) and by the European Union in the framework of the Cold Molecules TMR Network under Contract No. HPRN-CT-2002-00290. P. J. thanks the Office of Naval Research for partial support. C. C. is a Lise-Meitner research fellow of the FWF.

[1] E. Tiesinga, B.J. Verhaar, and H.T.C. Stoof, Phys. Rev. A **47**, 4114 (1993); S. Inouye *et al.*, Nature **392**, 151 (1998).
[2] S. Jochim *et al.*, Science **302**, 2101 (2003); published online 13 November 2003 (10.1126/science.1093280).
[3] M. Greiner, C. A. Regal, D. S. Jin, Nature **426**, 537 (2003).
[4] M. Zwierlein *et al.*, Phys. Rev. Lett. **91**, 250401 (2003).
[5] T. Bourdel *et al.*, Phys. Rev. Lett. **93**, 050401 (2004).
[6] R.G. Hulet, *KITP Conference on Quantum Gases*, Santa Barbara, CA, 10 - 14 May 2004.
[7] M. Bartenstein *et al.*, Phys. Rev. Lett. **92**, 120401 (2004); C. A. Regal, M. Greiner, D. S. Jin, Phys. Rev. Lett. **92**, 040403 (2004); M. W. Zwierlein *et al.*, Phys. Rev. Lett. **92**, 120403 (2004); J. Kinast *et al.*, Phys. Rev. Lett. **92**, 150402 (2004); M. Bartenstein *et al.*, Phys. Rev. Lett. **92**, 203201 (2004).
[8] C. Chin *et al.*, Science **305** 1128 (2004); published online 22 July 2004 (10.1126/science.1100818).
[9] D. M. Eagles, Phys. Rev. **186**, 456 (1969); A. J. Leggett, in *Modern Trends in the Theory of Condensed Matter*, edited by A. Pekalski and R. Przystawa (Springer-Verlag, Berlin), 1980; P. Nozières, S. Schmitt-Rink, J. Low Temp. Phys. **59**, 195 (1985); Q. Chen, J. Stajic, S. Tan and K. Levin, cond-mat/0404274.
[10] M. Houbiers, H.T.C. Stoof, W.I. McAlexander, and R.G. Hulet, Phys. Rev. A **57**, R1497 (1998).
[11] D. S. Petrov, C. Salomon, and G. V. Shlyapnikov, cond-mat/0309010.
[12] H. Heiselberg, Phys. Rev. A **63**, 043606 (2001); T.-L. Ho, Phys. Rev. Lett. **92**, 090402 (2004).
[13] K. Dieckmann *et al.*, Phys. Rev. Lett. **89**, 203201 (2002).
[14] K.M. O'Hara *et al.*, Phys. Rev. A **66**, 041401(R) (2002).
[15] S. Jochim *et al.*, Phys. Rev. Lett. **89**, 273202 (2002).
[16] T. Bourdel *et al.*, Phys. Rev. Lett. **91**, 020402 (2003).
[17] C. A. Regal, C. Ticknor, J. L. Bohn, and D. S. Jin, Nature **424** 47 (2003).
[18] C. H. Schunck *et al.*, cond-mat/0407373.
[19] S. Gupta *et al.*, Science **300**, 1723 (2003); published online May 8, 2003 (10.1126/science.1085335).
[20] J. Cubizolles *et al.* Phys. Rev. Lett. **91**, 240401 (2003); S. Jochim *et al.*, Phys. Rev. Lett. **91**, 240402 (2003).
[21] J. Vanier and C. Audoin, *The Quantum Physics of Atomic Frequency Standards*, (Adam Hilger Ltd, Bristol), 1989.
[22] C. Chin and P. Julienne, cond-mat/0408254.
[23] We assume an exponential decay of the particle number and fit $1-\mathrm{e}^{-\iota P(E)}$ to the loss signal, where ι depends on the rf power. In principle, we can also determine interaction parameters from E'. However, our fits yield large uncertainties for E'.
[24] H. T. C. Stoof, J. M. V. A. Koelman and B. J. Verhaar, Phys. Rev. B **38**, 4688 (1988).
[25] R. Côté, A. Dalgarno, and M.J. Jamieson, Phys. Rev. A **50**, 399 (1994)
[26] Z.-C. Yan, J.F. Babb, A. Dalgarno and G.W.F. Drake, Phys. Rev. A **54**, 2824 (1996)
[27] E.R.I. Abraham, W.I. McAlexander, J.M. Gerton, R.G. Hulet, R. Côté and A. Dalgarno, Phys. Rev. A **55**, R3299 (1997).

[28] A.J. Moerdijk, B.J. Verhaar, and A. Axelsson Phys. Rev. A **51**, 4852-4861 (1995)
[29] T. Köhler, E. Tiesinga, and P. S. Julienne, cond-mat/0408387.

References

[Abr97] E. R. I. Abraham, W. I. McAlexander, J. M. Gerton, R. G. Hulet, R. Côté, and A. Dalgarno, *Triplet s-wave resonance in ^{6}Li collisions and scattering lengths of ^{6}Li and ^{7}Li*, Phys. Rev. A **55**, R3299 (1997).

[Alt] A. Altmeyer, in preparation, Ph.D. thesis, Universität Innsbruck.

[Amo99] M. Amoruso, I. Meccoli, A. Minguzzi, and M. P. Tosi, *Collective excitations of a degenerate Fermi vapour in a magnetic trap*, Euro. Phys. J. D **7**, 441 (1999).

[And95] M. H. Anderson, J. R. Ensher, M. R. Matthews, C. E. Wieman, and E. A. Cornell, *Observation of Bose-Einstein Condensation in a Dilute Atomic Vapor*, Science **269**, 198 (1995).

[And97] M. R. Andrews, C. G. Townsend, H.-J. Miesner, D. S. Durfee, D. M. Kurn, and W. Ketterle, *Observation of Interference Between Two Bose-Einstein Condensates*, Science **275**, 637 (1997).

[And98] B. P. Anderson and M. A. Kasevich, *Macroscopic Quantum Interference from Atomic Tunnel Arrays*, Science **282**, 1686 (1998).

[Ang02] J. R. Anglin and W. Ketterle, *Bose-Einstein condensation of atomic gases*, Nature **416**, 211 (2002).

[Ari77] E. Arimondo, M. Inguscio, and P. Violino, *Experimental determination of the hyperfine structure in the alkali atoms*, Rev. Mod. Phys. **49**, 31 (1977).

[AS01] J. R. Abo-Shaeer, C. Raman, J. M. Vogels, and W. Ketterle, *Observation of Vortex Lattices in Bose-Einstein Condensates*, Science **292**, 476 (2001).

[Ast04] G. E. Astrakharchik, J. Boronat, J. Casulleras, and S. Giorgini, *Equation of State of a Fermi Gas in the BEC-BCS Crossover: A Quantum Monte Carlo Study*, Phys. Rev. Lett. **93**, 200404 (2004).

[Bak99] G. A. Baker, *Neutron matter model*, Phys. Rev. C **60**, 054311 (1999).

[Bar57] J. Bardeen, L. N. Cooper, and J. R. Schrieffer, *Theory of Superconductivity*, Phys. Rev. **108**, 1175 (1957).

[Bar98] M. A. Baranov and D. S. Petrov, *Critical temperature and Ginzburg-Landau equation for a trapped Fermi gas*, Phys. Rev. A **58**, R801 (1998).

[Bar00] M. A. Baranov and D. S. Petrov, *Low-energy collective excitations in a superfluid trapped Fermi gas*, Phys. Rev. A **62**, 041601 (2000).

[Bar04a] M. Bartenstein, A. Altmeyer, S. Riedl, S. Jochim, C. Chin, J. Hecker Denschlag, and R. Grimm, *Collective excitations of a degenerate gas at the BEC-BCS crossover*, Phys. Rev. Lett. **92**, 203201 (2004).

[Bar04b] M. Bartenstein, A. Altmeyer, S. Riedl, S. Jochim, C. Chin, J. Hecker Denschlag, and R. Grimm, *Crossover from a Molecular Bose-Einstein Condensate to a Degenerate Fermi Gas*, Phys. Rev. Lett. **92**, 120401 (2004).

[Bar04c] M. Bartenstein, A. Altmeyer, S. Riedl, R. Geursen, S. Jochim, C. Chin, J. Hecker Denschlag, R. Grimm, A. Simoni, E. Tiesinga, C. J. Williams, and P. S. Julienne, *Precise determination of ^{6}Li cold collision parameters by radio-frequency spectroscopy on weakly bound molecules* (2004), http://arxiv.org/abs/cond-mat/0408673.

[Bay96] G. Baym and C. J. Pethick, *Ground-State Properties of Magnetically Trapped Bose-Condensed Rubidium Gas*, Phys. Rev. Lett. **76**, 6 (1996).

[Bou03] T. Bourdel, J. Cubizolles, L. Khaykovich, K. M. F. Magalhães, S. J. J. M. F. Kokkelmans, G. V. Shlyapnikov, and C. Salomon, *Measurement of the Interaction Energy near a Feshbach Resonance in a ^{6}Li Fermi Gas*, Phys. Rev. Lett. **91**, 020402 (2003).

[Bou04] T. Bourdel, L. Khaykovich, J. Cubizolles, J. Zhang, F. Chevy, M. Teichmann, L. Tarruell, S. J. J. M. F. Kokkelmans, and C. Salomon, *Experimental Study of the BEC-BCS Crossover Region in Lithium 6*, Phys. Rev. Lett. **93**, 050401 (2004).

[Bre31] G. Breit and I. Rabi, *Measurement of nuclear spin*, Phys. Rev. **38**, 2082 (1931).

[Bru98] G. M. Bruun and K. Burnett, *Interacting Fermi gas in a harmonic trap*, Phys. Rev. A **58**, 2427 (1998).

[Bru99] G. M. Bruun and C. W. Clark, *Hydrodynamic Excitations of Trapped Fermi Gases*, Phys. Rev. Lett. **83**, 5415 (1999).

[Bru00] G. M. Bruun and C. W. Clark, *Ideal gases in time-dependent traps*, Phys. Rev. A **61**, 061601(R) (2000).

[Bru01a] G. M. Brunn and B. R. Mottelson, *Low Energy Collective Modes of a Superfluid Trapped Atomic Fermi Gas*, Phys. Rev. Lett. **87**, 270403 (2001).

[Bru01b] G. M. Bruun, P. Törmä, M. Rodriguez, and P. Zoller, *Laser probing of Cooper-paired trapped atoms*, Phys. Rev. A **64**, 033609 (2001).

[Bru01c] G. M. Bruun and L. Viverit, *Vortex state in superfluid trapped Fermi gases at zero temperature*, Phys. Rev. A **64**, 063606 (2001).

[Büc04] H. P. Büchler, P. Zoller, and W. Zwerger, *Spectroscopy of Superfluid Pairing in Atomic Fermi Gases*, Phys. Rev. Lett. **93**, 080401 (2004).

[Bul03a] A. Bulgac, *The spatial profile of the matter distribution in a dilute atomic-molecular Fermi cloud* (2003), http://arxiv.org/abs/cond-mat/0309358.

[Bul03b] A. Bulgac and Y. Yu, *Vortex State in a Strongly Coupled Dilute Atomic Fermionic Superfluid*, Phys. Rev. Lett. **91**, 190404 (2003).

[Bul04] A. Bulgac and G. F. Bertsch, *Collective oscillations of a trapped Fermi gas near the unitary limit* (2004), http://arxiv.org/cond-mat/0404687.

[Bur02] K. Burnett, P. S. Julienne, P. D. Lett, E. Tiesinga, and C. J. Williams, *Quantum encounters of the cold kind*, Nature **417**, 225 (2002).

[But97] D. A. Butts and D. S. Rokhsar, *Trapped Fermi gases*, Phys. Rev. A **55**, 4346 (1997).

[Car03] J. Carlson, S.-Y. Chang, V. Pandharipande, and K. Schmidt, *Superfluid Fermi Gases with Large Scattering Length*, Phys. Rev. Lett. **91**, 050401 (2003).

[Car04] L. D. Carr, G. Shlyapnikov, and Y. Castin, *Achieving a BCS Transition in an Atomic Fermi Gas*, Phys. Rev. Lett. **92**, 150404 (2004).

[Cha04] S. Y. Chang, V. R. Pandharipande, J. Carlson, and K. E. Schmidt, *Quantum Monte Carlo studies of superfluid Fermi gases*, Phys. Rev. A **70**, 043602 (2004).

[Che00] F. Chevy, K. W. Madison, and J. Dalibard, *Measurement of the Angular Momentum of a Rotating Bose-Einstein Condensate*, Phys. Rev. Lett. **85**, 2223 (2000).

[Che02] F. Chevy, V. Bretin, P. Rosenbusch, K. W. Madison, and J. Dalibard, *Transverse Breathing Mode of an Elongated Bose-Einstein Condensate*, Phys. Rev. Lett. **88**, 250402 (2002).

[Che04] Q. Chen, J. Stajic, S. Tan, and K. Levin, *BCS-BEC Crossover: From High Temperature Superconductors to Ultracold Superfluids* (2004), http://arxiv.org/cond-mat/0404274.

[Chi02] M. L. Chiofalo, S. J. J. M. F. Kokkelmans, J. N. Milstein, and M. J. Holland, *Signatures of Resonance Superfluidity in a Quantum Fermi Gas*, Phys. Rev. Lett. **88**, 090402 (2002).

[Chi04a] C. Chin, M. Bartenstein, A. Altmeyer, S. Riedl, S. Jochim, J. Hecker Denschlag, and R. Grimm, *Observation of the pairing gap in a strongly interacting Fermi gas*, Science **305**, 1128 (2004), published online 22 July 2004; 10.1126/science.1100818.

[Chi04b] C. Chin and R. Grimm, *Thermal equilibrium and efficient evaporation of an ultracold atom-molecule mixture*, Phys. Rev. A **69**, 033612 (2004).

[Chi05] C. Chin and P. S. Julienne, *Radio-frequency transitions on weakly bound ultracold molecules*, Phys. Rev. A **71**, 012713 (2005).

[Cho03] A. Cho, *Ultracold Atoms Spark a Hot Race*, Science **301**, 750 (2003), News Focus.

[Com99] R. Combescot, *Trapped ^{6}Li: A High T_c Superfluid?*, Phys. Rev. Lett. **83**, 3766 (1999).

[Com04a] R. Combescot and X. Leyronas, *Axial collective excitations of a degenerate Fermi gas in the BEC to unitarity crossover*, Europhys. Lett. **68**, 762 (2004).

[Com04b] R. Combescot and X. Leyronas, *Comment on "Collective excitations of a degenerate gas in the BEC-BCS crossover"*, Phys. Rev. Lett. **93**, 138901 (2004).

[Coo56] L. N. Cooper, *Bound Electron Pairs in a Degenerate Fermi Gas*, Phys. Rev. **104**, 1189 (1956).

[Cor00] S. L. Cornish, N. R. Claussen, J. L. Roberts, E. A. Cornell, and C. E. Wieman, *Stable ^{85}Rb Bose-Einstein Condensates with Widely Tunable Interactions*, Phys. Rev. Lett. **85**, 1795 (2000).

[Côt94] R. Côté, A. Dalgarno, and M. J. Jamieson, *Elastic scattering of two ^{7}Li atoms*, Phys. Rev. A **50**, 399 (1994).

[Cow02] S. Cowell, H. Heiselberg, I. E. Mazets, J. Morales, V. R. Pandharipande, and C. J. Pethick, *Cold Bose Gases with Large Scattering Lengths*, Phys. Rev. Lett. **88**, 210403 (2002).

[Coz03] M. Cozzini and S. Stringari, *Fermi Gases in Slowly Rotating Traps: Superfluid versus Collisional Hydrodynamics*, Phys. Rev. Lett. **91**, 070401 (2003).

[Cub03] J. Cubizolles, T. Bourdel, S. Kokkelmans, G. Shlyapnikov, and C. Salomon, *Production of Long-Lived Ultracold Li_2 Molecules from a Fermi Gas*, Phys. Rev. Lett. **91**, 240401 (2003).

[Dal99a] F. Dalfovo, S. Giorgini, L. P. Pitaevskii, and S. Stringari, *Theory of Bose-Einstein condensation in trapped gases*, Rev. Mod. Phys. **71**, 463 (1999).

[Dal99b] J. Dalibard, *Collisional dynamics of ultra-cold atomic gases*, in: M. Inguscio, S. Stringari, and C. E. Wieman (Eds.), *Proceedings of the International School of Physics - Enrico Fermi*, 321, IOS Press, 1999.

[Dav95] K. B. Davis, M.-O. Mewes, M. R. Andrews, N. J. van Druten, D. S. Durfee, D. M. Kurn, and W. Ketterle, *Bose-Einstein Condensation in a Gas of Sodium Atoms*, Phys. Rev. Lett. **75**, 3969 (1995).

[DeM98] B. DeMarco and D. S. Jin, *Exploring a quantum degenerate gas of fermionic atoms*, Phys. Rev. A **58**, R4267 (1998).

[DeM99a] B. DeMarco, J. L. Bohn, J. P. Burke, Jr., M. Holland, and D. S. Jin, *Measurement of p-Wave Threshold Law Using Evaporatively Cooled Fermionic Atoms*, Phys. Rev. Lett. **82**, 4208 (1999).

[DeM99b] B. DeMarco and D. S. Jin, *Onset of Fermi Degeneracy in a Trapped Atomic Gas*, Science **285**, 1703 (1999).

[Die02] K. Dieckmann, C. A. Stan, S. Gupta, Z. Hadzibabic, C. H. Schunck, and W. Ketterle, *Decay of an Ultracold Fermionic Lithium Gas near a Feshbach Resonance*, Phys. Rev. Lett. **89**, 203201 (2002).

[Die04] R. B. Diener and T.-L. Ho, *The Condition for Universality at Resonance and Direct Measurement of Pair Wavefunctions Using rf Spectroscopy* (2004), http://arxiv.org/abs/cond-mat/0405174.

[Don91] R. J. Donnelly, *Quantized Vortices in Helium II*, Campbridge University Press, Cambridge, 1991.

[Don01] E. A. Donley, N. R. Claussen, S. L. Cornish, J. L. Roberts, E. A. Cornell, and C. E. Wieman, *Dynamics of collapsing and exploding Bose-Einstein condensates*, Nature **412**, 295 (2001).

[Don02] E. A. Donley, N. R. Claussen, S. T. Thompson, and C. E. Wieman, *Atom-molecule coherence in a Bose-Einstein condensate*, Nature **417**, 529 (2002).

[Dür04] S. Dürr, A. Volz, T. Marte, and G. Rempe, *Observation of Molecules Produced from a Bose-Einstein Condensate*, Phys. Rev. Lett. **92**, 020406 (2004).

[Eag69] D. M. Eagles, *Possible Pairing without Superconductivity at Low Carrier Concentrations in Bulk and Thin-Film Superconducting Semiconductors*, Phys. Rev. **186**, 456 (1969).

[Els00] T. Elsässer, *Stehwellenfalle in einem Resonator*, diploma thesis, Max-Planck-Institut für Kernphysik, Heidelberg (2000).

[Fed98] P. O. Fedichev, G. V. Shlyapnikov, and J. T. M. Walraven, *Damping of Low-Energy Excitations of a Trapped Bose-Einstein Condensate at Finite Temperatures*, Phys. Rev. Lett. **80**, 2269 (1998).

[Fes58] H. Feshbach, *A Unified Theory of Nuclear Reactions*, Ann. Phys. **5**, 337 (1958).

[Geh03a] M. E. Gehm, *Preparation of an Optically-Trapped Degenerate Fermi Gas of ^{6}Li: Finding the Route to Degeneracy*, Ph.D. thesis, Duke University (2003).

[Geh03b] M. E. Gehm, S. L. Hemmer, S. R. Granade, K. M. O'Hara, and J. E. Thomas, *Mechanical stability of a strongly interacting Fermi gas of atoms*, Phys. Rev. A **68**, 011401(R) (2003).

[Gio96] S. Giorgini, L. P. Pitaevskii, and S. Stringari, *Condensate fraction and critical temperature of a trapped interacting Bose gas*, Phys. Rev. A **54**, R4633 (1996).

[Gio00] S. Giorgini, *Collisionless dynamics of dilute Bose gases: Role of quantum and thermal fluctuations*, Phys. Rev. A **61**, 063615 (2000).

[GO99] D. Guéry-Odelin, F. Zambelli, J. Dalibard, and S. Stringari, *Collective oscillations of a classical gas confined in harmonic traps*, Phys. Rev. A **60**, 4851 (1999).

[Gor61] L. P. Gorkov and T. K. Melik-Barkhudarov, *Contribution to the theory of superfluidity in an imperfect Fermi gas*, Sov. Phys. JETP **13**, 1018 (1961).

[Gra02] S. R. Granade, M. E. Gehm, K. M. O'Hara, and J. E. Thomas, *All-Optical Production of a Degenerate Fermi Gas*, Phys. Rev. Lett. **88**, 120405 (2002).

[Gre02] M. Greiner, O. Mandel, T. Esslinger, T. W. Hänsch, and I. Bloch, *Quantum phase transition from a superfluid to a Mott insulator in a gas of ultracold atoms*, Nature **415**, 39 (2002).

[Gre03] M. Greiner, C. A. Regal, and D. S. Jin, *Emergence of a molecular Bose-Einstein condensate from a Fermi gas*, Nature **426**, 540 (2003), doi:10.1038/nature02199; Published online 26 November 2003.

[Gre04] M. Greiner, C. C. A. Regal, and D. S. Jin, *Probing the excitation spectrum of a Fermi gas in the BCS-BEC crossover regime* (2004), http://arxiv.org/abs/cond-mat/0407381.

[Gri93] G. F. Gribakin and V. V. Flambaum, *Calculation of the scattering length in atomic collisions using the semiclassical approximation*, Phys. Rev. A **48**, 546 (1993).

[Gri97a] A. Griffin, W.-C. Wu, and S. Stringari, *Hydrodynamic Modes in a Trapped Bose Gas above the Bose-Einstein Transition*, Phys. Rev. Lett. **78**, 1838 (1997).

[Gri97b] A. Griffin and E. Zaremba, *First and second sound in a uniform Bose gas*, Phys. Rev. A **56**, 4839 (1997).

[Gri00] R. Grimm, M. Weidemüller, and Y. Ovchinnikov, *Optical dipole traps for neutral atoms*, Adv. At. Mol. Opt. Phys. **42** (2000).

[Gro61] E. P. Gross, *Structure in Quantized Vortex in Boson Systems*, Il Nuovo Cimento **20**, 454 (1961).

[Gup03] S. Gupta, Z. Hadzibabic, M. W. Zwierlein, C. A. Stan, K. Dieckmann, C. H. Schunck, E. G. M. van Kempen, B. J. Verhaar, and W. Ketterle, *Radio-Frequency Spectroscopy of Ultracold Fermions*, Science **300**, 1723 (2003).

[Hal01a] P. C. Haljan, B. P. Anderson, I. Coddington, and E. A. Cornell, *Use of Surface-Wave Spectroscopy to Characterize Tilt Modes of a Vortex in a Bose-Einstein Condensate*, Phys. Rev. Lett. **86**, 2922 (2001).

[Hal01b] P. C. Haljan, I. Coddington, P. Engels, and E. A. Cornell, *Driving Bose-Einstein-Condensate Vorticity with a Rotating Normal Cloud*, Phys. Rev. Lett. **87**, 210403 (2001).

[Hän80] T. W. Hänsch and B. Couillaud, *Laser frequency stabilization by polarization spectroscopy of a reflecting reference cavity*, Opt. Commun. **35**, 441 (1980).

[Hei01] H. Heiselberg, *Fermi systems with long scattering lengths*, Phys. Rev. A **63**, 043606 (2001).

[Hei04a] H. Heiselberg, *Collective Modes of Trapped Gases at the BEC-BCS Crossover*, Phys. Rev. Lett. **93**, 040402 (2004).

[Hei04b] H. Heiselberg, *Pairing gaps in Atomic Gases at the BCS-BEC Crossover* (2004), http://arxiv.org/abs/cond-mat/0406714.

[Hen03] G. Hendel, *Atom - Atom Wechselwirkung in einem ultrakalten, fermionischen Gas*, diploma thesis, Universität Innsbruck (2003).

[Her03] J. Herbig, T. Kraemer, M. Mark, T. Weber, C. Chin, H.-C. Nägerl, and R. Grimm, *Preparation of a Pure Molecular Quantum Gas*, Science **301**, 1510 (2003), published online 21 August 2003; 10.1126/science.1088876.

[Ho04a] T.-L. Ho, *Arrival of the Fermion Superfluid*, Science **305**, 1114 (2004).

[Ho04b] T.-L. Ho, *Universal Thermodynamics of Degenerate Quantum Gases in the Unitarity Limit*, Phys. Rev. Lett. **92**, 090402 (2004).

[Ho04c] T.-L. Ho and E. J. Mueller, *High Temperature Expansion Applied to Fermions near Feshbach Resonance*, Phys. Rev. Lett. **92**, 160404 (2004).

[Hod01] E. Hodby, G. Heckenblaikner, S. A. Hopkins, O. M. Maragó, and C. J. Foot, *Vortex nucleation in Bose-Einstein condensates in an oblate, purely magnetic potential*, Phys. Rev. Lett. **88**, 010405 (2001).

[Hof02] W. Hofstetter, J. I. Cirac, P. Zoller, E. Demler, and M. D. Lukin, *High-Temperature Superfluidity of Fermionic Atoms in Optical Lattices*, Phys. Rev. Lett. **89**, 220407 (2002).

[Hol01] M. Holland, S. J. J. M. F. Kokkelmans, M. L. Chiofalo, and R. Walser, *Resonance Superfluidity in a Quantum Degenerate Fermi Gas*, Phys. Rev. Lett. **87**, 120406 (2001).

[Hou97] M. Houbiers, R. Ferwerda, H. T. C. Stoof, W. I. McAlexander, C. A. Sackett, and R. G. Hulet, *Superfluid state of atomic ^{6}Li in a magnetic trap*, Phys. Rev. A **56**, 4864 (1997).

[Hou98] M. Houbiers, H. T. C. Stoof, W. I. McAlexander, and R. G. Hulet, *Elastic and inelastic collisions of Li-6 atoms in magnetic and optical traps*, Phys. Rev. A **57**, R1497 (1998).

[Hu04] H. Hu, A. Minguzzi, X.-J. Liu, and M. P. Tosi, *Collective modes and ballistic expansion of a Fermi gas in the BCS-BEC crossover*, Phys. Rev. Lett. **93**, 190403 (2004).

[Hua57] K. Huang and C. N. Yang, *Quantum-Mechanical Many-Body Problem with Hard-Sphere Interaction*, Phys. Rev. **105**, 767 (1957).

[Hua87] K. Huang, *Statistical Mechanics*, John Wiley & Sons, 1987, 2nd ed.

[Hul04] R. Hulet, *Conversion of an Atomic Fermi Gas to a Molecular Bose Einstein Condensate*, March, KITP Conference: Quantum Gases, Santa Barbara, CA; available online at http://online.kitp.ucsb.edu/online/gases_c04/hulet/ (2004).

[Ino98] S. Inouye, M. R. Andrews, J. Stenger, H.-J. Miesner, D. M. Stamper-Kurn, and W. Ketterle, *Observation of Feshbach resonances in a Bose-Einstein condensate*, Nature **392**, 151 (1998).

[Joc00] S. Jochim, *Aufbau einer Apparatur zum magnetooptischen Einfang von fermionischen Lithiumatomen*, diploma thesis, Max-Planck-Institut für Kernphysik, Heidelberg (2000).

[Joc02] S. Jochim, M. Bartenstein, G. Hendl, J. Hecker Denschlag, R. Grimm, A. Mosk, and M. Weidemüller, *Magnetic Field Control of Elastic Scattering in a Cold Gas of Fermionic Lithium Atoms*, Phys. Rev. Lett. **89**, 273202 (2002).

[Joc03a] S. Jochim, M. Bartenstein, A. Altmeyer, G. Hendl, S. Riedl, C. Chin, J. Hecker Denschlag, and R. Grimm, *Bose-Einstein Condensation of Molecules*, Science **301**, 2101 (2003), published online 13 November 2003; 10.1126/science.1093280.

[Joc03b] S. Jochim, M. Bartenstein, A. Altmeyer, G. Hendl, C. Chin, J. Hecker Denschlag, and R. Grimm, *Pure Gas of Optically Trapped Molecules Created from Fermionic Atoms*, Phys. Rev. Lett. **91**, 240402 (2003).

[Joc04] S. Jochim, *Bose-Einstein Condensation of Molecules*, Ph.D. thesis, Universität Innsbruck (2004).

[Jul92] P. Julienne, A. Smith, and K. Burnett, *Theory of collisions between laser-cooled atoms*, Advances in Atomic, Molecular, and Optical Physics **30**, 141 (1992).

[Kag97] Y. Kagan, E. L. Surkov, and G. V. Shlyapnikov, *Evolution of a Bose gas in anisotropic time-dependent traps*, Phys. Rev. A **55**, R18 (1997).

[Kem04] E. G. M. v. Kempen, B. Marcelis, and S. J. J. M. F. Kokkelmans, *Formation of fermionic molecules via interisotope Feshbach resonances*, Phys. Rev. A **70**, 050701(R) (2004).

[Ket99] W. Ketterle, D. S. Durfee, and D. M. Stamper-Kurn, *Making, probing and understanding Bose-Einstein condensates*, in: M. Inguscio, S. Stringari, and C. E. Wieman (Eds.), *Proceedings of the International School of Physics - Enrico Fermi*, 67, IOS Press, 1999.

[Kha02] L. Khaykovich, F. Schreck, G. Ferrari, T. Bourdel, J. Cubizolles, L. D. Carr, Y. Castin, and C. Salomon, *Formation of a Matter-Wave Bright Soliton*, Science **296**, 1290 (2002).

[Kim04a] Y. E. Kim and A. L. Zubarev, *Dynamics of Strongly Interacting Fermi Gases of Atoms in a Harmonic Trap*, Phys. Lett. A **327**, 397 (2004).

[Kim04b] Y. E. Kim and A. L. Zubarev, *Time-dependent density-functional theory for trapped strongly interacting fermionic atoms*, Phys. Rev. A **70**, 033612 (2004).

[Kin04a] J. Kinast, S. L. Hemmer, M. E. Gehm, A. Turlapov, and J. E. Thomas, *Evidence for Superfluidity in a Resonantly Interacting Fermi Gas*, Phys. Rev. Lett. **92**, 150402 (2004).

[Kin04b] J. Kinast, A. Turlapov, and J. E. Thomas, *Breakdown of hydrodynamics in the radial breathing mode of a strongly interacting Fermi gas*, Phys. Rev. A **70**, 051401(R) (2004).

[Kin04c] J. Kinnunen, M. Rodríguez, and P. Törmä, *Pairing Gap and In-Gap Excitations in Trapped Fermionic Superfluids*, Science **305**, 1131 (2004), published online 22 July 2004; 10.1126/science.1100782.

[Kin04d] J. Kinnunen, M. Rodríguez, and P. Törmä, *Signatures of Superfluidity for Feshbach-Resonant Fermi Gases*, Phys. Rev. Lett. **92**, 230403 (2004).

[Kin05] J. Kinast, A. Turlapov, and J. E. Thomas., *Heat Capacity of a Strongly Interacting Fermi Gas*, Science Express (2005), published online 27 January 2005; 10.1126/science.1109220.

[Kok02] S. J. J. M. F. Kokkelmans, J. N. Milstein, M. L. Chiofalo, R. Walser, and M. J. Holland1, *Resonance superfluidity: Renormalization of resonance scattering theory*, Phys. Rev. A **65**, 053617 (2002).

[Kok04] S. J. J. M. F. Kokkelmans, G. V. Shlyapnikov, and C. Salomon, *Degenerate atom-molecule mixture in a cold Fermi gas*, Phys. Rev. A **69**, 031602(R) (2004).

[Kra96] W. Krauth, *Quantum Monte Carlo Calculations for a Large Number of Bosons in a Harmonic Trap*, Phys. Rev. Lett. **77**, 3695 (1996).

[Lan77] L. D. Landau and E. M. Lifshitz, *Quantum Mechanics: Non-Relativistic Theory*, Pergamon Press, Oxford, 1977, 3rd ed.

[Lee57] T. D. Lee, K. Huang, and C. N. Yang, *Eigenvalues and Eigenfunctions of a Bose System of Hard Spheres and Its Low-Temperature Properties*, Phys. Rev. **106**, 1135 (1957).

[Leg80] A. J. Leggett, *Diatomic Molecules and Cooper Pairs*, in: A. Pekalski and R. Przystawa (Eds.), *Modern Trends in the Theory of Condensed Matter*, 13–27, Springer-Verlag, Berlin, 1980.

[Mad00a] K. W. Madison, F. Chevy, W. Wohlleben, and J. Dalibard, *Vortex Formation in a Stirred Bose-Einstein Condensate*, Phys. Rev. Lett. **84**, 806 (2000).

[Mad00b] K. W. Madison, F. Chevy, W. Wohlleben, and J. Dalibard, *Vortices in a stirred Bose-Einstein condensate*, J. Mod. Opt. **47**, 2715 (2000).

[Man04] N. Manini and L. Salasnich, *Bulk and Collective Properties of a Dilute Fermi Gas in the BCS-BEC Crossover* (2004), http://arxiv.org/abs/cond-mat/0407039.

[Mar04] B. Marcelis, E. G. M. van Kempen, B. J. Verhaar, and S. J. J. M. F. Kokkelmans, *Feshbach resonances with large background scattering length: Interplay with open-channel resonances*, Phys. Rev. A **70**, 012701 (2004).

[Mas04] P. Massignan, G. M. Bruun, and H. Smith, *Viscous relaxation and collective oscillations in a trapped Fermi gas near the unitarity limit* (2004), http://arxiv.org/abs/cond-mat/0409660.

[Mat99] M. R. Matthews, B. P. Anderson, P. C. Haljan, D. S. Hall, C. E. Wieman, and E. A. Cornell, *Vortices in a Bose-Einstein Condensate*, Phys. Rev. Lett. **83**, 2498 (1999).

[Men02] C. Menotti, P. Pedri, and S. Stringari, *Expansion of an Interacting Fermi Gas*, Phys. Rev. Lett. **89**, 250402 (2002).

[Mew96] M.-O. Mewes, M. R. Andrews, N. J. van Druten, D. M. Kurn, D. S. Durfee, C. G. Townsend, and W. Ketterle, *Collective Excitations of a Bose-Einstein Condensate in a Magnetic Trap*, Phys. Rev. Lett. **77**, 988 (1996).

[Mil02] J. N. Milstein, S. J. J. M. F. Kokkelmans, and M. J. Holland, *Resonance theory of the crossover from Bardeen-Cooper-Schrieffer superfluidity to Bose-Einstein condensation in a dilute Fermi gas*, Phys. Rev. A **66**, 043604 (2002).

[Mod03] G. Modugno, F. Ferlaino, R. Heidemann, G. Roati, and M. Inguscio, *Production of a Fermi gas of atoms in an optical lattice*, Phys. Rev. A **68**, 011601(R) (2003).

[Moe95] A. J. Moerdijk, B. J. Verhaar, and A. Axelsson, *Resonances in ultracold collisions of ^{6}Li, ^{7}Li, and ^{23}Na*, Phys. Rev. A **51**, 4852 (1995).

[Møl98] K. Mølmer, *Bose Condensates and Fermi Gases at Zero Temperature*, Phys. Rev. Lett. **80**, 1804 (1998).

[Mor01] H. Moritz, *Fermionisches Lithium in einer Resonatordipolfalle*, diploma thesis, Max-Planck-Institut für Kernphysik, Heidelberg (2001).

[Mos01] A. Mosk, S. Jochim, H. Moritz, T. Elsässer, M. Weidemüller, and R. Grimm, *Resonator-Enhanced Optical Dipole Trap for Fermionic Lithium Atoms*, Opt. Lett. **26**, 1837 (2001).

[Nar98] M. Naraschewski and D. M. Stamper-Kurn, *Analytical description of a trapped semi-ideal Bose gas at finite temperature*, Phys. Rev. A **58**, 2423 (1998).

[Noz85] P. Nozières and S. Schmitt-Rink, *Bose Condensation in an Attractive Fermion Gas: From Weak to Strong Coupling Superconductivity*, J. Low Temp. Phys. **59**, 195 (1985).

[Noz90] P. Noziéres and D. Pines, *The Theory of Quantum Liquids, Vol. II Superfluid Bose Liquids*, Addison-Wesley, 1990.

[O'H00] K. M. O'Hara, M. E. Gehm, S. R. Granade, S. Bali, and J. E. Thomas, *Stable, strongly attractive, two-state mixture of lithium fermions in an optical trap*, Phys. Rev. Lett. **85**, 2092 (2000).

[O'H01] K. M. O'Hara, M. E. Gehm, S. R. Granade, and J. E. Thomas, *Scaling laws for evaporative cooling in time-dependent optical traps*, Phys. Rev. A **64**, 051403(R) (2001).

[O'H02a] K. M. O'Hara, S. L. Hemmer, M. E. Gehm, S. R. Granade, and J. E. Thomas, *Observation of a Strongly Interacting Degenerate Fermi Gas of Atoms*, Science **298**, 2179 (2002).

[O'H02b] K. M. O'Hara, S. L. Hemmer, S. R. Granade, M. E. Gehm, J. E. Thomas, V. Venturi, E. Tiesinga, and C. J. Williams, *Measurement of the zero crossing in a Feshbach resonance of fermionic ^6Li*, Phys. Rev. A **66**, 041401(R) (2002).

[Oha02] Y. Ohashi and A. Griffin, *BCS-BEC Crossover in a Gas of Fermi Atoms with a Feshbach Resonance*, Phys. Rev. Lett. **89**, 130402 (2002).

[Oha03] Y. Ohashi and A. Griffin, *Superfluid transition temperature in a trapped gas of Fermi atoms with a Feshbach resonance*, Phys. Rev. A **67**, 033603 (2003).

[Ovc99] Y. B. Ovchinnikov, J. H. Müller, M. R. Doery, E. J. D. Vredenbregt, K. Helmerson, S. L. Rolston, and W. D. Phillips, *Diffraction of a Released Bose-Einstein Condensate by a Pulsed Standing Light Wave*, Phys. Rev. Lett. **83**, 284 (1999).

[Ped03] P. Pedri, D. Guéry-Odelin, and S. Stringari, *Dynamics of a classical gas including dissipative and mean-field effects*, Phys. Rev. A **68**, 043608 (2003).

[Per04a] A. Perali, P. Pieri, L. Pisani, and G. C. Strinati, *BCS-BEC Crossover at Finite Temperature for Superfluid Trapped Fermi Atoms*, Phys. Rev. Lett. **92**, 220404 (2004).

[Per04b] A. Perali, P. Pieri, and G. C. Strinati, *Quantitative Comparison between Theoretical Predictions and Experimental Results for the BCS-BEC Crossover*, Phys. Rev. Lett. **93**, 100404 (2004).

[Pet02] C. J. Pethick and H. Smith, *Bose-Einstein Condensation in Dilute Gases*, Cambridge University Press, 2002.

[Pet03] D. S. Petrov, *Three-body problem in Fermi gases with short-range interparticle interaction*, Phys. Rev. A **67**, 010703(R) (2003).

[Pet04] D. Petrov, C. Salomon, and G. Shlyapnikov, *Weakly bound dimers of fermionic atoms*, Phys. Rev. Lett. **93**, 090404 (2004).

[Pet05] D. S. Petrov, C. Salomon, and G. V. Shlyapnikov, *Scattering properties of weakly bound dimers of fermionic atoms*, Phys. Rev. A **71**, 012708 (2005).

[Pie00] P. Pieri and G. C. Strinati, *Strong-coupling limit in the evolution from BCS superconductivity to Bose-Einstein condensation*, Phys. Rev. B **61**, 15370 (2000).

[Pie04a] P. Pieri (2004), private communication.

[Pie04b] P. Pieri, L. Pisani, and G. C. Strinati, *BCS-BEC crossover at finite temperature in the broken-symmetry phase*, Phys. Rev. B **70**, 094508 (2004).

[Pit61] L. P. Pitaevskii, *Vortex lines in an imperfect Bose gas*, Sov. Phys. JETP **13**, 451 (1961).

[Pit98] L. Pitaevskii and S. Stringari, *Elementary Excitations in Trapped Bose-Einstein Condensed Gases Beyond the Mean-Field Approximation*, Phys. Rev. Lett. **81**, 4541 (1998).

[Pit02] L. Pitaevskii and S. Stringari, *The Quest for Superfluidity in Fermi Gases*, Science **298**, 2144 (2002).

[Pit03] L. Pitaevskii and S. Stringari, *Bose-Einstein Condensation*, Oxford University Press, 2003.

[Ran95] M. Randeria, *Crossover from BCS Theory to Bose-Einstein Condensation*, in: A. Griffin, D. Snoke, and S. Stringari (Eds.), *Bose-Einstein Condensation*, 355–392, Cambridge Univ. Press, Cambridge, 1995.

[Reg03a] C. A. Regal and D. S. Jin, *Measurement of Positive and Negative Scattering Lengths in a Fermi Gas of Atoms*, Phys. Rev. Lett. **90**, 230404 (2003).

[Reg03b] C. A. Regal, C. Ticknor, J. L. Bohn, and D. S. Jin, *Creation of ultracold molecules from a Fermi gas of atoms*, Nature **424**, 47 (2003).

[Reg03c] C. A. Regal, C. Ticknor, J. L. Bohn, and D. S. Jin, *Tuning p-Wave Interactions in an Ultracold Fermi Gas of Atoms*, Phys. Rev. Lett. **90**, 053201 (2003).

[Reg04a] C. A. Regal, M. Greiner, and D. S. Jin, *Lifetime of Molecule-Atom Mixtures near a Feshbach Resonance in* ^{40}K, Phys. Rev. Lett. **92**, 083201 (2004).

[Reg04b] C. A. Regal, M. Greiner, and D. S. Jin, *Observation of Resonance Condensation of Fermionic Atom Pairs*, Phys. Rev. Lett. **92**, 040403 (2004).

[Rie04] S. Riedl, *Untersuchung stark wechselwirkender fermionischer Quantengase mittels Absorptionsabbildung*, diploma thesis, Universität Innsbruck (2004).

[Sak94] J. J. Sakurai, *Modern Quantum Mechanics*, Addison-Wesley, 1994, revised ed.

[Sch99] U. Schünemann, H. Engler, R. Grimm, M. Weidemüller, and M. Zielonkowski, *Simple scheme for tunable frequency offset locking of two lasers*, Rev. Sci. Instr. **70**, 242 (1999).

[Sch01] F. Schreck, L. Khaykovich, K. L. Corwin, G. Ferrari, T. Bourdel, J. Cubizolles, and C. Salomon, *Quasipure Bose-Einstein Condensate Immersed in a Fermi Sea*, Phys. Rev. Lett. **87**, 080403 (2001).

[Sch04] C. H. Schunck, M. W. Zwierlein, C. Stan, S. M. F. Raupach, W. Ketterle, A. Simoni, E. Tiesinga, C. J. Williams, and P. S. Julienne, *Feshbach Resonances in Fermionic Lithium-6* (2004), http://arxiv.org/abs/cond-mat/0407373.

[Shi04] Y. Shin, M. Saba, T. A. Pasquini, W. Ketterle, D. E. Pritchard, and A. E. Leanhardt, *Atom Interferometry with Bose-Einstein Condensates in a Double-Well Potential*, Phys. Rev. Lett. **92**, 050405 (2004).

[Sim04] A. Simoni, E. Tiesinga, C. J. Williams, and P. S. Julienne (2004), private communication; the calculation is based on the data published in [Bar04c].

[SK98] D. M. Stamper-Kurn, H.-J. Miesner, S. Inouye, M. R. Andrews, and W. Ketterle, *Collisionless and Hydrodynamic Excitations of a Bose-Einstein Condensate*, Phys. Rev. Lett. **81**, 500 (1998).

[Söd99] J. Söding, D. Guéry-Odelin, P. Desbiolles, F. Chevy, H. Inamori, and J. Dalibard, *Three-body decay of a rubidium Bose-Einstein condensate*, Appl. Phys. B **69**, 257 (1999).

[Sta04] J. Stajic, J. N. Milstein, Q. Chen, M. L. Chiofalo, M. J. Holland, and K. Levin, *Nature of superfluidity in ultracold Fermi gases near Feshbach resonances*, Phys. Rev. A **69**, 063610 (2004).

[Ste99] J. Stenger, S. Inouye, A. P. Chikkatur, D. M. Stamper-Kurn, D. E. Pritchard, and W. Ketterle, *Bragg Spectroscopy of a Bose-Einstein Condensate*, Phys. Rev. Lett. **82**, 4569 (1999).

[Ste00] J. V. Steele, *Efective Field Theory Power Counting at Finite Density* (2000), nucl-th/0010066.

[Sto88] H. T. C. Stoof, J. M. V. A. Koelman, and B. J. Verhaar, *Spin-exchange and dipole relaxation rates in atomic hydrogen: Rigorous and simplified calculations*, Phys. Rev. B **38**, 4688 (1988).

[Sto96] H. T. C. Stoof, M. Houbiers, C. A. Sackett, and R. G. Hulet, *Superfluidity of Spin-Polarized ^{6}Li*, Phys. Rev. Lett. **76**, 10 (1996).

[Stö04] T. Stöferle, H. Moritz, C. Schori, M. Koöhl, and T. Esslinger, *Transition from a Strongly Interacting 1D Superfluid to a Mott Insulator*, Phys. Rev. Lett. **92**, 130403 (2004).

[Str96] S. Stringari, *Collective Excitations of a Trapped Bose-Condensed Gas*, Phys. Rev. Lett. **77**, 2360 (1996).

[Str02] K. E. Strecker, G. B. Partridge, A. G. Truscott, and R. G. Hulet, *Formation and propagation of matter-wave soliton trains*, Nature **417**, 150 (2002).

[Str03] K. E. Strecker, G. B. Partridge, and R. G. Hulet, *Conversion of an Atomic Fermi Gas to a Long-Lived Molecular Bose Gas*, Phys. Rev. Lett. **91**, 080406 (2003).

[Str04a] S. Stringari, *Collective oscillations of a trapped Fermi gas near a Feshbach resonance*, Europhys. Lett. **65**, 749 (2004).

[Str04b] S. Stringari, *Non linear corrections to the collective frequencies* (2004), private communication; a summary of his results is found in appendix B.

[Sun03] H. Suno, B. D. Esry, and C. H. Greene, *Recombination of Three Ultracold Fermionic Atoms*, Phys. Rev. Lett. **90**, 053202 (2003).

[Tie93] E. Tiesinga, B. J. Verhaar, and H. T. C. Stoof, *Threshold and resonance phenomena in ultracold ground-state collisions*, Phys. Rev. A **47**, 4114 (1993).

[Tim01] E. Timmermans, K. Furuya, P. W. Milonni, and A. K. Kerman, *Prospect of creating a composite Fermi-Bose superfluid*, Phys. Lett. A **285**, 228 (2001).

[Tin66] M. Tinkham, *Introduction to Superconductivity*, McGraw-Hill, New York, 1966.

[Tör00] P. Törmä and P. Zoller, *Laser Probing of Atomic Cooper Pairs*, Phys. Rev. Lett. **85**, 487 (2000).

[Tru01] A. G. Truscott, K. E. Strecker, W. I. McAlexander, G. B. Partridge, and R. G. Hulet, *Observation of Fermi Pressure in a Gas of Trapped Atoms*, Science **291**, 2570 (2001).

[Van89] J. Vanier and C. Audoin, *The Quantum Physics of Atomic Frequency Standards*, Adam Hilger, Bristol, UK, 1989.

[Vic99] L. Vichi and S. Stringari, *Collective oscillations of an interacting trapped Fermi gas*, Phys. Rev. A **60**, 4734 (1999).

[Vic00] L. Vichi, *Collisional Damping of the Collective Oscillations of a Trapped Fermi Gas*, J. Low. Temp. Phys. **121**, 177 (2000).

[Web03] T. Weber, J. Herbig, M. Mark, H.-C. Nägerl, and R. Grimm, *Bose-Einstein Condensation of Cesium*, Science **299**, 232 (2003).

[Wei99] J. Weiner, V. S. Bagnato, S. Zilio, and P. S. Julienne, *Experiments and theory in cold and ultracold collisions*, Rev. Mod. Phys. **71** (1999).

[Wei04] P. Weiss, *Extreme Impersonations*, Science News **166**, 186 (2004).

[Wil99] C. J. Williams, E. Tiesinga, P. S. Julienne, H. Wang, W. C. Stwalley, and P. L. Gould, *Determination of the scattering lengths of ^{39}K from 1_u photoassocitation line shapes*, Phys. Rev. A **60**, 4427 (1999).

[Wil04] J. E. Williams, N. Nygaard, and C. W. Clark, *Phase diagrams for an ideal gas mixture of fermionic atoms and bosonic molecules*, New Journal of Physics **6**, 123 (2004).

[Wu97] H. Wu, E. Arimondo, and C. J. Foot, *Dynamics of evaporative cooling for Bose-Einstein condensation*, Phys. Rev. A **56**, 560 (1997).

[Xu03] K. Xu, T. Mukaiyama, J. R. Abo-Shaeer, J. K. Chin, D. E. Miller, and W. Ketterle, *Formation of Quantum-Degenerate Sodium Molecules*, Phys. Rev. Lett. **91**, 210402 (2003).

[Yan96] Z.-C. Yan, J. F. Babb, A. Dalgarno, and G. W. F. Drake, *Variational calculations of dispersion coefficients for interactions among H, He, and Li atoms*, Phys. Rev. A **54**, 2824 (1996).

[Zam98] F. Zambelli and S. Stringari, *Quantized Vortices and Collective Oscillations of a Trapped Bose-Einstein Condensate*, Phys. Rev. Lett. **81**, 1754 (1998).

[Zam01] F. Zambelli and S. Stringari, *Moment of inertia and quadrupole response function of a trapped superfluid*, Phys. Rev. A **63**, 033602 (2001).

[Zar99] E. Zaremba, T. Nikuni, and A. Griffin, *Dynamics of Trapped Bose Gases at Finite Temperatures*, J. Low Temp. Phys. **116**, 277 (1999).

[Zha04] J. Zhanga, E. G. M. van Kempenc, T. Bourdela, L. Khaykovicha, J. Cubizollesa, F. Chevya, M. Teichmanna, L. Tarruella, S. J. J. M. F.Kokkelmansa, and C. Salomon, *P-wave Feshbach resonances of ultracold ^6Li*, Phys. Rev. A **70**, 030702(R) (2004).

[Zwi03] M. W. Zwierlein, C. A. Stan, C. H. Schunck, S. M. F. Raupach, S. Gupta, Z. Hadzibabic, and W. Ketterle, *Observation of Bose-Einstein Condensation of Molecules*, Phys. Rev. Lett. **91**, 250401 (2003).

[Zwi04] M. Zwierlein, C. A. Stan, C. H. Schunck, S. M. F. Raupach, A. J. Kerman, and W. Ketterle, *Condensation of Pairs of Fermionic Atoms near a Feshbach Resonance*, Phys. Rev. Lett. **92**, 120403 (2004).

Acknowledgement

First of all, I would like to thank my advisor Rudi Grimm for his support and advice throughout this thesis. Rudi was always available and willing to discuss any aspects of the experiment and his rich experience helped us to solve many problems that we would not have overcome otherwise. His sparkling enthusiasm for science is unforgettable and was a constant source of motivation.

Most of the time I had the pleasure to work together with the former Ph.D. student Selim Jochim. Since I joined the Lithium experiment in September 2001, I learned a lot from his rich experience. Together we setup the experimental apparatus, that had just been transferred from Heidelberg to Innsbruck. I am grateful for his many lessons on the experimental details and the great team work which lead to many important results. Selim has been a dependable colleague and friend throughout my years in Innsbruck.

I would also like to thank Gerhard Hendl who joined us in the beginning of 2002 as a diploma student. Unforgettable is his fast and precise soldering work and many of our electronic circuits that were essential for setting up a reliable and stable experiment carry his name.

I also want to express my thanks to the Ph.D. student Alexander Altmeyer, who joined our Lithium team in spring 2003. It was about that time that we saw the first loss in the atomic signal, which soon later turned out to be due to the formation of molecules. Alexander was an essential help during the modifications of the setup and during many long nights of measurements.

At about the same time the postdoc Cheng Chin joined our group. Cheng loved the molecules from the first date and produced new ideas for the next experiments long before the ongoing investigations had been finished. His calculations helped us a lot to understand our experimental results.

In autumn 2003 we were happy, that Stefan Riedl joined our Lithium crew as a diploma student. Soon after, Stefan made important contributions to the new setup and the subsequent measurements. After finishing his diploma thesis in summer 2004 we were fortune to convince him to continue working on the project as a Ph.D. student. I am sure that together with Alexander and our new postdoc Reece Geursen, the experiment lies in the best hands for further great research results.

I would also like to thank our staff scientist Johannes Hecker Denschlag. Johannes supported us continuously during all the years and was always available for discussions on the ongoing experiments.

I also want to express my thanks to all the other members of the Grimm group, who worked on the different projects. In particular I would like to thank Hanns-Christoph Nägerl, Matthias Theis, Jens Herbig, Michael Mark, Matthias Gustavsson, Tobias Kraemer, Gregor Thalhammer, Klaus Winkler, Bastian Engeser and the former group members Markus Hammes, Tino Weber and David Rychtarik for the various fruitful discussions and their helpful advices. With most of them I had the pleasure to organize the YAO conference, which was on the whole a lot of work but also a great

experience.

I also want to thank the non-scientific members of the institute. Our group secretary Christine Götsch-Obmascher for all the organization work and Manuel Kluibenschädl for helping with the computer network. I would also like to thank Anton Schönherr and Stefan Haslwanter from the mechanical workshop for their excellent work and for teaching me many useful tricks.

I want to thank all the members of the Grimm group for the nice atmosphere at and outside the university. I remember well the many winter days on the surrounding ski-slopes and the famous night tobogganing activities. In summer I enjoyed very much the numerous barbecues, where Alexander, also known as the "Schwenker" (German name for a very special kind of barbecue and the way of using it), did a phenomenal job.

Finally I would like to thank my family. They consistently supported and encouraged me during all my studies.

My greatest thank deserves Anna. She always believed in me and was on my side in times of great challenge and doubt. She was patient with my work and here Italian way of life also helped me to keep my eyes peeled for things outside of the university.

Thanks all of you!!!